

<http://researchcommons.waikato.ac.nz/>

## **Research Commons at the University of Waikato**

### **Copyright Statement:**

The digital copy of this thesis is protected by the Copyright Act 1994 (New Zealand).

The thesis may be consulted by you, provided you comply with the provisions of the Act and the following conditions of use:

- Any use you make of these documents or images must be for research or private study purposes only, and you may not make them available to any other person.
- Authors control the copyright of their thesis. You will recognise the author's right to be identified as the author of the thesis, and due acknowledgement will be made to the author where appropriate.
- You will obtain the author's permission before publishing any material from the thesis.

# The Influence of the Lithological and Geotechnical Properties of Rocks on the Morphology of Glacial Valleys

A thesis submitted in fulfilment  
of the requirements for the degree  
of  
Doctor of Philosophy in Earth Sciences  
at the  
University of Waikato

by

*Paul Christian Augustinus*



University of Waikato  
1988



## ABSTRACT

The glacial valley cross-profile has traditionally had its development attributed to the physical properties of the eroding glacier, with the input of the properties of the eroded rock mass to the development of the valley system considered in a purely qualitative sense.

The present study shows that the size of the outlet trough is directly related to the volume of ice discharged through it, estimated from the glacier contributing area. The trough size and morphological variations therein, can be partially attributed to the influence of the bedrock strength properties.

Rock intact strength measures showed little relationship to the form of the glacial trough. However, a modified rock mass strength method was developed and applied to a variety of morphological and geological terrains in the vicinity of the Main Divide of the New Zealand Southern Alps. The results indicate a significant correlation between the cross-valley form and mass strength (RMS) properties of the eroded bedrock. The RMS controls on the development of the trough were: joint spacing, joint orientation and joint continuity. The trend suggests that weaker, more densely jointed bedrock tends to develop broader, flatter valleys. RMS with respect to subaerial processes controls the extent of post-glacial/interglacial modification of the trough slope, and development of zones of weakened slope rock that could be preferentially exploited by subsequent glacier re-advances.

Due to their position astride the Alpine Fault, the New Zealand Southern Alps are subjected to high levels of shallow crustal horizontal stresses. The PHS directions are indicated by geodetic and earthquake first-motion studies, as well as conjugate shear joint and glacial valley orientations. The *in situ* stress field may control the location and extent of rock failure, when considered in conjunction with the high gravitational stresses induced by the extreme relief. Finite element models of typical glacial troughs suggest that rock intact strength properties control the likelihood and site of stress-induced bedrock failure.

Thus, the shape of a glacial trough depends not only on the physical properties of the glacier, but on the geotechnical properties of the host rockmass. The stress-induced controls on the site of rock mass failure are important controls on the locus of erosion. Following development of the glacial trough, considerable modification of the size and form of the valley cross-profile may occur depending on the mass strength of the de-buttressed slope rock.

## ACKNOWLEDGEMENTS

I would like to acknowledge my chief supervisor, Professor M.J. Selby for suggesting the topic and providing the opportunity, through research funds from the University Grants Committee, to undertake fieldwork in the Dry Valleys, Antarctica. Financial support from the Department of Earth Sciences, University of Waikato, enabled the project to be carried through to fruition.

Thanks must go to Professor J.M. Soons, Geography Department University of Canterbury, for allowing me access to the facilities of her Department during 1986; Dr Athol Carr, Department of Civil Engineering, University of Canterbury, for tutoring me in his SHELL finite element programme; and to the post-graduate students of the Geography Department for making my stay pleasurable and fruitful.

The co-operation of the Antarctic Division, DSIR personnel, and U.S. Navy squadron VXE6 is acknowledged during my sojourn in Antarctica over the 1984/85 summer, and the former during my frequent visits to the Antarctic Division Library and Map-room.

The chief rangers of Mount Cook, Westland, Aspiring and Fiordland National Parks are thanked for allowing me to conduct my research in their areas of jurisdiction; and for the free use of park huts.

This study was undertaken with the support of a Commonwealth Scholarship and Fellowship Plan Award administered by the New Zealand University Grants Committee.

Finally, I would like to thank my second supervisor, Roger Briggs, for proof reading and his constant pleas of "but its not my field". Fellow research students in the Earth Sciences Department, University of Waikato are particularly thanked for stimulating discussion and support over the years - without whose presence this work might have been completed a lot sooner!

## TABLE OF CONTENTS

	Page No.
ABSTRACT	ii
ACKNOWLEDGEMENTS	iii
TABLE OF CONTENTS	iv
LIST OF FIGURES	x
LIST OF TABLES	xiii
 CHAPTER ONE: INTRODUCTION	
1.1 <u>Statement of Problem</u>	1
1.2 <u>Aims of Study</u>	2
1.3 <u>Scope of Proposed Study</u>	3
1.4 <u>Literature Review</u>	
1.4.1 Glacial Erosion and Rock Quality	3
1.4.2 Glacial Erosion Processes	5
1.4.3 Rock Strength and Glacial Erosion	7
1.4.4 Influence of Rock Stress on Glacial Erosion	8
1.5 <u>Summary</u>	9
 CHAPTER TWO: GEOGRAPHIC AREAS OF INVESTIGATION: PHYSIOGRAPHY, GEOMORPHIC PROCESSES AND GEOLOGIC SETTING	
2.1 <u>Choice of Study Sites</u>	10
2.2 <u>Site Location and Physiography</u>	12
2.2.1 Fiordland Region	12
2.2.2 South-Central Fiordland Region	22
2.2.3 Mt. Aspiring Region	22
2.2.4 South Westland Region	27
2.2.5 Mt. Cook Region	32
2.2.6 McMurdo Dry Valleys	35
2.3 <u>Regional Geology and Tectonics of the Southern Part of     the Southern Alps</u>	
2.3.1 Introduction	38
2.3.2 Fiordland Region	41
2.3.3 Mt. Aspiring Region	43

2.3.4 South Westland Region	47
2.3.5 Mt. Cook Region	48
2.3.6 McMurdo Dry Valleys Region	50
2.4. <u>Summary</u>	53
CHAPTER THREE: MORPHOMETRY OF FIORDLAND OUTLET GLACIER TROUGHS: IMPLICATIONS FOR GLACIAL TROUGH DEVELOPMENT	
3.1 <u>Introduction</u>	54
3.2 <u>Quantification of the Morphology of Fiordland</u>	
3.2.1 Introduction	56
3.2.2 Outlet Glacier Trough Morphology	56
3.2.3 Delineation of Glacier Divides	60
3.2.4 Trough Morphometry	61
3.3 <u>Results and Discussion</u>	64
3.4 <u>Implications for Southern Alps Glacial Trough Development</u>	72
3.5 <u>Comparison With Some Antarctic Outlet Glacier Troughs</u>	73
3.6 <u>Summary and Conclusions</u>	80
CHAPTER FOUR: ROCK MASS STRENGTH CONTROLS ON THE MORPHOLOGY AND STABILITY OF GLACIAL VALLEY SLOPES	
4.1 <u>Introduction</u>	82
4.2 <u>Controls on the Stability of Alpine Rock Slopes</u>	82
4.3 <u>Methodology</u>	
4.3.1 Introduction	84
4.3.2 Techniques	85
4.4 <u>Regional Rock Mass Strength</u>	
4.4.1 Darran Mountains Region	85
4.4.2 South-Central Fiordland Region	91
4.4.3 Mt. Aspiring Region	91
4.4.4 South Westland Region	98
4.4.5 Mt. Cook Region	100
4.4.6 Summary RMS Results	101

4.5 <u>Rock Mass Strength Controls on Some Antarctic Dry Valley Landforms</u>	
4.5.1 Introduction	102
4.5.2 RMS and the Dry Valleys	102
4.5.2.1 Upper Wright Valley-Mt. Baldr	104
4.5.2.2 Mt Cerce-Olympus Range	104
4.5.3 Discussion of Results	106
4.5.4 Summary and Conclusions	110
4.6 <u>Modified RMS Method</u>	
4.6.1 Introduction	111
4.6.2 Modified RMS Method	112
4.6.3 Results	116
4.7 <u>Glacial Trough Morphometry</u>	
4.7.1 Introduction	116
4.7.2 Glacial Drainage Density	118
4.7.3 Parabolas As Glacial Valley Cross-Profile Analogues	121
4.7.4 Shape Factors	123
4.7.5 RMS Versus Valley Shape	123
4.7.6 Rock Intact Strength Versus Valley Shape	125
4.7.7 Relative Importance of the Erosion Processes	129
4.8 <u>Summary and Conclusions</u>	130
CHAPTER FIVE: INTACT STRENGTH PROPERTIES OF SOME ROCKS FROM NEW ZEALAND AND ANTARCTICA	
5.1 <u>Introduction</u>	133
5.2 <u>Methods</u>	133
5.3 <u>Correlations Between Rock Strength and Physical Properties</u>	
5.3.1 Introduction	134
5.3.2 Point Load Strength	134
5.3.3 Rock Physical Properties	134
5.3.4 Shore Hardness	137

5.3.5 Los Angeles Abrasion	138
5.3.6 Schmidt Hammer Rebound	138
5.4 <u>Effect of Saturation on Rock Strength</u>	140
5.5 <u>Implications of Strength Reduction of Saturated Rocks for Geomorphic Studies</u>	143
5.6 <u>Rock Intact Strength and Glacial Valley Morphology</u>	144
5.7 <u>Summary and Conclusions</u>	145
CHAPTER SIX: TECTONICS, STRESSES AND GLACIAL VALLEYS	
6.1 <u>Introduction</u>	146
6.2 <u>Regional Crustal Stress Patterns from Geomorphic Data</u>	
6.2.1 Introduction	147
6.2.2 Conjugate Shear Surfaces from Joint Patterns	147
6.2.3 Valley Trends	151
6.2.4 Lineaments	151
6.3 <u>Regional Crustal Stress Patterns in the Southern Alps from Joint and Valley Orientations</u>	
6.3.1 Northern Fiordland Region	153
6.3.2 South-Central Fiordland Region	157
6.3.3 Mt. Aspiring Region	159
6.3.4 South Westland Region	160
6.3.5 Mt. Cook Region	161
6.3.6 Implications of Valley Trends for Landscape Development	163
6.4 <u>In situ Rock Stress Determinations</u>	
6.4.1 Introduction	164
6.4.2 Central Otago	164
6.4.3 Fiordland	165
6.5 <u>Summary and Conclusions</u>	168
CHAPTER SEVEN: STRESS MODELLING AND THE DEVELOPMENT OF GLACIAL TROUGHS	
7.1 <u>Introduction</u>	169
7.1.1 Review of Modelling of Valley-Ridge Systems	170

7.2	<u>Finite Element Method</u>	
7.2.1	Introduction	173
7.2.2	Mesh Development	174
7.2.3	Data Input to the Model	174
7.2.4	Model Output	178
7.3	<u>Finite Element Models</u>	
7.3.1	Northern Fiordland	178
7.3.2	West Arm Manapouri	183
7.3.3	Greywacke Model-Mt Cook	185
7.3.4	Schist Model-South Westland	188
7.4	<u>Stress Evaluation: Implications for Slope Stability and Erosion Processes</u>	190
7.5	<u>Influence of the In situ Stress Regime on the Development of Some Antarctic Dry Valley Landforms</u>	
7.5.1	Introduction	192
7.5.2	Finite Element Analysis	192
7.5.3.1	FE Model- Mt. Thor	194
7.5.3.2	FE Model- Mt. Cerce	194
7.5.3	Development of Residual Stresses in Sandstone	197
7.5.4	Summary and Conclusions	199
CHAPTER EIGHT: SYNTHESIS		
8.1	<u>Introduction</u>	200
8.2	<u>Valley Initiation and Development</u>	200
8.3	<u>Interaction of RMS and Stress Field on Valley Development</u>	201
8.4	<u>Implications of Uplift, Erosion and Rock Strength for the Development of the Southern Alps Landscape</u>	
8.4.1	Introduction	204
8.4.2	Fiordland Region	206
8.4.3	Mt Aspiring-South Westland Region	207
8.4.4	Central Southern Alps-Westland to Mt Cook Regions	208
8.4.5	Antarctica	209
8.5	<u>Conclusions</u>	211

REFERENCES	212
APPENDIX ONE: ROCK MASS STRENGTH DATA SHEETS	234
APPENDIX TWO: MORPHOMETRIC DATA	240
APPENDIX THREE: ROCK INTACT STRENGTH DATA SHEETS AND METHODOLOGY	249



## LIST OF FIGURES

Figure	Page No.
2.1a. Location of study regions	11
b. Generalized geological map	11
2.2a-c. Valley and slope morphology, Fiordland	13-14
2.3. Summit accordance, Fiordland	17
2.4. Snow-line elevation, South Westland	18
2.5. Fiordland localities	19
2.6. Geomorphic map - northern Fiordland	21
2.7. Geomorphic map - south-central Fiordland	23
2.8. Geomorphic map - Mt. Aspiring	24
2.9a,b. Slope morphology, Mt. Aspiring	25
2.10. Summit-level envelope, Mt. Aspiring	26
2.11. Geomorphic map - Mt Cook-South Westland	29
2.12a-c. Slope morphology, Waiho Valley	30-31
2.13a-c. Slope morphology, Mt Cook region	33-34
2.14. Location map, Antarctica	36
2.15a. Cirque headed valley, Olympus Range	37
b. Taylor Valley, Antarctica	37
2.16. Principal horizontal shortening directions	40
2.17. Uplift and erosion rates, Southern Alps	40
2.18. South western South Island tectonics	42
2.19. Fiordland geology	44
2.20. Mt. Aspiring geology	46
2.21. South Westland geology	49
2.22. Mt. Cook geology	51
2.23. Wright-Victoria valley geology	52
3.1. Fiordland glacial limits	55
3.2. Summit-level envelope, Fiordland	57
3.3. Fiordland localities	58
3.4. Connectivity indices, Fiordland	62
3.5. Description of fiord morphometry	63

3.6.	Fiord locations	65
3.7a-c.	Fiord size-catchment area relationships	66
3.8.	Location of inland lakes	74
3.9.	Lake size-catchment area relationships	75
3.10.	Antarctic outlet trough size-catchment area relationships	77
4.1.	Rock mass strength envelope	86
4.2a-e.	Rock mass strength envelopes for each terrain	88
4.3.	Sheet jointing, northern Fiordland	90
4.4a,b.	Rock slides, Mt Aspiring area	92
4.5a.	Geomorphic map of Dart Glacier area	93
b.	Poles to joints, Dart Glacier area	94
4.6a,b.	Structurally controlled slopes	96
4.7.	Active slopes, Waiho Valley	99
4.8.	Mt Cook skyline	99
4.9.	RMS envelope, McMurdo Dry Valleys	103
4.10.	RMS slope transects	105
4.11.	Mt Cerce, Olympus Range	107
4.12.	Olympus Range profile transect	109
4.13.	Slope development model	109
4.14.	Joint control on glacial erosion	114
4.15a,b.	Glacial drainage density versus RMS	120
c,d.	Shape exponent 'c' versus RMS	120
4.16.	Valley cross-profile shape versus RMS	124
4.17.	Rock intact strength versus shape factor	127
4.18.	Rock intact strength versus form ratio	128
5.1.	Relationships between rock intact strength and physical properties	136
5.2.	Relationships between rock intact strength and physical properties	139
6.1.	Principal horizontal shortening directions	149
6.2.	Principal stresses and fracture development	150
6.3.	Rectification of drainage patterns	152

6.4.	Structural geometries in vicinity of Main Divide	154
6.5.	Preferred valley trends near Main Divide	156
6.6.	Crustal earthquake distribution	158
7.1.	Finite element boundary conditions and mesh	172
7.2.	FE meshes for glacial valley profiles	175
7.3.	Tectonic control on crustal stresses	177
7.4 & 5.	Model output, northern Fiordland	180-181
7.6.	Model output, West Arm Manapouri	184
7.7.	Model output, Tasman Valley	187
7.8.	Model output, Whymper Valley	189
7.9.	FE meshes for Olympus Range profiles	193
7.10.	Model output for Mt. Thor profile	195
7.11.	Model output for Mt. Cerce profile	196
7.12.	Sheeting joints, Mt. Dido	198
7.13.	Columnar jointing, Asgard Range	198
8.1.	Glacial trough development, Southern Alps	202
8.2.	Uplift and erosion rates, central Southern Alps	205

## LIST OF TABLES

Table	Page No.
2.1. Geomorphic symbols	20
3.1. Fiord size data	67
3.2. Comparison of correlation coefficients	69
3.3. Comparison of regression equations	69
3.4. Comparison of power equations	69
3.5. Dimensions of inland lakes	75
3.6. Dimensions of some Antarctic outlet glaciers	78
3.7. Regression equations for outlet glaciers	78
4.1. RMS classification weightings	86
4.6. Mean RMS and valley shape data	117
4.7. Correlation matrix shape-strength parameters	120
4.8. Mean intact strength parameters	126
4.9. Ranking of glacial erosion processes	129
5.1. Correlation matrix rock strength properties	135
5.2. Correlation matrix isotropic rock strength	135
5.3. Brazil tensile strength of water-saturated rocks in % of strength of oven-dried rocks	142
7.1. Geotechnical properties for FE models	179

## **Chapter One**

### **Introduction**

## CHAPTER ONE: INTRODUCTION

### 1.1. Statement Of Problem

The landscapes of the heavily glacierized Southern Alps are quite spectacular. Within them, the generally 'U'- shaped valleys of northern Fiordland and their inland counterparts in NW Nelson, contrast with the generally broader valleys eroded into the rock on the eastern side of the Main Divide. This variation has been attributed to the greater erosional resistance of the Fiordland plutonics relative to that of the closely jointed greywacke and schist of the Southern Alps (Suggate, 1982). However, little is known of the influence of rock quality on the erosion processes, both glacial and fluvial, that controlled the landscape development.

A considerable volume of literature is available on the qualitative assessment of rock resistance to erosion (e.g., Yatsu, 1966), but few attempts have been made to evaluate the mechanisms of rock resistance, and how this influences the processes acting on the rock (Selby, 1987). Although many ice-flow problems have been solved, rock mass behaviour under stress, beneath and adjacent to glaciers, has received little attention, but the extent to which geological structure exerts a close control on glacial erosion has been recognized (Nilsen, 1973; Roberts, 1974; Seppala, 1975; Addison, 1981). Recently, Harbor *et al.* (1988) used glacier sliding laws and spatial variations in rock resistance to simulate the interaction between ice flow, erosion patterns and topography in the long term evolution of glacial valleys. The models are highly idealized, although they do indicate the potential importance of rock quality to the development of glacial landforms.

The *in situ* rock strength properties, in particular rock mass strength (RMS), have recently been assigned a greater role in the geomorphic resistance-process-form model (Selby, 1980, 1982). The rock strength characteristics of the eroded rock mass have been shown to be important controls on slope evolution, as well as controlling the erosional development of certain morphological features (Selby, 1980; Gordon, 1981; Cooks, 1983; Moon and Selby, 1983; Nicholas and Dixon, 1986; Moon, 1986; Augustinus, 1987; Beckdahl, 1987). However, the extent to which RMS influences glacial erosional forms, and indeed the development of the final valley form, is yet to be shown in other than

a qualitative sense (Addison, 1981). This study is an attempt to evaluate the influence of rock mass properties on glacial valley morphology in the New Zealand geologic setting, and for comparison purposes, some ice-free valleys in the Transantarctic Mountains.

## 1.2. Aims Of Study

The aims of this study are 5- fold:

(a) The morphometric description of the glacial valley cross-profiles and the quantification of the variations displayed by the morphological terrains that characterize the Southern Alps, and for comparison purposes, the McMurdo Dry Valleys, Antarctica.

(b) The characterization of the *in situ*, rock mass and intact strength of specimens, from the viewpoint of examining slope stability, and the examination and quantification of rock resistance to glacial erosion. This involves:

1. the field mapping of lithology, bedrock structure and bedrock form, and determination of rock mass strength;

2. the identification of the physical properties of the rocks which control the mineralogical and bulk rock resistance to abrasion, and the controls on bedrock resistance to plucking.

(c) The examination of structural controls on glacial valley form, from the viewpoint of both valley orientation and valley cross-profile shape, as well as the influence on slope stability.

(d) The examination of the influence of the regional stress-field generated by Alpine Fault-induced tectonics and locally induced stresses on the development of the glacial landscape.

(e) Development of a unified model for the development of the Southern Alps glacierized landscape that might be applicable to glacierized terrains developed in similar tectonic settings elsewhere.

### 1.3. Scope Of Proposed Study

The breadth of the topic enabled the elucidation of only the most basic questions given the various constraints on this research. A full investigation of this type would require: 1) the skills of a glaciologist for the complete modelling of the various glacial systems, examined only peripherally in this study; 2) access to the machinery of the mining engineer for the complete *in situ* rock investigation, i.e. diamond drill rig, *in situ* rock strength testing equipment, and a stress cell for *in situ* stress measurement; 3) the skills of a computer scientist for the development of models, both simple and complex, to test the necessarily tentative models developed, and the investigation of many complex interactions.

The Southern Alps has a complex geology and glacial history about which little is known. As a direct result of the scale of the Southern Alps, the investigation was necessarily restricted to the field examination of the most accessible 'representative' glacial valleys within each of the glacierized terrains. Two months were spent examining glacially and/or subaerially modified slopes in the McMurdo Dry Valleys, Antarctica, in the summer of 1984/85. February - April 1985 was spent examining glacial valley slopes in the Northern Fiordland region, followed by several weeks studying glaciated rock slopes in the South Westland region. The latter part of the 1985/86 summer field season was spent studying the glacierized landscape in south-central Fiordland and the glaciated rockslopes of the Mt Cook region. The 1986/87 summer field season was occupied with examination of the glaciated landscapes of the Mt Aspiring and Mt Cook regions. A total of nine months was spent in the field.

### 1.4. Literature Review

#### 1.4.1. Glacial Erosion and Rock Quality

Modelling of the development of glacial troughs usually involves only the physical properties of the glacier (Boulton, 1974; Hallett, 1981, Roberts and Rood, 1984), largely ignoring the influence of the properties of the eroded bedrock on the erosion process and resultant valley form. The contribution of rock resistance to the glacial



erosion process has been assessed only qualitatively (e.g. Sugden, 1978) and it remains a stumbling block to the realistic assessment of glacial erosion and the development of the erosional landforms.

In a study of cirque evolution, Olyphant (1981a,b) argued that cirque downcutting occurs at a slower pace than does the wall recession. This was partly explained by considering erosion during a non-glacial interval, when mechanical weathering of exposed rock walls can result in cirque widening and lengthening (Olyphant, 1983). Olyphant's (1981a) study agreed with Graf's (1976, p.86) conclusion that "despite varying degrees of glacial dissection and geological variations, cirques tend towards a common shape of about equal length and width." A similar tendency towards uniformity of morphology is displayed by glacial troughs, which display a characteristic parabolic trough cross-profile form (Graf, 1970; Wheeler, 1984). Using a similar argument to that used for cirque development, the rock quality i.e. joint density, should be an important control on glacial erosion and the development of glacial troughs. However, this factor has been only qualitatively evaluated (Addison, 1981; Rastas and Seppala, 1981).

Several variables influence the erodibility of the bedrock, such as intact bed rock hardness, permeability and bedding attitude (Sugden and John, 1976), but fracture density is assumed to be the most important factor determining local variations in susceptibility to glacial erosion (Olyphant, 1981b, 1983). Theoretical modelling by Boulton (1974) suggested that glacial quarrying (crushing and plucking) should also be most effective on densely fractured bedrock. Indeed Morland and Morris (1977) concluded that the typical "roche moutonnée" form of obstacles on the glacier bed, at all scales from small hummocks to valley steps, cannot develop unless the rock is already jointed.

However, Andrews (1972) argued that intramountain variations in cirque development reflect both the duration and intensity of glacial erosion, rather than bedrock properties. According to Andrews and Le Masurier (1972), a strong empirical relationship between bedrock jointing and estimated erosion coefficients, is interpreted as evidence that the degree of glacial dissection is a function of rock susceptibility to long term glacial erosion processes. Variations in the forms of glacial troughs have been explained as due to intensity of glacial erosion, irrespective of the geological conditions (Girard,

1976; Aniya and Welch, 1981a). However, altitude and insolation effects are probably of minor importance in the development and enlargement of glacial valleys (Graf, 1970) and the controls on the glacial erosion processes in the outlet glacier trough are probably the dominant elements in glacial valley development (Boulton, 1974; Sugden, 1978).

As part of a study of landform evolution using ice flow modelling, Oerlemans (1984) examined glacial valley development under ice sheets and showed that where the ice sheet base is frozen to its substrate, temperature patterns control valley deepening as they control basal sliding. McIntyre (1985a) used a similar basal sliding model to explain the development of overdeepened outlet glacier troughs draining the East Antarctic Ice Sheet. However, except in Polar regions, these thermal influences are absent for typical glacial valleys. Harbor *et al.* (1988) modelled the progressive enlargement of an idealized V-shaped channel to produce a curved channel cross-section beneath a glacier. Provision of a zone of weaker rock at the valley base allowed the glacier to excavate a deeper trough. However, the bedrock model used in this study is unrealistic. A prerequisite for the development of a realistic model is the input of strength properties of the rock mass that control the glacial erosion process, rather than some ideal rock strength index that might have little influence on the erodibility of the rock mass.

#### 1.4.2. Glacial Erosion Processes

It has been generally accepted that the dominant controls on the development of the glacial erosional landforms are the factors controlling the processes of plucking and abrasion at the ice/rock interface (Embleton and King, 1975). More recently, the erosive action of high pressure subglacial water has received recognition as an important component of glacial erosion (Drewry, 1986). Erosion by glacial meltwater is considered a relatively minor component of the glacial erosion process (Drewry, 1986) and will not be considered here. The processes of plucking and abrasion involve: (1) the detachment of fragments from the rock surface; (2) comminution into progressively smaller fragments; and (3) the abrasion of the bedrock surface as the glacier sole slides over the bed, and is armoured with rock fragments of varying degrees of hardness.

## (1) Abrasion

Subglacial abrasion involves the entrainment of rock debris at the glacier base, and its sliding and comminution against the bedrock. The controls on subglacial abrasion are the subject of some dispute (Boulton, 1974; Hallett, 1979; 1981). The models diverge in the prediction of abrasion rates along the central parts of glacial troughs. Whereas Boulton's model has the abrasion rates reducing to zero and lodgement taking place, the Hallett approach maintains abrasion and successfully explains fiord depth (Roberts and Rood, 1984). In cold-based glaciers, most abrasion will occur when the debris bands enclosed in shear bands in the ice come into contact with bedrock protuberances (Boulton, 1974). Quantitatively, this abrasion will be far less than that beneath sliding temperate ice. Andrews (1972, 1975) compared rates of erosion for Pleistocene cold glaciers in east Baffin Island with those for temperate valley glaciers in Colorado, based on estimated rates of cirque excavation. Although processes other than abrasion will have operated, the contrast is considerable: 50-200 mm/kyr against 650-1300mm/kyr for temperate valley glaciers.

Abrasion is only one of the processes acting at the glacier base, and for the purposes of this study will only be referred to in a qualitative sense. Although undoubtedly an important component of the erosion process, its full assessment was beyond the scope of this study. It has been reviewed extensively by Drewry (1986).

## (2) Subglacial Plucking

The subglacial plucking process largely exploits pre-existing joints in the rock mass. Several processes have been suggested whereby entirely joint bound blocks may be pulled from the bed and incorporated into the glacier (Röthlisberger and Iken, 1981), or where partially joint-bound blocks may be further fractured and then incorporated (Boulton, 1974). A number of fracturing mechanisms have been suggested: (1) Regelation of meltwater in the lee-side positions may lead to ice growth in the interstices (Carol, 1947). However, it is unlikely that this process can occur at a scale greater than a few centimetres (Embleton and King, 1975). (2) Glacial unloading may cause dilation joints to open in the bedrock (Lewis, 1954). (3) Internal stresses induced in the rock hummock by the ice flow may lead to

stress release fracturing in lee-side positions (Boulton, 1974; Boulton *et al.*, 1979). (4) Boulders in traction in the basal ice have been observed to produce fracturing on the lee-sides of bedrock hummocks where pressures, and thus bedrock strengths, have been reduced (Boulton, 1979). Stresses of up to 8 MPa have been measured for subglacial rock fragments passing over a pressure plate (Hagen *et al.*, 1983).

All these processes may act at the base of temperate valley glaciers to allow the breakup and subglacial exploitation of the fractured rock mass. The various mechanisms of exploitation and entrainment of the debris subglacially have been well summarized by Drewry (1986). Similarly, Drewry (1986) has reviewed and made some perceptive additions to current knowledge on subglacial rock crushing and fracture so that only a brief review is necessary.

#### 1.4.3. Rock Strength and Glacial Erosion

At the scale of the contact between basal clasts and the bedrock, stresses induced by the contact were shown to be important controls on subglacial bedrock fracture (Ficker *et al.*, 1980). At the scale of the whole glacier, the ice mass will stress the bedrock surface and important stress differences will be developed due to variations in pressure at the ice-rock interface. Morland and Boulton (1975) modelled a simple bedrock hummock assuming elastic bedrock behaviour. As a corollary, Boulton (1974) showed that there was little difficulty in providing adequate forces for rock failure to occur subglacially. Indeed, according to Boulton (1974, p.24): 'a plucking process alone may suffice if joint bounded blocks exist, but some plucking process must operate to produce fractured masses in the lee-sides of bedrock hummocks where they are otherwise unjointed'.

The origin of the jointing can be wholly non-glacial, resulting from previous tectonic events. There may also be dilation joints of non-glacial type caused by the unloading of the bedrock by denudation. A structural control on glacial erosion has long been recognized. Zumberge (1955) demonstrated a structural alignment of glacial scour, with the structure controlling the depth of erosion. Similarly, many authors (e.g. Nilsen, 1973; Roberts, 1974; Seppala, 1975), considered faults, joints and dykes to determine the alignment of fiords and glacial troughs.

The relaxation of overburden and ice confining stresses was regarded by a number of authors to generate rock fracture immediately preceding or during glaciation, and hence to facilitate subglacial quarrying, often enhanced by freeze/thaw processes (Jahns, 1943; Lewis, 1954; Battey, 1960). Harland (1957) qualified this oversimplified picture of stress-release joint development irrespective of bedrock anisotropy, arguing that for stresses induced by variations in ice thickness to be effective, they would act by combining with the pre-existing rock stresses. The evaluation of rock stress input to the erosion process will be considered in Chapter 7.

Sheet jointing alone is not sufficient for joint block removal, there must also be near orthogonal intersecting joint sets that are more likely to be non-glacial in origin (Biro, 1968). The forms and characteristics of the ice scoured topography relate closely to bedrock structure, in particular bedding planes and foliations (Gordon, 1981; Rastas and Seppala, 1981).

#### 1.4.4. Influence of Rock Stress On Glacial Erosion

Ice sheets attain thicknesses of up to 5 km, and the normal stress at the glacier bed may reach 45 MPa and generate failure of the subglacial bedrock (Drewry, 1986). The strength properties of the eroded bedrock will have an important control on the geometry and magnitude of the glacially imposed stresses and thus on the mode of failure of the subglacial bedrock. Where rock fragments are entrained at the glacier sole, the stresses they transmit to the bedrock may be greatly magnified by point contacts as the clasts impinge on the bedrock (Hagen *et al.*, 1980). Such features as chattermarks are indicative of very high subglacial stresses and crushing-compressive failure of the bedrock. The repeated passage of subglacial clasts over a region of bedrock may give rise to loading cycles that will significantly reduce rock intact strength.

Stress concentrations at subglacial hummocks may allow tensile and shear failure of the bedrock (Boulton, 1974), as well as creating the potential for compressive failure at these sites. A low-pressure zone may exist on the lee-side position of subglacial hummocks in which tensile failure and fracture can occur (Boulton, 1974). Structural anisotropy, as produced by bedding and joint planes, may significantly weaken the subglacial bedrock and reduce the magnitude of the stresses

required for failure of the intact rock (Addison, 1981). Such a phenomenon is well known from engineering studies of rock behaviour under stress (i.e., Stacey, 1973).

Several factors require examination for an understanding of the part played by the glacier and entrained rock material in the crushing of bedrock. These include: (1) The nature of the applied stresses. This factor is reviewed and discussed in Chapter 7. (2) The physical characteristics of the rock mass, i.e., intact rock strength and the presence of pre-existing weaknesses such as joints and foliation, and their influence on rock strength and erosion resistance (reviewed in Chapters 4 and 5). (3) The influence of subglacial water is known to markedly reduce rock mass strength. (4) Methods of evacuation of the failed subglacial rock material. This latter factor has been reviewed in detail by Drewry (1986).

#### 1.5. Summary

At the scale of bedrock asperities and hummocks, the importance of the strength properties and stress within the subglacial bedrock have been recognized (Boulton, 1974; Drewry, 1986). Both Boulton *et al.* (1979) and Boulton and Jones (1979) argued that at the scale of the ice sheet, the permeability and porosity of the bedrock control subglacial drainage, and thus the mode of subglacial erosion. At the scale of the valley glacier, the physical properties of the glacier are commonly assumed to control the mode of erosion and development of the glacial trough form (Boulton, 1974; Roberts and Rood, 1984; Habor *et al.*, 1988). However, no quantitative research has been undertaken into the influence of the strength properties of the rock mass and the *in situ* stress field, on the development of the glacial trough size and shape.

## **Chapter Two**

### **Geographic Areas of**

### **Investigation: Physiography, Geomorphic**

### **Processes and Geological Setting**

## CHAPTER TWO: GEOGRAPHIC AREAS OF INVESTIGATION: PHYSIOGRAPHY, GEOMORPHIC PROCESSES AND GEOLOGICAL SETTING

### 2.1. Choice Of Study Sites

The aims, as set out in section 1.2, involve assessment of the influence of variations in lithology, geotechnical properties and geotectonic setting on the development and morphology of glaciated valleys. Consequently, the first step was to select study sites in the heavily glacierized portions of the Southern Alps.

To enable the study of the geotechnical and lithological variations within the basement rocks and their control on glacial valley form, it was necessary to examine glacierized troughs developed in a variety of rock types. Essentially unmodified and/or, minimally subaerially modified troughs were studied so that rock conditions were as close as possible to those that existed during glaciation.

The broad variations in valley morphology apparent across the Southern Alps, can be incorporated in 5 study regions (Fig. 2.1a): (1) wide, flat floored valleys developed within the greywackes of the Mt. Cook region ( $170^{\circ} 15'E-43^{\circ} 35'S$ ) and (2) chlorite grades II and III schists of the Mt Aspiring region ( $168^{\circ} 40'E-44^{\circ} 35'S$ ). These contrast markedly with the relatively deep and narrow troughs cut into (3) the plutonic basement of Northern Fiordland ( $168^{\circ} 05'E-44^{\circ} 40'S$ ), and (4) the chlorite-grades III,IV and garnet-oligoclase schists of South Westland ( $170^{\circ} 10'E-43^{\circ} 27'S$ ). Within Fiordland, a marked disparity is apparent between the overdeepened troughs of the Darran Mountains, and the relatively overwidened forms of (5) south-central Fiordland ( $167^{\circ} 05'E-45^{\circ} 35'S$ ). The general geology of the southern part of the Southern Alps and Fiordland is shown in Fig. 2.1b.

In addition to the investigation of sites in New Zealand, one summer season was spent investigating sites in the McMurdo Dry Valleys, Antarctica. Gunn and Warren (1962, p.60) noted that the Antarctic Dry Valleys "contrast with the much deeper and steeper glacial troughs of New Zealand". However, unlike the Southern Alps, the slopes had been subjected to considerable subaerial modification and are not directly comparable with those developed in the Southern Alps. Fieldwork in the Dry Valleys was undertaken to examine the



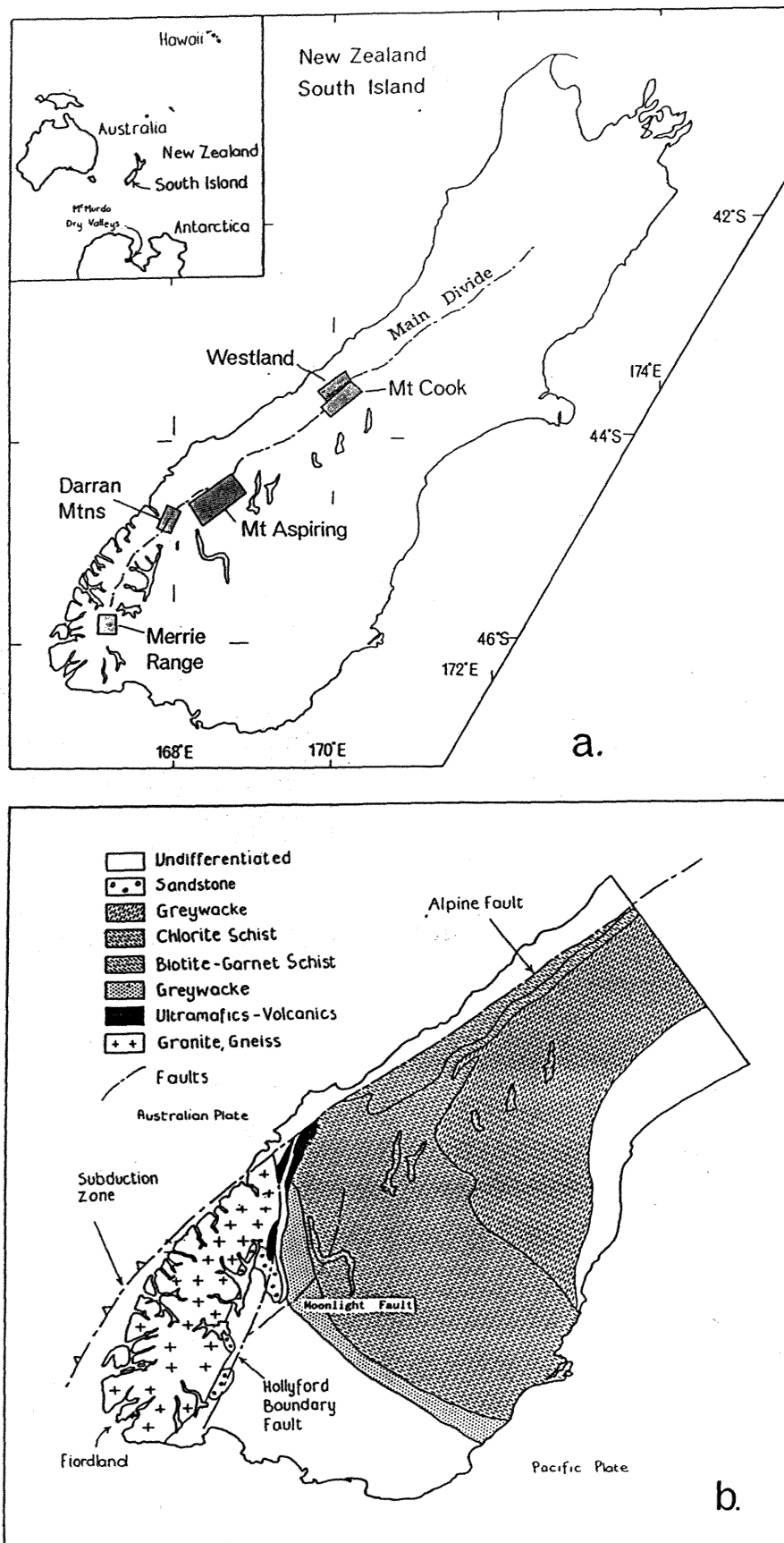


Figure 2.1. (a) Location of study areas, South Island New Zealand. (b) Generalized map of the geology and main tectonic elements in the southern half of the South Island. After Suggate (1978).

influence of variations in rock strength on the mode of subaerial and glacial landform development in a polar environment.

## 2.2. Site Location and Physiography

This section presents a brief description and review of each study region, including the physiography and currently active geomorphic processes.

### 2.2.1. Fiordland Region

For the purposes of this study, Fiordland has been subdivided into two broad subregions on the basis of their contrasting morphological features. The northern terrain, the Darran Mountains, is a region of overdeepened valleys separated by broad, gently sloping interfluves. The glacial valleys in Northern Fiordland contrast with the generally broad, shallow troughs with narrow interfluves developed in south-central Fiordland (Fig. 2.2a,b).

The Darran Mountains is a region of deep 'U' shaped valleys that have been spectacularly oversteepened by ice, and extensive, sometimes permanent snowfields remain perched above them. On the low angle valley shoulders defining the interfluves, thick winter snow packs accumulate. As a consequence, avalanche activity is high, both in winter and summer, and combined with the steep runout zones, is a strong modifying influence on the landscape. Avalanches are initiated on the broad, gently sloping valley shoulders and have frequently developed avalanche-impact tarns (Fitzharris and Owens, 1984).

Mixed snow avalanche/rockfalls are frequently a hazard on the Milford Road-Milford Track region, forcing the closure of the road for several days during most winters. Fitzharris and Owens (1980) identified avalanche tracks and made a hazard assessment of the Milford Road. Rockfalls are seemingly initiated on the valley shoulders, while the trough walls themselves are stable and frequently display the impact polish of the winter avalanches, especially near the major avalanche tracks. A further consequence of freeze/thaw processes on the shoulder rock, are the debris cones and aprons mantling the valley sides (Fig. 2.2c). Examination of the trough walls indicates a high degree of slope stability. This suggests that the

a.



b.





C.

Figure 2.2. (a) Typical view of glacial trough morphology, Cleddau Valley, northern Fiordland. Note the narrow, steep-sided nature of the troughs.  
 (b) A typical glacial valley, Hauroko Burn, in south-central Fiordland.  
 (c) Trough wall and talus slope, Gertrude Valley northern Fiordland. Note low-angle valley shoulder and slab glacier.



trough walls are not the source of the talus aprons, but rather the valley shoulders, from where weathered, frost-shattered rock probably participates in mixed snow/rock avalanches.

Talus or debris slopes are common features, providing the concave basal slope segments (Fig. 2.2c). High frequency, low magnitude rockfalls (apparently  $<10 \text{ m}^3$ ) are the most important debris input to the talus slopes. As with the Coast Range in British Columbia, the major rockfall trigger mechanisms are probably freeze-thaw activity, snowmelt and rainstorms, with some input of earthquake shaking (Ryder, 1981). There is therefore likely to be a marked seasonal and daily variation in rockfall patterns with maximum activity in spring, such as has been found in the Albertan Rocky Mountains (Luckman, 1976, 1981; Gardner, 1980).

Large magnitude/low frequency mass movements (rock slides, deep-seated cliff failure) are not common. There is little evidence for the inducement of large scale slope modification in northern Fiordland, unlike the situation in the Rockies (Gardner, 1980; Mollard, 1977), Iceland (Whalley *et al.*, 1983) and western Norway (Bjerrum and Jorstad, 1968). In Norway, large rock slides were probably triggered by deglaciation, as a result of changed stress/strain relationships following glacier recession (Bovis, 1982). The scarcity of large slope failures in northern Fiordland reflects the massive, relatively structureless nature of the plutonic and high grade metamorphic rocks.

Earthquakes are an important geomorphic agent in northern Fiordland. Earthquakes are indicative of high stresses within the crust, and because of the high strength of the Fiordland rocks, stress relief sometimes occurs by catastrophic brittle failure of the plutonic rocks. Micro-seismic studies (Scholz *et al.*, 1973) indicate a high level of low magnitude crustal seismicity in Fiordland, but large events of M7 or greater have been recorded (Davey and Smith, 1983). Due to the low population density and consequent lack of observers, few observations of earthquake-induced rockfall are available. Pearce and Watson (1986) found that earthquake-induced landsliding is the principal sediment supply mechanism in the granite bedrock terrain of NW Nelson, and a similar relationship may prevail in northern Fiordland.

In 1814-1820, Capt. Edwardson of the cutter 'Snapper', reported topographic changes at Doubtful Sound between a visit in 1814 and his return in 1820, and attributed it to seismic 'convulsion'. These changes included the disappearance of a river 2 miles long, of the lake that fed it, and of a lagoon (Eiby, 1968). From 1826-27 there was a regular succession of earthquakes, and associated uplift located 80 km to the north of Dusky Sound. Large landslides occurred along the whole intervening coast and in places trees were seen underwater (Eiby, 1968).

According to Benson *et al.* (1934), the most striking feature of the Fiordland topography is the general accord of summit levels (Fig. 2.3). Benson *et al.* (1934) argued that the planation of the surface was completed by the late Tertiary. Recently, Ward (1988a) defined a summit surface across the Fiordland block and argued that this surface must be a peneplain due to the variable erodibility of the rock it cuts across. Ward assigned a 2 Myr age to the surface, based on cross-cutting relationships with unfaulted Pliocene deposits. Fiordland seems to have been tilted and uplifted as a coherent block following the development of the erosion surface.

During the present century, there have been marked reductions in extent of the glaciers. No glacier mass balance studies have been carried out, although Chinn and Whitehouse (1978) estimated the present glaciation limit from an assessment of the current end of summer snowline elevation. The snowline and its complexity were found to increase to the north, correlating with higher precipitation and the location of topographic highs and depressions (Fig. 2.4).

The relatively fresh, unweathered nature of the plutonic and high grade metamorphic rocks in the region, and the lack of vegetation in the alpine zone, provide numerous good exposures for study. Access to the Darran Mountains is provided by the Te Anau-Milford road (Fig. 2.5), with the road itself following the Upper Hollyford Valley. Due to the rugged nature of the terrain and the attendant difficulty of access, only a restricted study and sampling programme was feasible. The general location of the field sites is indicated in Fig. 2.6).



Figure 2.3. Apparent summit accordance (planation surface ?) across south-central Fiordland. View west from Merrie Range.

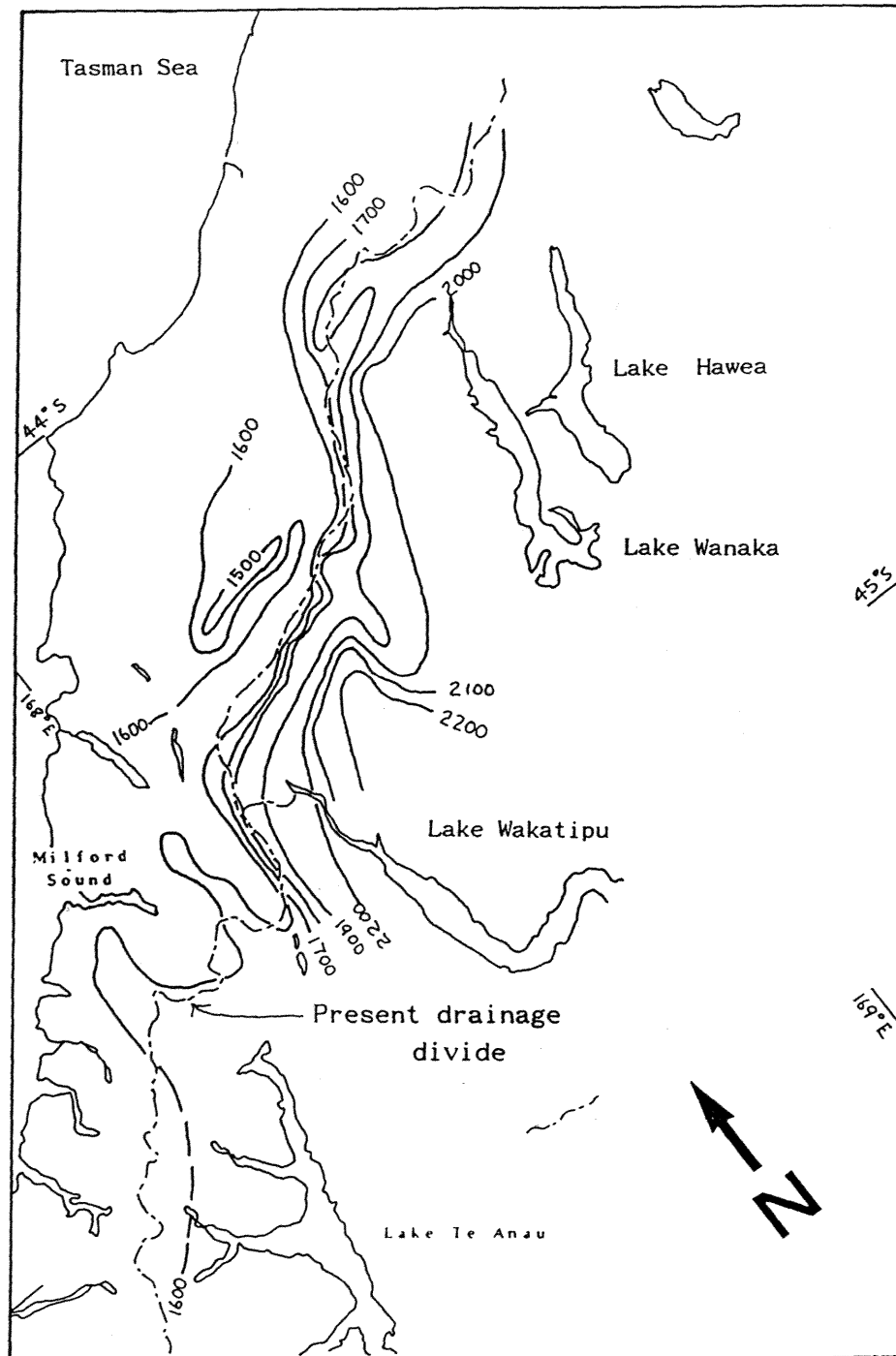


Figure 2.4. 1978 glacier snow-line elevation contours for the southern section of the glaciated Southern Alps. After Chinn and Whitehouse (1978). Contours in metres.



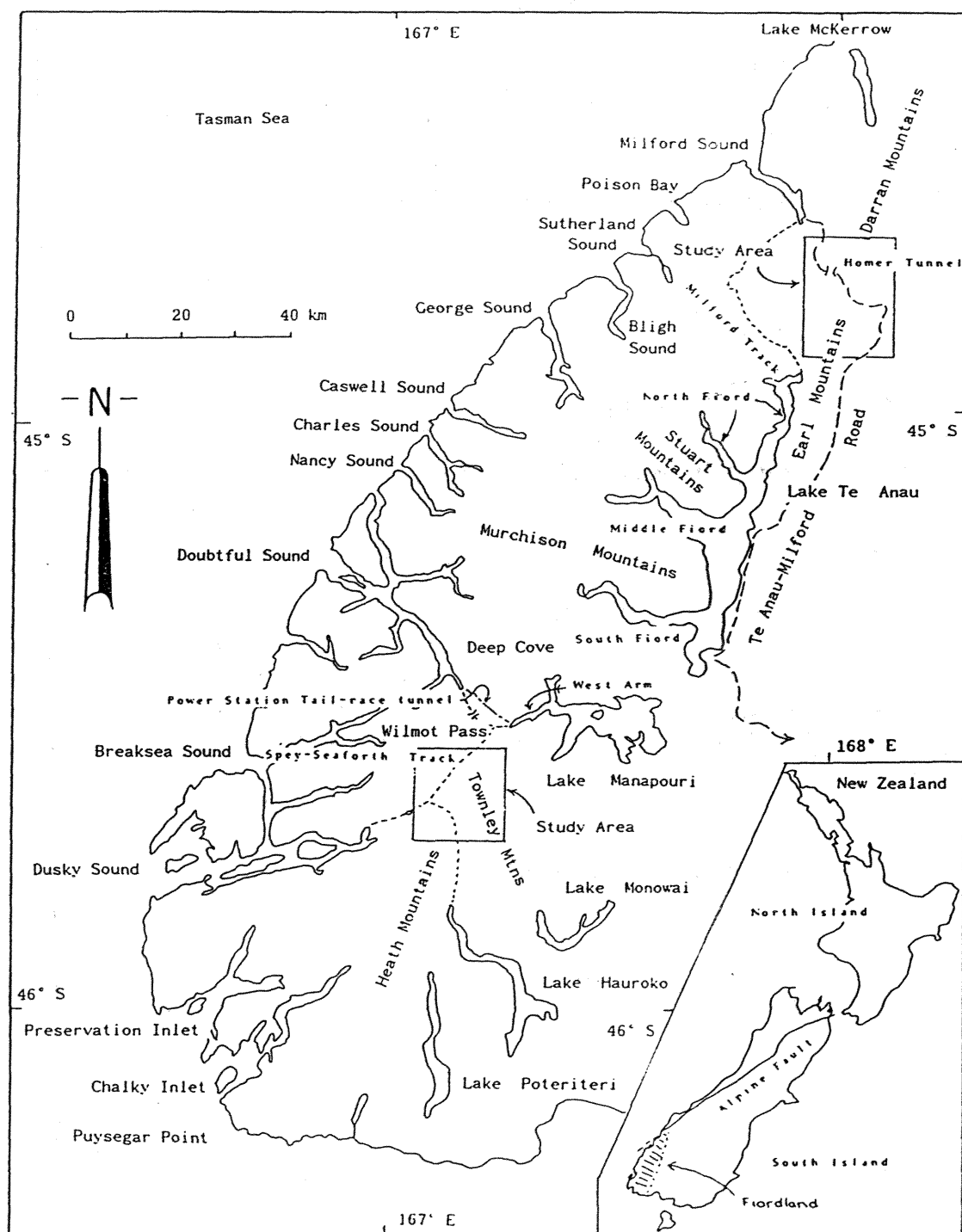


Figure 2.5. Fiordland localities mentioned in text.

## Geomorphological Mapping Symbols



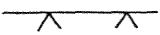
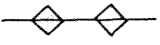
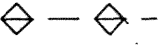

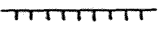
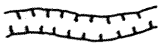
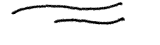
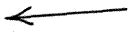


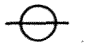


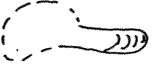


	Peak
	pass
	angular convex break of slope
	sharp ridge crest
	rounded ridge crest
	cliffs (bedrock >40°)
	sharp break of slope (fault, slide scar)
	gorge
	ridge-rent/tension crack
	foliation/bedding dip direction
	ground moraine & moraine ridge
	glacial outwash
	roches moutonnées (flow direction)
	cirque
	depositional terrace
	glacier
	rock-fall/rock slide & scar
	talus cone/debris slide
•2	site number

Table 2.1.

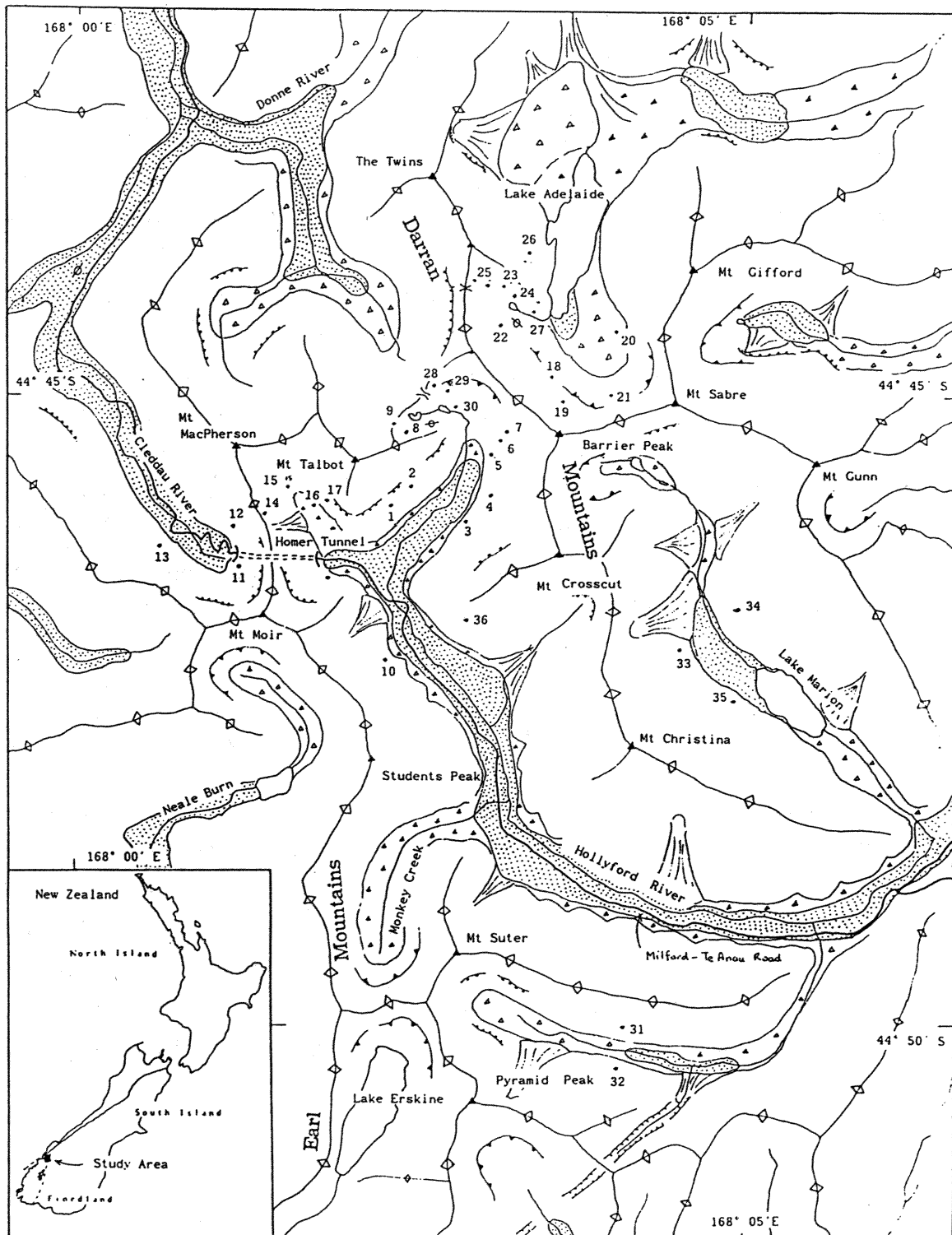


Figure 2.6. Simplified geomorphic map of northern Fiordland, showing location of study sites. Mapping symbols as given in Table 2.1.

### 2.2.2. South-Central Fiordland Region

This is a region of rugged mountains and deep, heavily glacierized valleys. The forest cover mantling the slopes is frequently heavy, restricting movement in the field to alpine ridges and the occasional deer and Fiordland National Park trails. The alpine zone commences at about 1500 m and the rolling 'knock and lochan' nature of the topography gives easy access to the 'tops' once the heavily vegetated lower slopes have been negotiated. Access to the region was by boat from two points: (1) to West Arm, Lake Manapouri and the Spey-Seaforth Track to Dusky Sound ; and (2) from the south by boat up Lake Hauroko for access to the Merrie and Heath Ranges (Fig. 2.7). Due to problems with the weather, the presence of squadrons of sandflies, difficulty of access and time constraints, only a restricted appraisal of the landscape and regional rock properties was feasible. Site locations are displayed in Fig. 2.7.

### 2.2.3. Mt. Aspiring Region

The Mt. Aspiring region is dominated by steep, jagged peaks, changing to broad troughs below the level of the glaciers. However, considerable variation in morphology is apparent, closely allied to the structural variations in the schist. Large, glacially over-deepened lakes were formed where the constrained valley glaciers debouched their ice onto the Otago lowland. Large ice-fields persist in the region i.e., the Bonar/Volta Glaciers and Olivine Ice Plateau (Fig. 2.8).

Besides the omnipresent glacial influence exemplified by the 'U' shaped trough profiles (Fig. 2.9a), considerable slope activity, both past and present, was observed. Summerville *et al.* (1983) described large scale collapse of the trough wall at the snout of the Dart glacier following glacier retreat from the 1850 moraines, and the thick supra-glacial debris cover points to the pervasiveness of slope-failure and rockfall. Bishop and Hislop (1983) described large, destructive rock slides at the head of the Waiatoto River and Gloomy Gorge, and Bell (1976, 1982) described destabilization and collapse of schist slopes in Central Otago postglacially and pointed to the controlling influence of structure/foliation on these processes (Fig. 2.9b). Whitehouse (1987), examined the relative contribution and importance of the various alpine slope processes.

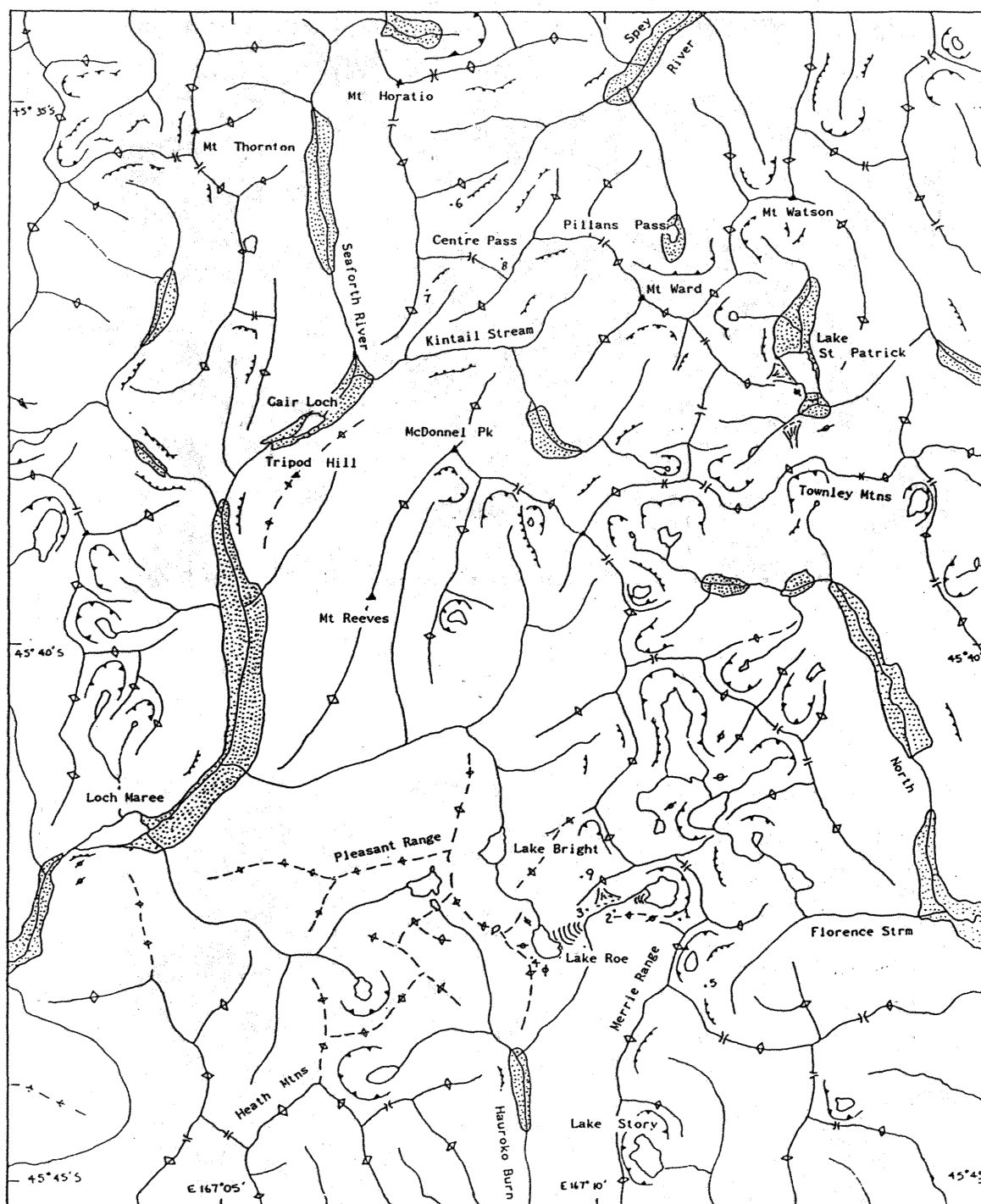


Figure 2.7. Simplified geomorphic map of part of south-central Fiordland, incorporating locations of study sites. Mapping symbols as given in Table 2.1.

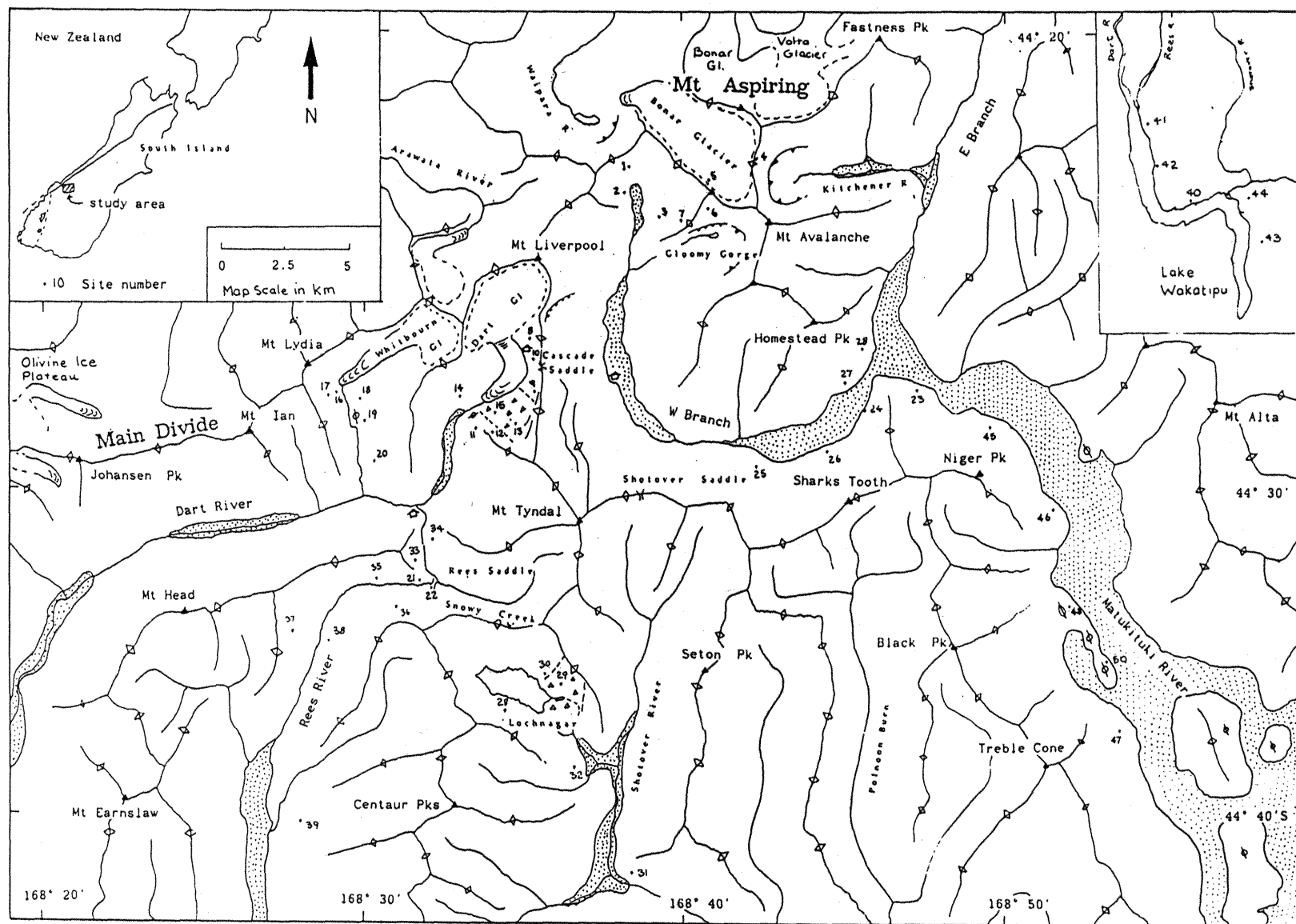


Figure 2.8. Location of study sites in Mt Aspiring region. Inset top right indicates location of profile outside the map area.



a.



b.

Figure 2.9. (a) Snowy Creek valley, a typical glacial trough developed in the schist of the Mt Aspiring region.  
 (b) Slide plane and debris chute on foliation-parallel schist slope, west branch, Matukituki Valley.







A summit-level envelope (section 3.2) was developed for the Mt Aspiring-South Westland region (Fig. 2.10) indicating the presence of a broadly domed erosion surface and topographic low over the Haast Pass area. The summit accordance must be attributed to limited erosion of an uplifted erosion surface, because there is no relationship between summit height and erodibility of the constituent rocks (Craw, 1985). A significant reduction in height of the surface eastwards coincides with the position of the Moonlight Fault, suggesting differential Quaternary uplift west of the Fault (Craw, 1985).

Earthquakes have been recognized as being a landscape modifier in the Aspiring block. Bishop and Hislop (1983) described large rockslides in the Upper Waipara and Gloomy gorge initiated by earthquakes, while J.Adams (1981), in an evaluation of earthquake dammed lakes in New Zealand, assigned Lochnagar to an earthquake initiated rockfall. Micro-earthquake surveys by Scholz *et al.* (1973) and Reyners *et al.* (1983) showed that earthquake activity is at a relatively low level, with a low frequency of high magnitude earthquakes. However, the overall high level of seismic risk (Hancox *et al.*, 1985) indicates the probable contribution of earthquakes to landsliding/landform modification.

Access to the study sites was via three points: (1) by road from Wanaka along the Matukituki Valley to Raspberry Flat; and from the west, access was by road from Glenorchy to (2) the Dart and (3) the Rees valleys. Profile locations are shown in Fig. 2.8.

#### 2.2.4. South Westland Region

The Main Divide at the Franz-Josef to Fox glacier region of South Westland forms a string of rugged peaks oriented NE-SW, parallel to the strike of the Alpine Fault (Fig. 2.11a,b). Secondary ranges of some 15 km in length strike NW perpendicular to the Main Divide. All of the rivers and larger streams of the region are glacier- and snow-fed. Rainfall is high: 5,000-12,000mm/yr, as are the uplift and denudation rates ~4-11mm/yr (H.Wellman, 1979; Whitehouse, 1987). Rivers are therefore large and fast-flowing, prone to frequent flooding and consequently have an unusually large erosion potential.

The high prevailing precipitation on the western side of the Main Divide that supplies the névés of the Franz Josef and Fox glaciers, is fed by the dominantly westerly airflow from the Tasman Sea.

The rugged topography and high orographic precipitation is given expression by the Franz Josef and Fox glaciers, each of which descend well below the snowline and are actively eroding and depositing debris in their overdeepened and oversteepened troughs. The late Pleistocene/Holocene glacial history of many of the glaciated Westland valleys has been documented in Wardle (1973), and for the Franz Josef Glacier by Sara (1968).

Roches moutonnées persist at Sentinel Rock car park and fault bound rock bars stretch across the Waiho Valley 200m down-glacier from the active snout (Fig. 2.11b). The rock bars were only exposed in 1965 with the retreat of the ice (Sara, 1968). Speight (1935) examined the Sentinel Rock forms, and proposed that they were fault-bounded uplift blocks, and glacially moulded with preferential removal of the brecciated debris.

The South Westland valleys, particularly near to the active glacier snouts, are relatively narrow and deep with broad intervening interfluves. A progressive widening of the troughs and reduction of the trough wall slope is evident with distance from the snout. Steeply dissected rectilinear slopes with thin debris cover dominate the landscape. Remnant landscapes are restricted mainly to the U-shaped valley heads, with high fluvial erosion rates resulting in the development of usually sharply V-shaped profiles (Griffith and McSaveney, 1983; Whitehouse, 1987)(Fig. 2.12a,b).

Rockfalls and snow avalanching are important processes locally, especially in the alpine zones. On slopes developed parallel to the foliation, large deep-seated rock slope failures form planar slopes with hummocky surfaces. Destabilization of the trough walls following the retreat of the glaciers is seen in the Franz Josef and Fox valleys. Failure of the slope rock by slab and wedge failure is common, particularly on the foliation and dominant joint sets (Fig. 2.12b). Gage (1966) described stress-relief slabbing of schist slopes near the Franz Josef glacier snout. This failure propagated rapidly after deglaciation (Fig. 2.12c). There is often little evidence remaining of the glacial origin of the valleys, with post-glacial

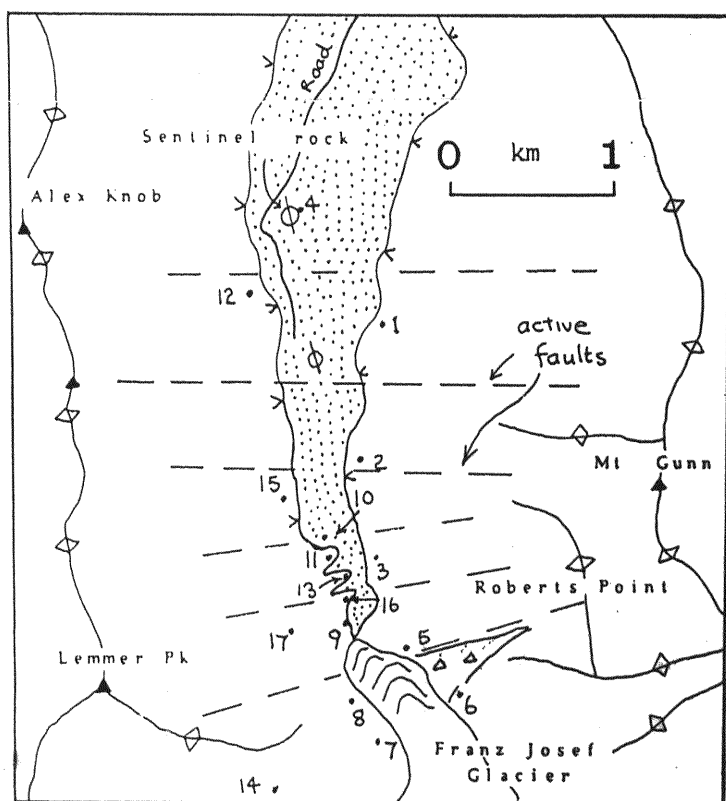
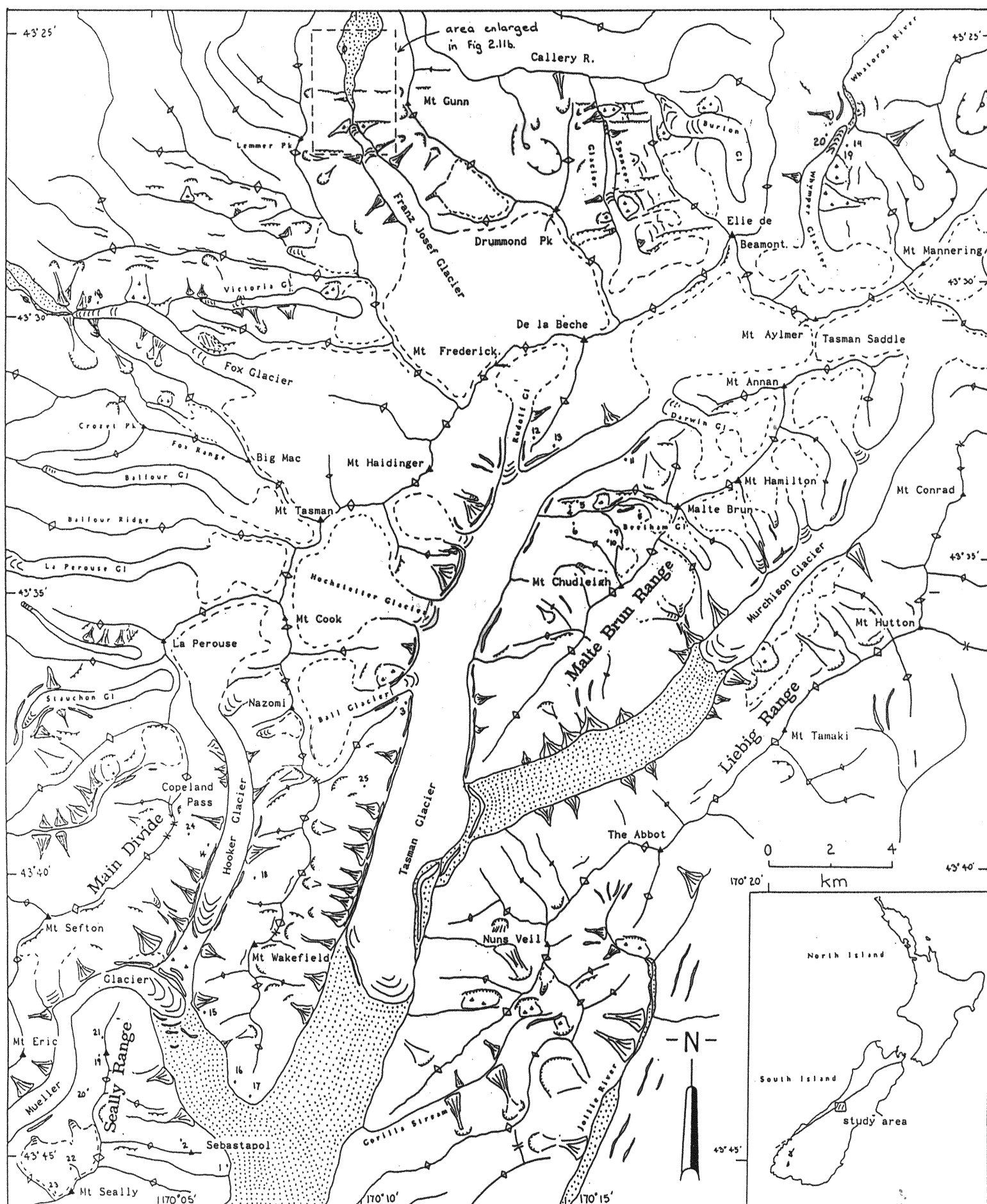


Figure 2.11. (a) Simplified geomorphic map of Mt. Cook and South Westland regions, incorporating location of study sites. Mapping symbols as given in Table 2.1.  
(b) Enlargement of Franz Josef Glacier area, showing profile locations. Glacier at 1978 position.



a.



b.





C.

Figure 2.12. (a) Rock bars (riegels) in front of the Franz Josef Glacier, Waiho Valley, South Westland.  
 (b) Foliation controlled slab failure and planar slide developed on schist slope, Whymper Glacier, South Westland. Note steep, stable slopes on the opposing valley wall.  
 (c) Stress-relief induced slab failure in schist, Franz Josef Glacier. Note the development of sheet jointing perpendicular to the foliation.

modification and high fluvial erosion rates resulting in rapid slope destabilization and mass movement (J.Adams, 1985; Whitehouse, 1987).

The West Coast is a seismically active region (Scholz *et al.*, 1973, Norris and Cooper, 1986). Although recent major earthquakes have not been centred on the Alpine Fault, they have been associated with nearby fractures and have been responsible for some impressive effects on the landforms of the region, such as the fault-boundedriegels in front of the Franz Josef Glacier (Fig. 2.12a,b).

Profile locations are shown in Fig. 2.11a,b. These valleys have mainly NW-SE and E-W valley trends. Examination of structural controls on slope form was of interest, so a valley system oriented N-S, the Whymper Valley, was also studied. Several other glaciers in the region were visited on a reconnaissance survey, but problems of access, and time constraints precluded their full examination.

#### 2.2.5. Mt. Cook Region

The Mt. Cook region is steep, mountainous and heavily glaciated, and is but a small section of the Torlesse terrain that dominates the eastern side of the Main Divide (Fig. 2.1a,b). The Torlesse rocks comprise massive to finely laminated greywacke and argillite with a complex structural history (Spörli, 1979; Findlay and Spörli, 1984). 24 profile sites were selected along the Hooker, Mueller and Tasman glaciers, as well as on tributary valleys and intervening ridges (Fig. 2.11a).

Intense glacierization of the Mt. Cook region has given rise to a landscape dominated by broad, relatively overwidened valleys and massive triangular interfluves (Fig. 2.13a,b). A strong structural control is evident from the development of the major valleys parallel to the bedding in the Torlesse rocks. The uplift rate ranges from 5-20 mm/yr and is broadly balanced by erosion (J.Adams, 1980).

The amount of precipitation ranges from approximately 800 mm/yr in the drier parts of the eastern mountains, to >5000mm/yr near to the crest of the Main Divide. Rock structures closely affect erosion processes and rates, with highly stressed, deformed and fractured rocks and intensely fractured argillite bands being much more susceptible to weathering and failure than the less deformed greywackes (Blair, 1972; Whitehouse, 1983). Major landslides > 1 Mm<sup>3</sup>



a.



b.





C.

Figure 2.13. (a) Mueller Glacier, Mt Cook National Park. Note wide valley, debris cones and thick supra-glacial debris cover.

(b) Unstable slope and debris cone above lateral moraine of the Tasman Glacier. This is typical of the rapid erosion undergone by the Torlesse greywacke and argillite close to the Main Divide.

(c) Anti-slope scarp/tension joint developed on greywacke slope above Ball Glacier.



commonly occur and many are associated with major faults and may have been triggered by earthquakes (Whitehouse, 1983, 1987). Earthquake activity is at a high level, although the events are mainly of low magnitude (Reyners *et al.*, 1983).

Glacially eroded 'U'-shaped bedrock troughs, horns, arêtes and cirques dominate the landscape. High winter snow avalanche activity is a characteristic of this region (Fitzharris *et al.*, 1983) and the frequent association of the latter with rockfall from the glacially oversteepened slopes is evident from the thick supraglacial debris cover. Rockfall and snow avalanche taluses form rectilinear slopes below ~1500m. High rockfall activity and the production of debris cones (Whitehouse, 1983) attest to the rapidity of wall destabilization (Fig. 2.13c). Anti-slope scarps frequently develop on the ridge crests parallel to the Main Divide (Whitehouse, 1987). The scarps may result from the movement of landslides, fault movement, loss of slope support following deglaciation or gravitational adjustments to the tensional input to the mountain landscape (Beck, 1968)(Fig. 2.13d). Recently, Prebble (1987) described the development of anti-slope scarps by rock mass bulging. Reduction of slope angles and coalescence of debris cones, create a general reduction of the landscape relief with distance from the glacier snout.

Close to the Main Divide, the 'typical' glacial valley slope developed in Torlesse rock displays: 1) a short convex summit characterized by active freeze/thaw processes; 2) a bevelled, veneered rock surface sometimes with buttresses and rock pinnacles projecting through the scree veneer; 3) a free-face or zone of steep rock ribs, often terminating in small free-faces separated by scree-filled schutes and funnels; and 4) a talus slope built beneath chute openings and sometimes coalescing talus fans (Fig. 2.13b).

#### 2.2.6. McMurdo Dry Valleys

As part of the field study of selected glacierized terrains, part of the 1984/85 summer field season was spent examining aspects of the glacierized/subaerially modified landscape of the McMurdo Dry Valleys, Antarctica (Fig. 2.14). Initially it was hoped to be able to undertake a comparative study of the relatively overwidened troughs developed by the cold/wet based glaciers in Antarctica, and the relatively overdeepened valleys eroded by wet-based glaciers in the New Zealand Southern Alps.

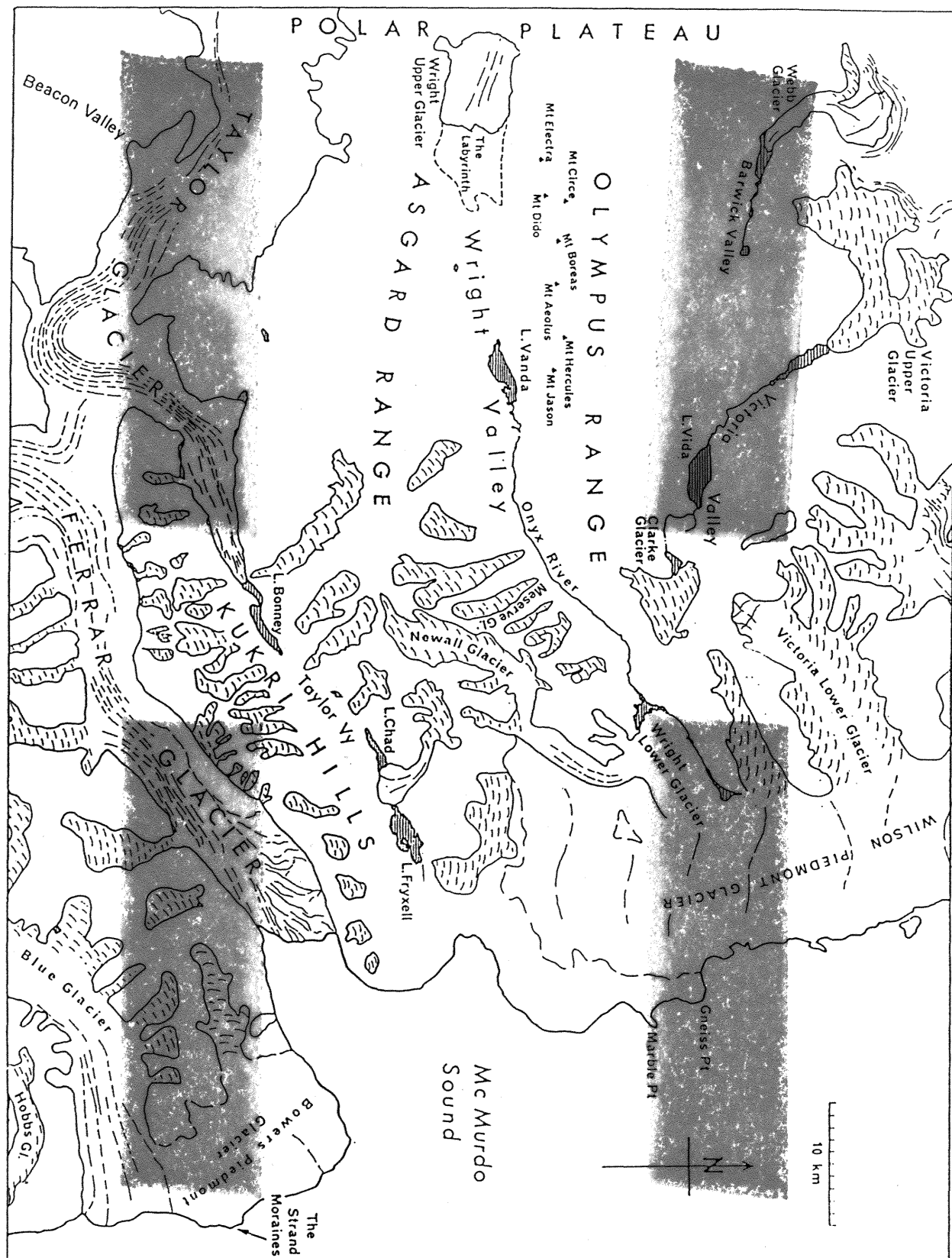


Figure 2.14. General location map, McMurdo Dry Valleys, Antarctica.



a.



b.

Figure 2.15. (a) Cirque headed valley in western-most Olympus Range above upper Wright Glacier, with partial development of a through valley.  
(b) Typical overwidened glacial trough, lower Taylor Valley, Antarctica.

The Dry Valleys are a predominantly ice-free region of intensely glacierized terrain. The landscape developed under a temperate glacial regime in the late Miocene (Denton *et al.*, 1984). Since the Pliocene, the valleys have been essentially ice-free, with occasional inundation by Ross Sea ice. Considerable subaerial modification of the slopes has occurred. Selby (1971, 1974) described many of the features and attributed them to salt weathering and progressive development of Richter denudation slopes.

In cross-section, three divisions of the Dry Valley area are apparent: (1) the deep valleys themselves; (2) glacial shoulders or benches, and structurally defined terraces; and (3) the network of cirques and cirque-headed alpine valleys that cut into the neighbouring ranges (Fig. 2.15a). The valleys exhibit broad 'U' shapes that are probably related in part to the resistance of the dolerite sills to vertical abrasion (Gunn and Warren, 1962). The valley floors, consistently 700-1200 m below the adjacent peaks, increase in width from about 1.5 km at their upper ends to about 4 km where they join, or terminate, e.g. Taylor Valley (Fig. 2.15b).

The cirque basins are believed to have been cut by local warm-based ice, in contrast to the cold ice that now occupies them and is not at present enlarging the basins (Selby and Wilson, 1971). Less than 15% of the cirques are occupied by ice masses, and in a few instances the divides between adjacent cirques have been eroded to form wind gaps. The ice-free cirques show marked differences in elevation, shape and degree of development, largely related to the stage of cirque development, rather than differences in lithology or orientation (Aniya and Welch, 1981a). Similarly, Aniya and Welch (1981b) argued that there is no evidence for a relationship between valley cross-profile form and lithology.

## 2.3. Regional Geology and Tectonics of the Southern Part of The Southern Alps

### 2.3.1. Introduction

The Southern Alps is a tectonically active region. The Alpine Fault is the major structural element of the region and is the controlling factor in the development of the tectonic regime (Fig.

2.1b). The Alpine Fault forms part of the Indian-Pacific plate boundary and passes through the South Island (Walcott, 1978). For most of the past 25 Myr it has behaved as a continental transform fault, resulting in 460 km of dextral offset of the formerly adjacent crystalline terrains of Fiordland and NW Nelson (Kamp and Fitzgerald, 1987). However, in the past 10-15 Myr the relative motion of the plate has been oblique in the vicinity of the South Island. A compressive component has gradually developed across the fault, and rapid uplift along the eastern side of the fault has formed the Southern Alps (Scholz *et al.* 1973; Walcott, 1978).

The present relative plate motion across the plate boundary in the Southern Alps is ~40 mm/yr, but only ~1/4 of this is on the Alpine Fault (Walcott, 1978, 1979). A large component of plate motion is thought to be taken up by the ductile deformation of the rocks east of the Alpine Fault (J.Adams, 1979). Koons (1987), studied the thermal and mechanical consequences of rapid uplift in the Southern Alps, and found that in addition to high crustal temperatures and associated high heat flow, rapid uplift produces a weakening of the crust by raising the depth of transition from brittle to ductile behaviour.

Compression across the plate boundary has caused Fiordland to be thrust over the oceanic crust of the Australian Plate. Subduction of the Australian Plate is actively occurring beneath Fiordland, with associated thrust and strike-slip tectonic regimes (Scholz *et al.*, 1973; Davey and Smith, 1983). The resulting uplift has been essentially epeirogenic, at least during the Pleistocene (Ward, 1988a). Further north, a predominance of strike-slip faulting on the eastern side of the Alps is associated with the Mt. Aspiring region (Fig. 2.16) and underthrusting of the Australian Plate. According to Allis (1981, 1986), both the inferred thermal regime and the variation in crustal thickness beneath the Southern Alps, suggest that the mode of crustal shortening changes considerably along the length of the Alpine Fault. In the central Alps, the crustal shortening is being accommodated predominantly by uplift and erosion of the continental crust of the Pacific Plate, as postulated by J.Adams (1980, 1985). Further south, crustal shortening is taken up by crustal thickening with a lesser uplift component. However, there is less uplift north of Mt Cook, and Allis (1986) attributed this to relief caused by subduction at the southern end of the Hikurangi subduction margin.

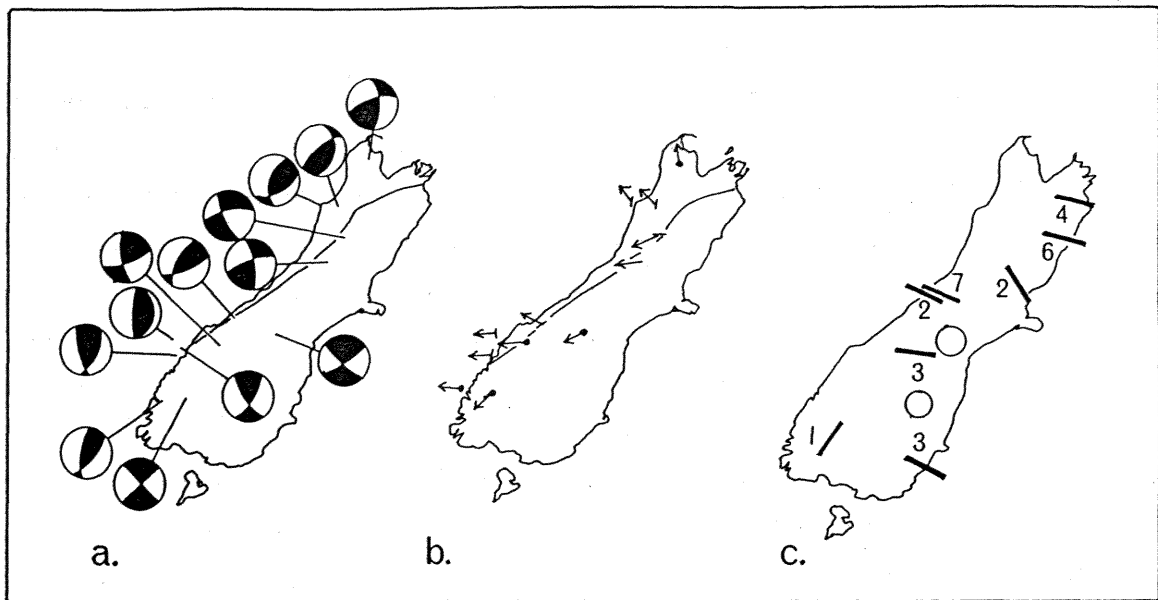


Figure 2.16.

(a) Compilation of fault plane solutions for shallow earthquakes and micro-earthquakes. All mechanisms are equal area projections of the upper focal hemisphere: compressional quadrants are shaded.

(b) Slip directions inferred from fault plane solutions. A dot indicates where the fault direction is in doubt; a bar indicates where the strike of the fault is known.

(c) Principal horizontal shortening directions from geodetic strain measurements, indicating the magnitude of the shear strain. Open circles indicate no measureable shear strain. After Walcott (1978).

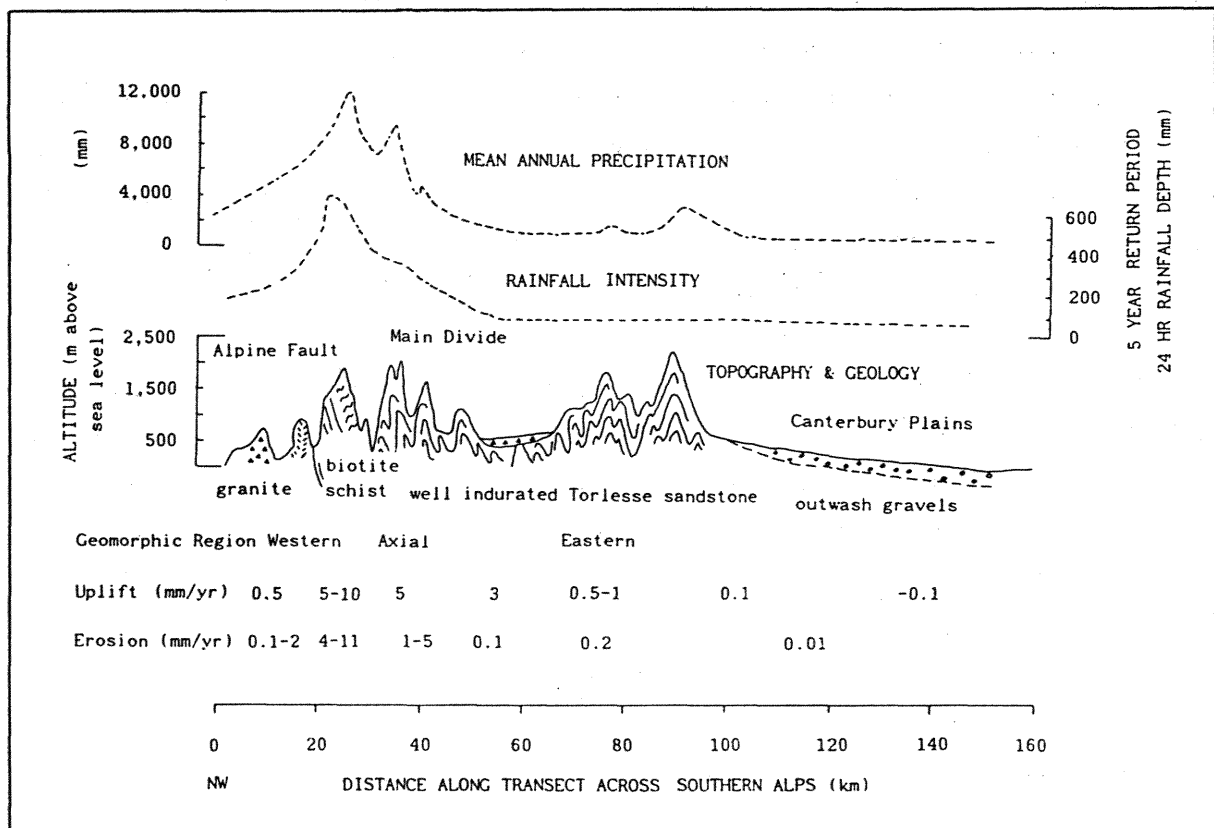


Figure 2.17. Cross-section through central Southern Alps showing precipitation, uplift rate and erosion rate variations across the Main Divide. After Whitehouse (1987).



J. Adams (1979) and H. Wellman (1979) inferred that a change from crustal thickening to predominantly uplift and erosion occurred in the last few Myrs. Furthermore, J. Adams (1980) suggested that the total amount of uplift and erosion adjacent to the Alpine Fault may exceed 50 km. C. Adams (1979, 1981) suggested that the amount of late Cenozoic uplift has not been greater than 10 km. In a study of erosion rates across the Southern Alps, J. Adams (1980, 1985) argued that the erosion of the upthrust plate edge is fast enough to balance uplift so that the mountains are in a dynamic steady state. This steady state is maintained by the interaction of uplift, relief, rainfall and erosion rates that restore this balance (Fig. 2.17). Estimates of the amount of erosion from river suspended sediment loads (Griffiths, 1981) relative to the estimated uplift rates, support the equilibrium model for the central Southern Alps (Whitehouse, 1987).

### 2.3.2. Fiordland Region

The Fiordland block lies at the boundary of the Pacific and Indian plates (Fig. 2.1b) and displays the elements of convergent and transcurrent plate margins (Walcott, 1978). Transcurrent motion at the plate boundary has transferred the Australian Plate northward relative to the Pacific Plate (Davey and Smith, 1983). Norris and Carter (1980) suggest there has been limited strike-slip movement along the Moonlight-Hollyford Fault, and that transcurrent movement is spread over a region of shear through Fiordland (Fig. 2.18).

Uplift rates of 1-6 mm/yr have been estimated for southern Fiordland by Bishop (1985), while Ward (1988a) calculated a rate of 0.9 mm/yr from correlations of presumed high-level marine terraces incised by glacial outwash surfaces. In northern Fiordland, Hull and Berryman (1986) derived uplift rates of 2.2 mm/yr from Holocene terraces on both sides of the Alpine fault adjacent to Lake McKerrow. At the Aurora cave system on the western side of lake Te Anau, Williams (1985) used a change in level of the main cave passages to date fluctuations in lake level. By comparison with terraces on the eastern side of Lake Te Anau, an average uplift rate of 2 mm/yr was derived for the Pleistocene. These uplift rates are scattered but are sufficient to indicate a substantial increase in the rate of uplift towards the north of the Fiordland micro-plate.

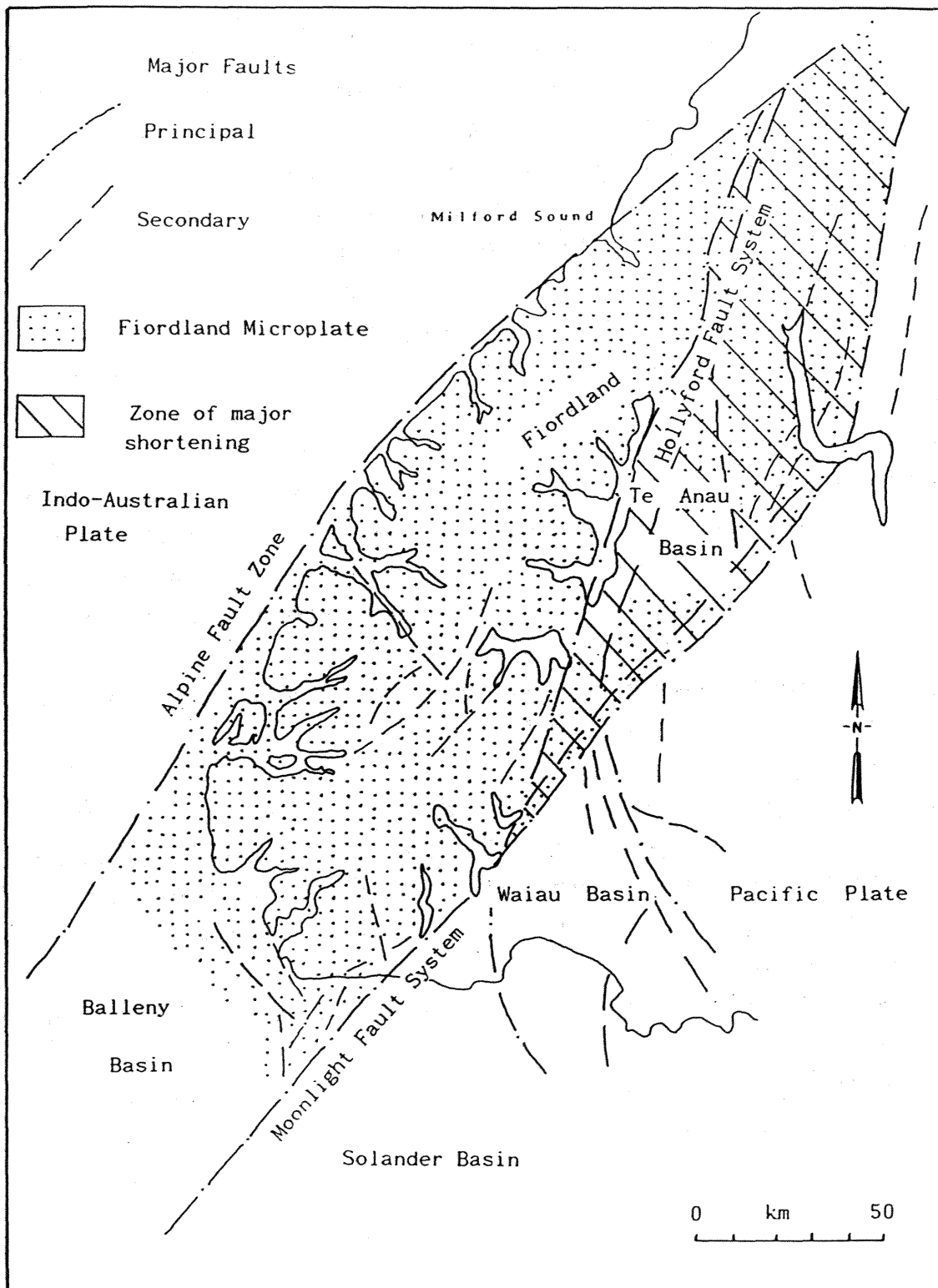


Figure 2.18. Regional structural and fault map of southwestern South Island. After Norris and Carter (1982).



Until comparatively recently, the only coverage of much of the area was from reconnaissance 1:250,000 mapping (e.g., Wood, 1960, 1962). A number of detailed bedrock studies have been completed in recent years (e.g., Williams and Harper, 1978; Gibson, 1982; Bradshaw, 1985). In the most recent synthesis of Fiordland geology, Oliver and Coggon, (1979) recognized four geological terrains on the basis of rock associations and comparative magnetic relief: a) western province, comprising lower crustal rocks of amphibolite and granulite facies; b) central province, comprising granite, granodiorites and amphibolite facies metasediments; c) western Fiordland belt comprising granulite facies metasediments; and d) eastern province of relatively young plutonics dominated by granites and diorites (Fig. 2.19). Recent work has refined this and enabled modelling of aspects of the metamorphic development of the Fiordland block (Mattinson *et al.*, 1986; Gibson *et al.*, 1988). The contact between the western and central provinces has been reinterpreted as a ductile shear zone separating lower and upper crustal plates generated during continental extension (Gibson *et al.*, 1988).

The crystalline basement of the Darrans Complex in northern Fiordland, consists largely of intrusive layered to massive igneous rocks. These grade autometamorphically into hornblende diorites, both on a local scale along joints and dykes, and regionally from the Darran Mountains westward towards Milford Sound (Blattner, 1978; Williams and Smith, 1983). Overall, the Darrans Intrusives (Williams and Harper, 1978; Williams and Smith, 1983) are relatively homogeneous, except for variations in texture and occasional bands of xenoliths and intrusive layering (Blattner, 1978). Folds and foliated rocks are not characteristic of the intrusives, and foliation, where developed is generally associated with faults, shear zones or contacts.

### 2.3.3. Mt. Aspiring Region

The Mt. Aspiring terrain extends northwards from the crystalline Fiordland Terrain on the eastern side of the Alpine Fault, and the region is subjected to highly oblique compression (Fig. 2.1b & 2.16). Earthquake first-motion studies by Scholz *et al.* (1973), and Davey and Smith (1983) indicate a generally E-W oriented PHS direction, with strike-slip faulting predominating. At the Alpine Fault, thrust faulting is developed and is predominantly highly oblique (Reyners *et*

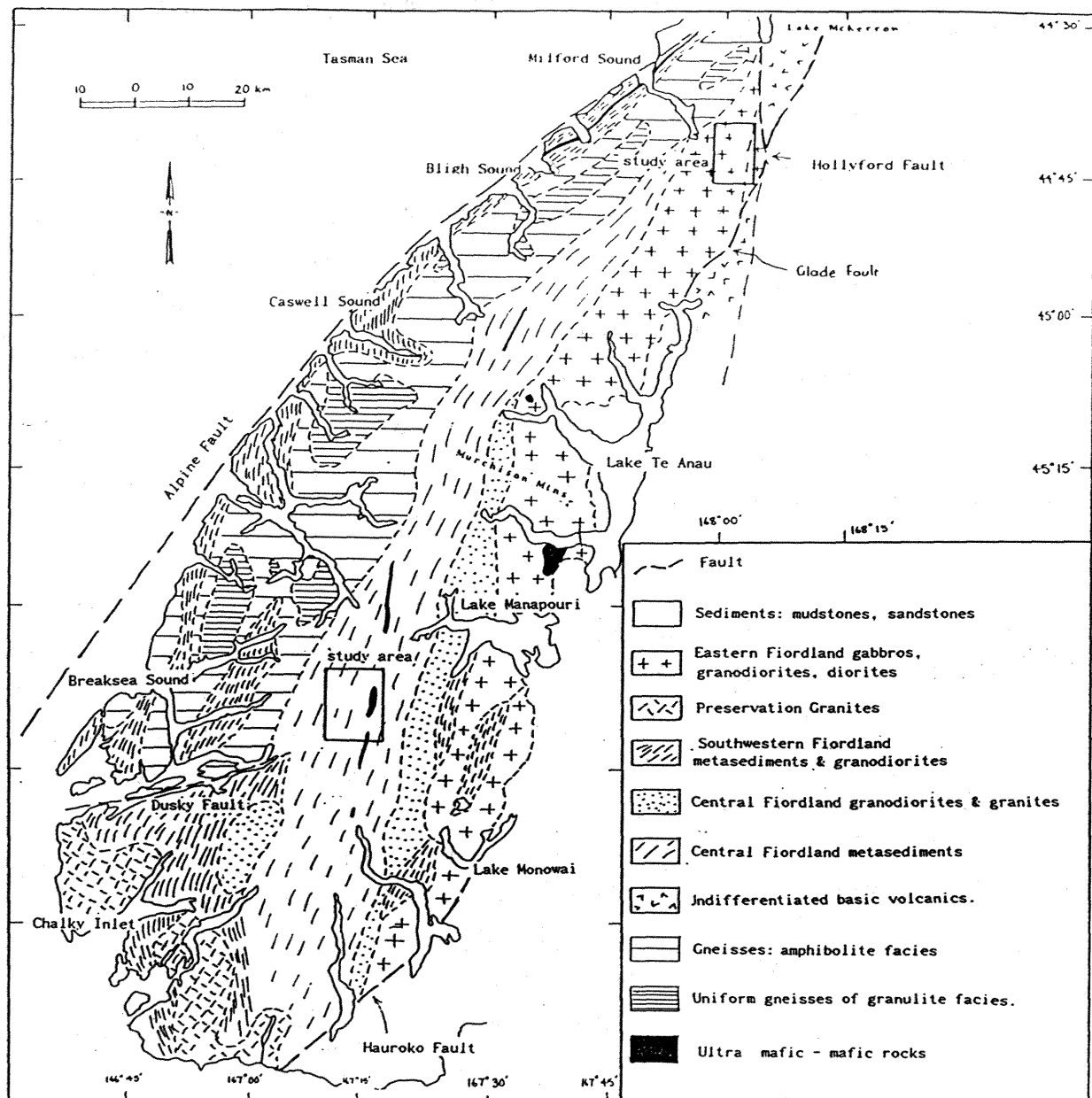


Figure 2.19. Generalized geological map of the Fiordland Block. After Oliver and Coggon (1979).

al., 1983). Crustal thickening occurs due to underthrusting of the Australian Plate (Allis, 1986).

Late Cenozoic activity and differential uplift along the Moonlight Fault is suggested by generally greater peak elevations and higher relief mountains on the eastern side of the fault (Fig. 2.10). Comparatively erosion resistant greenschist forms some of the high peaks immediately west of the fault, and greenschist is also common on the eastern side of the fault (Fig. 2.20), so that the topographic variation is unlikely to be due to differential erosion (Craw, 1985). The Moonlight Fault still has active epicentres located near its surface trace (Scholz *et al.*, 1973), and the topographic expression of the fault argues for significant relatively recent movement.

The Moonlight fault is apparently a single major dislocation surface north of Lake Wakatipu, but further south the zone is up to one km wide involving several crush zones and fault planes (Fig. 2.18). Associated features genetically related to the fault movements include kink folds and possible conjugate faults striking  $\sim 60^\circ$  away from the main zone (Turnbull *et al.*, 1975). The geometry of the late Cenozoic movement on the two groups of faults suggests that the faults were not formed as new fractures during the late Cenozoic but by rejuvenation along pre-existing lines of weakness (Norris *et al.*, 1978). Uplift rates on the eastern side of the Alpine Fault during the late Cenozoic of 5 mm/yr (Cooper and Bishop, 1979), and 5.6 mm/yr estimated from flights of presumed marine terrace remnants (Bull and Cooper, 1986, 1988), confirm rapid uplift east of the Alpine Fault. However, the results of Bull and Cooper (1986) have been questioned by Ward (1988b). Kamp *et al.* (submitted) used the ages of annealed fission tracks in zircon and apatites from the schist to derive uplift rates of 2.6-4.6 mm/yr since the initiation of late Cenozoic uplift.

The structure of the terrain is dominated by the Alpine and Moonlight faults, with the foliated and fractured schist comprising a highly deformed terrain subjected to several deformations (Craw, 1985). The regional geology is shown in Fig. 2.20. Detailed examination by Craw (1984) showed that there is significant lithologic variation on a regional scale. There are two major rock types in the Otago schist: (1) quartzofeldspathic schist or greyschist, and (2) greenschist. Craw (1984) mapped psammitic schist, two types of pelitic

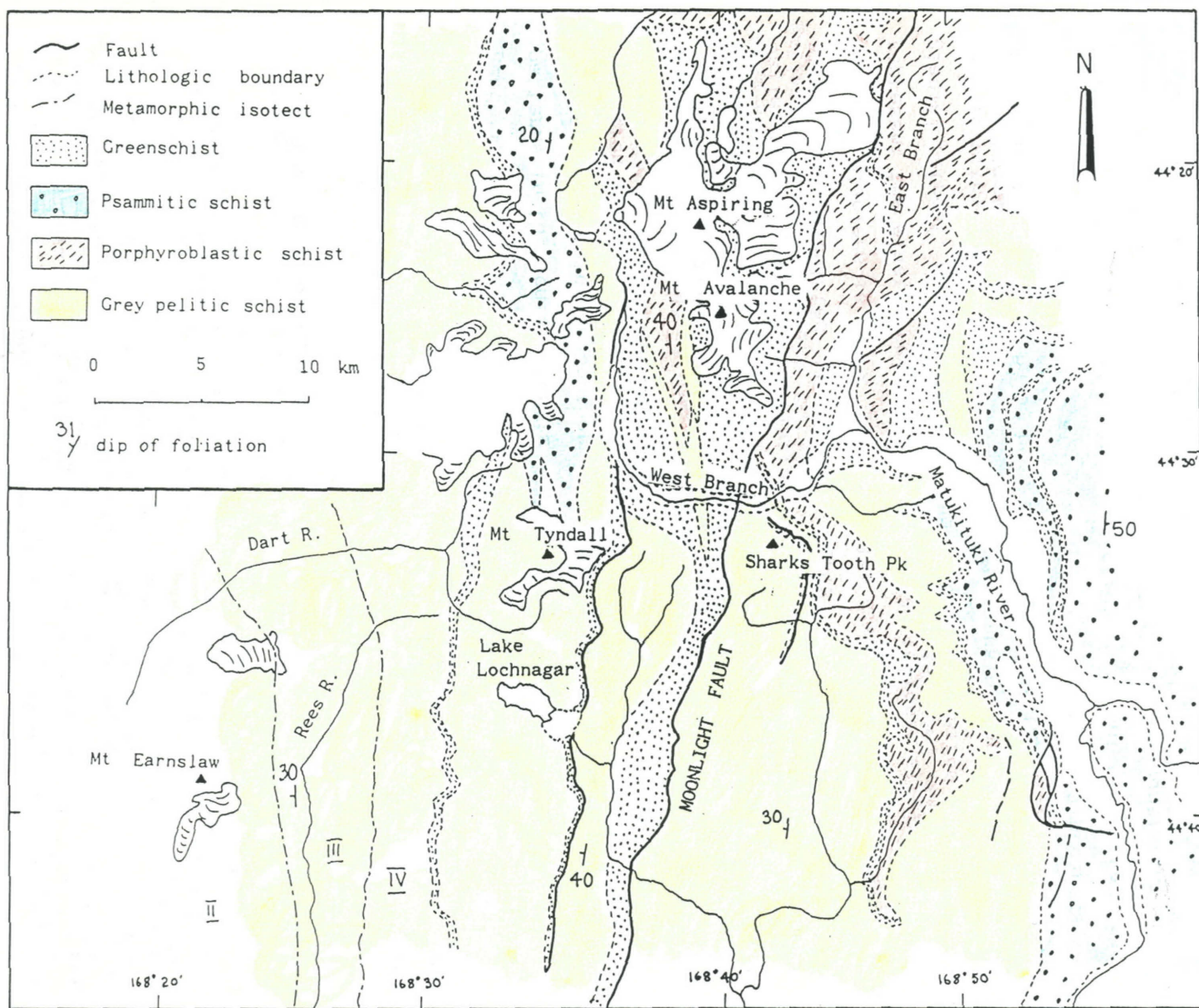


Figure 2.20. Generalized geological map of the Mt Aspiring region showing main structural elements and metamorphic zones. After Crow (1984, 1985).

schist (grey and porphyroblastic) and four types of greenschist (light, spotted, foliated, and epidote-rich) recognizable on outcrop scale in textural zone 4. Craw (1984) divided the area into two lithologic associations, the 'Aspiring Association' and the eastern 'Wanaka Association', separated by a north trending poorly defined but lithologically gradational boundary. The Aspiring Association is made up predominantly of pelitic rock types with much greenschist and ultramafic horizons. The Wanaka association consists largely of psammitic schists with subordinate pelitic schist and greenschist.

#### 2.3.4. South Westland Region

The glacierized landscape of South Westland on the eastern side of the Alpine Fault, is a zone subjected to highly oblique compression (Fig. 2.16). Earthquake first-motion studies by Scholz *et al.* (1973), geodetic strain studies (Walcott, 1978), and studies of fracture patterns in the schist (Norris and Cooper, 1986), confirm the current convergence within the Southern Alps and allow the present WNW-ESE PHS direction to be calculated (Fig. 2.16).

Norris and Cooper (1986) examined small displacements of recently deglaciated surfaces across mesoscopic fractures in the Franz Josef Valley, and argued for correlation with the PHS direction. The shear strain rate calculated by Walcott (1979) from geodetic measurements near the glaciers is  $7 \times 10^{-7}/\text{yr}$ . The displacements were argued to represent the elastic release of accumulated tectonic strain following glacial retreat. However, Norris and Cooper recognized that the area may lie within an area of high creep strain. The schists exposed within the Waiho Valley have been uplifted during the Late Quaternary uplift of the Alps. Holm *et al.*, (1987) suggested a progressive rotation of the subhorizontal PHS direction in an anticlockwise sense with the most recent structures giving PHS directions consistent with the geodetic and micro-earthquake data.

Bull and Cooper (1986, 1988) used flights of presumed wave-cut marine terraces to calculate late Cenozoic uplift rates of  $\sim 7.8 \text{ mm/yr}$  in the schist of the Franz Josef area, although Ward (1988b) argued that their data, and therefore the derived uplift rates, are erroneous. Bull and Cooper's estimate is lower than the estimated uplift rates of 10-20 mm/yr from terrace tilt measurements by J. Adams (1979) and Wellman (1979).

The geologically and structurally complex nature of the Main Divide has been studied in some detail (e.g., Gunn, 1960; Warren, 1967; Findlay, 1979; Findlay, 1987; Craw *et al.*, 1987). The rocks west of the Divide and bounded on their western side by the Alpine Fault are mostly schists of varying metamorphic grade. The schists change from chlorite-muscovite subfacies at the Main Divide, to garnet-oligoclase schists of amphibolite facies metamorphism in the west. The rocks exposed in the Franz Josef, Fox and Whymper valleys are interspersed quartzo-feldspathic biotite to garnetiferous schist, with minor amounts of chlorite schist near the present glacier snouts (Fig.2.21).

Locally the structure is dominated by tight isoclinal folding with the axial plane striking NE-SW, nearly parallel to the Alpine Fault (Gunn, 1960). Four phases of deformation have been recognized (Findlay, 1979, 1987) forming a Tertiary megashear belt formed of steeply dipping, anastomosing, kilometre-scale, ductile shear zones originating from redistributed movement within the plate boundary (Findlay, 1987). Gunn defined 2 major fault systems: a) those trending E-W; b) those trending NW-SE perpendicular to the axial plane of the folds, and a third group, the Alpine and associated faults. The NW-SE faults are oriented parallel to the AC joint system, with the shear stress likely to be relieved by slip along these pre-existing fractures.

#### 2.3.5. Mt. Cook Region

The Mt. Cook region is a zone of oblique convergence, with the eastern side of the Alpine Fault moving south and also being thrust westward relative to the Australian Plate (Walcott, 1978). First-motion studies of micro-earthquakes (Scholz *et al.*, 1973), indicate that the PHS axis is subhorizontal, although the extension varies from shallow to steeply plunging. Unlike the Fiordland and Mt Aspiring terrains, where considerable underthrusting of the Pacific Plate is occurring, the amount decreases northward and is probably minimal north of Mt. Cook (Allis, 1981, 1986). In the central Southern Alps, crustal shortening is being accommodated by uplift and erosion of the Pacific Plate (J.Adams, 1980).

The glaciers of the Mt. Cook region lie within the Torlesse terrane, an extensive suite of Carboniferous-Triassic greywacke consisting of indurated, poorly-sorted, polymict sandstones, and

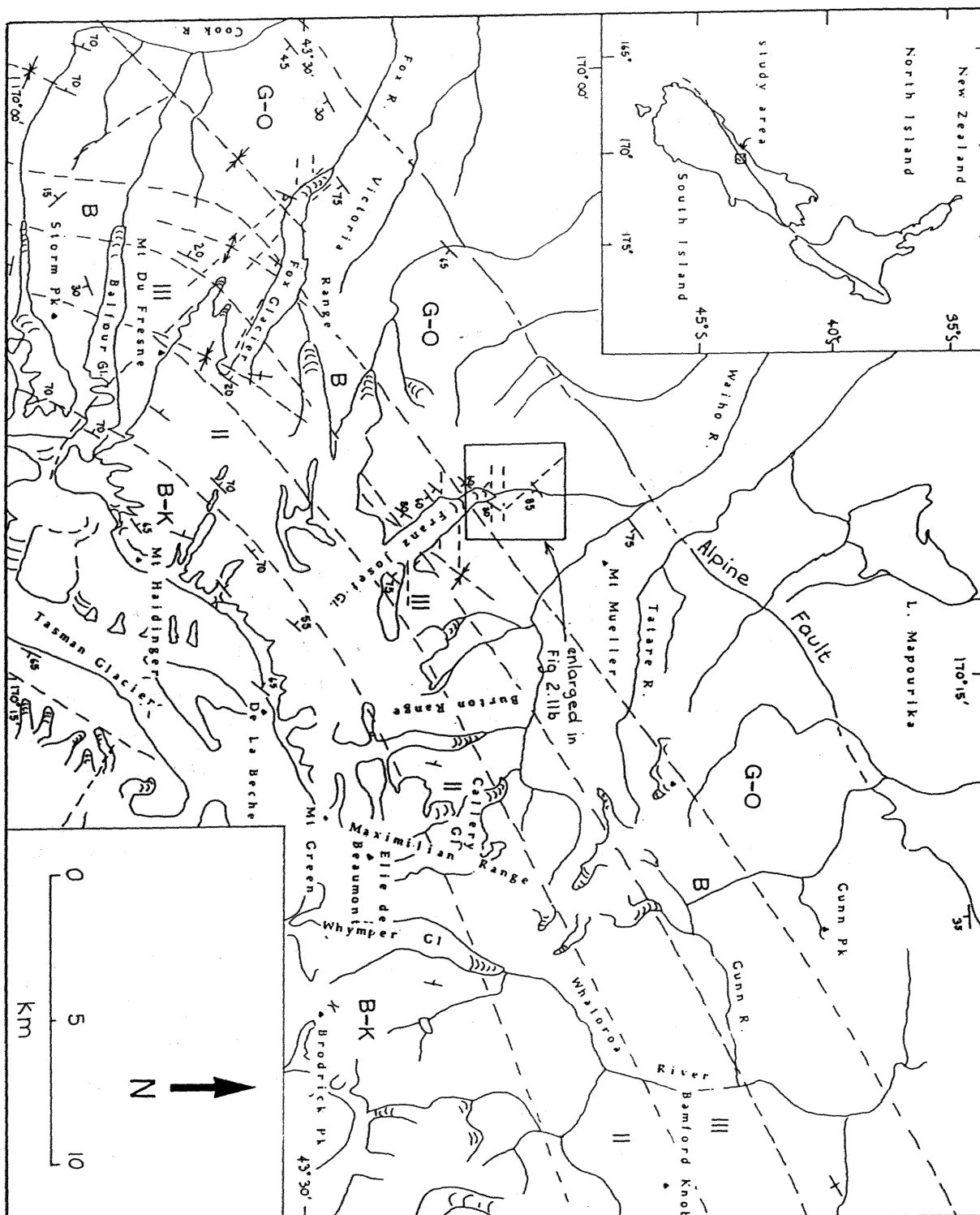


Figure 2.21. Generalized geological and structural map of South Westland region in the vicinity of the Waiho-Fox valleys, showing metamorphic boundaries. G-O = garnet-oligoclase zone, B = biotite zone, II and III = chlorite textural zones, B-K = chlorite subzone I. After Warren (1967).



mudstones (Findlay and Spörli, 1984). In the Hooker-Mueller Valleys, the Torlesse rocks consist mainly of four lithotypes: thin-bedded sandstone with minor siltstone; thick-bedded massive sandstone; thin-bedded sandstone with black mudstone; and finely-bedded muddy siltstone. Similar rock units occur in the Malte Brun Range where Waterhouse (1985) mapped in detail the lithology and structure of the Torlesse. A generalized geology and structure map of the region is shown in Fig. 2.22.

The structure of the Mt. Cook Range is dominated by large, north-facing, steeply plunging folds. The Main-Divide, on the western side of the Hooker Valley is formed of west dipping beds, broken by WNW dipping faults. Findlay and Spörli (1984) recognized four episodes of folding and dislocation of the Torlesse by oblique-slip faults. Strata and faults strike predominantly N-S to NE-SW and appear to control the main drainage lines.

#### 2.3.6. McMurdo Dry Valleys Region

Unlike the New Zealand Southern Alps and most other major Cenozoic mountain ranges of the world, the uplift of the Transantarctic Mountains (TAM) was not accompanied by thrusting or andesitic volcanism, although some step-faulting is developed on the Ross Sea side of the TAM. Rather, the uplift has been exclusively by vertical crustal movement with gentle tilting of the fault blocks (Fitzgerald *et al.* 1986; Gleadow and Fitzgerald, 1987). Fission track dating studies by Fitzgerald *et al.* (1986), show that there has been ~5 km of uplift since the early Eocene, associated with passive rifting. Despite the high elevations, gravity modelling suggests that the crust beneath the mountains is only 40-45 km thick (Bentley, 1983). Recent extensional tectonism in the Ross Embayment is indicated by unusually high heat flows in the Dry Valleys area (Decker and Bucher, 1982). The values suggest unusually high conductive heat transfer through anomalously thin lithosphere, as occurs in other modern continental extension terrains such as the Basin and Range Province (Decker and Bucher, 1982).

The geology of the Dry Valleys and site locations are shown in Fig. 2.23. The basement complex consists of tightly folded, steeply dipping Koettlitz Group metasediments and plutonics (Granite Harbour Intrusives) of Early Palaeozoic age (Findlay *et al.*, 1984). The granite-gneiss is flanked by the Larsen Granodiorite, and localized



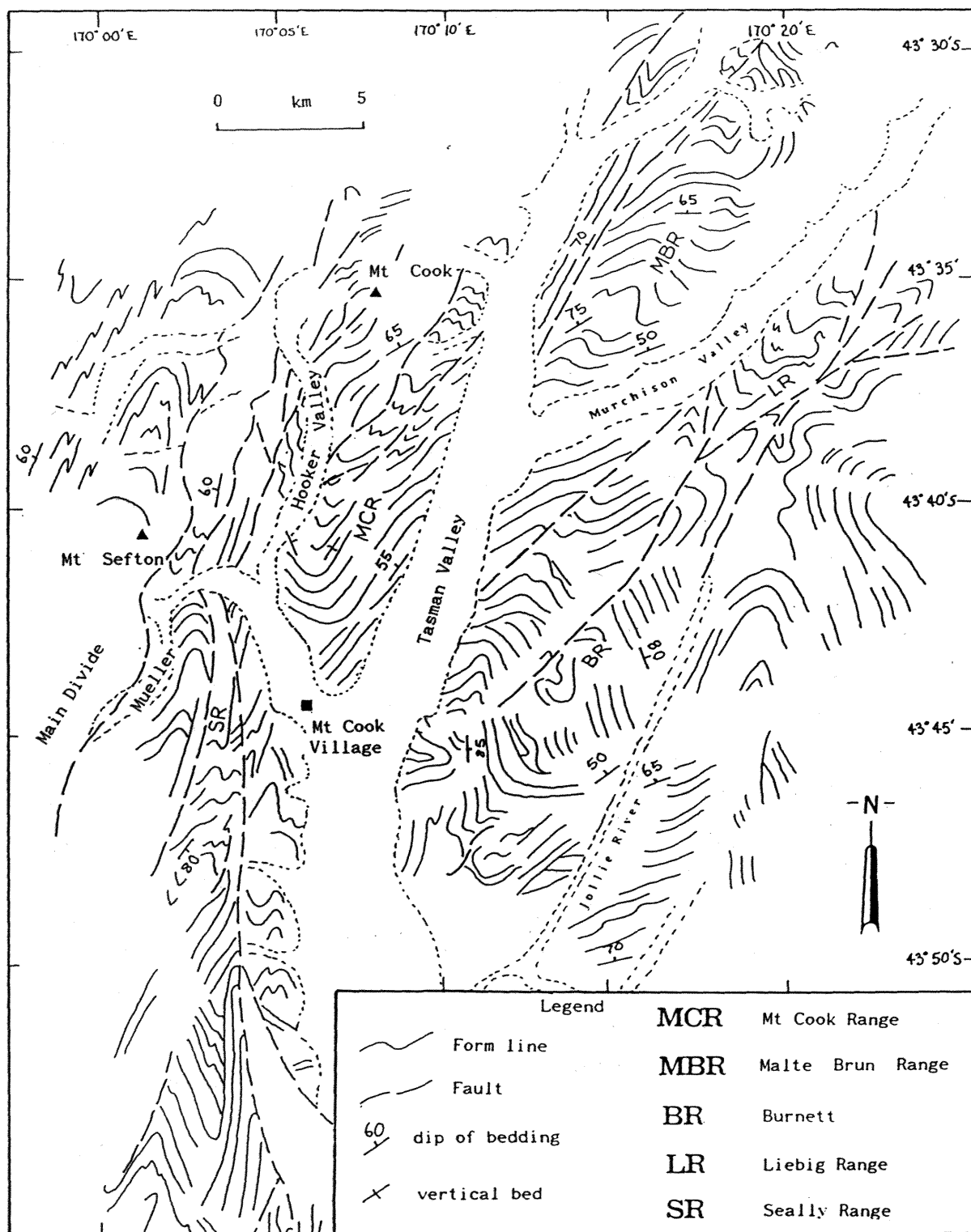
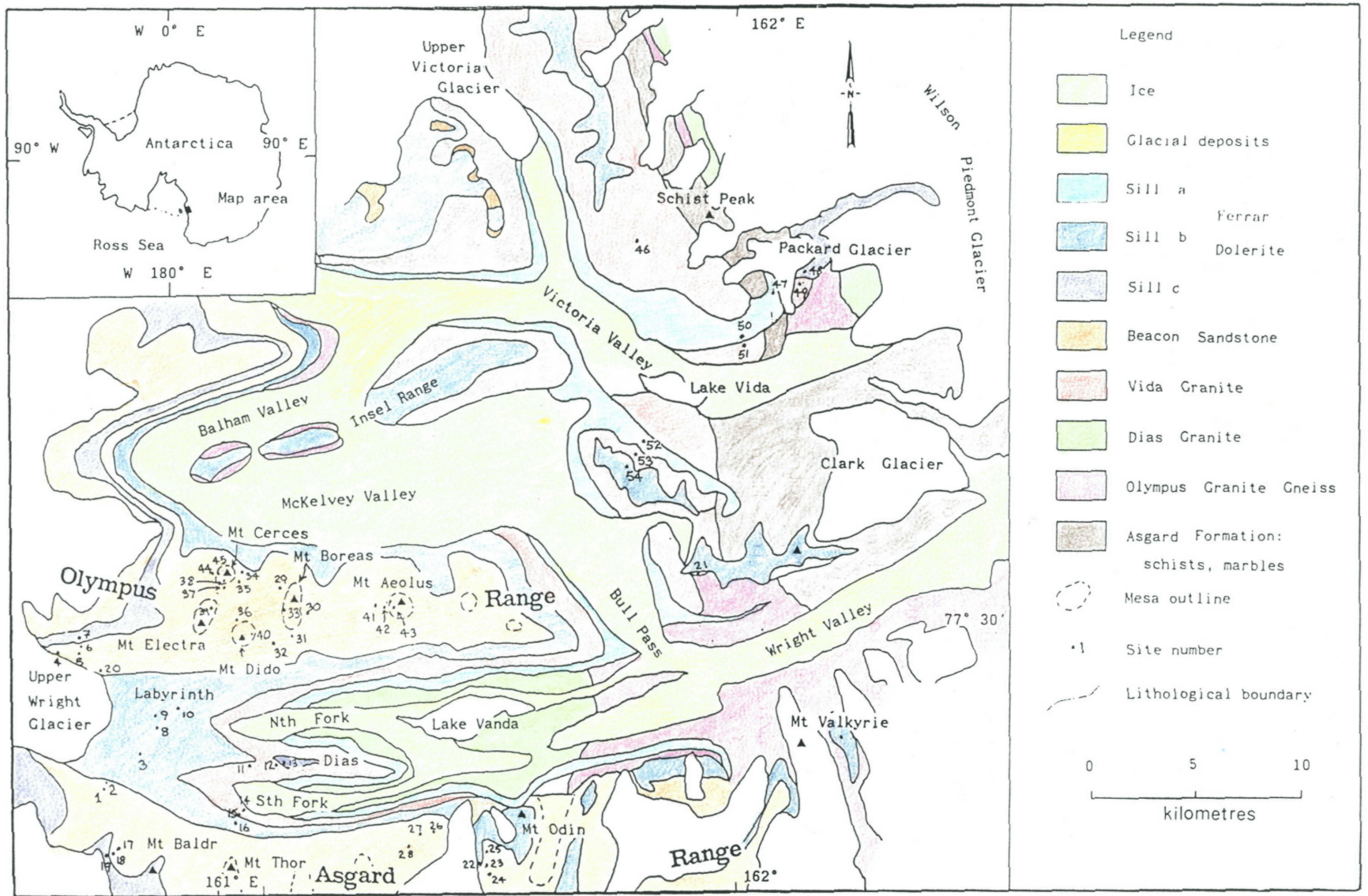


Figure 2.22. Generalized structural and geological map of Mt Cook region. Note strong structural control on the orientation of the main valleys draining the eastern side of the Main Divide. After Findlay and Sporli (1984).



tabular bodies of Theseus Granodiorite intrude all three. The basement rock was uplifted and eroded to form the Kukri erosion surface upon which a thick sedimentary sequence- the Beacon Supergroup -accumulated (McKelvey *et al.*, 1977). Both the basement complex and the Beacon Supergroup were intruded during the early Jurassic by dolerite dykes and sills of the Ferrar Group (Gunn and Warren, 1962).

#### 2.4. Summary

Aspects of the geomorphological and geological features of the central and southern parts of the Southern Alps have been documented. The glacierized landscape of the Southern Alps of the Main Divide cannot be understood without consideration of the regional geology and tectonics. The objective of the remainder of this study is to attempt to relate aspects of the tectonic and glacial erosional geomorphology in the vicinity of the Main Divide to bedrock properties and structure.

## **Chapter Three**

### **Morphometry of Fiord Trough Outlets**

#### **Implications for Glacial Trough Development**

## CHAPTER THREE: MORPHOMETRY OF FIORDLAND OUTLET GLACIER TROUGHS: IMPLICATIONS FOR GLACIAL TROUGH DEVELOPMENT

### 3.1. Introduction

The Fiordland region is the only morphological terrain of the Southern Alps that has not suffered extensive post-glacial modification. As a consequence, the valleys present in Fiordland owe their morphology wholly to glacial processes and rock resistance, providing a suitable terrain for the isolation and examination of glacial input to development of a glacial valley system.

Little is known of the Pleistocene glacial history of Fiordland, other than from the glacial geologic studies of Fitzharris (1967) and McKellar (1973) on the eastern margin of the region. The deposits necessary for the elucidation of the early Pleistocene glacial history have not been preserved due to the intensity of the subsequent glaciations (McKellar, 1982). The sequence of Fiordland glaciations elucidated by McKellar (1973) is shown in Fig. 3.1. No radiometric ages are available for the sequences shown, but the oldest preserved Moat Creek advance may be mid-Pleistocene (McKellar, 1973). From the radial pattern of troughs and fiords in south-central Fiordland, Linton (1957) suggested that a central ice-cap and attendant radiating outlet glaciers dominated the development of the glacierized landscape. McKellar (1982) argued that it was only during the last, Otiran, glacial stage that the glaciers eroded the overdeepened valleys close to their present shape. Bruun *et al.* (1955) studied the bottom profile and side slopes of Milford Sound, and argued that the last glacial advance truncated an older valley profile shaped by ice earlier in the Otiran glaciation when the valley floor was 300-400m higher than present.

The lack of even basic geomorphic data and the remoteness of the region necessitated the application of a variety of remote sensing techniques to permit an empirical evaluation of the influence of the Pleistocene glacial system on Fiordland Block morphogenesis; in particular, the development of the over-steepened and deepened troughs and fiords.

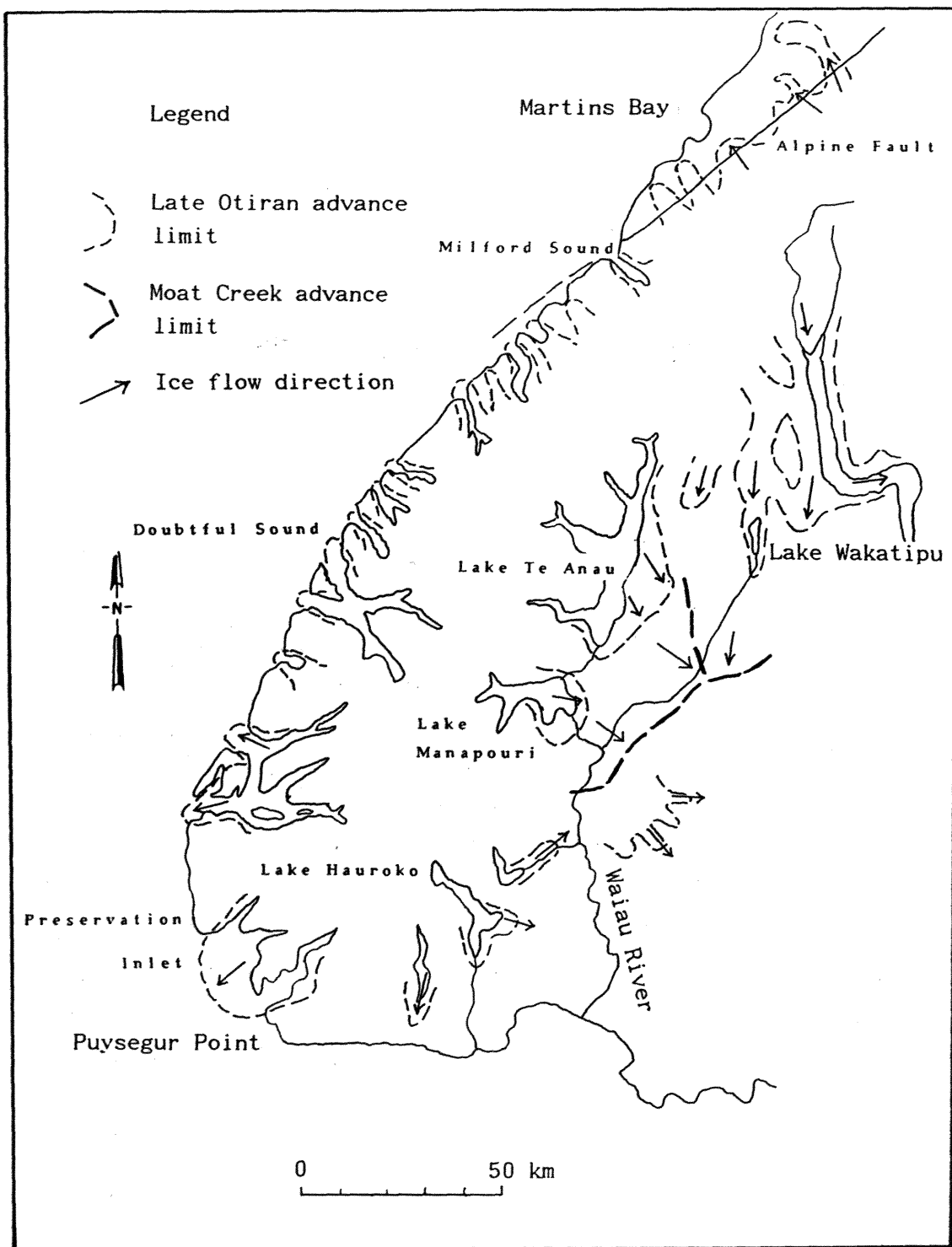


Figure 3.1. Map of Fiordland showing maximum extent of the Pleistocene glacial advances. Adapted from NZGS Miscellaneous Series Map 6, 1973.

### 3.2. Quantification of The Morphology of Fiordland

#### 3.2.1. Introduction

A summit-envelope surface was generated for the Fiordland Block by the method of Ryder (1981) to enable the quantification and description of the apparent summit accordance/erosion surface. The procedure involved dividing Fiordland into 10 mile square sectors on 1:63,360 topographic maps (New Zealand Mapping Service Series 1) and averaging the heights of the 5 highest peaks in each sector. The data points were contoured to give the pattern shown in Fig. 3.2. A broadly domed upland surface was delineated, sloping gently seaward from centres over the Murchison Mountains and Wilmot Pass regions. North of the Murchisons towards the Darran/Earl Mountains, a distinct dislocation in the summit envelope occurs, where it steepens rapidly towards a higher summit surface over northern Fiordland. Another break in the surface occurs along the eastern boundary of the Fiordland block, coinciding with the Hollyford Fault system, east of which are the plains of the Waiau and Te Anau basins. The locations of the sites mentioned in the text are displayed in Fig. 3.3.

Corresponding to this upland surface are a series of radiating outlet troughs and fiords that had been attributed by Linton (1957) to the effects of radiating outlet glaciers from a central ice-cap located over south-central Fiordland. Linton argued that the dispersive tendency of a major ice-centre is capable of imposing a system of radiating outlet troughs on the pre-glacial landscape, even if the valley pattern of the region is only partially favourable to the development of such a system. Linton argued that where valleys oriented in the right direction are not available, the ice-centre will adapt the existing valley pattern by overriding watersheds and linking existing valley elements. This habit of ice-caps will be used shortly as the rationale for a method of delineating the ice-cap locations.

#### 3.2.2. Outlet Glacier Trough Morphology

A clear relationship between glacier activity, the volume of ice flowing through the outlet trough, and the resultant trough size and form, has been demonstrated in British Columbia (Roberts and Rood, 1984), West Greenland (Haynes, 1972) and for the Laurentide ice sheet (Sugden, 1978). These studies were undertaken on terrains of ice-sheet

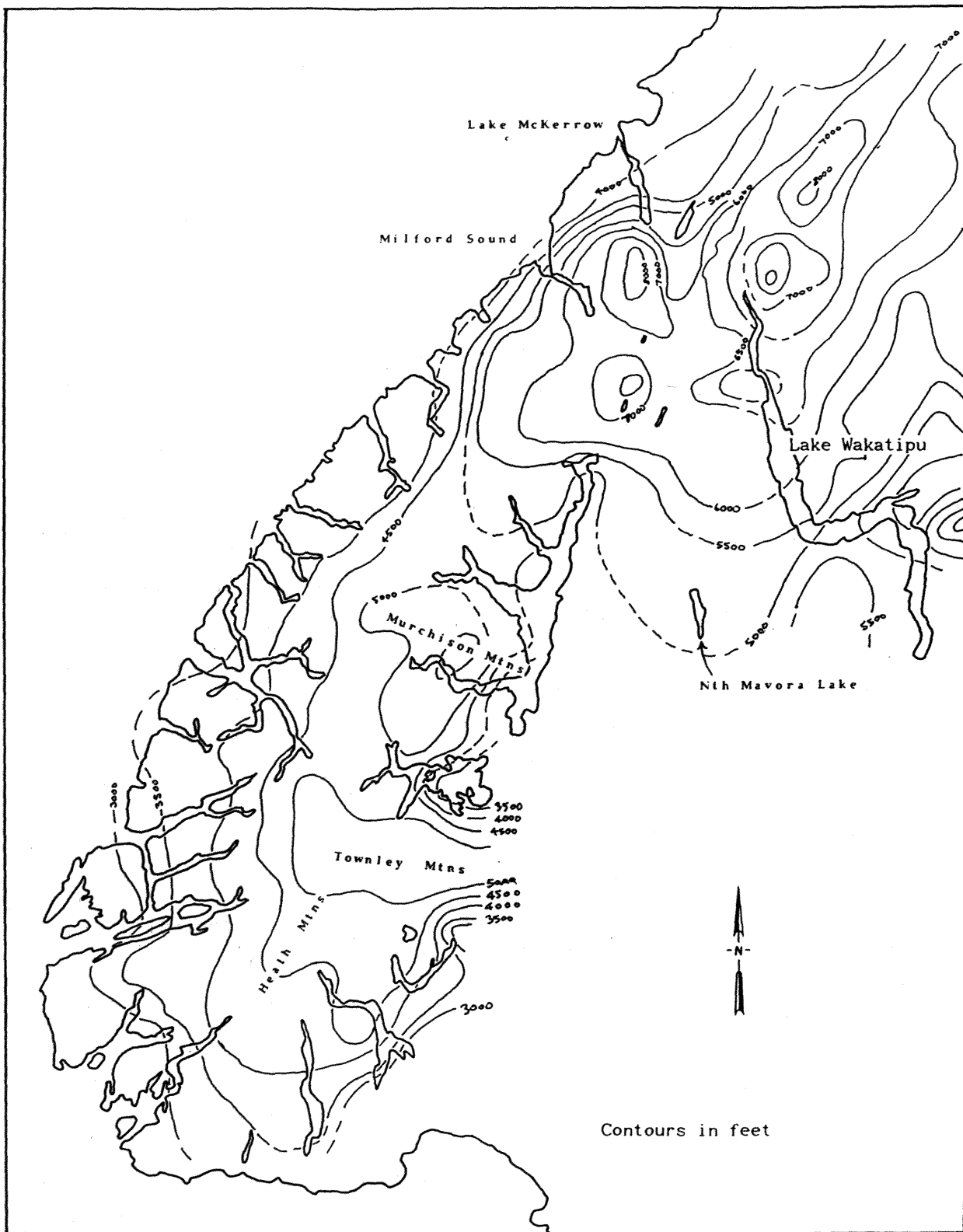


Figure 3.2. Summit level envelope (planation surface ?) for the Fiordland region. Note the broadly domed nature of the surface over Fiordland with apparent westward tilting.



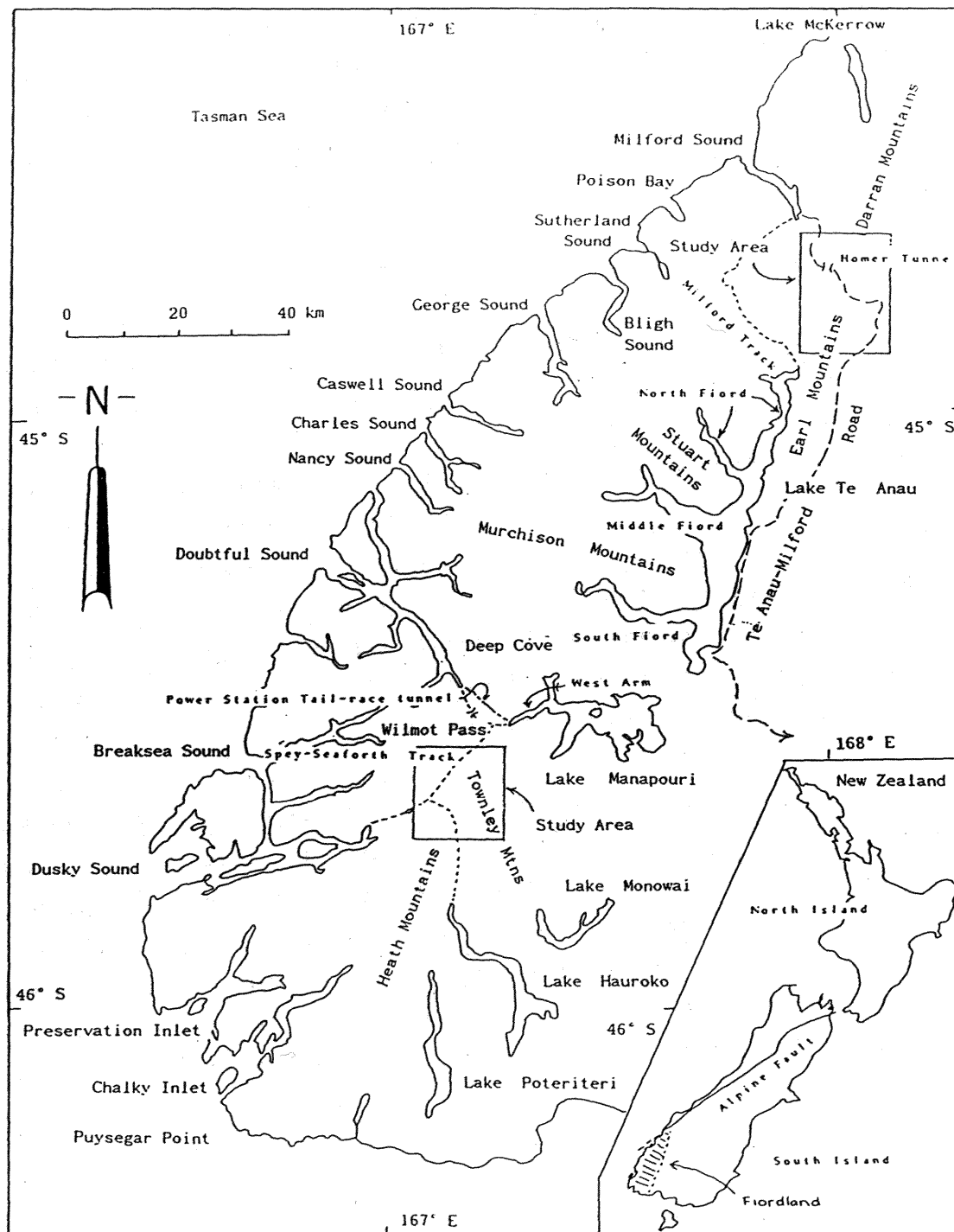


Figure 3.3. Map of Fiordland showing locations of geographic features referred to in text. Fiordland study areas indicated.

glaciation where the glaciers are essentially cold-based, except along the outlet troughs where channellized flow may allow basal melting and the development of a landscape of selective linear erosion (Sugden, 1974; 1978). However, such a relationship between outlet trough form and discharge may differ for regions developed under more temperate glacial conditions such as probably existed in the Southern Alps, New Zealand.

To enable analysis of the relationship of glacier activity to outlet trough form and volume, a range of trough size descriptors was measured. The parameters quantified are: (1) outlet trough width; (2) trough depth; (3) trough length; (4) trough cross-sectional area; and (5) the catchment area for each outlet trough. However, these factors must be measured relative to some datum plane of near constant relative position across the region of interest. Haynes (1972) measured the upper limit of the trough from the level of the Tertiary erosion surface that defines a convenient datum surface across West Greenland. Roberts and Rood (1984) employed sea-level as the datum surface for their British Columbia fiord troughs. The details of measurement of the morphometric parameters will be outlined shortly.

The obvious datum of sea-level was selected for this study. However, for the data derived relative to this surface to give meaningful results, constant uplift rates across Fiordland must be assumed. The geological evidence suggests increasing uplift rates to the north of the block, associated with northward migration of the subduction zone that delineates the western boundary of Fiordland. Fortunately, an erosion surface of probable late Pliocene age (Ward, 1988a) persists across south-central Fiordland (Fig. 3.3). The trough size parameters were measured relative to each datum surface.

A potential source of error is the use of the catchment area of each outlet trough as a measure of the glacier contributing area present under equilibrium glacier conditions. Haynes (1972) suggested that deviations from the regression surface greater than the standard error of estimate, may be due to the glaciers overtopping their divides. Similarly, Roberts and Rood (1984) suggested that although catchment area provides a good estimate of the glacier contributing area (stressing the importance of the topographic high as the crucial feature separating glacier flow in the ice-field), the topographic highs and ice-divides are not invariably coincident as the divides can

be overridden. Thus an attempt was made to assess the importance of overriding of divides in the development of the Fiordland landscape.

### 3.2.3. Delineation of Glacier Divides

Evaluation of the position and influence of the ice-divides on the development of the Fiordland glacierized landscape is hampered by the lack of information on the form of the equilibrium glacial system. Linton (1957) argued that the glacial ice-centre will adapt to the existing valley pattern by overriding watersheds and linking the existing valley elements. The concept of progressive modification of the landscape by multiple watershed breaching was applied by Haynes (1977) to the study of ice-sheet overriding in Scotland. If a central ice cap develops, it is assumed that the valleys will become increasingly interconnected. For local ice-caps the modification will be at a maximum near the ice-centre, decreasing with distance along the outlet troughs. Modification is defined by reduction in divide breaching and pirating caused by progressive lowering of the outlet glacier with distance from the névé. Haynes (1977) developed a technique for quantifying this relationship based on graph theory, that, has been used to assess the connectivity of transport networks (Kansky, 1963). Haynes applied these topological measures to the glacial valley patterns of Scotland and parts of Greenland. This technique of measuring valley connectivity was applied to the Fiordland Block to enable delineation of the ice centres and their relationship to the drainage divides.

$$\text{The } \alpha \text{-index (index of connectivity). } \alpha = \frac{E - V + G}{2V - 5} \quad (1)$$

where E is the number of links, V is the number of nodes; and G is the number of free linkages in the system. Fiordland-Mt. Aspiring region was divided into 148 sectors from 1:63,360 topographic maps. The troughs were checked for glacial origin by examination of aerial photographs, and divide breaches defined as glacially moulded features at least 100 m deep. In areas where only a few watershed breaches occurred, care was taken to include whole valley networks, because otherwise the effect of valley connections that exist would be nullified (Haynes, 1977). Problems were encountered in keeping the sample areas the same size. Consequently, natural boundaries, like the major outlet glacier troughs, were used to delineate sample areas.

The  $\alpha$ -values were plotted at the mid-point of each sector and the data contoured (Fig. 3.4). The distribution of connectivity indices suggests the development of 3 ice-caps, broadly coincident with the peaks in the upland surface (Fig. 3.3). Within the limits of accuracy of the technique, the ice divides correspond to the present drainage divide, confirming that the topographic highs controlled the location of the ice-caps and ice flow patterns. Glacier flow radiated into each basin with the contribution to each outlet trough being proportional to the size of the ice-cap in each basin. Deviations from this idealized surface undoubtedly occurred, especially with the likelihood of ice-cap asymmetry and the volume of ice contributing to the seaward glaciers being greater than that to the lee-ward outlet glaciers due to the dominance of snow-bearing winds from the west. Over the Milford Track region of northern Fiordland, the modelled ice-centre is located some 10 km east of the drainage divide (Fig. 3.4).

#### 3.2.4. Trough Morphometry

i. Trough width: calculated relative to sea-level, and in the case of the inland fiords, lake level. Using sea-level as datum, fiord widths were calculated by dividing the area of the fiord surface at present sea-level by the length of each fiord from the head to the mouth, or where it joins another fiord (Fig. 3.5a). Since the troughs are nearly parallel-sided, this measure provides a good estimate of fiord width (Roberts and Rood, 1984).

ii. Trough depth: calculated relative to both reference surfaces. Trough depth was measured relative to the upland surface (summit envelope), as well as below sea-level (Fig. 3.5b). The maximum, rather than the mean depth was used in this study as it was thought to be indicative of the degree of glacial scour. However, this maximum depth does not represent the full magnitude of fiord deepening, due to sediment infill and flattening of the basin floor (Stanton and Pickard, 1981). The depth of the inland fiords with respect to sea-level was not included in this study.

iii. Trough cross-sectional area: measured relative to both the upland surface (delineated by the summit envelope) and below sea-level (Fig. 3.5c). The trough cross-sectional area below sea-level was only calculated for the coastal fiords and not for the overdeepened inland

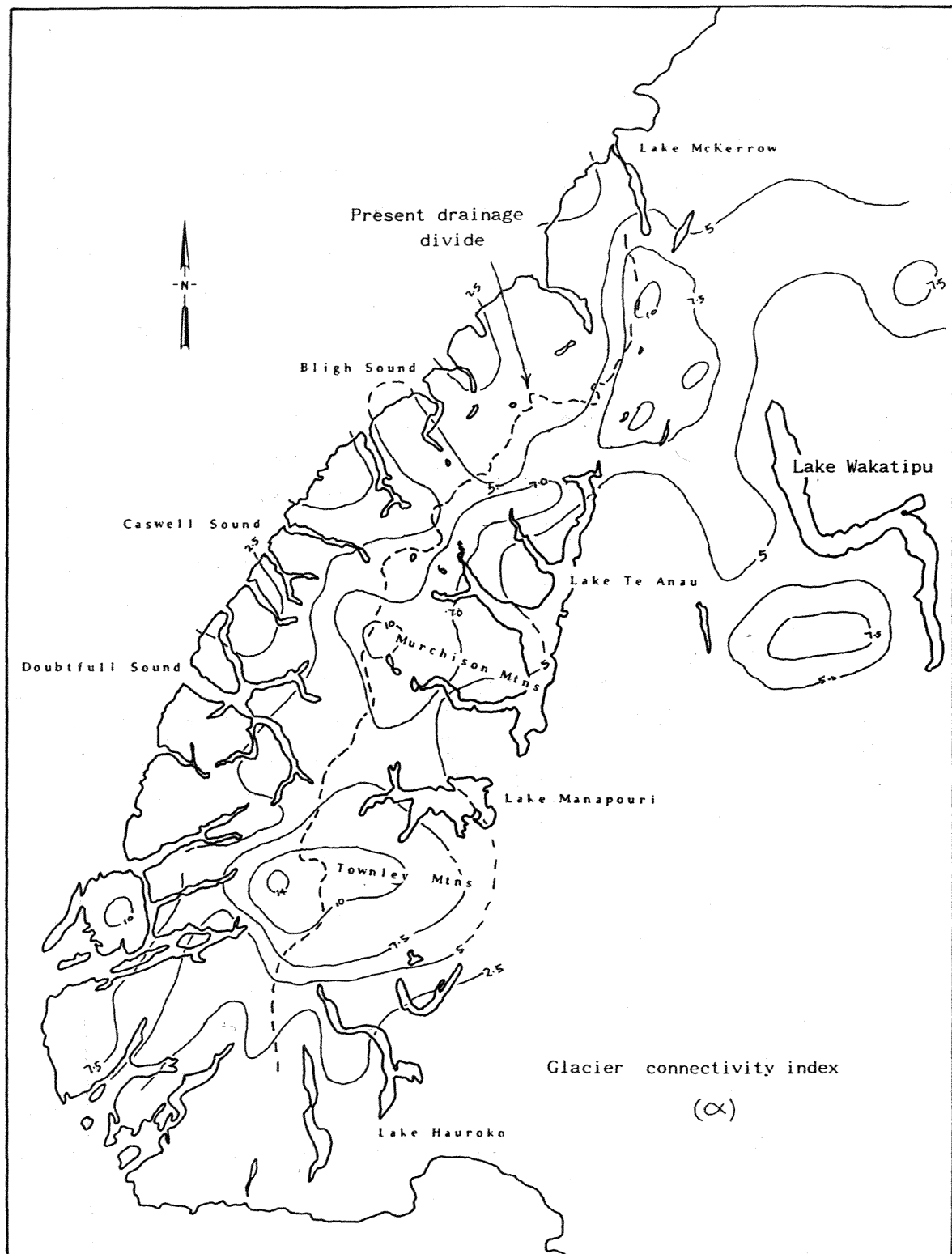


Figure 3.4. Connectivity indices ( $\alpha$ ) for the Fiordland region. Note the definition of 3 broad domes and the relative position of the present drainage divide.

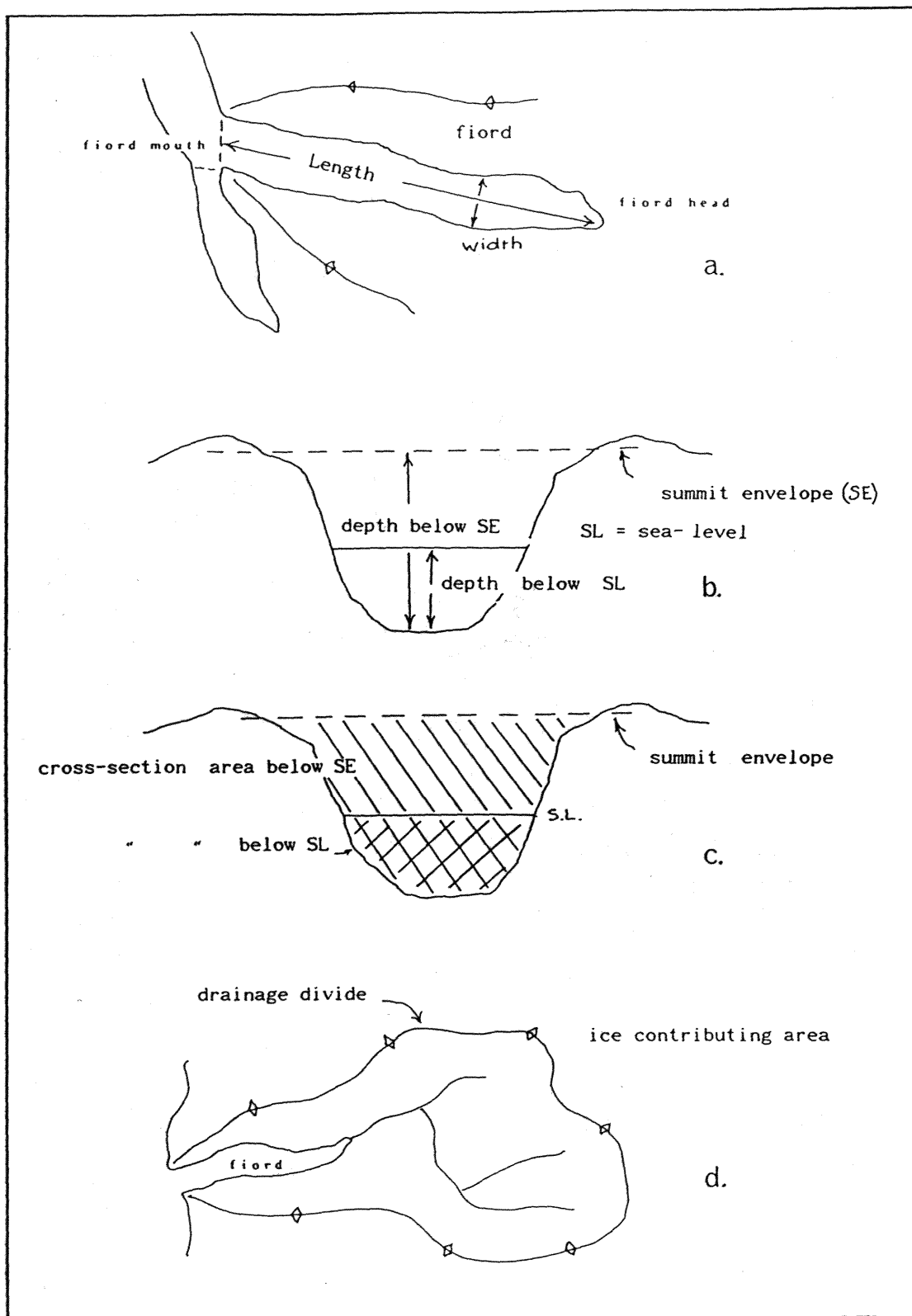


Figure 3.5. Description of fiord morphometry: (a) fiord width and length; (b) fiord depth below sea-level and depth below summit envelope; (c) fiord cross-sectional area below sea-level and below summit envelope; (d) ice contributing area to the fiord.

basins. The cross-sectional area for each outlet fiord is the mean of 5 measurements for each trough.

iv. Trough length: measured from the head to the mouth of the fiord trough. The mouth of the fiord was defined as being where the fiord enters the ocean, or where it joins another fiord. The head of the fiord is the upstream limit of inundation by the sea or lake (fig. 3.5a). In every fiord trough used in this study, bedrock (?) sills exist at the fiord mouth and at least one overdeepened basin is developed (Stanton and Pickard, 1981).

v. Ice contributing area: measured as the present day drainage area above the mouth of the fiord, and including the contribution of slopes above the fiord side walls (Fig. 3.5d). The problems and assumptions associated with this parameter have already been discussed.

The data generated for each fiord basin are given in Table 3.1. Individual data points have been deleted from the analysis where adequate bathymetric maps were not available. The location of the fiords is shown in Fig. 3.6.

### 3.3. Results and Discussion

All of the outlet trough form indices were found to have some degree of correlation with glacier contributing area (Fig. 3.7a-c). The glacier contributing area is the fiord system's equivalent of the total area of the drainage basin. The general form of the power equation relating valley length and catchment area is:

$$L_f = aA_f^b \quad (2)$$

$L_f$  is the fiord size factor,  $A_f$  is the ice contributing area. For equation (2) to be dimensionally balanced, the exponent  $b$  must have a value of 0.5 (Bull, 1975). If this is the case, then the relation between the variables is isometric because a change in fiord size will be directly proportional to a change in glacier contributing area. The concept of allometry can be defined as the analysis of proportional changes in the size of a geomorphic system, usually expressed in the form of a power equation (Bull, 1975; Church and Mark, 1980). Roberts and Rood (1984) found that fiord size parameters are proportionately



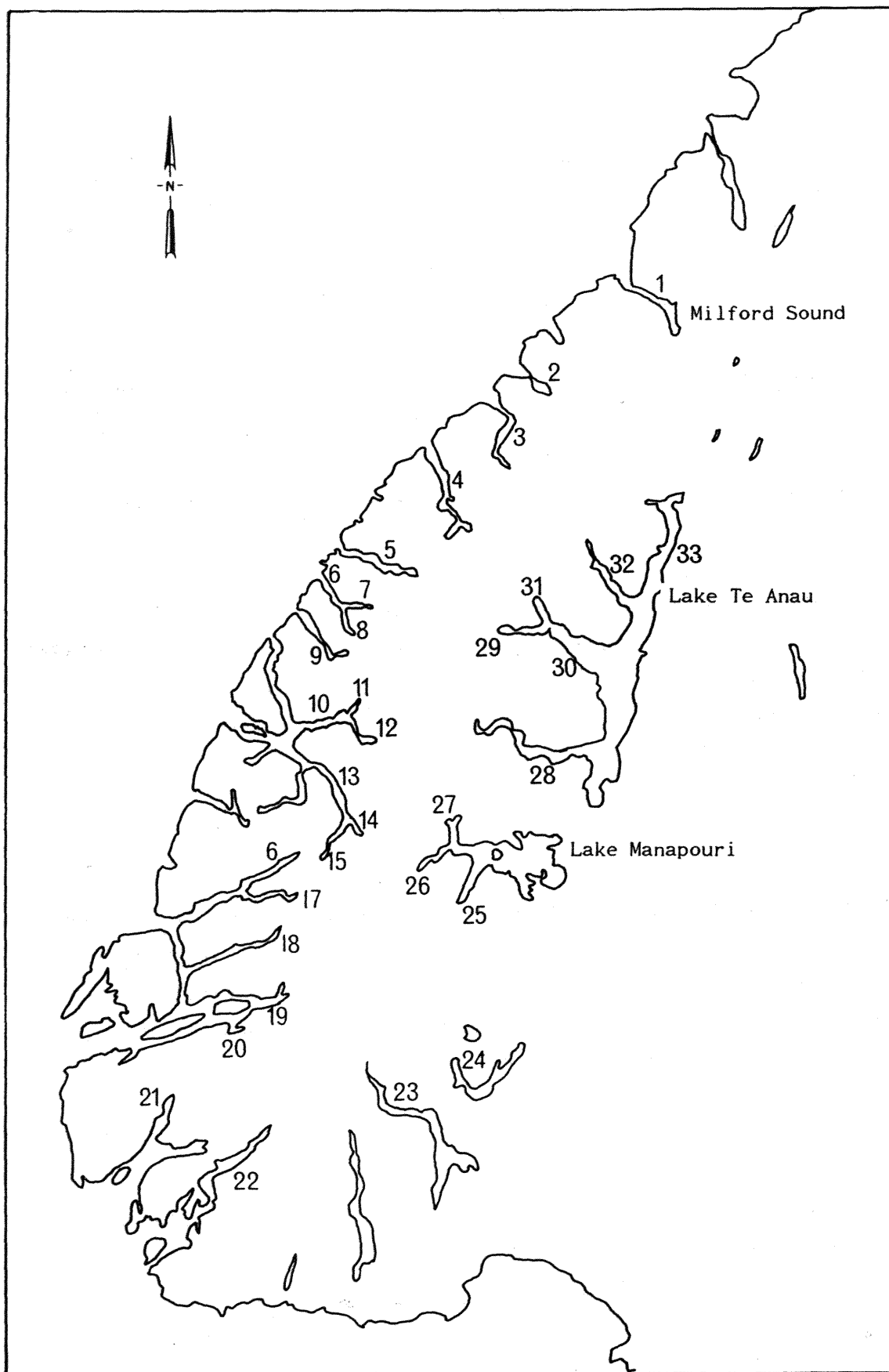


Figure 3.6. Location of the fiords used in this study. Numbers correspond to the fiords listed in Table 3.1.

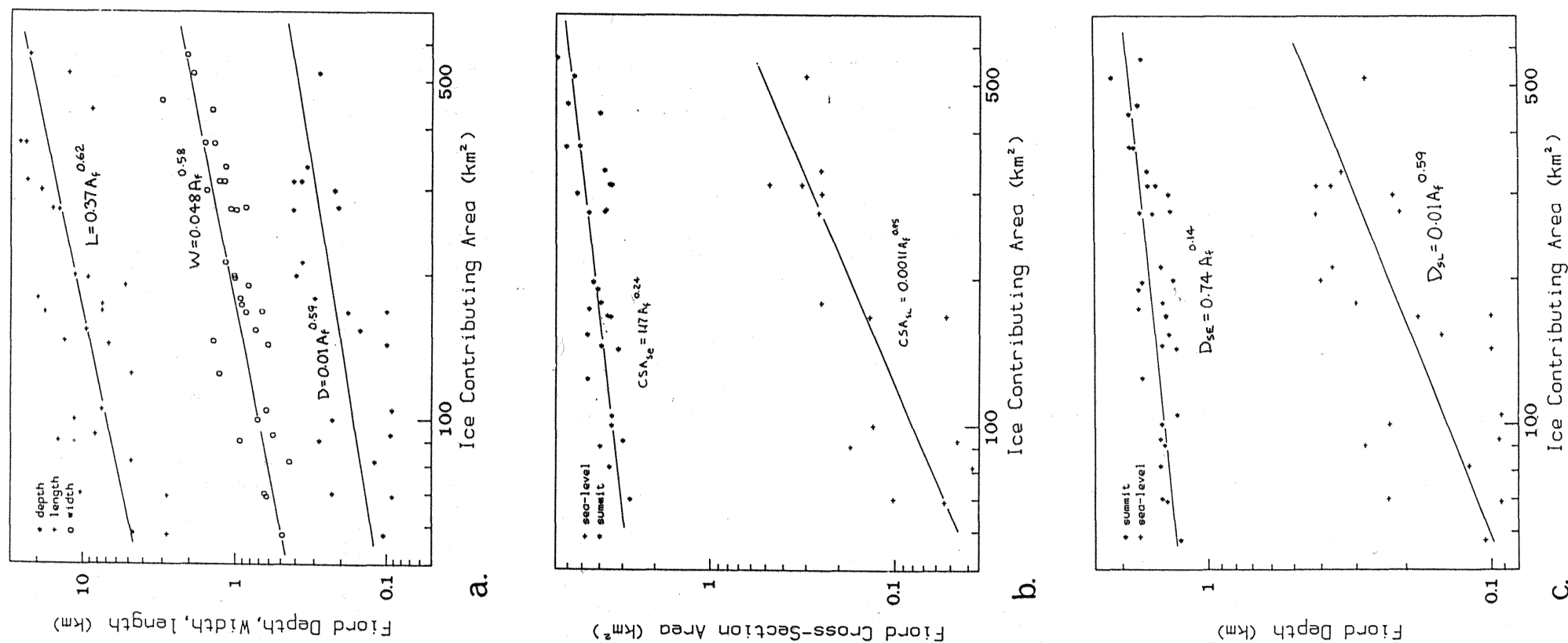


Figure 3.7. Relationship between ice contributing area and fiord size properties: (a) fiord length, width, and depth below sea-level; (b) fiord cross-sectional area below summit level envelope and sea-level; (c) fiord depth below summit level envelope and sea-level. SE = summit envelope SL = sea-level

Table 3.1. Size of some Fiordland outlet glacial troughs

Fiord	Width (km)	Depth Total (km)	Depth SL Below SL (km)	Cross-Section Area Total (km <sup>2</sup> )	Cross-Section Area Below SL (km <sup>2</sup> )	Length (km)	Catchment Area (km <sup>2</sup> )	Distance To Sea (km)
1. Milford Sound	1.94	2.17	0.278	5.55	0.302	12.5	519.2	14.0
2. Sutherland Sound	0.76	1.37	0.150	4.69	-----	9.50	152.8	15.0
3. Bligh Sound	0.88	1.40	0.181	3.49	0.137	17.8	166.6	17.5
4. George Sound	1.58	1.37	0.222	5.36	0.249	18.8	298.4	17.0
5. Caswell Sound	1.01	1.56	0.416	4.61	0.258	14.3	271.9	22.0
6. Emelius Arm	0.63	1.29	0.100	3.19	-----	6.80	142.6	21.3
7. Gold Arm	0.64	1.28	0.092	3.44	-----	7.50	104.4	18.5
8. Charles Sound	0.88	1.35	0.210	3.71	-----	-----	275.3	17.3
9. Nancy Sound	0.96	1.42	0.279	4.00	0.174	14.5	090.3	19.3
10. Bradshaw Basin	1.21	1.62	0.415	3.46	0.319	-----	311.0	27.0
11. Precipace Cove	0.64	1.39	0.092	3.93	0.054	2.80	069.1	22.0
12. Gaer Arm	0.69	1.40	0.100	3.64	0.053	7.50	167.4	28.8
13. Deep Cove	0.45	1.47	0.120	3.55	0.038	4.80	081.7	34.3
14. Hall Arm	0.58	1.47	0.094	3.01	0.046	8.30	092.9	28.0
15. Malaspina Arm	1.19	1.63	0.338	3.79	0.252	-----	332.7	30.5
16. Vancouver Arm	0.73	1.45	0.228	3.45	0.131	11.3	099.8	19.3
17. Broughton Arm	0.66	1.45	0.230	2.74	0.102	10.3	070.0	21.0
18. Wet Jacket Arm	0.96	1.44	0.300	3.95	0.250	19.8	178.2	26.0
19. Second Cove	1.20	1.46	0.364	-----	-----	-----	211.6	18.5
20. Fanny Bay	0.50	1.25	0.105	-----	-----	2.80	057.5	30.0
21. Edwardson Sound	1.05	1.32	0.400	-----	-----	11.3	198.6	23.3
22. Long Sound	1.31	1.52	0.368	4.18	0.480	23.3	311.3	41.0
23. Lake Hauroko	1.40	1.81	-----	6.13	-----	23.8	372.0	55.5
24. Lake Monowai	1.44	1.45	-----	3.94	-----	13.2	144.8	65.5
Lake Manapouri								
25. South Arm	1.45	1.88	-----	4.00	-----	8.80	436.8	51.3
26. West Arm	0.94	1.75	-----	4.59	-----	7.50	172.8	42.0
27. North Arm	0.85	1.75	-----	4.12	-----	5.30	189.5	41.5
Lake Te Anau								
28. South Fiord	1.62	1.87	-----	5.16	-----	26.0	373.0	35.8
29. Middle Fiord	3.13	1.75	-----	6.01	-----	-----	456.5	36.0
30. South-West Arm	1.04	1.70	-----	4.35	-----	9.30	196.2	30.8
31. North Fiord	1.10	1.73	-----	3.77	-----	15.8	273.1	28.7
32. North-West Arm	1.31	1.70	-----	4.68	-----	4.80	123.8	29.0
33. Camp Basin	2.13	1.70	-----	6.87	-----	22.3	568.0	32.8

SL = sea-level, total = below summit envelope.

adjusted to variations in glacier contributing area following the form of equation (2). When  $b < 0.5$ , this is the condition of negative isometry, whilst  $b > 0.5$  reflects the condition of positive allometry.

Varying degrees of negative and near perfect isometry were obtained for the regression of fiord size variables against glacier contributing area (Tables 3.2-4). The variables fiord depth below sea level, and fiord width and length, displayed near perfect isometry. Fiord depth below the summit envelope and fiord cross-section area displayed varying degrees of negative isometry. This suggests that the erosion of the outlet troughs increased in direct proportion to the volume of ice discharged through them (Fig. 3.7). That is, with increases in glacier discharge through the channel and/or ice velocity, erosional adjustment will be by a proportional increase in fiord deepening, widening and lengthening.

However, fiord depth below the summit envelope displays considerable negative isometry, indicating a slow response of overall fiord deepening to increases in ice discharge. This suggests that fiord troughs are equilibrium forms well adjusted to discharge. The results are displayed in Fig. 3.7. All of the morphometric parameters employed in this study were found to be significantly correlated with glacier contributing area at the 95% confidence level (Table 3.2).

Deviation of the residuals from the regression surface larger than the standard error of estimate suggest the presence of anomalously large or small fiords, although the regression equation itself is not a true expression of the relationship between trough size and the volume of ice discharged through it. It is merely the expression best fitting the data and so includes the effects of other factors. This means that small deviations from the regression surface cannot be accorded any geomorphological significance, although several deviations do appear to have geomorphological explanations.

The fact that glacial troughs are equilibrium forms whose size is related to the volume of ice discharged through them has long been recognized. Penck (1905), termed this relationship the law of adjusted cross-sections, a theme developed for glacierized basins by Haynes (1972) and Roberts and Rood (1984). In the Fiordland region several of the fiords are anomalously deep with respect to the size of their catchments. In particular, Caswell Sound is anomalously deep relative

Table 3.2. Comparison of Correlations and regressions for different regions

Correlation Coefficient This Study      Haynes (1972)		t This Study	p This Study	Coefficient of Determination This Study      Roberts & Rood (1984)      Haynes (1972)		
$r_{1,7} = 0.84$	$r_{4,7} = 0.71$	8.51	.0005	$R_{1,7} = 70.0$	$R_{1,7} = 48.2$	$R_{4,7} = 50.93$
$r_{2,7} = 0.66$		4.83	.0005	$R_{2,7} = 42.9$	$R_{6,7} = 82.7$	
$r_{3,7} = 0.64$		3.76	.001	$R_{3,7} = 41.4$		
$r_{4,7} = 0.68$		4.93	.0005	$R_{4,7} = 46.5$		
$r_{5,7} = 0.78$		4.51	.0005	$R_{5,7} = 61.0$		
$r_{6,7} = 0.67$		4.62	.0005	$R_{6,7} = 45.1$		
$R_{4,74} = 0.65$	$R_{4,74} = 0.93$	4.50	.005	$R_{4,74} = 46.9$		$R_{4,74} = 86.97$
$R_{2,74} = 0.70$		3.8	.0005	$R_{2,74} = 49.2$		
$R_{6,74} = 0.68$		3.95	.0005	$R_{6,74} = 45.7$		

1 = fiord width, 2 = fiord depth below summit envelop, 3 = fiord depth below sea level, 4 = fiord cross-section area below summit envelop, 5 = fiord cross-section area below sea-level, 6 = fiord length, 7 = drainage basin area, 8 = distance from sea.  
t = Student's t distribution, p = level of significance.

Table 3.3. Comparison Of Regression Equations

Regression Equations This Study	Roberts & Rood (1984)	Haynes (1972)
$\log y_1 = -1.32 + 0.58 \log x_7$ $\log y_2 = -0.129 + 0.14 \log x_7$ $\log y_3 = -1.99 + 0.59 \log x_7$ $\log y_4 = -0.068 + 0.24 \log x_7$ $\log y_5 = -2.95 + 0.95 \log x_7$ $\log y_6 = -0.44 + 0.62 \log x_7$ $\log y_3 = -0.26 + 0.130 \log x_4 + 0.12 \log x_7$ $\log y_4 = 0.034 + 0.234 \log x_7 + 0.033 \log x_8$ $\log y_6 = -0.076 - 0.200 \log x_4 + 0.620 \log x_7$	$\log y_1 = -0.478 + 0.245 \log x_7$ $\log y_3 = -1.61 + 0.355 \log x_7$ $\log y_6 = -0.049 + 0.48 \log x_7$	$\log y_4 = -0.23 + 0.387 \log x_7$  $\log y_4 = 0.144 + 0.523 \log x_7 - 0.077 \log x_8$

Shows relationship between catchment areas (y) trough size parameters (x). Subscript numbers as given in Table 3.2.

Table 3.4. Comparison of Power Equations

Power Equations This study	Roberts & Rood (1984)	Haynes (1972)
$y_1 = 0.048 A_f^{0.58}$ $0.48 < b < 0.68$	$y_1 = 0.333 A_f^{0.25}$ $0.1 < b < 0.4$	$y_4 = 0.589 A_f^{0.39}$
$y_2 = 0.74 A_f^{0.14}$ $0.1 < b < 0.18$	$y_3 = 0.025 A_f^{0.36}$ $0.21 < b < 0.51$	
$y_3 = 0.01 A_f^{0.59}$ $0.4 < b < 0.78$		
$y_4 = 1.17 A_f^{0.24}$ $0.17 < b < 0.31$		
$y_5 = 0.0011 A_f^{0.95}$ $0.72 < b < 1.18$	$y_6 = 0.893 A_f^{0.48}$ $0.35 < b < 0.61$	
$y_6 = 0.366 A_f^{0.62}$ $0.42 < b < 0.64$		

$A_t$  = ice contributing area to outlet troughs

$y$  = trough size parameters, subscript numbers as in Table 3.2

$b$  = power equation exponent ( $y = ax^b$ )

to sea level, a factor that may be explained by lithology, structure and/or the addition of ice from adjacent catchments. Unfortunately, little is known of the structure of the area, so that the possibility of potential glacier exploitation of a weakened fault zone cannot be evaluated. Caswell Sound is located well to the north of the Murchison ice-centre (Fig. 3.4), so the addition of ice from outside the catchment is unlikely to have been a significant contributing factor to the glacial overdeepening of the fiord.

Several of the major outlet troughs are anomalously shallow with respect to sea-level, such as: Bounty Basin, Bligh Sound; Elder Basin, George Sound; Hall Arm, Doubtful Sound; and Sutherland Sound. The apparent 'under-development' of Bligh, George and Sutherland sounds can be attributed to a changing tectonic regime and uplift following the development of the equilibrium glacial system in the mid-Pleistocene.

Overwidening of the outlet troughs is another feature displayed by several of the fiords. Arran Basin and Middle Fiord, Lake Te Anau; lakes Monowai and Hauroko are good examples, and can generally be explained by preferential glacier exploitation of weakened rock at the faulted contact of the Fiordland crystalline basement rocks with the relatively soft Tertiary sediments to the east (Fig. 2.1b). However, the contribution of post-glacial sediment infill to the shallowing of the troughs cannot be underestimated, as shown by the frequently broad, flat trough floors. As these troughs are distally located with respect to the ice-centres, the additional factor of ice contribution from outside the catchment may be a minor, but certainly not the dominant factor in the overwidening of the troughs.

Comparison of the power equations and coefficients of determination derived in this study with those of Roberts and Rood (1984) and Haynes (1972) (Table 3.4), indicates some interesting differences. Roberts and Rood used a principal axis approach to the least squares estimation. This required recalculation of the power equations from their data to enable a comparison with the power equations developed for Fiordland. Roberts and Rood (1984) compared Hack's (1957) power equation relating stream length to catchment area, against their fiord length equation:

$$\begin{aligned} L_d &= 5.1A_d^{0.6} & (\text{Hack, 1957}) \\ \frac{L_d}{L_f} &= \frac{5.1A_d^{0.6}}{0.81A_f^{0.5}} = 6.3A_f^{0.1} & (3) \\ L_f &= 0.81A_f^{0.5} & (\text{Roberts and Rood, 1984}) \end{aligned}$$

where  $L_d$  and  $L_f$  are stream length and fiord length, whilst  $A_d$  and  $A_f$  are stream catchment area and ice contributing area respectively. Since the exponents are nearly equivalent, the coefficient 'a' was considered to be indicative of the scale difference between the systems, implying that stream lengths are at least six times as long as the measured fiord lengths over the range of drainage basin/ice contributing areas considered. A similar comparison of the power equations derived from this study and those of Haynes (1972) and Roberts and Rood (1984) gave the following results:

$$\begin{aligned} L_a &= 0.366A_f^{0.62} \\ \frac{L_a}{L_r} &= \frac{0.366A_f^{0.62}}{0.893A_f^{0.48}} = 0.41A_f^{0.14} & (4) \\ L_r &= 0.893A_f^{0.48} \end{aligned}$$

$$\begin{aligned} D_a &= 0.01A_f^{0.59} \\ \frac{D_a}{D_r} &= \frac{0.01A_f^{0.59}}{0.025A_f^{0.36}} = 0.4A_f^{0.23} & (5) \\ D_r &= 0.025A_f^{0.36} \end{aligned}$$

$$\begin{aligned} CSA_a &= 1.17A_f^{0.24} \\ \frac{CSA_a}{CSA_h} &= \frac{1.17A_f^{0.24}}{0.59A_f^{0.39}} = 1.98A_f^{0.15} & (6) \\ CSA_h &= 0.59A_f^{0.39} \end{aligned}$$

where  $L_a$  = fiord lengths obtained in this study;  $L_r$  = fiord lengths obtained by Roberts and Rood (1984);  $D_a$  = fiord depths obtained in this study;  $D_r$  = fiord depths obtained by Roberts and Rood (1984);  $CSA_a$  = fiord cross-sectional areas obtained in this study; and  $CSA_h$  = fiord cross-sectional area obtained by Haynes (1972).

Fiord width 'b' exponent obtained for the Fiordland troughs is significantly different to that of Roberts and Rood (1984) (Table 3.4), negating the validity of a comparison of these factors. However, equation (5) suggests that the British Columbia fiords are 2.5 times the depth of their Fiordland counterparts over the range of glacier contributing areas considered. Similarly, examination of equation (4) suggests that the fiords developed in British Columbia are 2.4 times longer than their New Zealand counterparts for the same glacier contributing area. Conversely, outlet troughs from the West Greenland



Ice Sheet are only half the cross-sectional area of the New Zealand fiords (equation 6). This difference suggests more intense glacier erosion for the temperate outlet glaciers of Fiordland. The marked 'over-lengthening' of the British Columbia fiords relative to the New Zealand fiords suggests either: (1) a fundamental difference in erosion processes between the two regions; or (2) differences in controls on the point of fiord overdeepening, and thus, mode of erosional development of the fiord. In Fiordland the length of the fiord troughs is largely constrained by the lithological and tectonic boundaries of the Fiordland Block, beyond which overdeepened troughs are not developed (Fig. 2.19).

The examination of the Fiordland glacial system suggests that the outlet troughs are probably equilibrium forms adjusted to the maximum ice volume discharged through them. As long as the glaciers in subsequent glaciations attain similar or reduced levels with similar glacial conditions, this equilibrium trough form should be maintained and slowly enlarged. This model can be used to examine the forms of glacierized troughs formed elsewhere in the Southern Alps, and to assess the influence of such factors as bedrock structure and rock mass strength on trough development.

### 3.4. Implications For Southern Alps Glacial Trough Development

An objective of this study was to examine the influence of the geotechnical properties of the rock mass upon the development of the glacierized troughs contained thereon. Hence, it was necessary to identify the effect of the various factors that are thought to be controlling erosion and development of the trough form. The study region must comprise relatively uniform, massive, near structureless bedrock, so that structural control on the development of the glacial troughs is minimized. This will enable the isolation of the input of the glaciological characteristics to the model. An important prerequisite is that the form of the subglacially moulded trough is known, and that the processes are acting uniformly across the area. Unfortunately, the trough morphology is rarely preserved after deglaciation due to destabilization and failure of the oversteepened rock slopes. Consequently, a region of high rock mass strength and stability, preserving the details of the glacial moulding, is required.

A further pre-requisite is that the troughs examined are equilibrium trough forms developed during maximal glacial conditions. In a study of the Laurentide ice-sheet, Sugden (1978) argued that intense, long period glacierization develops troughs that are essentially adjusted to the maximum discharge of ice through them. An area of relative structural and geotechnical uniformity exists in the form of the intensely glacierized Fiordland Block.

Analysis of fiord trough form and size in Fiordland indicates that the size of the outlet trough is adjusted to the volume of ice discharged through it, although the trough form differs between northern and south-central Fiordland. This methodology was applied to the examination of glacially overdeepened inland lakes on the eastern side of the Southern Alps (Table 3.5; Fig. 3.8). However, these inland lakes cannot be directly correlated with each other or the Fiordland basins, because there is no suitable constant datum from which to measure the trough size parameters. Lake level is of little utility, other than locally since different amounts of aggradation (differing sedimentation rates (Pickrill and Irwin, 1983)) have occurred, and other than at lakes Pukaki, Tekapo, and Ohau, the glacial sequences are not sufficiently well documented for dated lateral moraines to be used as datum surfaces.

Application of the best-fit regression surfaces and equations developed for the Fiordland outlet troughs, to the inland lakes developed in the schist and greywacke/argillite on the eastern side of the Main Divide, allows some evaluation of the mode of erosional development of the inland lakes. Examination of Fig. 3.9 indicates that lakes such as Wanaka, Tekapo and Pukaki are all over-widened with respect to the Fiordland equilibrium glacial system. To a first approximation, glacial exploitation and erosion of the densely jointed and foliated schists and greywacke valleys appears to be by preferential widening rather than deepening.

### 3.5. Comparison With Some Antarctic Outlet Glacier Troughs

Ice streams are the most dynamic element of large ice sheets, they are lubricated by water at the bed and slide rapidly with velocities in excess of several hundred metres per year (Drewry, 1983). Consequently, it would be expected that they would be the dominant element in the erosion of the bedrock producing such features as

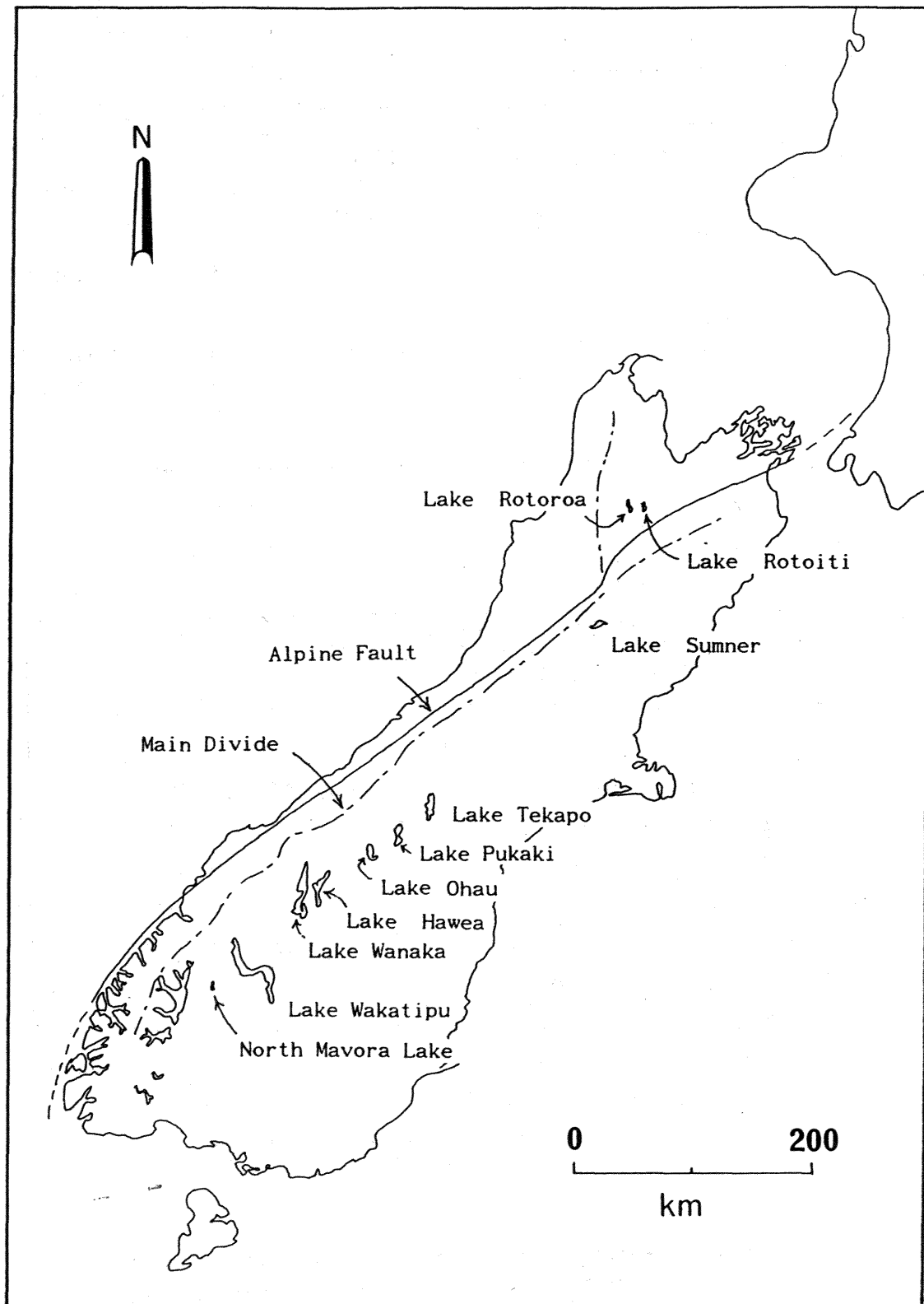


Figure 3.8. Location of the lakes used in this study, eastern side of the Main Divide of the Southern Alps.

Table 3.5. Dimensions of the inland lakes

Lake Name	Width (km)	Depth (km)	Length (km)	Catchment area (km <sup>2</sup> )
1. Lake Rotoroa	1.2	0.145	10.0	346
2. Lake Rotoiti	0.48	0.072	4.8	185
3. Lake Sumner	1.77	0.135	6.5	275
4. Lake Tekapo	6.55	0.170	12.8	968
5. Lake Pukaki	9.35	0.130	16.5	1075
6. Lake Ohau	3.9	0.129	10.5	964
7. Lake Hawea	2.1	0.160	19.0	852
8. Lake Wanaka	3.7	0.311	14.0	1159
9. Lake Wakatipu	4.2	0.380	26.9	1732
10. North Mavora Lake	0.95	0.077	11.0	277

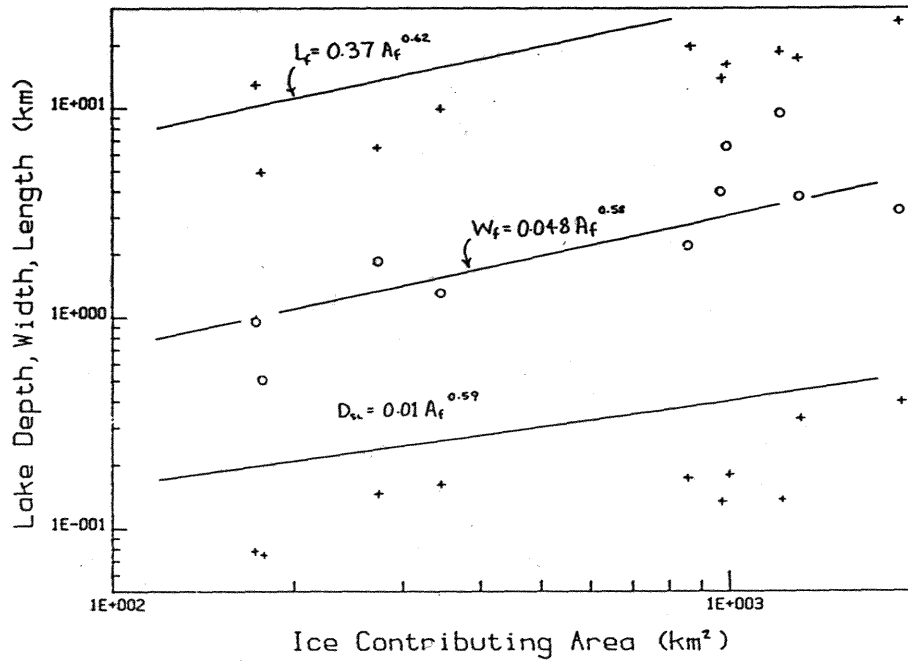


Figure 3.9. Comparison of the size and glacier contributing areas for the inland lakes with the best-fit equations developed for the Fiordland outlet troughs. Note the generally undersize nature of the lake basins, although a tendency towards overwidening is developed for the troughs cut into greywacke basement.

troughs and fiords (Sugden, 1978; McIntyre, 1985a). Ice streams characterized by deeply incised beds are rather like true outlet glaciers despite their lack of visible confining walls (Bentley, 1987). Small East Antarctic ice streams have surface profile that are not greatly different from the standard equilibrium profile for sheet flow ice, although they do show the characteristic concave upwards profile towards the coast (McIntyre, 1985a). Driving stresses peak near the coast in both East Antarctic ice streams and outlet glaciers. In configuration, ice flux and driving stress, there is little difference between ice streams such as the Lambert Glacier and outlet glaciers such as the Byrd (Bentley, 1987).

The West Antarctic outlet glaciers differ from their East Antarctic counterparts in having relatively poorly developed subglacial troughs, and lower surface elevations. This is probably due to the deep-lying glacial floor in West Antarctica rather than any inherently different character of the ice streams themselves (Bentley, 1987). However, the ice streams draining into the Ross Ice Shelf occupy wide, relatively shallow depressions of only a few hundred metres depth (Rose, 1979; Shabtaie *et al.*, 1987) contrasting with the deep bedrock troughs excavated by large outlet troughs draining the East Antarctic ice sheet. Drewry and Robin (1983) suggested that the subtle bedform associated with active ice streams in West Antarctica may mean that the ice flow in this area is either relatively youthful or transient. The Marie Byrd Land ice streams are more closely related to ice shelves than to terrestrial ice, and appear to represent landward extensions of the ice shelf (McIntyre, 1985a). Their behaviour is consistent with ice which is flowing under the influence of lateral spreading rather than the basal shearing which dominates terrestrial ice flow.

Haynes (1972) in Greenland, and Sugden (1978) for the Laurentide ice sheet, suggested that a strong relationship exists between the size of the outlet glacier and the discharge (ice flux) through them. A limited study was undertaken to test for the development of similar relationships with the Antarctic ice streams and outlet glaciers. Best-fit regression equations were obtained for the relationship between ice stream depth and width, and glacier contributing area. Insufficient information was available on the flux of the Antarctic outlet glaciers, necessitating the application of glacier contributing area as a surrogate index. Antarctic trough size data are given in Tables 3.6 & 3.7, and correlations displayed graphically in Fig. 3.10.

Table 3.6. Correlations, regressions and power equations developed for Antarctic outlet troughs and ice streams.

Correlation Coefficient	t	p	Coefficient of Determination	Power Equation
$r_{W,A} = 0.94$	11.84	.0005	$R_{W,A} = 87.5$	$y_W = 0.387 A_f^{0.34}$ $0.17 < b < 0.51$
$r_{D,A} = 0.79$	4.82	.0005	$R_{D,A} = 62.4$	$y_D = 0.089 A_f^{0.23}$ $-0.03 < b < 0.44$

Subscript W = trough width, D = trough depth, A = ice contributing area,

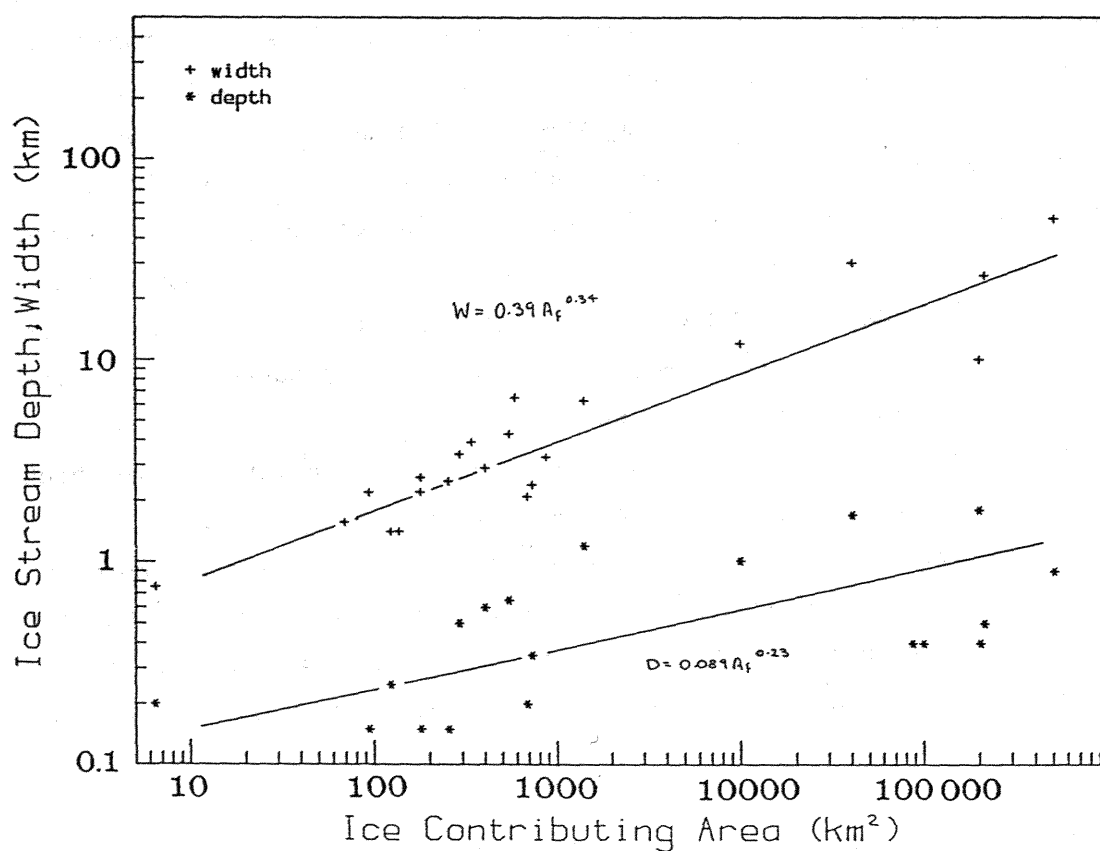


Figure 3.10. Relationship between glacier contributing areas and Antarctic outlet ice stream properties of width and depth.

Table 3.7. Selected morphometric properties of some Antarctic outlet glaciers and ice streams.

Outlet Trough	Ice Contributing Area (km <sup>2</sup> )	Ice Stream Width (km)	Depth of glaciers (km)	Glacier Velocity (km/yr)
Koettlitz Glacier	290	3.4	0.5	
Victoria Upper	180	2.6	0.15	
Walcott Glacier	69	1.56	-	
Hobbs Glacier	94	2.2	0.15	
Webb Glacier	124	1.4	0.25	
Ironside Glacier	874	3.3	-	
Recoil Glacier	545	4.3	0.65	
Stafford Glacier	179	2.2	-	
Cosmonaut Glacier	731	2.4	0.35	
Heartfield Glacier	253	2.5	0.15	
Parker Glacier	137	1.4	-	
Ice Breaker Glacier	588	6.5	-	
Fitzgerald Glacier	338	3.9	-	
Pitkevitch Glacier	402	2.9	0.6	
Pilot Glacier	685	2.1	0.2	
Packard Glacier	6.4	0.75	0.2	
Taylor Glacier ^	1410	6.3	1.2	0.01
Hays Glacier +	10,000	12.0	1.01	1.0
Lambert Glacier *	986,000	54	2.6	0.25
Rutford Ice Stream ~	40,500	30	1.7	0.4
Pine Island Glacier #	214,000	26	0.5	2.1
Shiraze Glacier !	200,000	10	1.8	2.5

Sources: + Meier (1983), \* McIntyre (1985b), ^ Robinson (1984), ~ Morgan *et al.* (1982), Crabtree and Doake (1982), ! Fujii (1981). All others interpolated from U.S.G.S 1:250,000 reconnaissance topographic maps.



Comparison of the power equations calculated for the Fiordland and Antarctic outlet troughs was attempted, although detailed geomorphic interpretations were not possible.

$$\begin{aligned} W_a &= 0.387A_f^{0.34} \\ \frac{\quad}{\quad} &= 8.06A_f^{0.24} \end{aligned} \quad (7)$$

$$W_f = 0.048A_f^{0.58}$$

$$\begin{aligned} D_a &= 0.089A_f^{0.23} \\ \frac{\quad}{\quad} &= 0.076A_f^{0.01} \end{aligned} \quad (8)$$

$$D_f = 1.17A_f^{0.24}$$

where  $W_a$  and  $D_a$  refer to the power equation developed for the width and depth of the Antarctic outlet troughs respectively;  $W_f$  and  $D_f$  refer to the equations developed for the width and depth below the planation surface for the Fiordland troughs.

Nevertheless, the results suggest that the Antarctic outlet glaciers and ice streams are adjusted to glacier discharge as was argued by Bentley (1987), and the Antarctic outlet glacier troughs are significantly wider than their Fiordland counterparts over the range of glacier contributing areas considered (equation 7). However, examination of equation (8) suggests significant relative over-deepening of the Fiordland troughs.

Examination of equation (9) shows that the Antarctic outlet trough widths are of similar proportional adjustment to ice flux to that of their British Columbia counterparts.

$$\begin{aligned} W_a &= 0.387A_f^{0.34} \\ \frac{\quad}{\quad} &= 1.16A_f^{0.09} \end{aligned} \quad (9)$$

$$W_r = 0.333A_f^{0.25}$$

where  $W_r$  refers to the power equation for fiord width in British Columbia.

The Antarctic outlet glaciers and ice streams are apparently overwidened, but under-deepened with respect to the equivalent elements in the Fiordland glacial landscape. The over-size nature of the Antarctic outlet troughs is probably a consequence of trough enlargement during earlier periods of high discharge, rather than development in accordance with the ice volumes supplied by the present

ice-divides. This follows the model of development of outlet troughs draining the Laurentide ice sheet (Sugden, 1978; England, 1986), with the present outlet glaciers not being sufficiently active to generate significant changes in trough size and form.

Comparison of the shapes of Antarctic outlet troughs, both presently ice-free (Aniya and Welch, 1981a) and subglacial (Drewry, 1972), indicates that the outlet troughs have attained a constant near parabolic form, minimally modified by subsequent glacial erosion. The present forms of the Antarctic outlet glacial troughs are probably a consequence of the predominance of slow abrasion at the base of the glaciers and the long period of glacial occupation (P. Wellman, 1988). This follows Boulton (1974), Roberts and Rood (1984) in suggesting that in the early stages of glacial erosion, such as the relatively youthful glacial valleys in the New Zealand Southern Alps, glacial deepening proceeds more rapidly than widening. However, with increasing length of occupation and scale, there is an almost exclusive tendency towards trough widening. This may also be explained by limiting conditions for glacial erosion, whereby once a certain glacier thickness and velocity is attained, the glacier can no longer scour its bed, and lodgement and preferential widening will occur (Boulton, 1974).

There is considerable variation in the subglacial conditions operating at the scale of the Antarctic outlet glaciers and ice streams. McIntyre (1985a) argued that many of the large outlet glaciers draining the East Antarctic ice sheet are at pressure melting point at their base, allowing the erosion and persistence of overdeepened subglacial troughs. However, the smaller outlet glaciers draining through the Transantarctic Mountains in the Ross Sea region are probably largely frozen to their bases, although Drewry (1982) and Robinson (1984) showed that limited areas of subglacial water exit. Thus, the process of erosional development of the Antarctic outlet troughs is largely a product of their age and size.

### 3.6. Summary and Conclusions

Outlet glacier trough size, and to a certain extent shape, appears to be controlled by the glacier flux through them. This relationship appears to hold in glacial systems of all types and scales. Closer examination of the relationship for the glacial troughs developed in

the New Zealand Southern Alps suggests that glacial exploitation and erosion of the closely jointed and foliated schist and greywacke valleys appears to be by preferential widening rather than deepening. Thus, whilst glacier discharge directly controls the size of the outlet troughs, the properties of the host bedrock may influence the final trough shape. This will be considered more fully in the following chapters.

## **Chapter Four**

### **Rock Mass Strength**

**Controls on the Morphology and**

**Stability of Glacial Valley Slopes**

## CHAPTER FOUR: ROCK MASS STRENGTH CONTROLS ON THE MORPHOLOGY AND STABILITY OF GLACIAL VALLEY SLOPES

### 4.1. Introduction

The Rock Mass Strength (RMS) classification of Selby (1980), as modified by Moon (1984), was applied to recently deglaciated trough slopes in a variety of terrains in the vicinity of the Main Divide of the Southern Alps. This was to enable the examination of the influence of rock mass properties on variation in glacial trough form and development. The RMS method has been applied successfully in a wide variety of climate and landform systems from the Namib Desert to Antarctica (Selby, 1980). Slopes adjusted to their RMS are common in nature, and the frequent recognition of oversteepened slopes undercut by erosion processes, and structurally controlled rock benches of lower slope angle, indicates its utility in resistance-form studies. This method has been rigorously tested by Moon and Selby (1983), Moon (1984, 1986) and Abrahams and Parsons (1987) as a reliable method of stability analysis for geomorphic purposes. It is a modification of existing engineering geology rock mass classifications (e.g., Bienawski, 1974, 1979).

Glacially oversteepened slopes have a brief life-span in most recently deglaciated alpine valleys (Luckman, 1976; Bovis, 1982). The slopes tend to evolve towards strength equilibrium slopes as cross-joints open in the rock mass, and as joint blocks rotate, slide, or fall (Selby, 1982). To test this hypothesis in glacial environments, recently deglaciated valleys in the Southern Alps, developed in a variety of rock types, were examined. The RMS classification was applied to detect controls on slope form, and to test for progressive development of equilibrium slopes with time and distance from the glacier snout.

### 4.2. Controls on the Stability of Alpine Rock Slopes.

In many studies of alpine geomorphology, steep rock walls have received little attention (Embleton and Whalley, 1979; Caine, 1982), either because their development appears to be intuitively simple or due to difficulties of fieldwork. In the Canadian Rockies and granites/gneisses of western Norway, most of the stability problems

arise in glacially undercut slopes re-equilibrating to the changed stress conditions produced by undercutting and removal of the buttressing glacier (Barton, 1971; Bovis, 1982; Savage and Varnes, 1987). Most of the unstable rock slopes probably fail during and shortly after glacier retreat (Bjerrum and Jorstad, 1968; Whalley *et al.*, 1983). However, failures are not limited to this period. From the degree of lichen development on the talus deposits and the fresh scars on the rock slopes, it is evident that the processes have continued through time and are still quite active today.

Rock falls and slides of cohesive rock are the most common slope degradation processes. The geometry and kinematics of the slides tend to be controlled by discontinuities in the slide mass (Cruden, 1976; Bruce and Cruden, 1977). Typically, the major part of the rupture surface is parallel to bedding, or on the controlling discontinuity set, with movement caused by erosion at the foot and lateral margins of the block (Bruce and Cruden, 1977).

However, in the Coast Mountains of British Columbia (Ryder, 1981; Bovis, 1982) and western Norway (Bjerrum and Jorstad, 1968), it was noted that competent, massive rock often displays sufficient strength to maintain stable steep slopes of considerable height. The stability is dependent on factors that change with time and the result is a gradual deterioration of conditions until sliding occurs. The rate of loss of stability depends on local factors such as topography, nature and structure of the rockmass, and climatic conditions. The climatic conditions include the influence of snow-melt, which increases the water pressure in the joints, and of freeze/thaw on rock shatter and rock weakening. Whalley *et al.* (1983) postulated that during deglaciation high cleft water pressures would have occurred in rock joints favourably oriented with respect to the glacier, reducing the mass strength and stable angle with respect to sliding.

To obtain some understanding of why the failure of glacial valley rock slopes has occurred, the problem has to be considerably simplified. In each area it is assumed that the pre-glacial rock mass stood at an angle below that of its limiting stability as governed by the RMS, and only with the glacial erosional undercutting of the slopes did these rock masses develop steep-sided troughs. A rock slope is able to support a load in unconfined compression so that the rock mass as a whole does behave like a cohesive body. The shear plane

limits the vertical height of the slope, and will be modified to form a 'zig-zag' zone through the rock mass due to its discontinuous nature.

At the same time as the slope is created and enhanced through the removal of the outermost part of the rock mass, internal stress conditions often result in the development of a zone of tension in the upper part of the slope (Scheidegger, 1963; Stacey, 1973). The stress input to the slope development will be considered more fully in Ch.7. When a steep slope has been created, regardless of the lithology, the geometry of the rock mass weaknesses often makes failure inevitable (Selby, 1982). The factors that have perpetuated failure through time are the internal factors active within a rock mass. These are: (1) residual, self weight and tectonically induced stresses; (2) cleft water pressure; (3) degree of weathering of the rock mass (Wywroll, 1977); and 4) joint propagation in the rock slope (Selby, 1982).

Inductive work on alpine cliffs has emphasized two aspects: (1) their form, especially with respect to structural controls and rock strength (Selby, 1982); and (2) their role as the source of debris input to the talus slopes beneath them (Gardner, 1980; Statham and Francis, 1986). Collapse of the cliff face by slab failure is probably a strain-controlled process, i.e., with accelerating motion until a critical threshold is passed and failure occurs. During the period preceding ultimate failure, fractures should be propagated along potential shear surfaces and previously intact rock until the effective resistance of the rock to sliding is reduced to that of the shear strength along its fractures and joints (Selby, 1982). Thus, it is not only the intact strength properties of the rock mass, but the geometry, spacing and width of the rock joints that are the main controls on the stability of steep rock slopes.

#### 4.3. Methodology

##### 4.3.1. Introduction

Several methods of RMS assessment have been proposed (Bienawski, 1974, 1979; Selby, 1980). This study uses Selby's (1980) classification, with further breakdown of the measured parameters using the modified RMS chart of Moon (1984). Eight parameters are incorporated in the classification system. These are: intact rock

strength, joint width, joint spacing, continuity, joint orientation, state of rock weathering, joint roughness and groundwater outflow. To each of these is allotted a weighting dependent on the relative influence of that parameter. Each parameter was given a rating (r) on a discontinuous scale (Moon, 1984). The sum of r's for the rockmass is known as the rock mass strength (RMS) rating. The advantage of the system is that it is easily applied in the field, using portable equipment.

#### 4.3.2. Techniques

Measurements of the RMS properties followed the method given in Selby (1980), and each parameter was weighted according to the modified scale of Moon (1984) (Table 4.1). For the graphical representation of the system, the total RMS rating is plotted against slope inclination at each site (Fig. 4.1). Superimposed on the plot is the RMS envelope as refined by Abrahams and Parsons (1987). The results of the RMS profiles will be compared from region to region.

Geomorphologists have long recognized that slope failure frequently occurs along discontinuities such as joints, bedding planes, foliations and faults rather than through intact rock (e.g., Barton and Choubey, 1977). As suggested by Brown (1981), no distinction between joint sets was made when measuring joint spacing at each profile site. This was largely due to frequent inability to decipher individual joint sets due to the apparently random nature of the fractures in the slope. Scanline surveys were from 5-25 m in length. In any attempt to assess RMS influence on glacial erosion processes, the random fractures are undoubtedly of paramount importance in controlling the size of the joint blocks available for glacial plucking.

### 4.4. Regional Rock Mass Strength

#### 4.4.1. Darran Mountains Region

The Darran Mountains region of northern Fiordland is largely comprised of massive, structureless gabbro and diorite. The RMS-slope inclination relationship for all sites is shown in Fig. 4.2a. It is immediately apparent that many of the steep slope profiles fall within the strength equilibrium region of the graph. Many of the lower slope



Table 4.1. Geomorphological rock mass strength measurement system.  
After Moon (1984).

	Very strong				Strong				Moderate				Weak				Very weak			
Intact strength Rating	100-70	69-57	56-53	52-50	49-48	47-46	45-44	43-42	41-40	39-38	37-36	35-33	32-29	28-25	24-17	<17				
	20	19	18	17	16	15	14	13	12	11	10	9	8	7	6	5				
Weathering Rating	Unweathered				Slightly weathered				Moderately weathered				Highly weathered				Completely weathered			
	10				9				7				5				3			
Joint spacing (m)	>3	3-	2.2-	1.9-	1.6-	1.4-	1.2-	1.0-	0.8-	0.7-	0.6-	0.5-	0.4-	0.3-	0.25-	0.2-	0.15-	0.1-	0.07-	0.05-
	2.2	1.9	1.6	1.4	1.2	1.0	0.8	0.7	0.6	0.5	0.4	0.3	0.25	0.2	0.15	0.1	0.07	0.05	0.03	0.025
Rating	30	29	28	27	26	25	24	23	22	21	20	19	18	17	16	15	14	13	12	11
Joint orientation Rating	> 30° into slope				< 30° into slope				Horizontal and vertical				< 30° out of slope				> 30° out of slope			
	20				18				14				9				5			
Joint width Rating	< 0.1 mm				0.1-1 mm				1-5 mm				5-20 mm				> 20 mm			
	7				6				5				4				2			
Joint continuity Rating	None continuous				Few continuous				Continuous, no infill				Continuous, thin infill				Continuous, thick infill			
	7				6				5				4				1			
Groundwater Rating	None				Trace				Slight				Moderate				Great			
	6				5				4				3				1			

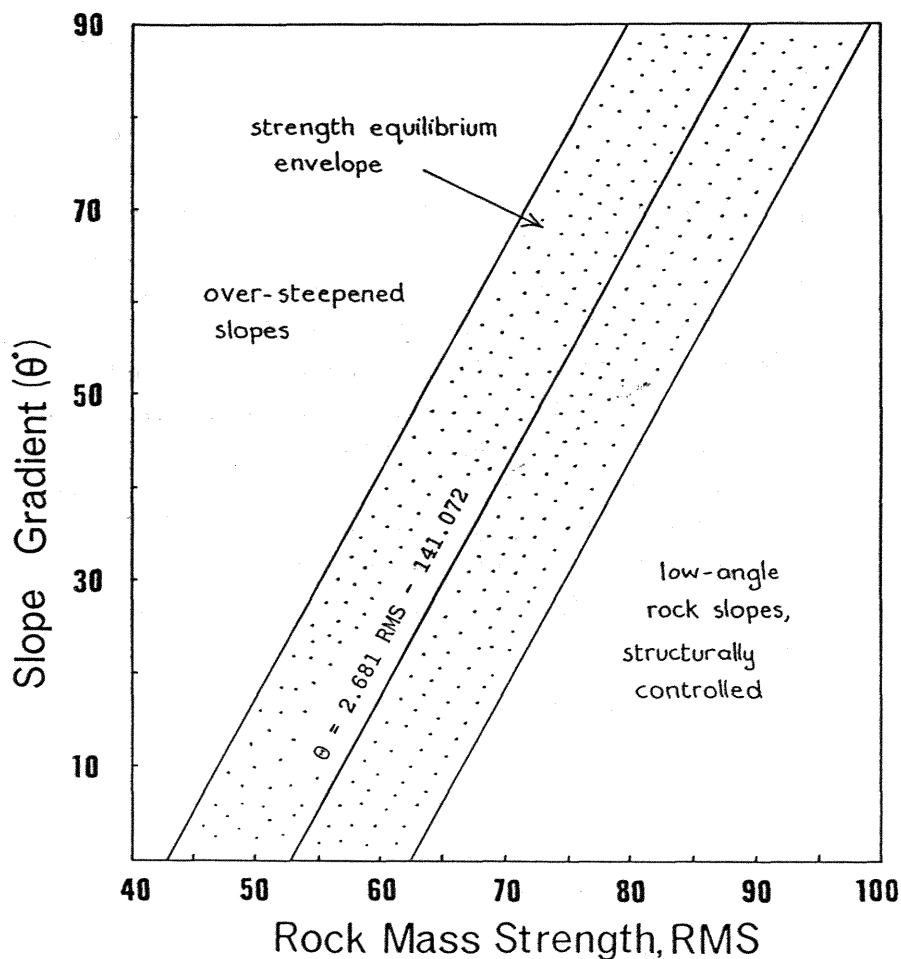


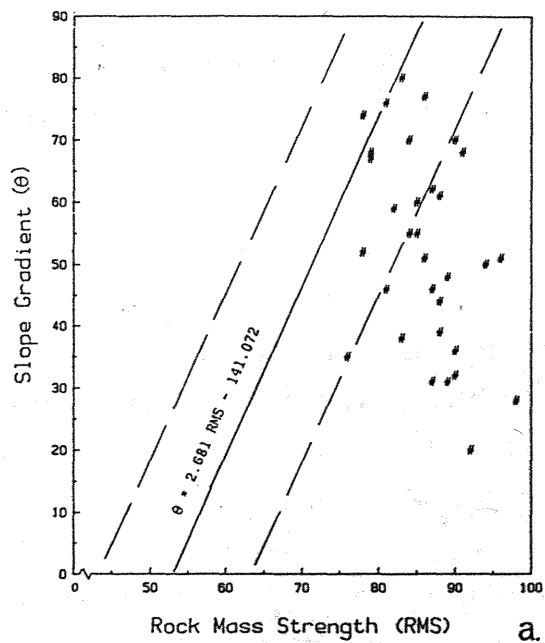
Figure 4.1. Graph of rock slope gradient against rock mass strength indicating strength equilibrium relationship and envelope. Note the controls on slopes lying above or falling below the strength equilibrium envelope. After Abrahams and Parsons (1987).

Figure 4.2. Relationship between rock mass strength and rock slope inclination for valley wall slopes from deglaciated troughs in the vicinity of the Main Divide, Southern Alps. Note that few slopes are oversteepened.

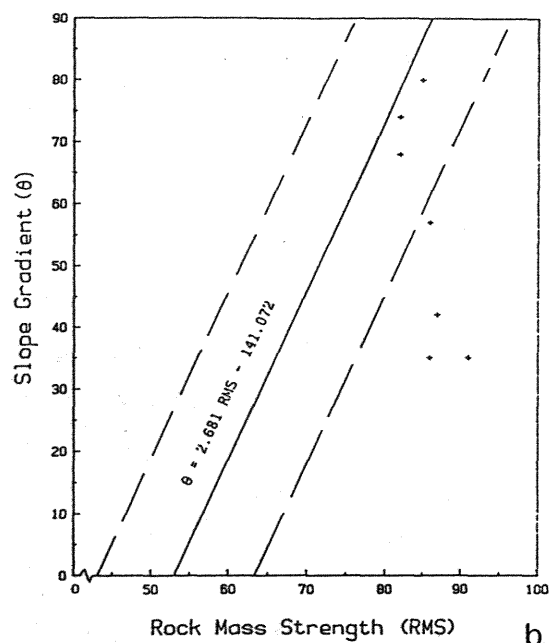
(a) Northern Fiordland plutonic rocks. Note control of sheeting joints on the morphology of low-angle slopes.

(b) South-central Fiordland plutonics and amphibolites.

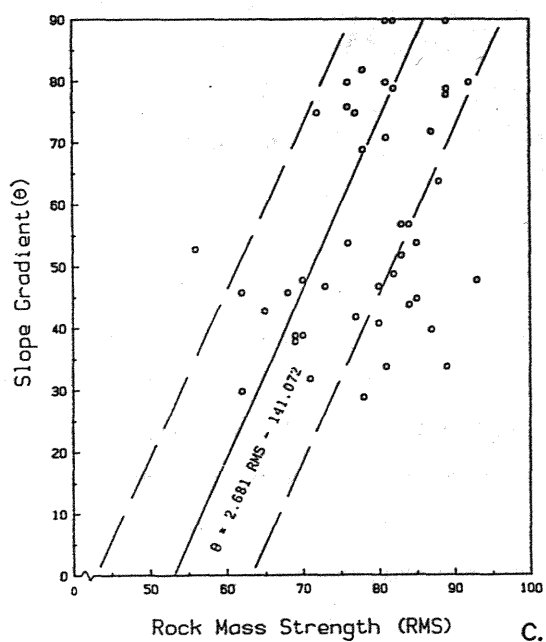
(c) Mt. Aspiring region schist slopes. (d) South Westland schist slopes. Sheeting joints and foliation control the morphology of most slopes; (e) Mt. Cook greywacke and argillite. Slopes falling below envelope are structurally controlled.



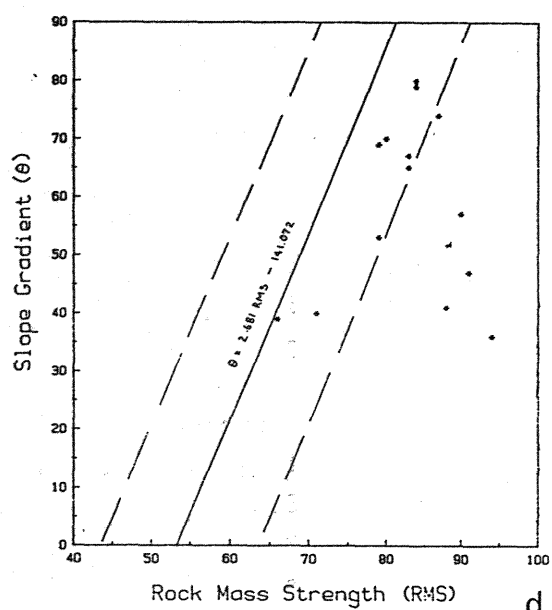
a.



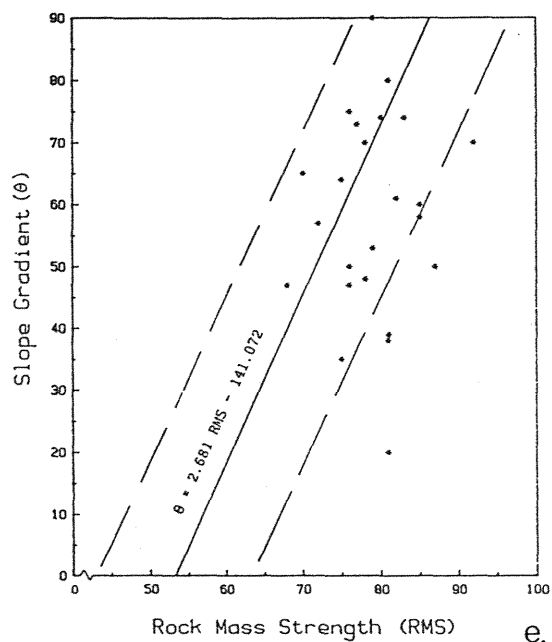
b.



c.



d.



e.

segments are low-angle rock slopes (Fig. 4.2a). With increasing height up the slope, the concave nature of the slope profile generates steep, strength equilibrium sections.

The surfaces of the rock slopes are defined by well developed curved sheeting joints and/or regional tectonic joint elements, and are independent of geological boundaries. The sheeting joints are nearly vertical towards the upper part of the slope, but are concave and have reduced slope towards the toe (Fig. 4.3). All sheeting joints are probably of stress relief origin and formed in connection with stress changes that accompanied the erosion of the valleys. Further evidence for their origin as surficial stress relief features lies in the fact that their spacing increases considerably into the slope. Many low-angle rock slopes have their morphology controlled by the sheeting joints (Fig. 4.2a). These low-angle slopes are far lower than that allowed by the RMS properties of the slope rock. This reflects slope modification by glacial erosion processes associated with development and control by stress-relief jointing.

The massive slabs delineated by the sheeting joints are frequently buttressed by rock with tightly closed cross-joints dipping at low angle into the slope. This property imparts considerable stability to the slopes. The sheeting joints rarely extend over the full height of the slope. Toppling and wedge failures are rare, and deep-seated failures or anti-slope scarps such as those found in Norway (Bjerrum and Jorstad, 1968) and the Coast Mountains of British Columbia (Mollard, 1977), have not been identified. Most slope failures are small planar slides which are generally controlled by the sheeting joints.

The plutonic rock mass has a relatively uniform range of Schmidt hammer hardness values despite mineralogical and textural variations observed in outcrop. The most important difference between the sites are those of the controlling joint orientations and joint spacings. The RMS assessment indicates that many of the steep slopes developed on the plutonics display equilibrium forms and have been little modified since deglaciation. Failure of the slopes will not occur until cross-joints open, probably aided by freeze-thaw and high seasonally-controlled water pressures in the joints.



Figure 4.3. Concave upwards sheeting joints developed in diorite, Adelaide Valley, northern Fiordland.

The high RMS of the northern Fiordland plutonic rock results in the high degree of stability of the glacially undercut trough walls following glacier recession. The steep rock slopes will be progressively reduced to a lower gradient controlled by the slope processes, the opening of cross-joints, and the weathering and progressive degradation of the joint surfaces.

#### 4.4.2. South-Central Fiordland Region

The south-central Fiordland area largely comprises massive granites, schists and amphibolites. The RMS-slope inclination relationships for all sites are plotted in Fig. 4.2b. Only a limited number of profile sites were selected due to time constraints and difficulties of access; the location of the profile sites is given in Fig. 2.7. It is immediately apparent that all slopes fall within or below the strength equilibrium region of the RMS-slope graph (Fig. 4.2b). The majority of the slopes are stable, and unlike the situation in northern Fiordland, the low-angle slopes seldom have their morphology controlled by sheeting joints. The glacially moulded rock slopes generally display considerably lower slopes than their RMS suggests could be sustained. This may be a consequence of the dominance of glacial moulding by the Pleistocene ice-cap and radiating outlet glaciers (Chapter 3) on the development of the glacierized morphology, i.e., the trough slopes are adjusted to equilibrium glacial conditions, rather than adjusted to the rock mass strength of the eroded basement.

#### 4.4.3. Mt. Aspiring Region

The Mt Aspiring region comprises strongly foliated psammitic and pelitic schist with minor greenschist. As far as possible, RMS profiles were measured on a wide variety of schist types and slopes displaying a variety of structural/foliation controls. Unlike the case in Northern Fiordland, few recently deglaciated, unvegetated slopes were stable. Landslides and rockfall are common, with failure occurring typically on foliation planes (Figs. 4.4 and 4.5). Major causes of sliding appear to be: erosion at the foot of dip slopes; removal of the buttressing ice; and earthquake shaking. The RMS data are displayed graphically with respect to the appropriate slope inclination in Fig. 4.2c.



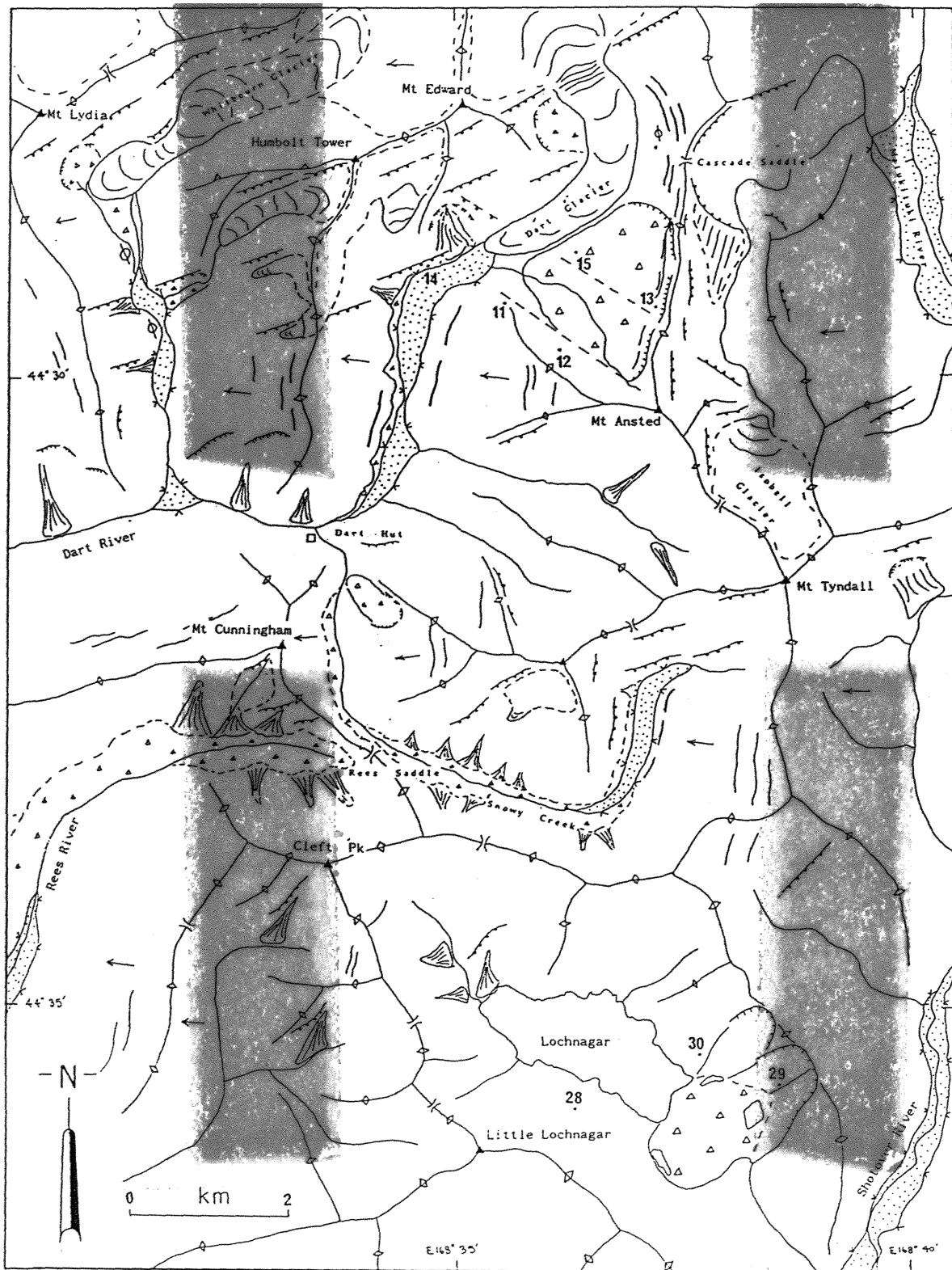


a.



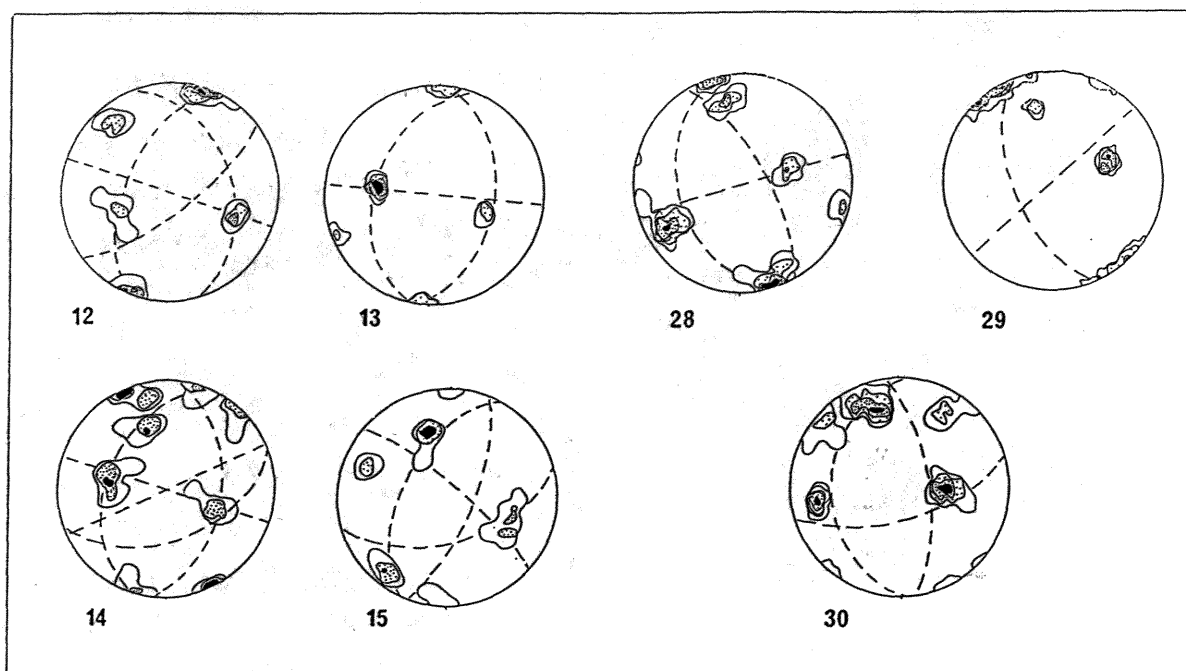
b.

Figure 4.4. (a) Planar rock slide at snout of Dart Glacier, Mt Aspiring National Park. Note foliation controlled slide plane with slope below equilibrium angle. (b) Lochnagar, dammed by a large rock slide. An example of a large natural wedge failure.



a.





b.

Figure 4.5. (a) Geomorphic map of central Mt. Aspiring National Park, showing (b) fracture set geometry and the location of major rock slides above the Dart Glacier and damming Lochnagar. Mapping symbols as given in Table 2.1.

(b) Schmidt net contour plots of poles to joints and foliation, indicating structural elements controlling the rock slides. Numbers refer to locations on (a) geomorphic map. No. 12. 4, 8, 12, 16% per 1% area, 29 points. No. 13: 4, 8, 12, 16% per 1% area, 31 points. No. 14. 4, 8, 12% per 1% area, 32 points. No. 15: 4, 8, 12% per 1% area, 21 points. No. 28: 3, 6, 9, 12, 15% per 1% area, 30 points. No. 29: 3, 6, 9, 12% per 1% area, 37 points. No. 30: 3, 6, 9, 12% per 1% area, 33 points.

**Lower hemisphere projections**

The use of the Schmidt hammer was limited for the quartz-mica schist, with its uneven surface texture having a significant effect on the readings. In addition, the use of the Schmidt hammer parallel to the schistosity was frequently inhibited by the destructive collapse of the mica laminae under the hammer impact, thereby lessening the impact considerably. Despite the problems, a limited number of readings were obtained which were able to be used and integrated into a RMS study. Joint widths varied considerably, with wide tensile joints dominating the unstable slopes. Combined with high joint water pressures, the joint properties contribute significantly to the development of rockfall and slope failure.

Rockslides are not evenly distributed among the slope types. Most of the rock slides occur on dip and overdip slopes (slopes in which the foliation is inclined more steeply than slope = overdip; foliation with a similar inclination to that of the slope = dip slope; foliation more gently inclined than slope = underdip). The foliation planes facilitate rock slides because of their continuity and frequency in the slopes. In overdip, dip and underdip slopes, the bedrock possesses a dip direction similar to the surface of the slope. Few of the slopes fall within the oversteepened region of the graph, with the majority falling within the bounds of the strength equilibrium envelope (this may be largely fortuitous as the slopes have had insufficient time to equilibrate to subaerial conditions), or the low angle, structurally controlled domain (Fig. 4.2c). The undercut to near undercut slopes are primarily structurally controlled, with joints dipping gently-to-steeply into the buttressing basal rock units. Cross-joints of tectonic origin do not appear to penetrate far into the slope rock, thus largely preventing the breakup and failure of the rock mass. Few of the cross-joints are continuous, with most terminating at the foliation surfaces, except where the slopes are controlled by near vertical fault trends (Fig. 4.6a).

Examination of dip slopes indicates that most are stable with respect to present conditions. However, it would only take high cleft water pressures, coupled with minor earthquake shaking, to activate/reactivate slides on unbuttressed, as well as buttressed dip-slopes. Such a scenario is envisaged for the incidence of the ridge foundering/collapse and sliding of an intact schist block that dammed Lake Lochnagar (Fig. 4.4b, 4.5). Failure occurred on an active splay fault of the Moonlight Fault that defines the eastern boundary of the slide zone and developed as a large wedge failure. Failure at the



a.



b.

Figure 4.6. (a) Joint plane/fault controlled valley trend and slopes, Dart Glacier, Mt. Aspiring National Park. Note supra-glacial debris and unstable slopes.

(b) Foliation controlled anti-slope scarps developed near the crest of schist slopes above the Dart Glacier. Lateral moraines in foreground, scarps in background. Antislope scarps 5-6 metres high

fault plane occurred along a thin ( $\sim 0.5\text{m}$ ) band of highly sheared and fractured cataclasite, whose brittle nature would allow the rapid rupture and extension of the slide plane. The examination of scarps and scars indicate that more than one cliff collapse has occurred.

Progressive failure and modification of the bare rock slopes is apparent, with planar and wedge slides, and slumping being the dominant processes. At the snout of the Dart Glacier, a large planar rock slide occurred following the recession of the Dart Glacier from its 1850 position (Summerville *et al.*, 1983) (Fig. 4.4a and 4.5). High water pressures on the slide surface were probably important, as well as the attendant stress/strain redistribution in the slope.

Dip-slopes in the schist are frequently destabilized by the glacial removal of the material buttressing the slope toe. The removal of the glacier buttress allows the lateral expansion of the valley wall rock. This sometimes occurs in the form of large planar and wedge slides, especially in planar foliated pelitic greyschist, such as that at the snout of the Dart Glacier. The roughness of the planar slide surface is a major control on the stability of the slope and the incidence of slides (Cruden, 1976). Slides occur mainly where the planar foliation surface in the schist has a low joint roughness coefficient and the rock is compact and massively jointed. This reflects the reduction in shear strength along the surface with increasing block size due to reduction in contact area across the surface (Bandis *et al.*, 1981). High joint water pressures would reduce this strength and enhance failure. However, deformed/sheared schist is usually closely jointed and large slides were seldom found to occur in rock slopes comprised of such rock, although slumping is common. This may reflect the fact that small blocks have the ability to rotate slightly and so maintain contact with small-scale roughness features. This would increase the shear strength of a potential slide surface and reduce the probability of a slide involving a cohesive mass, unless a major energy input to the system, such as a large earthquake, occurs.

Near the crest of the strike-ridges such as the upper Dart Valley, upward-facing scarps are frequently formed (Fig. 4.6b). The scarps appear to develop as a result of valley-ward sliding of large planar blocks on foliation controlled surfaces. The foundering of the ridges is probably a result of glacial removal of the slope toe and buttress

so that sliding on the relatively smooth foliation surface is permitted. The slope collapse is controlled by the rhythmic alternation of beds of competent massively jointed greenschist and more closely jointed, plane foliated pelitic greyschist. These uphill facing scarps become local catchment basins for snow and meltwater which can then drain downslope through the rockmass along the foliation plane joints. This will increase the cleft water pressure and result in seasonally enhanced acceleration of the downward slope movement, especially with erosional removal of the slope toe, allowing the foliation weakness/slide plane to 'daylight'.

#### 4.4.4. South Westland Region

This region of predominantly quartzo-feldspathic garnet to chlorite schist, displays similar properties to the chlorite II and III zone grey and green-schist encountered in the Mt Aspiring region. In South Westland the highly foliated schists display cross-cutting tectonic and stress-relief jointing that combine to control the slope orientation and form.

The locations of the RMS profiles are displayed in Fig. 2.11a,b. Profiles were undertaken both parallel and perpendicular to the foliation to enable assessment of extent of joint control on the slopes. Generally the valleys cut the foliation at a high angle, with the major outlet troughs, i.e., the Franz Josef and Fox valleys, following probable fault shear zones (Gunn, 1960). Slopes are generally controlled by tectonic/stress-relief jointing, with some toppling of large joint-bound blocks and planar/wedge failure on foliation bound blocks. A result of the control of slopes by near vertical tectonic joint sets is that the slopes are of high mass strength (Fig. 4.2d) and relatively stable. This enables the persistence of steep slopes until cross-joints open and debris slides on cross-cutting fault zones and slabbing progressively denude the slopes. All rock units are of high RMS, and fall within either the low angle or strength equilibrium slope regions of the graph (Fig. 4.2d).

Valley slopes eroded parallel to the foliation i.e., the Spencer and Whymper glacier trough walls, display the same dip-slope controlled character to that encountered in the lower grade schist of the Mt Aspiring region. Unstable dip-slopes rapidly equilibrate following glacier and meltwater undercutting of the slope toe, giving rise to large planar slides. The slopes and valleys are often cross-





Figure 4.7. Rock bars, active faults and debris schutes in front of the Franz Josef Glacier, South Westland.



Figure 4.8. Mt Cook skyline, the low points in the range are defined by thick beds of low RMS argillite.

cut by active faults that contribute large wedge failures and act as chutes for debris slides (Fig. 4.7). The opposite valley wall is buttressed by the into-slope dip of the foliation joints, and failure occurs only when cross-joints develop. These slopes are steep and generally stable, following the removal of the buttressing ice. Without favourably oriented penetrative joint sets, failure is slow.

The Schmidt hammer readings for the schist are variable, depending on the relative proportions and thickness of the mica/quartz laminae. Due to their resistance to weathering, the quartz laminae tend to project above the surface and give spurious readings. Similarly, readings taken parallel to the foliation depend on the thickness and relative proportions of the quartz laminae. The joint spacing is also variable. However, the spacing is generally wide within the massive compact slide blocks, except where active faults generate shattered failure zones. The joints are generally open and moderately smooth allowing free water movement and high potential cleft water pressures, which are further favoured by the high degree of continuity of the major joint sets.

#### 4.4.5. Mt. Cook Region

The basement rock of the Mt Cook region comprises closely bedded and jointed greywacke and argillite. An attempt was made to examine slopes developed in valleys with varying orientations, structural domains and perceived lithological controls. The profile sites are shown in Fig. 2.11a. Rock slopes at high angles to the bedding/structure were unstable even near the glacier snouts. The trough walls rarely retained their glacial character and are frequently mantled by thick talus slopes.

Schmidt hammer readings taken on the greywacke and argillite rock slopes were monotonously uniform. The major strength difference between the greywacke and argillite is the close joint spacing in the argillite rock slopes. Climbers derisively refer to the argillite as 'Weetbix', with its fissile character giving it a reputation for unsafe holds. This factor is an obvious control on the character of the skyline of the Mt. Cook Ranges (Fig. 4.8). In the Maltebrun and Liebig ranges, bands of closely jointed argillite control the location of the saddles in the ranges and the glacial-diffuence cols, due to its low resistance to erosional processes. Conversely, the prominent peaks such as Maltebrun, comprise mainly competent, more massively

jointed greywacke/sandstone. Such a situation has been described from the Akaishi Range, Southern Japan Alps (Matsuoka, 1983), where closely jointed shale of low tensile strength defines the low points in the range. Joint widths vary, but are generally closely spaced, open, continuous and interlocking.

The bedding plane joints are an important control on the slope orientation and stability in the Mt Cook region. None of the slopes examined were found to be oversteepened/undercut with respect to their RMS, falling in the strength equilibrium/low angle region of the graph (Fig. 4.2e). Intact strength, spacing and width of the joints varies, but it is the orientation of the controlling joint set that dominates the stability and patterns of slope modification.

#### 4.4.6. Summary RMS Results

The conclusion of Selby (1982) that rock slopes retreat at angles that preserve their strength equilibrium is supported by a study of glacial valley rock slopes. Progressive slope reduction and modification occurs with time and distance from the glacier snout. However, this only occurs if the resistance of the rock mass does not change with depth into the rock mass. This appears to be the case for the closely jointed schist and greywacke slopes, but the granites display surface slopes controlled by sheeting joints. This joint set often consists of several sets of joints at various distances from the surface of the slope. The spacing between the joints increases with depth into the slope, so that with the progressive failure of the surface rock, the RMS will change, as will resistance to the erosion processes. This will occur until cross-joints open to allow failure to proceed.



#### 4.5. Rock Mass Strength Controls On Some Antarctic Dry Valley Landforms

##### 4.5.1. Introduction

A purpose of this study was to examine quantitatively the role of rock resistance (RMS) and fabric as potential controls on cliff form and retreat in the McMurdo Dry Valleys, Antarctica. Several studies have examined sandstone cliff form and retreat with respect to rock structure, strength and climate elsewhere, but the relative importance of these factors has been studied in Antarctica only by Selby (1980).

Schumm and Chorley (1966) analysed the mechanisms and rate of cliff retreat in the Colorado Plateau region with respect to the characteristics and structure of the scarp rock. They found that the main controlling factors on cliff retreat were rock resistance as determined by cementation and porosity, and orientation and spacing of joints and bedding planes. Nicholas and Dixon (1986) examined the controls on sandstone scarp form in the Canyonlands National Park, Utah, and established that rock fabric (fracture orientation and spacing) rather than resistance (UCS, porosity, etc.) was the main factor regulating the scarp morphology.

##### 4.5.2. RMS And The Dry Valleys

The method of Selby (1980), as modified by Moon (1984), was applied to assess the RMS of rock slopes on distinct landform assemblages developed in the McMurdo Dry Valleys. The strength equilibrium slopes require sufficient time to adjust, and the McMurdo Dry Valleys is an area that has been ice-free and climatically stable for ~4 Myr (Selby, 1980). There is little weathering, no slope wash, almost no meltwater, no vegetation and no ground water flow. This makes it ideal for the study of slopes and landform evolution.

The location of the RMS profile sites is shown in Fig. 2.23. The examination of the RMS-slope inclination graph (Fig. 4.9) indicates a strong relationship between high RMS values for lithological units and those units occupying the high relief positions. However, a number of discrepancies are evident which will be examined with reference to several composite profile transects.

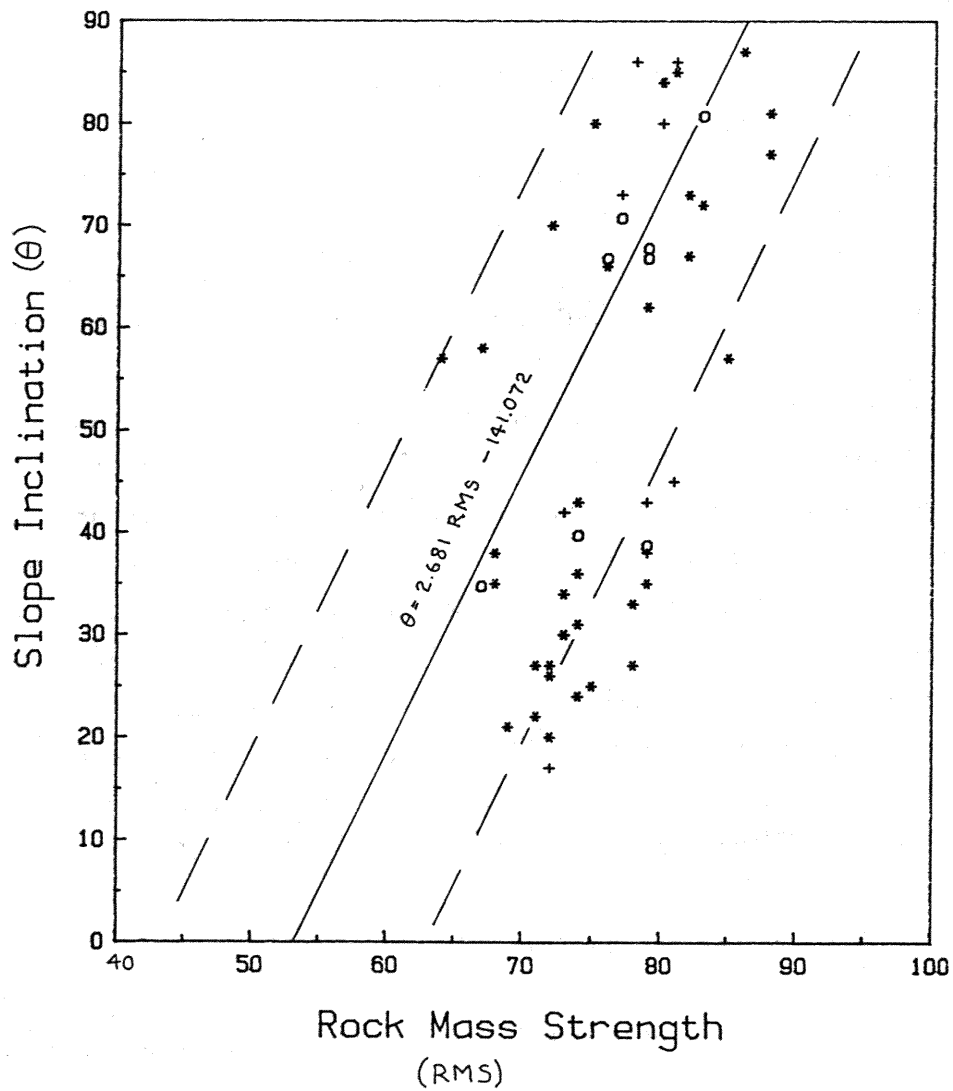


Figure 4.9. Relationship between rock mass strength and slope inclination for all slopes studied in the McMurdo Dry Valleys, Antarctica. \*: Beacon Supergroup Sandstones, +: Dolerite, o: Granites/gneisses.

#### 4.5.2.1. Upper Wright Valley-Mt Baldr

The valley transect is illustrated in Fig. 4.10a. The morphology of the area is dominated by the channelized forms of the Labyrinth in front of the snout of the Upper Wright Glacier. The cliffs mantling the Labyrinth are developed in relatively weak Beacon Supergroup sediments with a capping of hard, resistant Ferrar Dolerite.

On the southern side of the Upper Wright Valley below Mt Baldr on the Asgard Range, glacial deposits and slope debris, mantle low-angle slopes developed on closely bedded and jointed Altar Mountain Sandstone. Given the relatively high strength of the lower slope unit, it is interpreted as a Richter denudation slope, above which steep slopes are developed in closely bedded Arena Sandstone of similar RMS. The upper slope is in apparent strength equilibrium, with failure developed along slope-parallel unloading joints, allowing the progressive retreat of the upper slope unit. This retreat will result in the eventual development of a rectilinear slope unit.

Above the floor of the Tyrol cirque, the backwall comprises relatively massive Beacon Heights Orthoquartzite, with a cap of closely jointed Ferrar Dolerite. Thus, the backwall of the cirque comprises three distinct slope units (Fig. 4.10a). The lower steep slope displays high RMS and is in strength equilibrium. The backwall changes abruptly to more closely jointed sandstone of lower RMS and is also in strength equilibrium. Surficial sheeting joints are not strongly developed. The regular horizontal and vertical jointing of the resistant dolerite cap, defines a steep but stable slope which may gradually retreat through undercutting of the sandstone and by toppling failure.

#### 4.4.2.2. Mt Cerce-Olympus Range

The Olympus Range between the Airdevronsix Ice-falls and Mt Jason (Fig. 2.14 and 2.23) comprises a series of mesas developed in the Beacon Supergroup sediments. A cap of resistant Ferrar Dolerite persists only on the western end of the range; at the eastern end, the absence of dolerite is probably due to the westward tilt of the Beacon strata and intense glacial erosion removing the dolerite and upper layers of the Beacon Supergroup sediments.

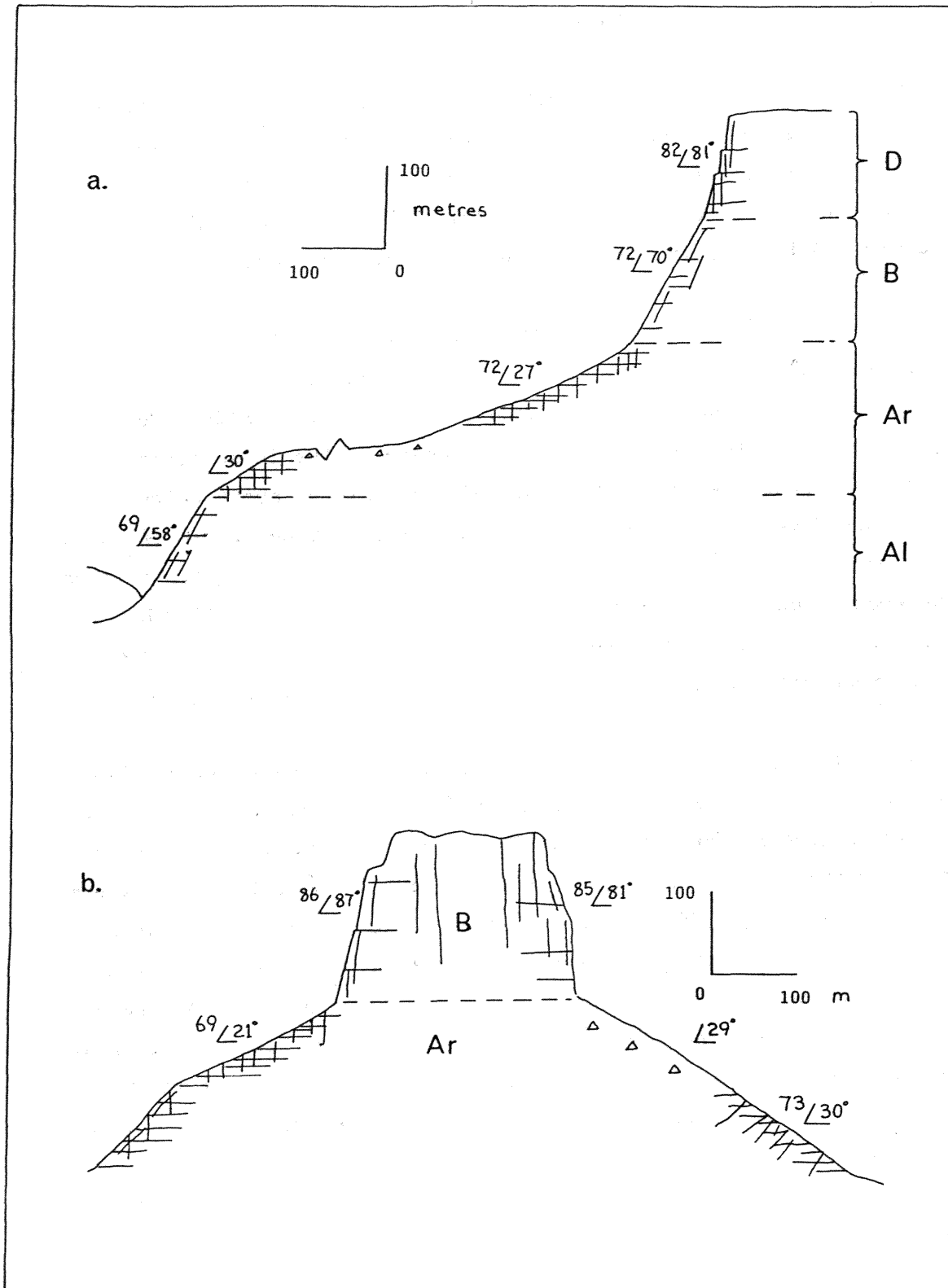


Figure 4.10. Slope transects indicating RMS and slope inclination for:  
 (a) Mt Thor, Asgard Range; (b) Mt Cerce, Olympus Range.  
 Letters refer to lithologies from Fig. 4.12.

A transect was conducted E-W across Mt Cerce on the Olympus Range (Fig. 4.10b). The steep upper section of the mesa comprises resistant Beacon Heights Orthoquartzite with frequently massive joint blocks, overlying relatively gentle slopes developed in closely jointed Arena Sandstone. No dolerite cap persists eastward of Mt Electra. The boundary between the two formations is transitional (McKelvey *et al.*, 1977). The Beacon Orthoquartzite is a remarkably uniform formation composed almost entirely of very mature quartz arenites.

The transect displays several distinct slope elements. The lower gentle slopes developed in the Arena Sandstone have several distinct breaks in slope culminating in the near vertical slopes developed on the Beacon Orthoquartzite cap rock. The main features of the ridges are the nearly vertical free-faces and the massive vertical and near vertical joints that divide the quartzite into blocks of 200-300 metres (Selby, 1974). Selby described the origin of the free-faces as due to the progressive release of internal stresses as the rock wall retreats. The unloading blocks are 1-5 metres thick and all begin at the foot of the cliff and terminate vertically in an overhang. At the end of each ridge, large tension joints have opened. Where these joints dip steeply into the slope, they give rise to large outward displacements at the ridge crest before commencement of toppling and fracturing at the column base.

The low-angle slopes formed on the closely jointed and bedded Arena Sandstone generally display slopes lower than their RMS properties would allow them to sustain. This supports their interpretation as rectilinear denudation slopes (Selby, 1974). The lack of, or only a thin, debris veneer on the slopes, is a response to weathering and wind abrasion that has rapidly comminuted the debris and eroded flute marks into the stable low angle slopes (Selby, 1977; Malin, 1984). The progressive slope modification and retreat to develop these rectilinear slopes results in the progressive undercutting of the orthoquartzite. This allows the opening of joints and toppling of massively jointed dolerite blocks.

#### 4.5.3. Discussion Of Results

The landforms of the McMurdo Oasis are developed in formerly glaciated valleys and largely display slopes in strength equilibrium. On the western-most Olympus Range, the resistant mesas developed in



Figure 4.11. Mt Cerce, Olympus Range, a resistant mesa developed in Beacon Heights Orthoquartzite. The underlying Altar Mountain Sandstone displays the characteristics of low-angle Richter denudation slopes.

the Beacon Heights Orthoquartzite dominate the landscape. Below the orthoquartzite, low-angle sandstone slopes display the characteristics of Richter denudation slopes (Bakker and Le-Heux, 1952; Selby, 1971) grading into wide, flat valley floors (Fig. 4.11). Denton *et al.* (1984) attributed these forms to glacial moulding by an over-riding Miocene ice-sheet, with the flow of the ice-streams highly oblique to that of the present valley system. The remnant orthoquartzite ridges were identified as roches moutonnées. Support for the model was largely in the form of 'lee-side' plunge pools, recognized on the Asgard and Olympus ranges, plus the roche moutonnée-like form of the mesas and ridges. However, supporting evidence from the glacial deposits and erratic distribution is not forthcoming (Selby, 1985). Selby argued that it is equally plausible that the mesas developed from progressive backwall retreat of the Miocene cirque walls (Selby and Wilson, 1971).

Selby's (1974, 1985) model of progressive subaerial development of the mesas is supported by the results of this study. However, this is not to imply that glacial erosion has not had an input to the landform development, but rather that the postglacial subaerial modification has been the dominant process in the development of the present high altitude landscape. Many of the troughs in the Olympus and Asgard ranges display forms that are relatively short (cirque backwall to rock lip distance). However, on the lee-side, relatively long basins with breached headwalls are commonly developed (Aniya and Welch, 1981b). Selby (1985) suggested that many such features might have resulted from the development of closely spaced cirques that enlarged headwards, thus breaching the headwall divide or arête and creating the 'through valley'.

An examination of Fig. 4.12. indicates a reasonable correlation between the RMS of the rock units and those units occupying consistent positions with respect to the Olympus Range morphology. At the western end of the range, Ferrar dolerite caps upper Beacon Supergroup sediments and the presently empty cirques are in an incipient stage of rectilinear slope development. High RMS Beacon Heights Orthoquartzite underlies the dolerite and allows the development of steep slopes of considerable stability. Further to the east at Mts. Electra and Dido, the steep slopes of the resistant mesas are formed on Beacon Orthoquartzite, underlying which, relatively weak, lower RMS Arena Sandstone has developed rectilinear denudation slopes. The intervening cirque floor is cut into higher RMS Altar Mountain Sandstone.

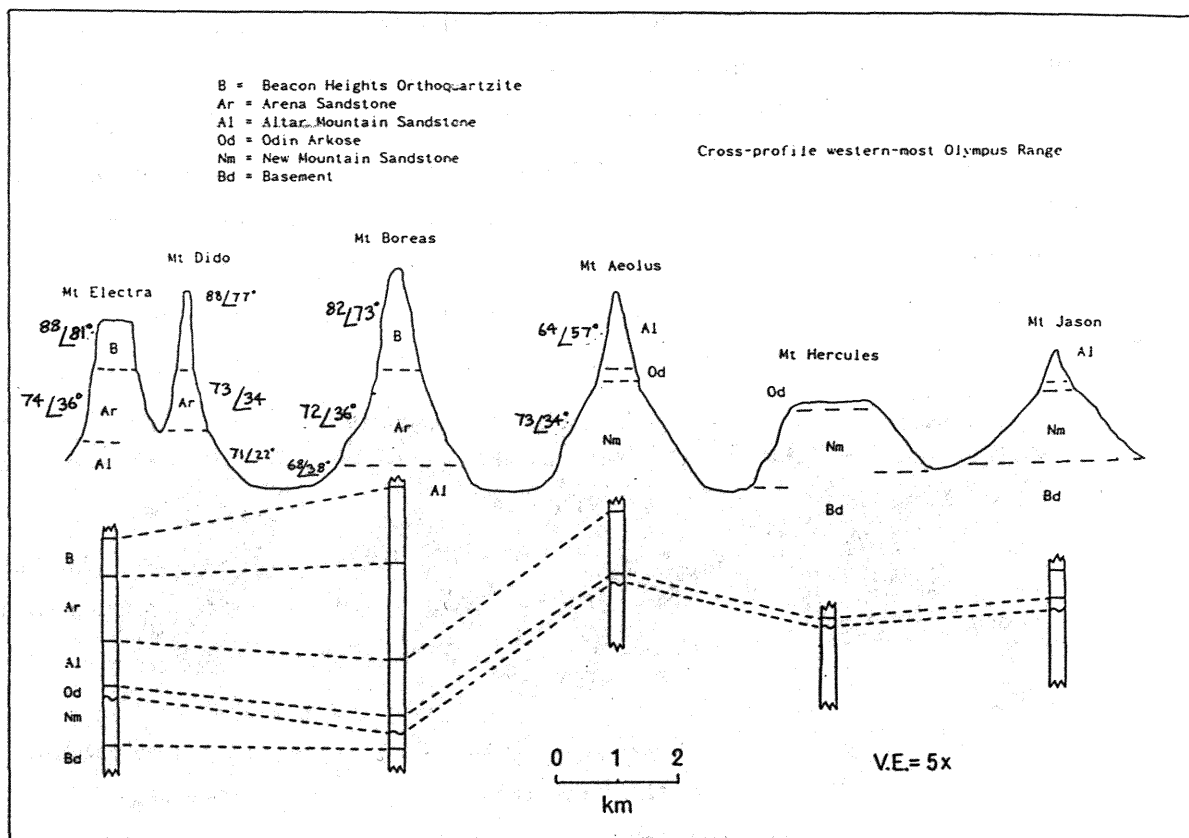


Figure 4.12. Profile transect across the western-most Olympus Range .  
Note the relationship between RMS and morphology.

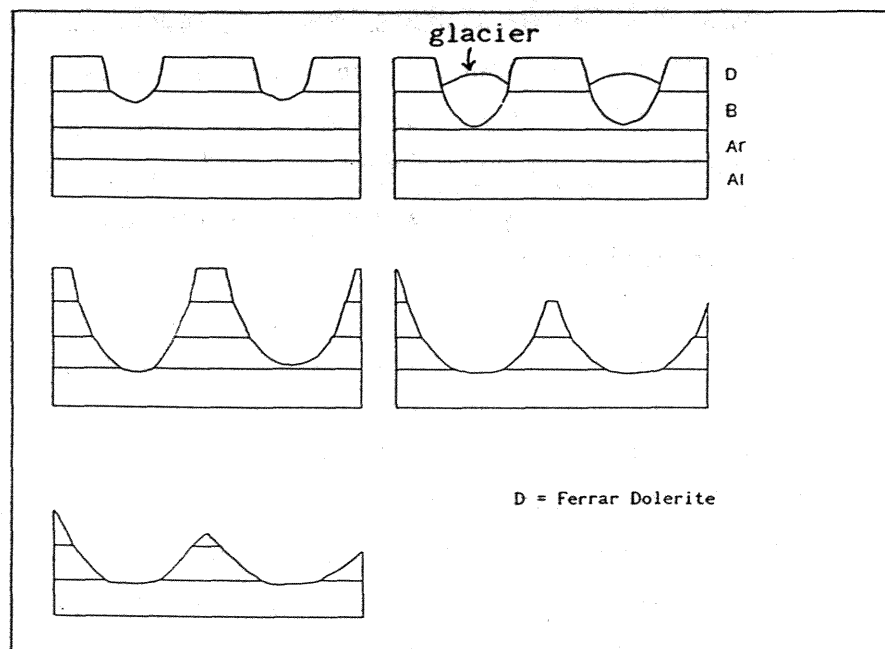


Figure 4.13. A simple model for the development of the morphology of the Olympus Range. The model involves the progressive removal of the capping dolerite sill, slope retreat and widening of the through valley. Symbols refer to rock units given in Fig. 4.12 (above).



In the vicinity of Mt Hercules only low-angle slopes cut into New Mountain sandstone persist as rectilinear denudation slopes, with a thin cap of more resistant Odin Arkose allowing the development of minor cliff sections. Mt. Jason is a low peak at the eastern end of the Olympus Range and displays a basically rectilinear slope form developed in low RMS New Mountain Sandstone.

The model of the development of the Olympus Range morphology involves the progressive removal of the dolerite cap and undercutting of the sandstone slopes. A postulated pre-glacial surface is shown in Fig. 4.13 whereby fluvially cut channels in the capping Ferrar Dolerite are enlarged and have their form enhanced by the development of temperate cirque glaciers (Selby and Wilson, 1971) until the present cirque forms were attained. The model involves the progressive removal of the capping Ferrar Dolerite from the eastern and central part of the range. A combination of Miocene temperate cirque/small valley glaciers and subaerial slope denudation resulted in the progressive undercutting of the dolerite cap via tensile failure and erosion of the Beacon Supergroup sediments.

#### 4.5.4. Summary and Conclusions

The results of this study show that the RMS classification can be applied to the interpretation of the development of some McMurdo Dry Valley slopes. The Olympus and Asgard Range landscapes, especially those developed in the Beacon Supergroup sediments, are shown to have their development in space and time controlled by the RMS properties of the rock strata. Where less resistant strata are exposed for a long period to subaerial denudation, then the slope retreat and the development of the ultimate Richter denudation slope is the final stage in the slope creation process. Along the Olympus Range, a progression towards an increase in the degree of trough and slope modification occurs, until the presence of a thick dolerite cap allows only incipient cirque basin development. This is a consequence of the eastward dip of the strata and the progressive removal of the thick dolerite cap towards the western end of the Olympus Range.

## 4.6. Modified RMS Method

### 4.6.1. Introduction

The RMS classification was developed for the examination of the stability of rock slopes with respect to subaerial processes. However, rock resistance with respect to erosion processes, especially those processes acting subglacially, are of different character to those controlling subaerial slope stability. Consequently, an attempt was made to modify the RMS classification to enable it to be used as an indicator of rock erosional resistance, and to examine whether RMS properties of the slope rock had a major influence on the size and shape of the glacial trough.

Cooks (1983) examined the influence of rock strength on drainage basin morphometry and was able to demonstrate that the development of the drainage basin morphometry depended largely on the strength of the bedrock underlying them. However, this study ignored the influence of rock jointing on rock strength and slope development. It has long been recognized in engineering geological studies that the jointing of the rock mass is the major control on rock slope development and hence on erosion (Hoek, 1983). Such factors as the state of weathering, joint width, continuity and spacing, were found to be critical in controlling *in situ* rock strength, and hence slope stability, erosion resistance and geomorphic development (Selby, 1982, 1987).

A modified RMS assessment of rock slopes in recently deglaciated troughs was undertaken for each morphological terrain. The profile sites were considered to have been minimally modified following deglaciation. Unfortunately, the character of the valley floor rock can rarely be assessed directly, due to the frequent presence of a thick valley fill. However, it is considered that towards the valley heads, where the degree of fill is minimal, the RMS character of the basal section of the slope unit is a valid surrogate for that at the valley base.

#### 4.6.2. Modified RMS Method

Glacial erosion of the rock bed involves plucking and abrasion as the primary processes at the ice-rock contact. Abrasion is difficult to assess and model. Hence, plucking at the glacier base, particularly in heavily jointed terrains, has been considered to be the major component of the glacial erosion process (Drewry, 1986). For subglacial plucking to proceed, the obvious control is the presence and pervasiveness of surficial rock jointing. Factors such as joint density, continuity and width, should control the ease of removal of the rock directly at the glacier sole. Joints also control bedrock permeability, and therefore water pressure in the joints, enhancing rock failure and joint block removal. However, the subglacial behaviour of the rock mass is difficult to model accurately, because the only information on the rock available is from what remains after glacier retreat. There are few published observations on the subglacial behaviour of the rock mass. Exceptions include Vivian and Bocquet (1973), Vivian (1979), Boulton *et al.* (1979) at the Glacier d'Argentière, and Hagen *et al.* (1983) at the Bondhusbreen Glacier, Norway.

The properties used in the modified RMS method are mainly those of Selby (1980), as modified by Moon (1984) but with several modifications. The changes were necessary because several of the parameters in the standard RMS classification could not be evaluated, or were irrelevant with respect to glacial erosion processes. The modifications are as following:

a) While subglacial water pressure, particularly in the rock joints is important (i.e., the heat pump mechanism for subglacial joint block removal (Robin, 1976; Röthlisberger and Iken, 1981)), this variable cannot be quantified because of the difficulty of access to the bedrock. Consequently, subglacial water pressure was regarded as a constant and given a zero rating for the purposes of this classification.

b) Similarly, joint width was regarded as a constant, since under glacial loading most joints are likely to be closed, other than the critical joints for failure and water penetration. Consequently this factor was neglected in the classification. Joint width is difficult to assess, but will be important on the low pressure side of

subglacial hummocks, with basal water pressures acting like a hydraulic jack (Röthlisberger and Iken, 1981). Joint width was given a zero rating for the purposes of this classification.

c) Joint spacing was assessed following the method of Selby (1980). A scanline survey at least 10m long was undertaken parallel to direction of glacier flow, and data were weighted according to the scheme given by Moon (1984)(Table 4.1).

d) Joint orientation and continuity are also difficult parameters to quantify. The exact combination of joint orientations that control block size and permit glacial excavation of the rock mass is not known, but will depend on both the physical properties of the glacier and the joint properties of the rockmass. Thus, a standardized approach had to be taken, ignoring the unknown and unquantifiable inputs to the system. This involved the examination of the present bedrock conditions which were assumed to be similar to those pertaining during glacial exploitation of the bedrock. Joint orientation was clearly important from the viewpoint of glacial excavation, although fracture orientation alone was considered to be inadequate because the continuity of the joints and block size influence the ease of joint block removal. This interrelationship of strength factors has been recognized in studies of rock excavation by machinery (Abdullatif and Cruden, 1983).

Hence, joint orientation and continuity were combined on a scale out of 20, with intermediate weightings given according to perceived resistance to subglacial plucking following the general joint orientation weighting scheme given in Selby (1980). The individual joint continuity rating (Table 4.1) was not input to the modified RMS classification. The weightings are necessarily subjective, and difficult to quantify and may not pertain directly to the subglacial conditions. Nevertheless, they are considered to be the best that can be achieved in this study. The weightings applied and their basis with respect to the rock mass characteristics, are shown diagrammatically in Fig. 4.14.

In the usual models of bedrock plucking at the glacier base, a hummock with a lee-side low pressure zone is required (Boulton, 1974; Röthlisberger and Iken, 1981). At the lower end of the scale, upglacier-dipping joint sets, combined with cross-cutting, interconnected sets, result in maximum ease of removal and were given

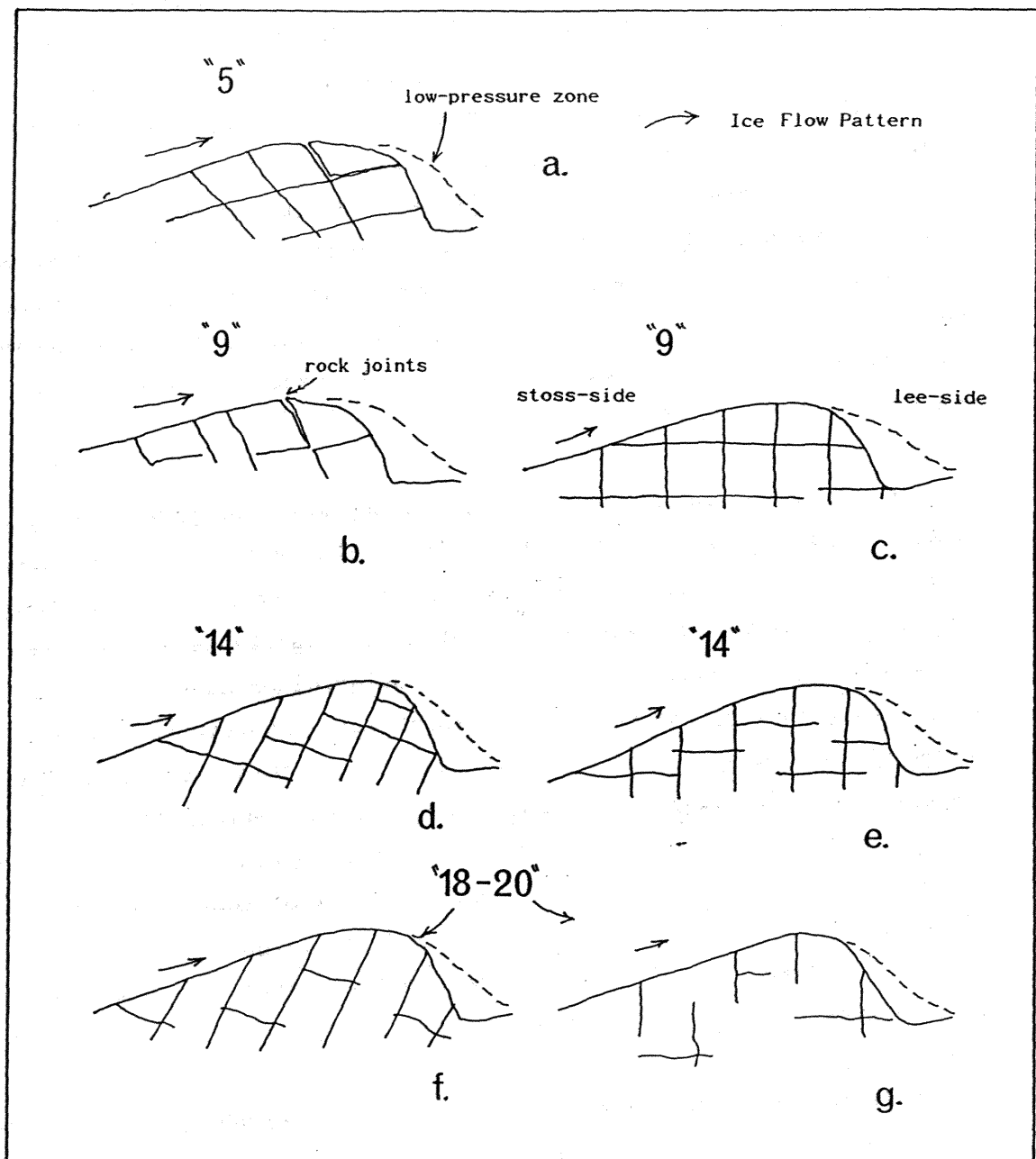


Figure 4.14. Relationship of joint orientation and continuity to glacier flow over a hummock, and assigned mass strength weightings (numerals).

a weighting of '5' (Fig. 4.14a). A rating of '9' was given where: (a) upglacier dipping surface joints showed poor continuity with cross-cutting joint sets, and (b) where near vertical dipping joints with good connectivity and interconnecting cross-cutting joint sets could allow relative ease of excavation (Fig. 4.14b,c).

A rating of '14' was assigned where near vertical joints with poor continuity, and steeply downglacier dipping joint sets with good connectivity persisted (Fig. 4.14d,e). A rating of '18-20' was generally assigned to rock with non-penetrative vertical to steeply down-glacier dipping joints, and/or horizontal sheeting joints with few cross-cutting joints (Fig. 4.14f,g). These combinations were considered to define the highest rock mass resistance to the subglacial plucking process.

e) The abrasion process is an important component of glacial erosion (Hallett, 1979; Metcalf, 1979). The relative importance of subglacial abrasion resistance to glacial erosion is not known. However, geotechnical methods of abrasion resistance estimation can be used as a surrogate of perceived subglacial erosion resistance. A strong correlation between Los Angeles abrasion resistance and Schmidt hardness (Kazi and Al-Mansour, 1980; Chapter 5, this study), indicates that the Schmidt hammer rebound can be used as a surrogate measure of bedrock abrasion resistance. Thus, the Schmidt hardness rating used in the modified RMS classification is an index of subglacial abrasion resistance as well as rock hardness and resistance to fracture, so that the rating scheme allows the most important aspects of the glacial erosion process to be evaluated.

While the RMS classification scheme of Selby (1980) gives a rating out of 100, the present modified scheme deletes three of Selby's parameters and the rating is out of 80, so that the individual parameters are given a proportionately greater weighting in the modified RMS classification. However, in the modified scheme the individual parameters follow the general weighting given in Table 4.1, except for joint orientation and continuity, for which the combined rating scheme given in Fig. 4.14 was followed. The modified classification scheme used is considered to be the best that can be achieved, and adequate for the purposes of this study.

#### 4.6.3. Results

The modified RMS method was applied to a variety of deglaciated troughs cut into 5 different lithologies. The bedrock profile sites compared here are those studied for standard RMS assessment, and the data for each of the lithologies are displayed in Appendix One and summarized in Table 4.6. For each morphological terrain, the mean modified RMS values were calculated for comparison with the mean of the morphometric indices. The methods used and results obtained will be detailed shortly. Examination of Table 4.6 suggests that, despite a wide variation in effective erosion resistance within each region, distinct differences emerge when related to the glacial valley morphometry.

Individual modified RMS values were not plotted against individual site shape indices due to: (1) considerable variations in strength properties and consequent lack of representativeness of samples taken from individual sites; (2) variations in form between and within adjacent valleys apparently unrelated to RMS; (3) the small scale maps (1:63,360) from which the morphometric data were derived, are of dubious accuracy; and 4) further operator error in the assumptions involved, such as estimations of trimline height. The mean value from each region was considered to reduce the compound error and allow comparison between the study regions.

#### 4.7. Glacial Valley Morphometry

##### 4.7.1. Introduction

While the study has so far been primarily concerned with the RMS properties of the eroded bedrock, for this data to be applied to the examination of the erosional landforms, the existence of a genetic relationship between rock strength and shape of the appropriate erosional landform must be demonstrated. To this end, a variety of morphometric properties of glacial valleys were investigated.

Studies of the rock profile under existing glaciers by gravity surveys (Kanasewich, 1963) and radio-echo sounding (Drewry, 1972), indicated a parabolic form for the cross-profile. Nye (1965) showed, on theoretical grounds, that parabolic or ellipsoidal channels are the

Table 4.6. Summary of rock mass strength (RMS) and valley shape data.

Study area	South Westland	Mt Cook	Mt Aspiring	Nth Fiordland	Sth Fiordland
Rock Type	Biotite schist	Greywacke/ argillite	Grey/green schist	Diorite/ gabbro	Granite/ metamorphics
Form ratio (FR)	1.56 $\pm$ 0.21	1.77 $\pm$ 0.19	1.79 $\pm$ 0.25	1.08 $\pm$ 0.13	1.39 $\pm$ 0.22
CoV	13.4	11.0	14.2	12.2	15.4
Shape Factor (f)	0.48 $\pm$ 0.04	0.52 $\pm$ 0.02	0.48 $\pm$ 0.04	0.43 $\pm$ 0.04	0.46 $\pm$ 0.04
CoV	8.0	4.4	7.4	8.9	8.6
Drainage density (km <sup>-1</sup> )	0.56 $\pm$ 0.07	0.40 $\pm$ 0.06	0.36 $\pm$ 0.07	0.71 $\pm$ 0.13	
CoV	12.8	14.2	18.8	17.9	
Exponent 'a'	6231 $\pm$ 634	7015 $\pm$ 574	6267 $\pm$ 873	5592 $\pm$ 1140	4372 $\pm$ 1126
CoV	10.5	8.5	14.5	19.3	26.6
Exponent 'b'	1.37 $\pm$ 0.26	1.16 $\pm$ 0.17	1.23 $\pm$ 0.27	2.14 $\pm$ 0.44	1.45 $\pm$ 0.33
CoV	19.9	15.5	22.6	21.3	23.1
Exponent 'c'	1.89 $\times 10^{-4}$	1.15 $\times 10^{-4}$	1.11 $\times 10^{-4}$	3.02 $\times 10^{-4}$	1.80 $\times 10^{-4}$
	+ 0.71 $\times 10^{-4}$	+ 0.36 $\times 10^{-4}$	+ 0.31 $\times 10^{-4}$	+ 0.78 $\times 10^{-4}$	+ 0.47 $\times 10^{-4}$
CoV	38.9	32.1	29.2	26.5	26.3
Modified RMS	64.4 $\pm$ 5.6	57.0 $\pm$ 5.3	58.2 $\pm$ 6.2	68.9 $\pm$ 4.3	67.7 $\pm$ 4.8
CoV	9.1	9.2	10.6	6.2	7.2
RMS (subaerial)	83.1 $\pm$ 7.4	79.1 $\pm$ 5.3	78.7 $\pm$ 8.5	86.2 $\pm$ 5.1	85.6 $\pm$ 3.1
CoV	9.0	6.7	10.8	6.0	3.6

CoV = coefficient of variation.



most efficient forms for the discharge of ice. Reynaud (1973) calculated shear stresses across the cross-profile of Athabasca Glacier, and showed that a 'U' shaped trough has approximately 50% more capacity than a 'V' shaped one for a given width and depth.

Svensson (1959) first applied mathematical analysis to the description of the glacial valley cross-profile, concluding that the cross-section was parabolic. Graf (1970) and Doornkamp and King (1971) found that a parabola best approximates trough shape, which suggests that the simple power curve  $y = ax^b$  can be used to approximate the cross-section of glacial troughs. Wheeler (1984) suggested that a better method is to use a second order polynomial equation ( $y = a + bx + cx^2$ ), so that the cross-section can be described with one symmetrical curve. The curve generated is not significantly constrained in either direction and can be used to describe the complete cross-section with one symmetrical curve.

However, these studies were regarded purely as curve fitting exercises and little attempt was made by these authors to assess the mode of formation of the valleys and the influence of the bedrock properties thereon. Using a different approach, Aniya and Welch (1981a,b) fitted curves to valley and cirque cross-profiles in the McMurdo Dry Valleys, Antarctica, in an attempt to assess the ability of the curve to accurately estimate sediment depth on the valley floor. As a corollary to this work, Aniya and Welch (1981a,b) suggested that morphological differences between the valleys and cirques reflect various stages in trough and cirque development, rather than differences in lithology or orientation.

#### 4.7.2. Glacial Drainage Density

In the present study, glacial drainage density (density of glacially moulded troughs) was assessed for at least 14 troughs from each region (Table 4.6). No major differences were encountered between regions despite major variation in rock quality and structural controls. This in a large part reflects the controlling influence of glacial erosion whereby an essentially equilibrium glacial valley system is created. Nevertheless, comparison of rock mass strength measures with glacial drainage density indicates a strong positive correlation (Fig. 4.15a,b, Table 4.7). A trend towards increasing

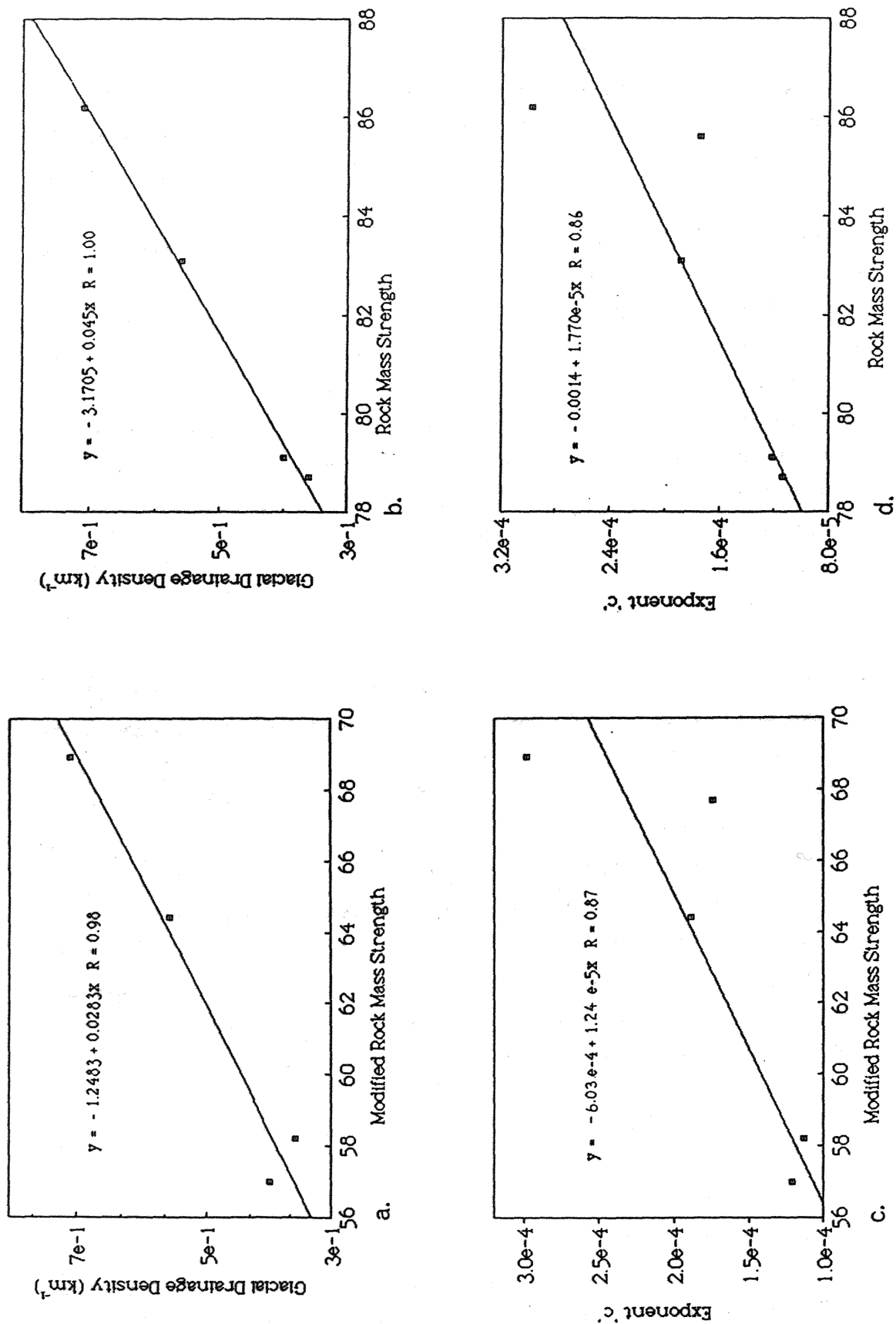


Figure 4.15. (a) and (b) Graphical representation of relationship between glacierized drainage density and mass strength of the bedrock. (c) and (d) Relationship between rock mass strength and valley shape, as indicated by the exponent 'c'. Note the strong control of RMS on the morphometric variables in each case.

Table 4.7. Correlation matrix for rock field and laboratory strength versus valley shape measures.

	FR	f	Density	a	b	c	Mod RMS	RMS	Shore	LA	Schmidt
FR	1.0										
f	0.89 p<0.05	1.0									
Density	-0.97 p<0.1	-0.81 ns	1.0								
a	0.62 ns	0.70 ns	-0.78 ns	1.0							
b	-0.95 p<0.05	-0.88 p=0.05	0.92 p<0.1	-0.42 ns	1.0						
c	-0.97 p<0.01	-0.86 p<0.07	0.99 p<0.02	-0.43 ns	0.97 p<0.01	1.0					
Mod RMS	-0.93 p<0.05	-0.87 p=0.05	0.98 p<0.05	-0.79 ns	0.79 ns	0.87 p<0.06	1.0				
RMS	-0.93 p<0.05	-0.82 p<0.1	0.99 p<0.005	-0.78 ns	0.78 ns	0.86 p<0.06	0.99 p<0.001	1.0			
Shore	-0.39 ns	0.02 ns	0.33 ns	-0.16 ns	0.28 ns	0.30 ns	0.27 ns	0.38 ns	1.0		
LA	-0.11 ns	-0.55 ns	0.06 ns	-0.29 ns	0.22 ns	0.12 ns	0.19 ns	0.07 ns	-0.83 p<0.1	1.0	
Schmidt	-0.21 ns	0.17 ns	0.10 ns	-0.10 ns	0.11 ns	0.09 ns	0.08 ns	0.20 ns	0.97 p<0.01	-0.84 p<0.1	1.0

ns = not significant at 90% level, p = level of significance

FR = form ratio, f = shape factor, density = glacial drainage density, a = exponent 'a', b = exponent 'b', c = exponent 'c', mod RMS = modified rock mass strength, RMS = rock mass strength (subaerial), shore = shore hardness, LA = Los Angeles abrasion resistance, Schmidt = Schmidt hammer rebound.

drainage density with increase in rock mass strength is developed. This is an apparently anomalous result, for drainage density would be expected to be highest in the weakest rocks (Cooks, 1983).

The relatively high glacierized drainage density obtained for the Fiordland region is probably inherited from the pre-glacial fluvial system with minimal modification. Following inception of the glacial system, the high rock mass strength would permit only relatively slow landscape modification, so that the present glacierized drainage is a palimpsest of the equilibrium glacial and fluvial drainage system. Conversely, in the relatively low RMS rocks of the Mts Cook and Aspiring regions, erosion and denudation rates are significantly higher (J.Adams, 1980; Whitehouse, 1987), allowing divide reduction, drainage capture and the development of large outlet glacial troughs along lines of structural weakness. This has resulted in progressive reduction of the glacial drainage density. The zone of highest uplift and erosion on the western side of the central Southern Alps displays higher glacierized drainage density than the greywacke terrain on the eastern side of the Main Divide (Table 4.6). This pattern is largely a reflection of rapid uplift, and rapid fluvial and glacial erosion preferentially exploiting, and having the geometry maintained, by zones of structural weakness.

#### 4.7.3. Parabolas As Glacial Valley Cross-Profile Analogues

Valley-side slope inclination was of limited utility in the description of the glacially moulded rock slopes due to the pervasiveness of structural controls on slope form. An attempt was made to fit parabolic curves to the slopes to enable their numerical description. However, structural controls and difficulty in matching the valley profiles reduced the utility of this method. Another problem was the nature of the topographic maps available for the analyses. The small scale and frequent inaccuracy of the 1:63,360 topographic maps reduced their suitability for detailed morphometric analyses. Insufficient time and resources were available to allow detailed field surveying of the slopes.

However, the small scale of the maps was sufficient to allow the generation of quadratic curves to fit the complete cross-profile, without the need to treat the opposing valley sides separately. The curve:

$$Y = a + bX + cX^2$$

(1)

can extend below the zero datum of the coordinate system used and its turning point can be both altitudinally and laterally shifted relative to the mid-point of the valley through the general character and asymmetry of the cross-section (Wheeler, 1984). Better fit to the valley cross-profiles can be obtained by fitting third or fourth-order polynomials, but the problems in interpreting the derived equations outweigh their usefulness. Good quality aerial photographs were used to identify the surface materials and to supplement the maps, with limited ground control. Within each study region, the relatively uniform structure and lithology holds the effects of geology constant. At least 15 curves were fitted to representative troughs from each region and the mean values of the derived 'a', 'b' and 'c' coefficients are given in Table 4.6. The quadratic equations derived at each site, the regression coefficient and the number of data points used to derive each equation are tabulated in Appendix Two.

The exponent 'c' is sensitive to the slope of the parabola, so that if the parabola is a good fit to the glacial valley cross-section, then 'c' is a good indicator of the variation in slope inclination between the terrains. An increase in 'c' reflects a steepening and narrowing of the curve, whilst 'a' and 'b' control the location of the curve turning-point and are inter-related. Consequently, the exponent 'c' appears to be the most appropriate exponent for application as a valley shape index. This is supported by the relationship between form ratio, shape factor and the 'c' exponent (Table 4.7).

The relationships between the exponents 'a', 'b' and 'c' and regional modified and subaerial rock mass strength are displayed Table 4.7. Correlations significant at the 90% or higher level are only developed for the relationship between the coefficient 'c' and the mass strength of the bedrock in each morphological terrain (Fig. 4.15c,d, Table 4.7). If the 'c' exponent is a good profile shape descriptor, then following the relationship outlined above, the increase in 'c' with increasing RMS reflects a narrowing and steepening of the troughs, and vice-versa for reduction in RMS. Further, the correlation of 'c' with glacial drainage density indicates a narrowing and steepening of the valleys with increase in the latter (Table 4.7). This reflects the obvious auto-correlation between the two factors and RMS control on the development of the landscape.

#### 4.7.4. Shape Factors

The form ratio (FR) (Graf, 1970; Andrews, 1972) is a useful measure of trough form, but it is not by itself an adequate form descriptor as U- and V- shaped troughs can have the same FR. Graf recommended the application of the FR with a parabolic curve descriptor. However, with regard to the aims of this study, a combined approach was not suitable. A single measure that would adequately quantify the trough cross-profile form was required.

The Form Ratio, as defined by Andrews (1972, 1975), and shape factor (f) of Nye (1965) and Mathews (1967), were utilized as trough shape indices. Form Ratio (FR) was defined as the width of the trough at the trimline divided by two times the valley depth below the trimline. At least 15 FRs were measured for each region and the means calculated (Table. 4.6). The height of the trimline was estimated from the upper level of glacial planation. In the Mt. Aspiring and Fiordland areas assessment was made both from aerial photographs and in the field. In the South Westland and Mt. Cook regions, the glaciation limit was derived from reconstructions of the late Pleistocene glacial system by Mathews (1967) and Porter (1975). The shape factor (f) is defined as:  $f = \text{Cross-section area/height of trimline above the thalweg} \times \text{trough perimeter}$ . The mean value for each region was obtained, with at least 15 readings taken per region and the results tabulated in Table 4.6.

A strong negative correlation was obtained for the relationship between f and modified RMS significant at 95% confidence level ( $r = -0.87$ , Table 4.7, Fig. 4.16a,b). This correlation improved to  $r = -0.93$  when FR rather than f was used in the analysis (Fig. 4.16c,d). This indicates that as the modified RMS (i.e., resistance to glacial erosion) increases, a trend towards reduction in FR and f develops, i.e., the development of deeper, narrower glacial troughs. Conversely, with reduction in modified RMS, the valleys tend to become relatively overwidened.

#### 4.7.5. RMS Versus Valley Shape

The relationship between the valley shape measures and rock mass strength indicates the presence of a strong causal relationship between the two sets of factors. However, it must be realized that

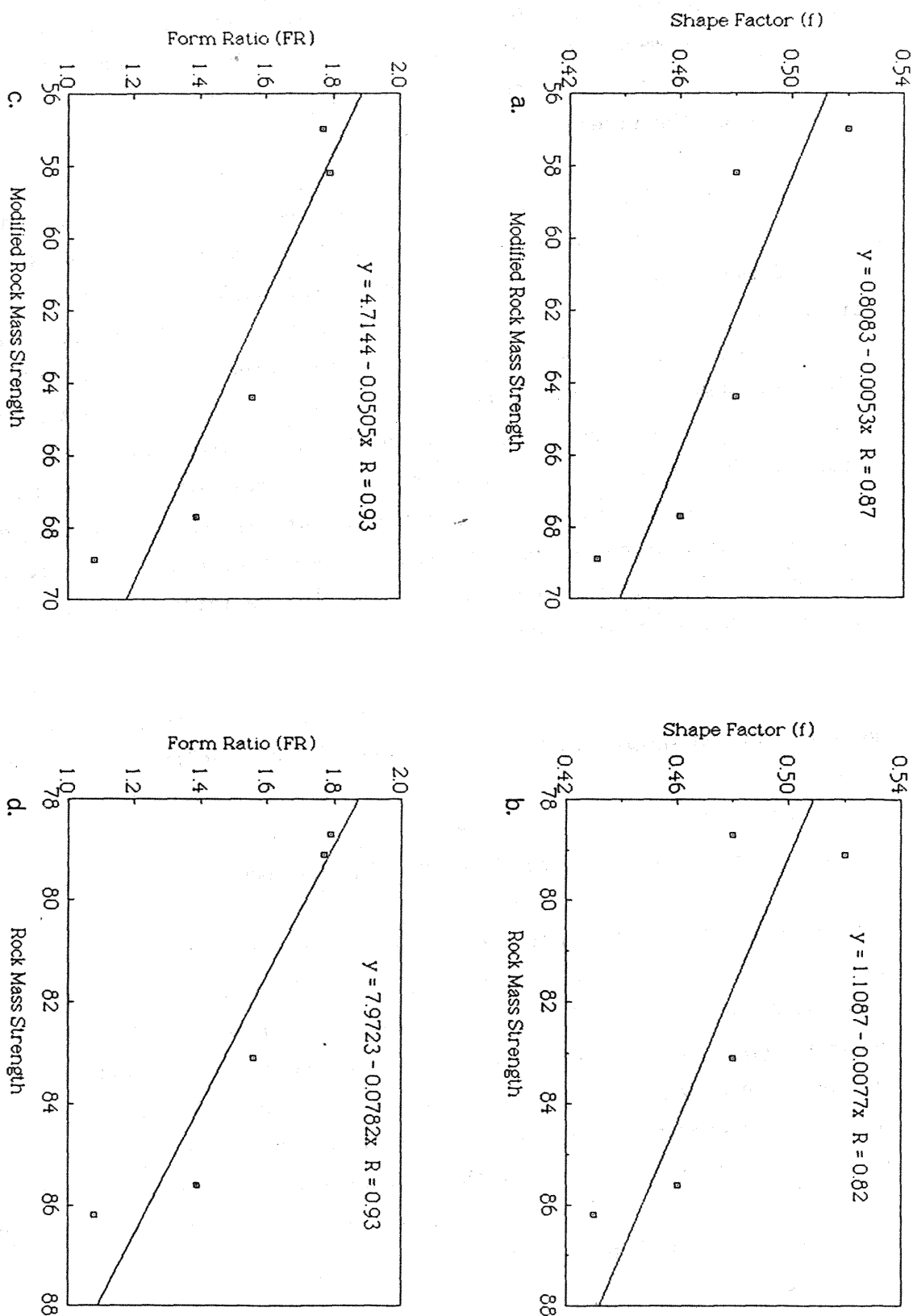


Figure 4.16. Relationship between rock mass strength with respect to glacial and subaerial processes and trough cross-profile shape. (a) and (b) Relationship between RMS and valley cross-profile shape factor (f). (c) and (d) Relationship between RMS and valley cross profile form ratio (FR).

these are only general trends with marked departures from the mean regression surfaces being apparent. Further, for the RMS of foliated schist and greywacke, the standard error of the data about the mean regression surface is large. This fact reflects controls of the foliation on the strength of the rock.

Further analysis was attempted using the shape measures and mean RMS with respect to subaerial processes. Examination of Figs. 4.15b, 4.16b,d and Table 4.7, indicates that a strong negative correlation significant at the 95% level, was obtained for RMS versus shape measures exponent 'c', form ratio and shape factor. The trend confirms that in weaker, highly jointed rock masses, such as the Aspiring schist and Mt. Cook greywacke, broader flatter troughs are developed. Thus, the RMS properties of the slope rock control the amount and rate of slope retreat. Preferential widening of the troughs and consequent slope destabilization occurs except where structural controls are paramount. Conversely, the high erosion resistance, plus high stability to subaerial processes of the northern Fiordland plutonic rocks has given rise to deep, narrow troughs where deepening has apparently exceeded widening. The high RMS of the slope rock in northern Fiordland allows the troughs to maintain their deep, narrow form.

#### 4.7.6. Rock Intact Strength Versus Valley Shape

Cooks (1983) argued that the morphology of fluvial valleys was largely controlled by the intact rock strength properties of the host rock mass. In particular, tensile, elastic moduli, U.C.S and peak shear strength values were found to be strongly correlated with slope, and drainage density. Thus, an attempt was made to quantify aspects of the intact strength of the rock masses from each of the study regions and to test for correlations with estimates of glacial trough shape. The methods of rock strength analysis and results are detailed in Appendix Three and Chapter Five.

Mean intact strength values were plotted against glacierized drainage density, exponent 'c', form ratio and shape factor for each region (Figs. 4.17, 4.18). The rock strength values are given in Table 4.8 and correlations in Table 4.7. Note the wide standard deviations in strength caused by the foliation of the schist. No clear trends are developed, confirming that the variations in the intact strength



Table 4.8. Mean intact strength parameters for each morphological terrain

Study area	South Westland	Mt Cook	Mt Aspiring	Nth Fiordland	Sth Fiordland
Rock type	Biotite schist	Greywacke/ argillite	Grey/green schist	Diorite/ gabbro	Granite/ metamorphics
Point load strength (MPa)	$8.19 \pm 1.24 +$ $2.86 \pm 0.29 //$	$11.21 \pm 0.15$	$5.85 \pm 2.55 +$ $1.81 \pm 0.90 //$	$5.50 \pm 1.31$	$5.32 \pm 1.44$
Brazil tensile strength (MPa)	$11.03 \pm 2.45 +$ $5.08 \pm 0.15 //$	$20.14 \pm 1.34$	$6.78 \pm 1.16 +$	$8.49 \pm 1.91$	----
Shore hardness	$61.0 \pm 7.1 +$	$83.6 \pm 8.1$	$49.7 \pm 8.9 +$	$76.6 \pm 3.7$	$78.1 \pm 3.3$
Los Angeles Abrasion (%)	$27.3 \pm 3.3$	$13.2 \pm 2.1$	$38.1 \pm 6.4$	$29.2 \pm 5.9$	$25.4 \pm 3.1$
Schmidt hammer rebound	$51.5 \pm 3.1$	$64.5 \pm 4.4$	$49.5 \pm 6.9$	$58.5 \pm 2.8$	$61.1 \pm 4.7$

+ refers to tests conducted perpendicular to foliation, // refers to tests parallel to foliation.

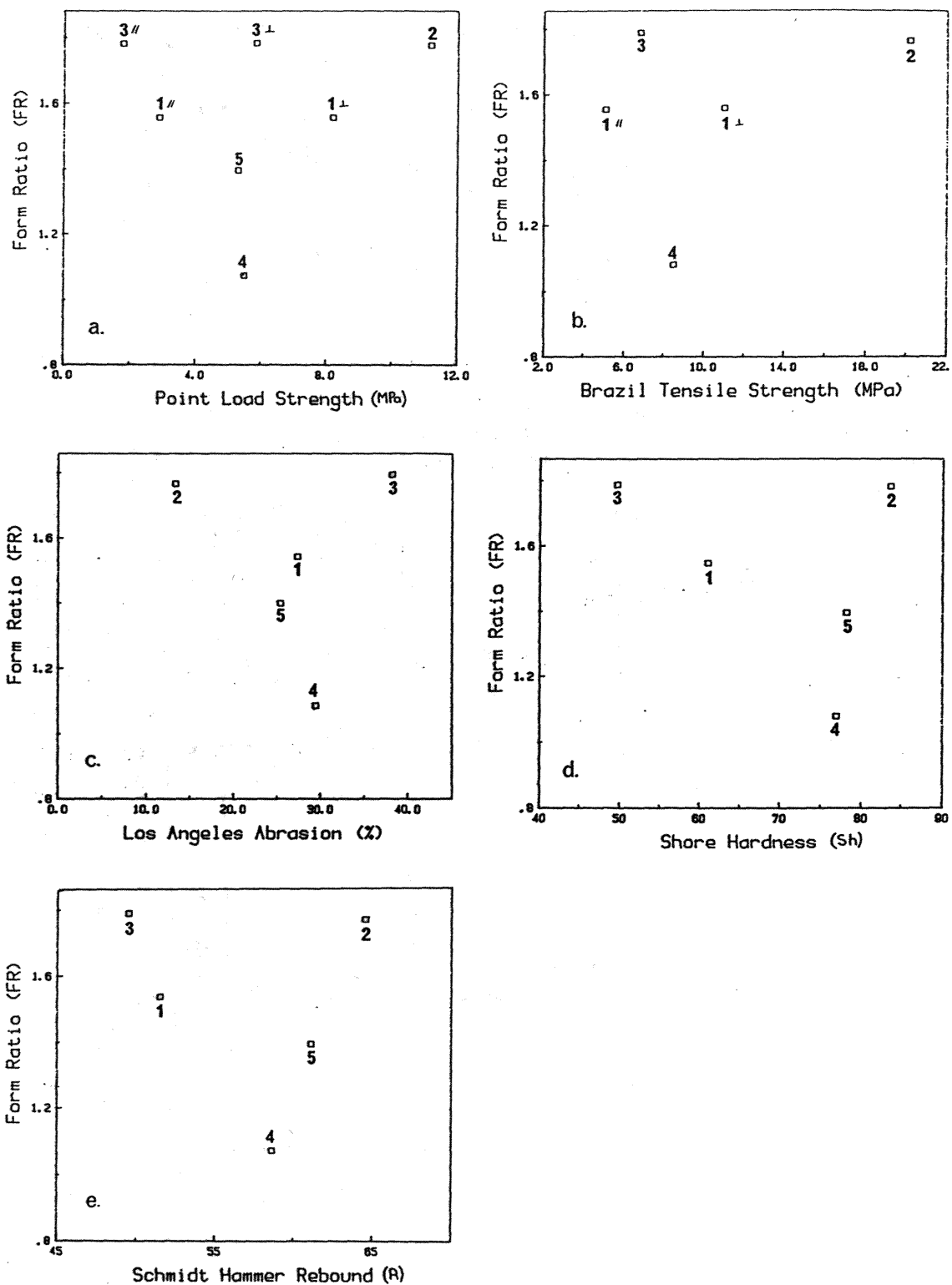


Figure 4.17. Relationship between point load strength, Brazil tensile strength, abrasion resistance, Shore hardness, Schmidt hammer rebound and the valley cross-profile shape factor (f). //: tested parallel to foliation, +: tested perpendicular to foliation, 1. South Westland, 2. Mt Cook, 3. Mt Aspiring, 4. northern Fiordland, 5. south-central Fiordland.

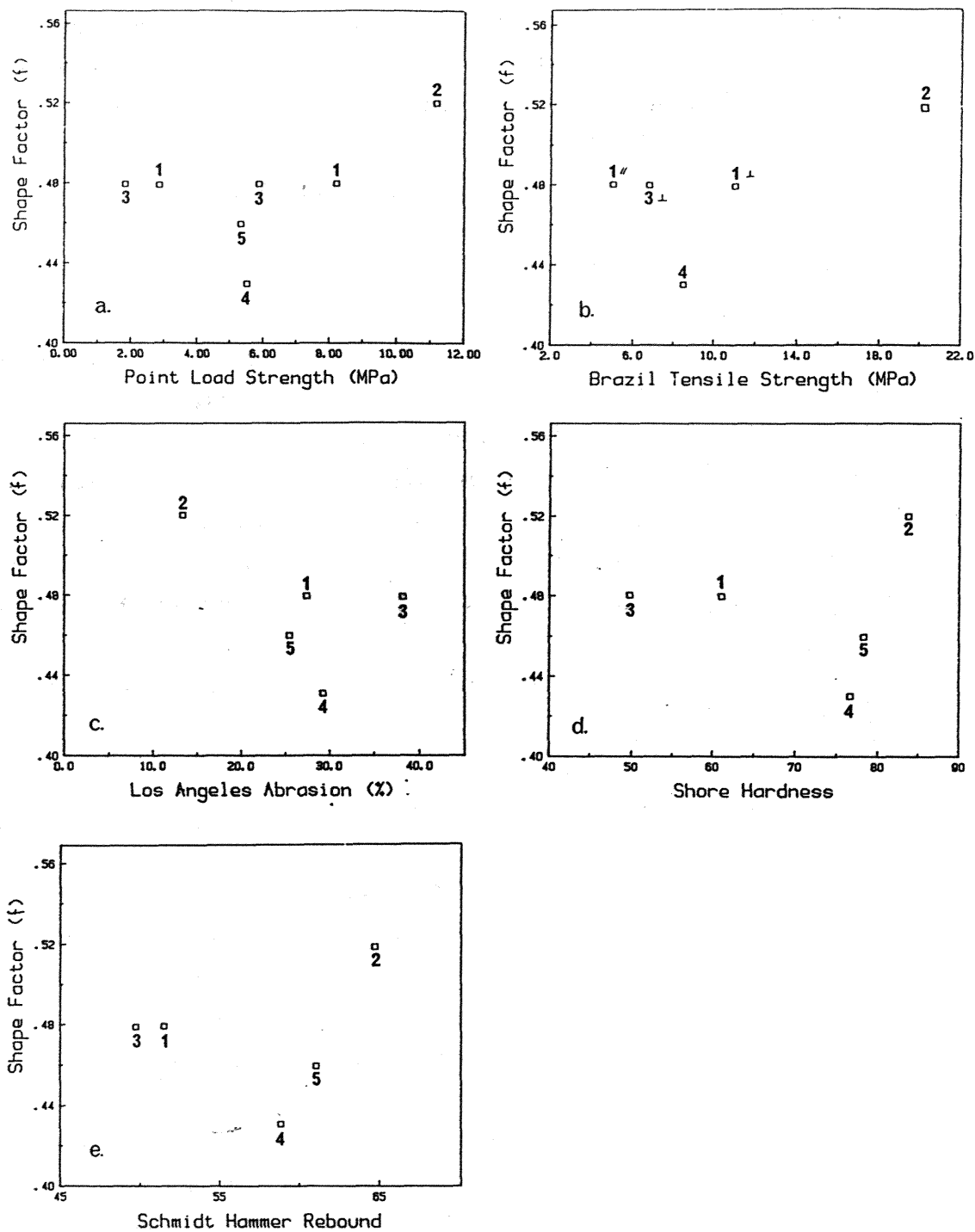


Figure 4.18. Relationship between point load strength, Brazil tensile strength, abrasion resistance, Shore hardness, Schmidt hammer rebound and valley cross-profile form ratio (FR). Symbols and numerals as given in Fig. 4.17.

properties of the host bedrock have little impact on the mode of erosional development and enlargement of the glacial troughs. However, when the RMS (joint) properties of the bedrock are considered, statistically significant correlations are developed, possibly reflecting the control of the RMS properties of the bedrock on the development of the erosional landscape (Fig. 4.16).

#### 4.7.7. Relative Importance of Erosion Processes.

The apparent control of the RMS properties of the bedrock on the mode of erosional development of the glacial troughs and final valley cross-profile form, has important implications for assessment of the relative contributions of subglacial plucking and abrasion to the forms resulting from the glacial erosion process. Absolute rates of erosion and the relative rank of the different mechanisms are affected by the geotechnical properties of the bedrock traversed by the ice.

The total mass of material eroded per unit area ( $\psi$ ) may be expressed in the form:

$$\psi = \iint_a [M_a + M_d + M_m + M_q] da \quad (2)$$

where  $M_a$  = mass of material removed by abrasion,  $M_d$  = mass of material removed by plucking,  $M_m$  = mass of material removed by meltwater,  $M_q$  = mass of material removed in solution by meltwater erosion, and  $a$  = area of glacier bed. However, the problem is to determine the relative contribution of each parameter and to assess their variability.

Drewry (1986) recognized that the present state of knowledge is insufficient to allow the separation of the various glacial erosive mechanisms or to permit assessment of relative rates. However, Drewry provided a crude ranking of the importance of each of the mechanisms:

Table 4.9. Ranking of glacial erosion processes.

Mode of erosion	Cold base	Warm base Hard rock	Soft rock
Abrasion	2	2	1
Crushing/fracture	1	1	2
Mechanical action of meltwater	3	3	
Solution in meltwater		4	4

where 1 = highest and 4 = the lowest.

However, use of the terms hard and soft as descriptors of rock strength properties is inadequate, as hard rock may be densely jointed, and soft rock massively jointed, giving the latter greater resistance to glacial plucking. In this study, it has been shown that the relationship between intact rock strength and the form of the glacial trough is poorly developed. In particular, rock abrasion resistance was found to be a non-significant factor with respect to final trough shape. The RMS, especially the joint properties of the bedrock, best explained the variations in trough form. The greywacke displays high abrasion resistance, but the close joint spacing gives it a low RMS, allowing rapid subglacial erosion by plucking and trough enlargement. Clearly, the assignation of relative importance of the various erosion processes is fraught with difficulty, with the contribution of each largely controlled by the strength properties of the eroded rock mass.

#### 4.8. Summary and Conclusions

The rock mass strength properties, stability and failure mechanisms of some alpine rock slopes have been catalogued. The work was undertaken both from the viewpoint of examining mode of slope development on different lithologies, and for evaluation of the resistance to subglacial erosion. These studies suggest the following:

- (1) Steep alpine rock slopes generally display equilibrium RMS forms, unless strong structural elements are evident, or they have been reduced to Richter denudation slopes.
- (2) After deglaciation and recession of the slope buttressing glacier, the steep slopes are destabilized by the changing stress conditions, and re-equilibrate rapidly with respect to subaerial processes towards RMS equilibrium forms.
- (3) The trough slopes have forms closely related to the RMS of their rock. The steep rock slopes formed on plutonic rocks in Fiordland have high RMS, and remain stable, displaying no evidence of deep-seated rock slope failures. Retreat is by rockfall/avalanche exploitation of the surficial sheeting joints. Modification of the slope rock is slow. Conversely, the closely jointed and foliated schist and greywacke are

relatively unstable and have their slopes controlled by the orientation of the foliation and dominant pre-existing tectonic joint sets. Modification of the slope rock is rapid.

(4) Selby's (1982) premise that rock slopes retreat at angles that preserve their strength equilibrium is supported for glacial trough slopes developed in closely jointed rock. Progressive slope reduction towards equilibrium forms occurs with distance from the glacier snout.

(5) The common textbook description of glacial valleys as being oversteepened (e.g., Embleton and King, 1975) is shown to be an inadequate generalization, at least with respect to the glacial troughs developed in the New Zealand Southern Alps. Oversteepening, if developed, is shown to be only a brief phase in the life-span of the slopes.

(6) The statement by Cooks (1983) that selected properties of intact bedrock control the form of fluvial valley forms, cannot be extended to glacial valleys. Rather, it has been shown here that the properties of the whole rock mass, as assessed by the RMS method, are the dominant controls on the geometry of glacial trough enlargement and final trough form.

## Chapter Five

# Intact Strength and Physical Properties of Some Rocks From New Zealand and Antarctica

## CHAPTER FIVE: INTACT STRENGTH PROPERTIES OF SOME ROCKS FROM NEW ZEALAND AND ANTARCTICA

### 5.1. Introduction

Rock intact strength and its control on landforms is a recurrent theme in the literature. However, few quantitative assessments have been made of the influence of rock strength on landform development (Cooks, 1979, 1983; Nicholas and Dixon, 1986). The geomechanical properties of rocks from selected profiles in each study region were assessed. The laboratory rock strength tests were undertaken to enable: (1) a comparison with *in situ* RMS tests, (2) evaluation of the geomechanical properties of the rocks for input to the finite element stress analysis (Ch. 7), and (3) the evaluation of the resistance of the rock to erosion processes and its variation between morphological terrains. Rock samples were taken from parts of both the New Zealand Southern Alps and McMurdo Dry Valleys, Antarctica.

### 5.2. Methods

Large oriented rock samples were selected in the field and intact strength measured in the laboratory. Unfortunately, frequent difficulty of access and removal of rock material allowed only limited amounts of sample to be retrieved, and as a result, only a limited geotechnical programme could be attempted. For the purposes of this study, the important rock properties were: (1) density, (2) porosity, (3) point load strength, (4) Brazil tensile strength, (5) intact shear strength, (6) dynamic elastic moduli and Poisson's ratio, (7) Los Angeles abrasion resistance, and (8) Shore hardness. Values obtained from field Schmidt hammer rebound measurements were added for comparison purposes. Methods and results are detailed in Appendix 3.

Correlation and regression analyses were applied to the data to test for relationships between the various rock strength measures and enable the estimation of intact strength where insufficient material was available. The relationships were assumed to be linear unless a plot revealed a distinct curvilinear trend. Further tests were undertaken on vacuum saturated samples where sufficient material was available to examine the strength changes that result from saturation of the rock.



### 5.3. Correlations Between Rock Intact Strength and Physical Properties

#### 5.3.1. Introduction

The following section presents the results of correlations of the various strength indices. Deere and Miller (1966) presented the results and comparisons of rock strength indices from 27 different lithologies, which are used for comparison in this study.

#### 5.3.2. Point Load Strength

Uniaxial compressive strength (UCS) is widely used as a practical measure of intact rock strength. However, the point load strength test is often used to estimate the UCS value, since considerably more sample preparation is required for UCS determination (Broch and Franklin, 1972). UCS was not measured in this study, although the correction of Bieniawski (1975) was applied to the relevant point load indices to allow the calculation of  $E_{30-50}$  (dynamic elastic moduli at 30-50% of UCS).

Indirect tensile tests have been correlated with UCS and point load strength. Szlavín, 1974 and Gunsallis and Kulhawy (1983) obtained strong correlations between point load and Brazil tensile strength. In the present study, an 'r' value of 0.89, significant at the 1% level, was calculated for the correlation of the point load index with the appropriate Brazil tensile strength value (Table 5.12; Fig. 5.1a). This strong correlation was expected because the point index was originally developed as a method of determining indirect tensile strength (Deere and Miller, 1966).

#### 5.3.3. Rock Physical Properties

Unit weight is, in the literature, commonly linked with UCS. D'Andrea *et al.* (1964) and Smorodinov *et al.* (1970) obtained strong correlations between the two indices, although Deere and Miller (1966) obtained an 'r' value of only 0.604 for their data. Using point load index as an estimator of UCS, a correlation coefficient of 0.67 was obtained in the present study, significant at the 1% level (Table 5.1, Fig. 5.1b). The trend is towards higher strength with greater density, although there is considerable scatter about the 'best-fit' line.

Table 5.1 Correlation coefficients of rock strength and physical properties for some rocks from New Zealand and Antarctica.

	Poros.	Pt.Ld. (dry)	Pt.Ld. (sat)	Braz.T. (dry)	Braz.T. (sat)	Sonic (dry)	Sonic (sat)	Cohes. (sat)	Shore (dry)	Shore (sat)	L.A. (dry)	Schmidt
Density (dry)	-0.84 p<.001	0.67 p<.005		0.56 p<.05		0.65L p<.05			0.28 ns		0.77 p<.01	0.27 ns
Density (sat)	-0.79 p<.001		0.65 p<.05		0.58L p<.1		0.66 p<.1	0.34 ns		0.09 ns		0.25 ns
Poros.	1.0	-0.75L p<.01	-0.87L p<.01	-0.85L p<.001	-0.9 p<.005	-0.69 p<.01	-0.76 p<.005	-0.76 p<.01	-0.67L p<.005	-0.66L p<.01	-0.92L p<.001	-0.62L p<.001
Pt.Ld. (dry)		1.0		0.89 p<.001		0.52 p<.05			0.23 ns		-0.79L p<.001	0.63L p<.05
Pt.Ld. (sat)			1.0		0.87 p<.05		0.87 p<.05	0.71 ns		0.53 ns		0.72L p<.05
Braz.T. (dry)				1.0		0.68 p<.005			0.47 p<.1		-0.8 p<.001	0.78 p<.001
Braz.T. (sat)					1.0		0.65 p<.05	0.74 p<.05		0.6 p<.05		0.73 p<.005
Sonic (dry)						1.0			0.58 ns		-0.70 p<.01	0.54 p<.1
Sonic (sat)							1.0	0.64 p<.05		0.55 ns		0.63 p<.05
Cohes. (sat)								1.0		0.59 p<.1	-0.8L p<.05	0.62 p<.1
Shore (dry)									1.0		-0.7 p<.005	0.43 ns
Shore (sat)										1.0		0.32 ns
L.A. (dry)											1.0	-0.64L p<.005

Poros. = porosity, Pt.Ld. = point load strength, Braz.T. = Brazil tensile strength, sonic = p-wave velocity  
 cohes. = cohesive strength, Shore = Shore hardness, L.A. = Los Angeles Abrasion, Schmidt = Schmidt hammer rebound, Dry = tests  
 in oven-dried state, sat = tested in vacuum saturated state.  
 p = level of significance, ns = not significant at 90% level.

Table 5.2. Correlation coefficients for some isotropic igneous rock strength and physical properties

	Poros.	Pt.Ld. (dry)	Pt.Ld. (sat)	Braz.T. (dry)	Braz.T. (sat)	Sonic (dry)	Sonic (sat)	Cohes. (sat)	Shore (dry)	Shore (sat)	L.A. (dry)	Schmidt
Density (dry)	-0.93 p<.0001	0.7L p<.1		0.71L p<.01		0.63L p<.1			-0.31 ns		-0.64 p<.05	0.7 p<.05
Density (sat)	-0.93 p<.0001		0.78 p<.1		0.64L p<.1		0.77 p<.01	0.25 ns		-0.42 ns		0.7 p<.05
Poros.	1.0	0.87L p<.005	-0.85 p<.05	-0.88 p<.005	-0.76L p<.05	-0.73L p<.05	-0.91 p<.0001	-0.23L ns	-0.03L ns	-0.11L ns	0.85L p<.001	-0.68L p<.05
Pt.Ld. (dry)		1.0		0.9 p<.0001		0.61 p<.1			-0.15 ns		-0.9L p<.005	0.60 p<.1
Pt.Ld. (sat)			1.0		0.93 p<.1		0.84 p<.05	0.41 ns		0.48 ns		0.86 p<.05
Braz.T. (dry)				1.0		0.62 p<.06			0.03 ns		-0.86L p<.0001	0.68 p<.05
Braz.T. (sat)					1.0		0.63 p<.1	0.3 ns		0.54 ns		0.73 p<.05
Sonic (dry)						1.0			0.03 ns		-0.65 p<.01	0.47 ns
Sonic (sat)							1.0	0.3 ns		0.36 ns		0.53 ns
Cohes. (sat)								1.0		-0.56 ns		0.15 ns
Shore (dry)									1.0		-0.36 ns	-0.23 ns
Shore (sat)										1.0		-0.17 ns
L.A. (dry)											1.0	-0.72 p<.05

p = level of significance, ns = not significant, L = log-linear relationship.  
 Column descriptors as given in Table 5.1

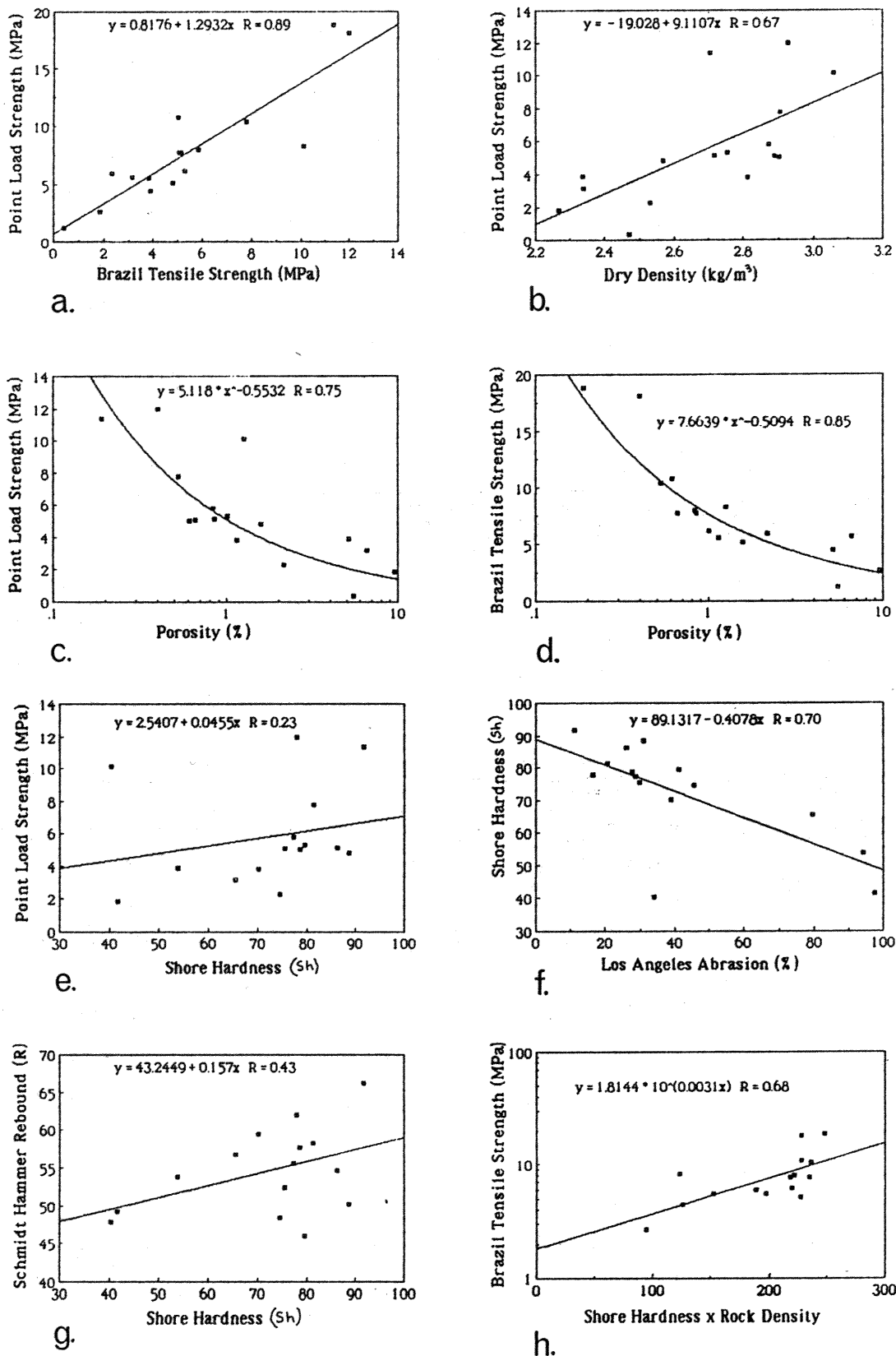


Figure 5.1. (a)-(h) Relationships between some rock intact strength and physical parameters. Details of comparisons given in text.

Smorodinov *et al.* (1970) obtained a strong relationship between UCS and rock porosity. In this study, a curvilinear relationship with a correlation of  $r = -0.75$  was determined for the point load strength of oven-dried rock as a surrogate of the UCS, indicating that the strength decreases with an increase in porosity (Table 5.1, Fig. 5.1c). However, when foliated rock and sandstone are deleted from the analysis, 'r' values of -0.87 and -0.90 were calculated for dry and saturated rock respectively (Table 5.2). Brazil tensile strength displays a similar curvilinear relationship with porosity (Tables 5.1 & 2, Fig. 5.1d).

#### 5.3.4. Shore Hardness

The Shore Hardness (Sh) test is a convenient and rapid method of comparing the hardness of rocks. The Shore hardness test was developed to determine the hardness of metals, and as metals are homogeneous, one rebound reading is enough to give a representative Shore hardness value. However, rocks are not homogeneous, being composed of a number of minerals and a single reading would not be representative of the complete specimen. Consequently, at least 20 readings were taken on a range of mineral types and the mean value considered to be representative of the whole rock (Brown *et al.*, 1981).

Deere and Miller (1966) obtained a strong correlation of 0.897 between UCS and Shore hardness, whilst Szlavins (1974) calculated an 'r' value of 0.84 for the same relationship. In this study, point load strength was used as a surrogate for UCS, and correlation with Shore hardness yields non-significant 'r' values of 0.23 & 0.53 for oven-dried and saturated tests respectively (Table 5.1, Fig. 5.1e). Szlavins (1974) determined an 'r' value of 0.81 for correlation of tensile strength and Shore hardness. However, in the present study, relatively poor, significant correlations of 0.47 and 0.6 were calculated for oven-dried and saturated rocks respectively (Table 5.1).

Deere and Miller (1966) calculated an 'r' value of 0.785 for the relationship between abrasion resistance and Shore hardness, while in the present study,  $r = -0.70$  was calculated for Los Angeles abrasion resistance versus Shore hardness for all rocks studied (Table 5.1, Fig. 5.1f), reducing to a non-significant -0.36 when only isotropic rocks are considered (Table 5.2). Nevertheless, the significant

correlation of the former suggests that Shore hardness could be used as a valid estimator of Los Angeles abrasion resistance.

Deere and Miller (1966) obtained an 'r' value of 0.872 for the relationship between Shore hardness and Schmidt hammer rebound. However, in this study, an 'r' value of only 0.43 (Table 5.1, Fig. 5.1g) was obtained for the same correlation, reducing to -0.13 when only isotropic igneous rocks were analysed (Table 5.2). This result and the poor correlation between Shore hardness and point load strength, suggests that the Shore hardness technique is not by itself a valid indicator of the strength of the whole rock. However, when Shore hardness is multiplied by rock density, a strong curvilinear relationship with rock strength is apparent (Fig. 5.1h).

#### 5.3.5. Los Angeles Abrasion

Examination of Tables 5.1 and 2 indicates that the Los Angeles (LA) abrasion index is significantly correlated with several rock intact strength and physical properties. As expected, it is strongly correlated with porosity (-0.92, Fig. 5.2a), rock density (0.77, Fig. 5.2b), point load strength (0.79, Fig. 5.2c) and Brazil tensile strength (0.88, Fig. 5.2d). The theory behind these correlations is that with increase in rock density, porosity reduces, the area of grain/grain contacts and the degree of crystal/grain interlocking increases, thus increasing the bulk rock abrasion resistance. Los Angeles abrasion resistance displays a significant correlation with Shore hardness (Fig. 5.1f). The strength of this correlation is improved by multiplying the Shore hardness by the appropriate dry rock density value (Fig. 5.2e).

#### 5.3.6. Schmidt Hammer Rebound

Field estimations of the compressive strength of *in situ* rock were obtained by means of a Schmidt hammer. Although the instrument actually measures hammer rebound due to rock elasticity, this value has been directly correlated with UCS (Day, 1980). Correlation of Schmidt hammer rebound values with intact strength measures yield the expected significant 'r' values (Tables 5.1 and 2). Deere and Miller (1966) obtained a correlation coefficient of 0.88 for Schmidt hammer rebound versus UCS, and the relationship is curvilinear. This result is reflected in the present study by an 'r' value for point load strength versus Schmidt hammer rebound of 0.63 (Fig. 5.2f), improving

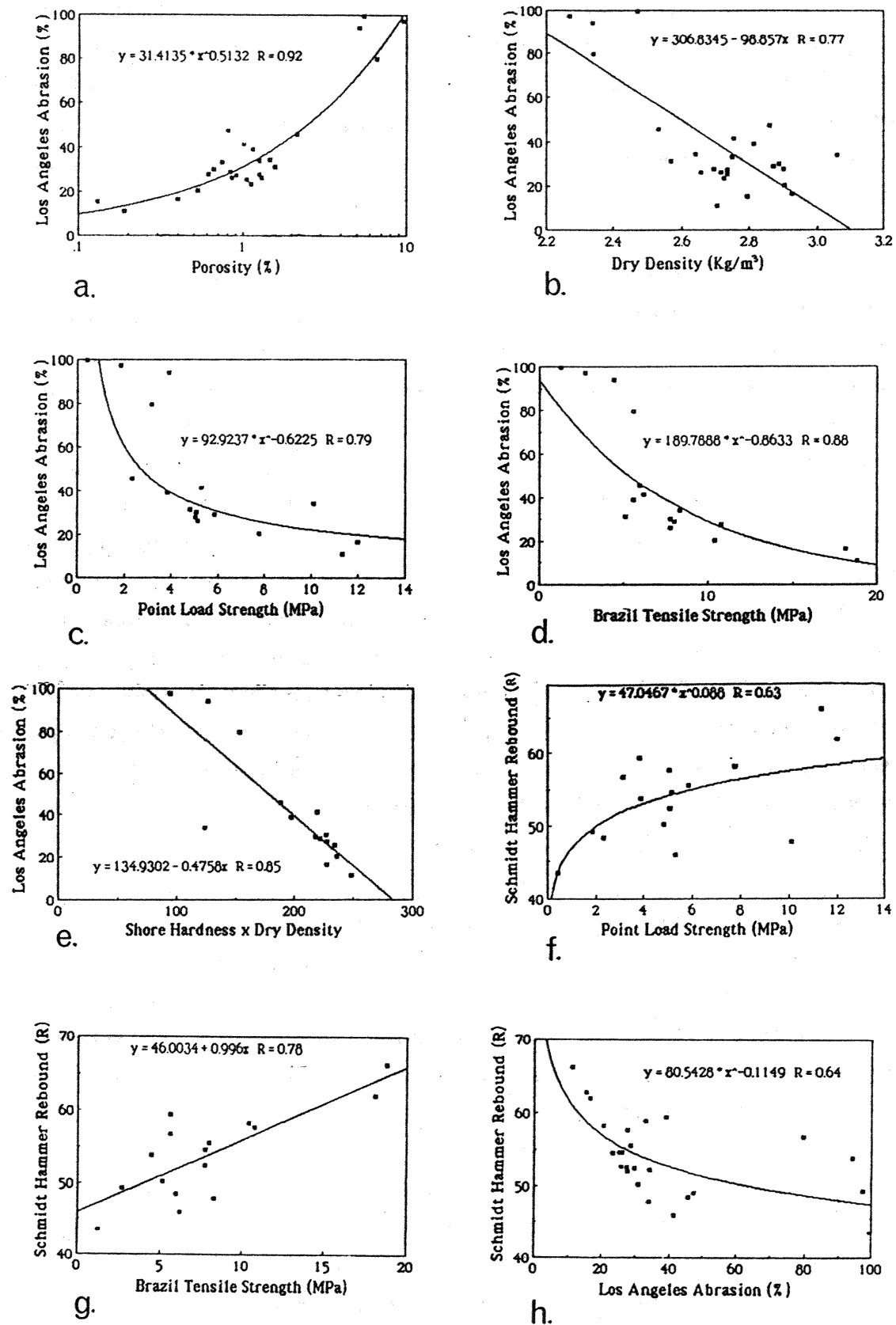


Figure 5.2. (a)-(h) Relationships between some rock intact strength and physical parameters.

to 0.72 when only saturated rocks are considered (Table 5.1). Similarly, correlation of Schmidt rebound and Brazil tensile strength of oven-dried rock gave ' $r$ ' = 0.78 (Table 5.1, Fig. 5.2g). The results of these analyses indicate that the Schmidt hammer can be used as a valid field measure of the UCS and tensile strength of the rocks studied.

Kazi and Al-Mansour (1980) obtained a reasonably constant proportionality between Los Angeles abrasion resistance of aggregates and Schmidt hammer rebound from the parent rock materials. This reflects the strong relationship between abrasion resistance and UCS obtained by Deere and Miller (1966) of ' $r$ ' = 0.78. In the present study, a curvilinear relationship, with a significant ' $r$ ' value of -0.64 was obtained for all rock types (Table. 5.1, Fig. 5.2h), improving to -0.72 when the foliated rocks (sandstone and schist) were removed from the analysis (Table 5.2). This result supports the premise of Kazi and Al-Mansour (1980) that the Schmidt hammer is a sensitive indicator of abrasion resistance for isotropic, igneous rocks. Since the Schmidt hammer can be used as an indicator of rock abrasion resistance, it was incorporated into the modified RMS scheme (section 4.6) to allow the quantitative evaluation of spatial variations in rock resistance to subglacial abrasion.

#### 5.4. Effect of Saturation on Rock Strength

Strength tests were undertaken on vacuum saturated rock samples where sufficient material was available. This was to enable the examination of strength changes that result from wetting/drying of the rock. There is a paucity of research into the effects of saturation on rock strength, although Broch (1974, 1979) used the point load strength index to investigate this change. Broch (1979) found that despite a general trend to strength reduction with saturation, some fine-grained non-porous rocks display a significant strength increase. As general conclusions, Broch (1979) argued that: (1) the strength reduction is progressively greater as the mafic mineral content increases, (2) strength reduction increases with the increasing development of schistosity and anisotropy.

Colbeck and Wiik (1965) determined that the saturated strength of quartz sandstone was only 50% of oven-dry strength. Michalopoulos and Triandafilidis (1976) conducted tests on several different lithologies

and concluded that the UCS reduces by ~20% when saturated, and the effect is further reduced with decreasing porosity. Similarly, Gunsallus and Kulhawy (1984) found that the effects of saturation are more pronounced as the rock tends from coarsely crystalline to fine-grained. With coarse crystalline rocks, strength changed little upon saturation due to their low porosity; while for coarse clastic and fine-grained sandstone, UCS drops were obtained of 30-40% and 50-70% respectively. Barton (1982) noted that saturated fracture toughness decreases 10-60% from the dry toughness depending on rock type. Water may affect the crack propagation in rock by chemically reacting with material at the crack tip and/or by mechanically reducing friction in the process zone.

The percentage tensile strength reductions/increases obtained upon saturation of the rock are displayed in Table 5.3 for all rock types examined. The general trend is similar to that determined by Broch (1979) using the point load strength index, but with some important differences. Fine-grained, non-porous greywacke was found to have a significant tensile strength increase upon saturation, a trend reflected by point load strength tests (Table 5.3, Appendix 3). Broch (1979) encountered similar properties for his fine-grained, non-porous rocks. The greatest strength reduction was obtained with foliated, highly anisotropic schist, despite its relatively low porosity. Strength reduction in the schist is significantly higher when it is tested perpendicular rather than parallel to the foliation. This probably reflects the geometry of the drainage pathways in the schist, and failure along mica bands parallel to the foliation. Free water drainage is apparently controlled by the planar quartz laminae in the schist (Hall, 1987).

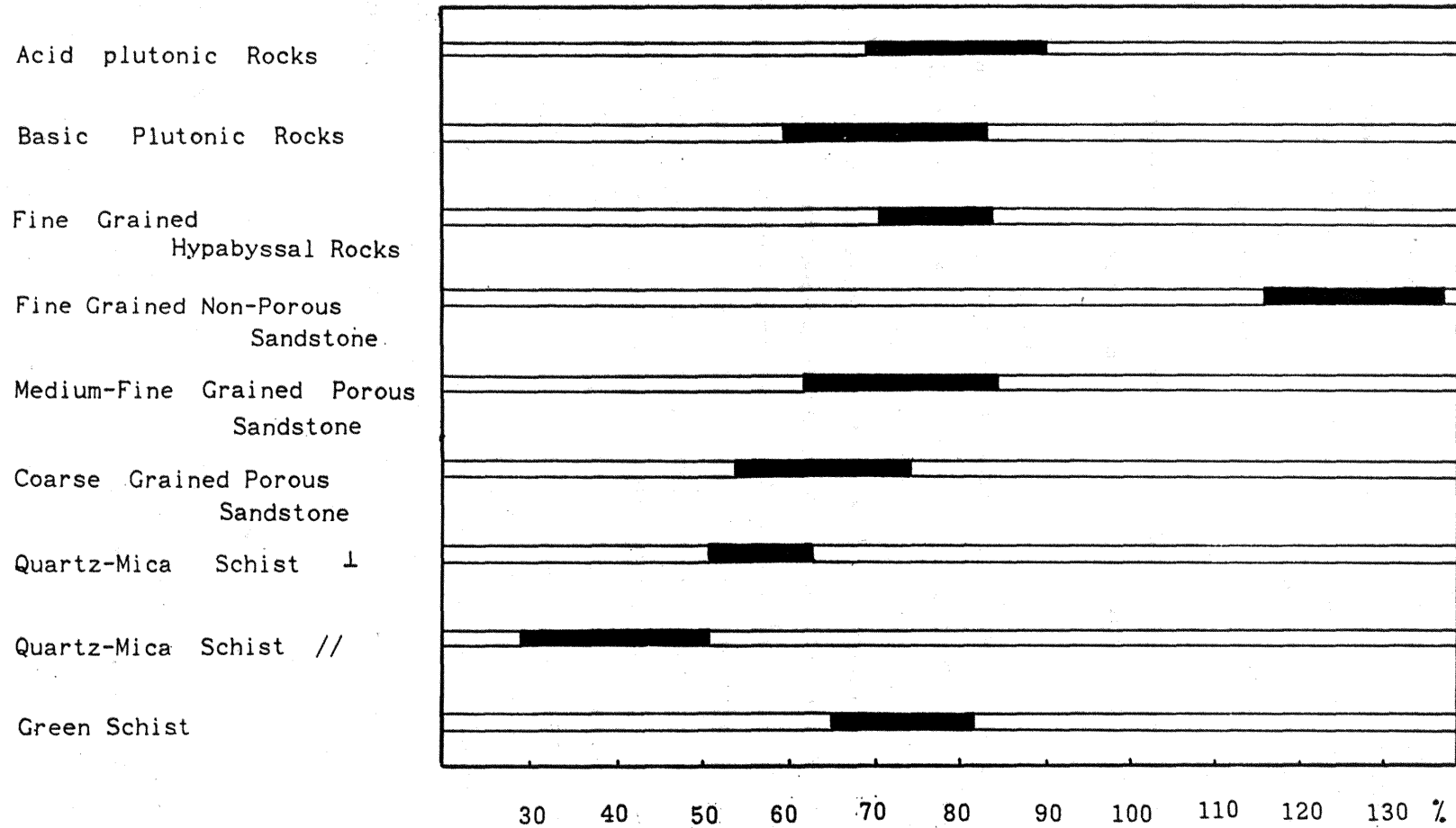
Greater percentage strength reduction is developed in basic plutonic, relative to acid plutonic rocks. A similar trend is observed when comparing fine and coarse-grained porous sandstones, although insufficient data are available to define this unequivocally. This trend is somewhat different to that encountered by Gunsallus and Kulhawy (1984), in which the fine-grained sandstone displayed the greater strength reduction. This latter trend was explained by the effective stress concept (Terzaghi, 1945), whereby effective stress (total stress minus pore water pressure) controls the rock failure stress as long as the rock has low grain contact area and connected pore space. However, this mechanism is unlikely to operate in low porosity, impermeable plutonic rocks.



Table 5.3

BRAZIL TENSILE STRENGTH OF WATER SATURATED ROCKS  
IN % OF STRENGTH OF OVEN DRY ROCKS

TYPES AND GROUPS OF ROCKS



## 5.5. Implications of Strength Reduction of Saturated Rock For Geomorphic Studies

The results of this study have important implications for the strength and failure of rock in the alpine glacial environment, and rates and modes of surficial rock weathering. The latter is beyond the scope of this study but has been recently evaluated by Hall (1987). Hall (1986) recognized that the actual amount of water and its distribution in the rock is critical for weathering studies, not just the presence of water in the rock and its water absorbing capacity. Hall (1986) further recognized that laboratory experiments on saturated rock samples are poor representatives of field conditions.

The porosity and permeability of the bedrock was argued by Boulton and Jones (1979) and Boulton *et al.* (1979) to control subglacial drainage, and thus the mode of subglacial erosion at the scale of continental ice-sheets. However, the permeability of the intact rock is a minor factor at the scale of the glacial valley cross-profile, where rock failure and subglacial exploitation of the weakened rock is primarily controlled by the presence and geometry of the major discontinuities, and resultant cleft water pressures.

In the subglacial and near pro-glacial situation, significant strength changes may result from high meltwater concentrations. The probability of saturated rock *in situ*, could markedly reduce the stresses required to cause failure of the intact (or jointed) rock. Such a strength decrease is particularly marked in the highly foliated schists, where rock swelling, failure and hence erosion, are strongly influenced by the geometrical relations of the foliation to the slope (Hall, 1987). Coarse crystalline and low porosity rocks are least influenced by water saturation. For porous, saturated foliated rocks, fracture initiation due to freezing is an important source of rock weakening and joint propagation (Walder and Hallett, 1985).

The apparent strength increase of saturated greywacke and marked reduction in strength in the foliated schist may help explain the development of the central Southern Alps landscape. Rock mass strength studies suggest that the unweathered schist in South Westland has a higher strength and erosion resistance than the greywacke on the eastern side of the Main Divide. However, erosion rates are

significantly higher in the schist to the west, so that the highest mountains are developed in the greywacke on the eastern side of the Main Divide (J. Adams, 1980, 1985; Whitehouse, 1987, Kamp *et al.*, submitted).

A partial explanation for this apparent paradox lies in the significantly greater weatherability of the schist (J. Adams, 1985). This factor would allow rapid physical and chemical breakup of the rock, and rapid erosion by fluvial and glacial processes. Fahey (1983) examined frost action and hydration effects on schist from Central Otago, New Zealand and demonstrated that frost action, associated with the volumetric expansion of pore water upon freezing, was 3 to 4 times more effective than hydration in the breakup of the schist. Freeze-thaw is thus a powerful potential source of rock disintegration. When this process is coupled with the high degree of saturated strength reduction and stress-induced fracturing of the schist, it may allow rapid rock physical and chemical weathering and erosion in favoured topographic and climatic situations. The RMS assessments were made on near unweathered schist surfaces, so that the derived RMS values for the South Westland study region are not representative of the whole schist terrain. Nevertheless, the high potential weatherability of the schist indicates that freeze-thaw and hydration-induced break-up of the rock may be a major component of the rapid denudation of the schist mountains. Thus, the RMS properties of the eroded rock mass may be of minor importance in the overall development of the central Southern Alps alpine landscape due to under-assessment of the importance of the weathering process in this study.

#### 5.6. Rock Intact Strength and Glacial Valley Morphology

The rock intact strength properties derived from this study were compared with the forms of the glacial troughs developed on each bedrock type (Section 4.7.4). No clear relationship between rock intact strength and form was apparent, indicating that the intact strength properties alone are insufficient to explain the mode of erosional development of the troughs. This is contrary to the experience of Cooks (1983) who argued that the geotechnical properties of the rocks had a strong control on the morphometric properties of fluvial drainage basins developed thereon.

However, Cooks (1983) ignored the input of rock jointing to erosion and landform development, whereas in the present study, a strong correlation was demonstrated between the field rock mass strength properties and the shape of the glacial valleys (Section 4.6). This indicates that studies of rock control on landform development must involve the rock mass strength properties of the bedrock, as intact strength properties of the rock mass alone are inadequate for realistic *in situ* rock strength characterization for the purposes of evaluating rock resistance to erosional processes.

## 5.7. Summary and Conclusions

The intact strength and some physical properties of rocks from the New Zealand Southern Alps and the McMurdo Dry Valleys, Antarctica were determined. Correlations between a variety of rock physical and intact strength properties were evaluated and compared with some published studies. The influence of moisture on rock strength was examined by comparison of oven-dried and vacuum-saturated rock strength. Saturation was found to significantly reduce the intact strength of most rock types studied, with strongly foliated schists displaying the greatest strength reduction. This weakening in saturated rocks has important implications for rock failure and subsequent erosion, particularly in glacial environments. Further, saturation greatly reduces the *in situ* stresses required for the rock to fail.

## **Chapter Six**

### **Tectonics, Stresses and Glacial Valleys**

### 6.1. Introduction

The Southern Alps is a tectonically active compressional mountain belt subjected to rapid uplift and denudation (H. Wellman, 1979; J. Adams, 1980). Geomorphological research in similar compressional terrains elsewhere in the world have shown that the tectonically-induced stress field has a significant influence on the erosional landforms developed thereon (Scheidegger and Ai, 1986). In such mountain belts, the tectonic stress-field may be the dominant stress component and the interaction with the processes of erosion by water and ice may be a major control on the morphogenesis of these regions (Scheidegger, 1980; Gerber, 1980). The Southern Alps, the European Alps and the Himalayas, are all well known examples of compressional mountain belts that have largely undergone intense glacierization as a result of uplift. The glaciers, in turn, have had a major influence on the development of the extreme relief characteristic of these regions.

The state of stress in the Earth's crust varies from place to place. Direct effects of the stress-field are observed in mines and tunnels as stress-relief fracturing and inferred from micro-earthquakes (McGarr, *et al.*, 1975). Other geological features such as valley morphology and valley trend are thought to be influenced by the geotectonic stress-field (Scheidegger and Ai, 1986). Four major sources of stress may be active in rock bodies: gravitational, tectonic, thermal and residual. These stress modes and their geomorphic importance have been examined by Scheidegger (1982a) and Selby *et al.*, (1988).

In this section, an attempt will be made to evaluate various lines of geomorphologic evidence for the nature of the neotectonic stress-field near the Main Divide of the Southern Alps. It will be shown that an understanding of regional tectonics is necessary to understand the morphogenesis of the Southern Alps glacierized landscape.

## 6.2. Regional Crustal Stress Patterns From Geomorphic Data

### 6.2.1. Introduction

The Southern Alps developed as a direct result of the collision of the Indo-Australian and Pacific lithospheric plates (H. Wellman, 1979). Evidence for the type and orientation of the principal stresses in the shallow crust resulting from this collision come from a number of sources. The orientation of valleys and fracture sets have been interpreted as a result of the regional crustal stress-field (Scheidegger, 1979a, 1980; Hancock, 1985; Bevan and Hancock, 1986), and earthquake first-motion and geodetic strain measurements are likewise constrained by the orientation and relative magnitudes of the principal stress axes (Scholz *et al.*, 1973; Walcott, 1978; Zoback and Zoback, 1980; Gough and Gough, 1987). Rock fracture and glacial valley trends will be examined in each region and inferred principal stress directions (PHS) compared to the known PHS directions determined using other methods. A brief review will be given of each geomorphic method of neotectonic stress-field interpretation.

### 6.2.2. Conjugate Shear Surfaces From Joint Patterns

Covenient units for the estimation of the tectonic stress-field, are the ubiquitous young fractures encountered in rock outcrops (Kohlbeck and Scheidegger, 1977; Hancock, 1985). A joint is any visible crack or fracture without displacement in an exposed rock mass. Gerber and Scheidegger (1975), and Scheidegger (1979a) found that the joints generally occur in three sets in an outcrop, with two being near vertical and a third near horizontal. The vertical joint sets were identified as tectonic joints defining Mohr-type fracture surfaces in a biaxial stress field. They are entirely independent of lithology or of previous rock deformations, and the regularities can be quantified by statistical procedures (Kohlbeck and Scheidegger, 1977).

In Mohr-type fractures, the bisectrix of the smaller angle is the greatest compression direction, and the least for the larger angle (Price, 1966). However, the 20 angles are often 60°-90° and Scheidegger (1979a, 1983) suggested that the large angles between the joint sets may indicate that fracture is not Mohr-type, but the result of some ductile slippage process. That is, the joints are responses to

some flow process induced in the horizontal plane by momentarily acting tectonic stresses. According to Scheidegger (1980), since the tectonic stress-field is constant over a wide area, joint measurements from several outcrops can be combined. Local disturbances will disappear and joint orientations generated by tectonic stresses will reinforce each other and increase their frequency.

However, there are problems with the assumptions implicit in Scheidegger's method. For example, Scheidegger (1980, 1982b, 1983) regards many joints, especially those belonging to orthogonal vertical sets, as shears even when, as in the Appalachian Plateau (Engelder and Geiser, 1980; Engelder, 1982, 1982b; Holst, 1982) the same sets have been interpreted as extensional fractures. Investigators working in other terrains (e.g. Hancock, 1985, Bevan and Hancock, 1986) have attributed some sets to shear failure and others, enclosing small dihedral ( $2\theta$ ) angles to failure in shear-extension transition. However, the terrains investigated adjacent to the Main Divide are strike-slip regions in which  $\sigma_1 > \sigma_2 > \sigma_3$ , and  $\sigma_1$  and  $\sigma_2$  are in the same horizontal plane and the minor stress  $\sigma_3$  vertical (Fig. 6.1). Conjugate shear fractures developed in such a stress field should be near vertical with an acute angle of separation ( $2\theta$ ) of from  $45^\circ$  to  $60^\circ$  (Hancock, 1985) (Fig. 6.2). A range of natural  $2\theta$  values is to be expected knowing that  $\phi$  (internal friction angle) varies with lithology and that there is a transition from single extension to paired shear fractures (Fig. 6.2). Thus, for the purposes of this study, the assumption of shear origin for the vertical fractures observed is assumed to be valid except where otherwise indicated.

At each field site, the fracture pattern was examined and quantified by representation as poles to planes on a Schmidt net contour diagram. Only relatively fresh, unweathered joints were measured. It must be emphasized that the present study of bedrock jointing was initially undertaken from the viewpoint of examination of structural/joint control on glacial valley slopes and their development. Hence, the principal criteria for determining microtectonic sequence: abutting and overprinting relationships and the offset of one structure by another (Hobbs *et al.*, 1976), were noted in only a few cases. The allocation of individual joint planes to sets was made on the basis of computer plotted diagrams of poles to joints, although Hancock (1985) suggested that the allocation of a joint surface to a set should be accomplished in the field on the basis of visible angular relationships between adjacent joint planes.



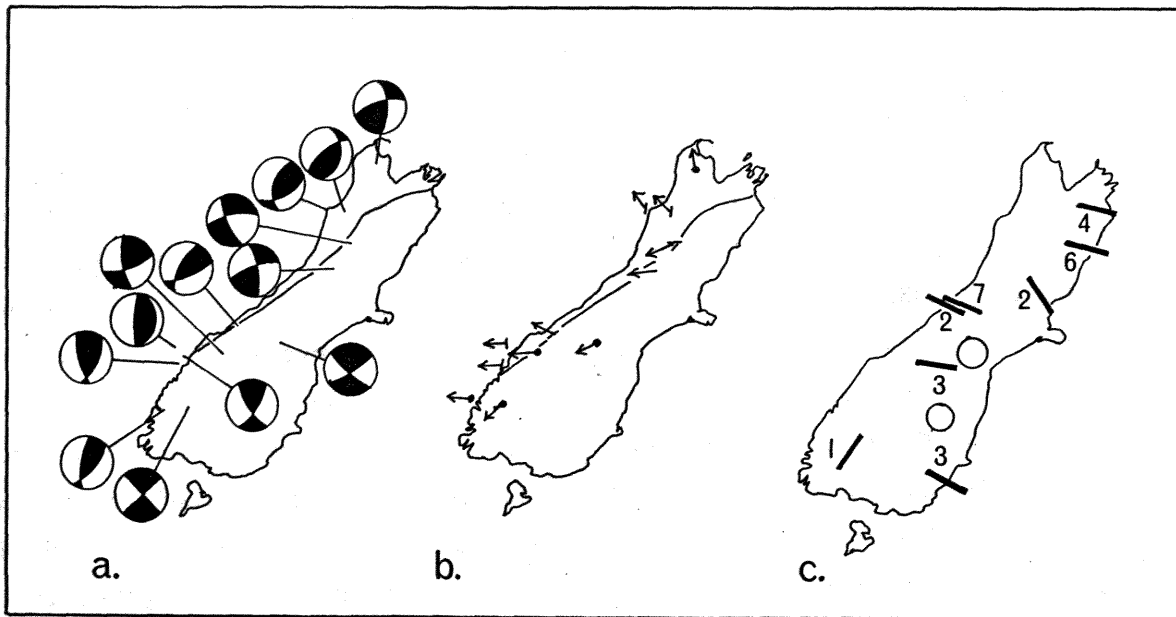


Figure 6.1. (a) Compilation of fault plane solutions for shallow earthquakes and micro-earthquakes. All mechanisms are equal area projections of the upper focal hemisphere: compressional quadrants are shaded.  
 (b) Slip directions inferred from fault plane solutions. A dot indicates where the fault direction is in doubt; a bar indicates where the strike of the fault is known.  
 (c) Principal horizontal shortening directions from geodetic strain measurements, indicating the magnitude of the shear strain. Open circles indicate no measureable shear strain. After Walcott (1978).

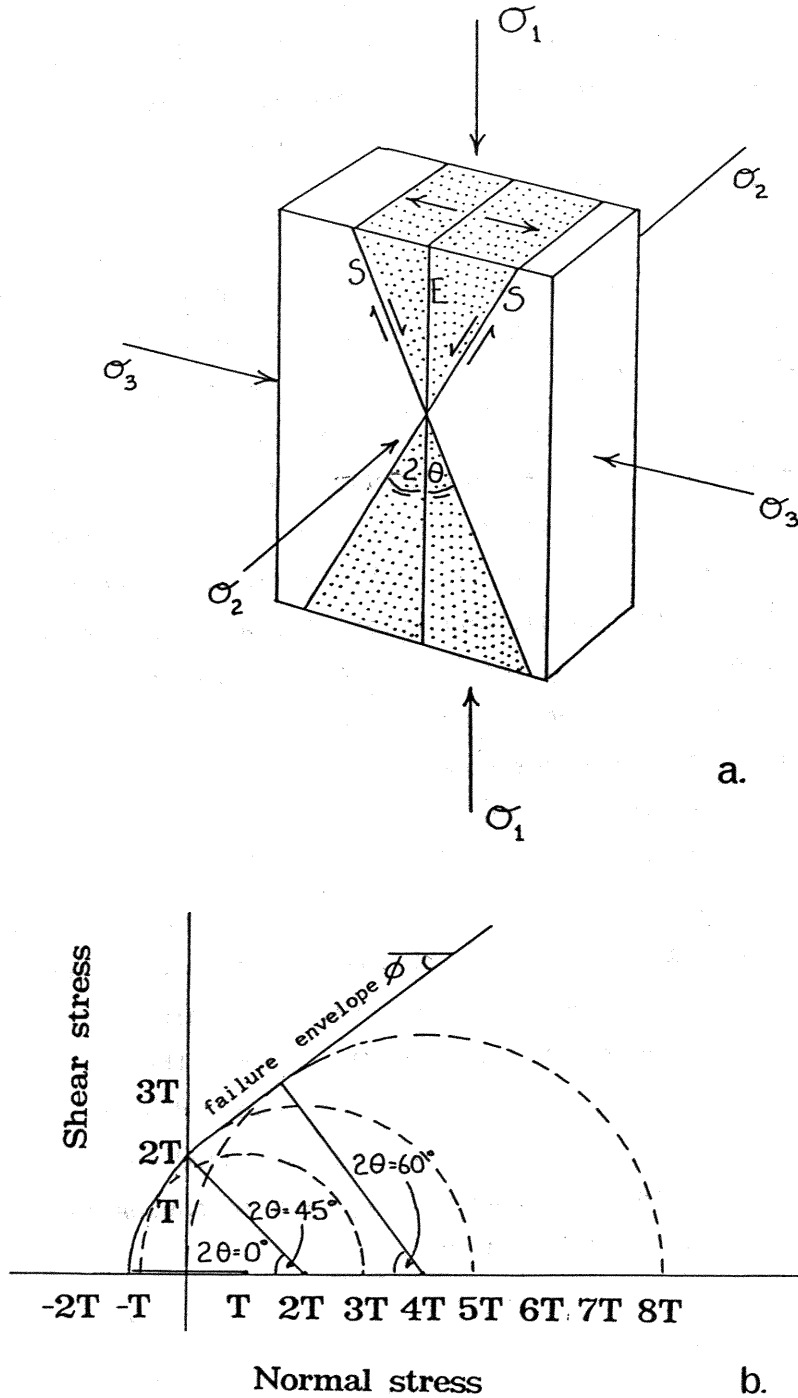


Figure 6.2. Block diagram showing relationships between principal stresses ( $\sigma_1 > \sigma_2 > \sigma_3$ ) and an extension fracture (E) and conjugate shear fractures (S) developed in a mechanically isotropic brittle rock. Stipple indicates the quadrants within which hybrid fractures form. (b) Composite failure envelope and Mohr circles constructed for  $2\theta = 0, 45$  and  $60^\circ$ . T: tensile strength.  $\phi$ : angle of internal friction.

Thus, the PHS directions interpreted from the fracture data collected in this study cannot be assigned any conclusive microtectonic origin on the basis of fracture architecture, although their 20 angles, and angular relationships with PHS directions determined using other means, suggest that the genetic interpretations may be valid.

### 6.2.3. Valley Trends

Scheidegger (1979b) argued that valley trends are not random, but reflect regional tectonic stress-fields. Scheidegger (1980) developed a procedure whereby the valley flow patterns were rectified, and a statistical analysis conducted, with the length of the valley segment used as the weight in subsequent statistical evaluation (Fig. 6.3). On the basis of the rectification procedure, river drainage nets in the Himalayas (Scheidegger, 1979b), Switzerland (Scheidegger, 1980), Alberta (Scheidegger, 1983), and Tibet (Ai and Scheidegger, 1981), as well as studies of glacial valley patterns (Scheidegger and Ai, 1986), have consistently yielded a non-random pattern. The preferred orientations generally correspond to the shear surface of the regional neotectonic stress-field (Scheidegger, 1980).

The method of rectification and evaluation of glacial valley patterns was attempted for parts of the New Zealand Southern Alps, the results and implications of which will be discussed shortly. The preferred valley trends were determined using the method of Emerson (1985). The length and orientation of each drainage segment was measured with the length of each segment used as the statistical weight. Rose diagrams were produced for each morphological terrain and indicate the preferred valley trends.

### 6.2.4. Lineaments

Lineaments detected as major surface features on Landsat imagery and aerial photography have been argued to be a consequence of the tectonic stress-field (Scheidegger and Ai, 1986). In the Southern Alps, New Zealand, Landsat imagery has been used for the mapping of lineaments. They were interpreted to be a reflection of surface structural, seismotectonic and geomorphic features (Oliver, 1983). Norris (1979) showed how a rectangular pattern of lineaments inherited from early Cainozoic rifting was transformed into a rhombic pattern by dextral strike-slip and collision along the Alpine Fault. Yeats (1987)

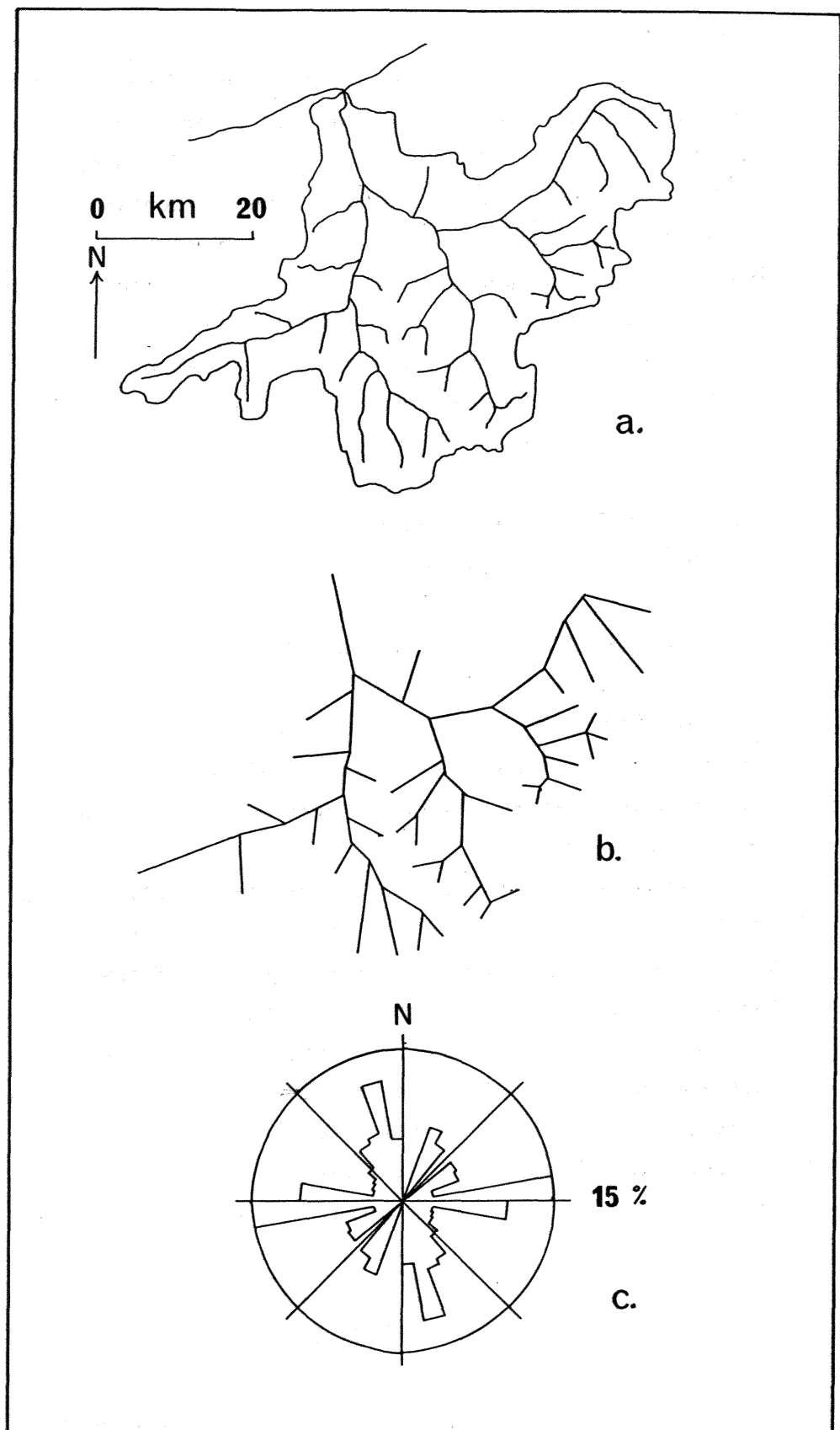


Figure 6.3. Rectification of drainage nets: (a) delineation of catchment and valley system; (b) rectification 'smoothing out' of wiggly lines; (c) weighted orientation frequencies for rectified valley segments. After Scheidegger (1980).

used landsat imagery to examine the late Cenozoic deformation of Central Otago. In the central North Island, Spörli (1987) modelled the tectonic development of lineaments interpreted from air photos. According to Oliver (1983) and Yeats (1987), most of the lineaments observed are undoubtedly related to the horizontal strain field due to the tectonic setting. However, the lineaments observed from Landsat imagery and aerial photographs are not necessarily indicators of the near surface crustal stress field as they may represent the overprinting of several successive stress regimes over time (Norris, 1979; Oliver, 1983). The lineaments will not be considered further here.

### 6.3. Regional Crustal Stress Patterns In The Southern Alps From Joint and Valley Orientations

#### 6.3.1. Northern Fiordland Region

More than one generation of fractures was indicated by cross-cutting relationships and quartz infilling of the joints. However, only relatively fresh, unfilled joints were measured in this study. The joints usually displayed no displacement and had a simple extensional character. The between-site variation in orientation of fracture sets is considerable and is probably a reflection of the extreme topography and the proximity to free faces. However, when all the joint data sets were combined, two strong near vertical orientation maxima are found to be developed (Fig. 6.4a). These are interpreted as conjugate shear surfaces in a biaxial stress field. Two low-angle joint sets strike ~NW-SE (Fig. 6.4a). These surfaces represent the sheeting joints developed in the plutonic rocks and may follow the shape of the original land surface (Chapman and Rioux, 1958).

If the bisectrix of the smaller angle is taken as the PHS direction, with the fracture trends defining conjugate shear surfaces, the interpolated PHS direction is NW-SE, highly oblique to the trend of the Alpine Fault. However, the  $2\theta$  angle is  $> 60^\circ$  and earthquake focal plane solutions indicate a generally E-W PHS direction for the region (Fig. 6.1a; Scholz *et al.* 1973; Davey and Smith, 1983). The focal plane solutions give the expected reverse thrusting at the coast associated with thrusting at the Alpine Fault boundary (Scholz *et al.*, 1973). In the interior of the Fiordland micro-plate, the solutions indicate a strike-slip stress regime, similarly oriented E-W.

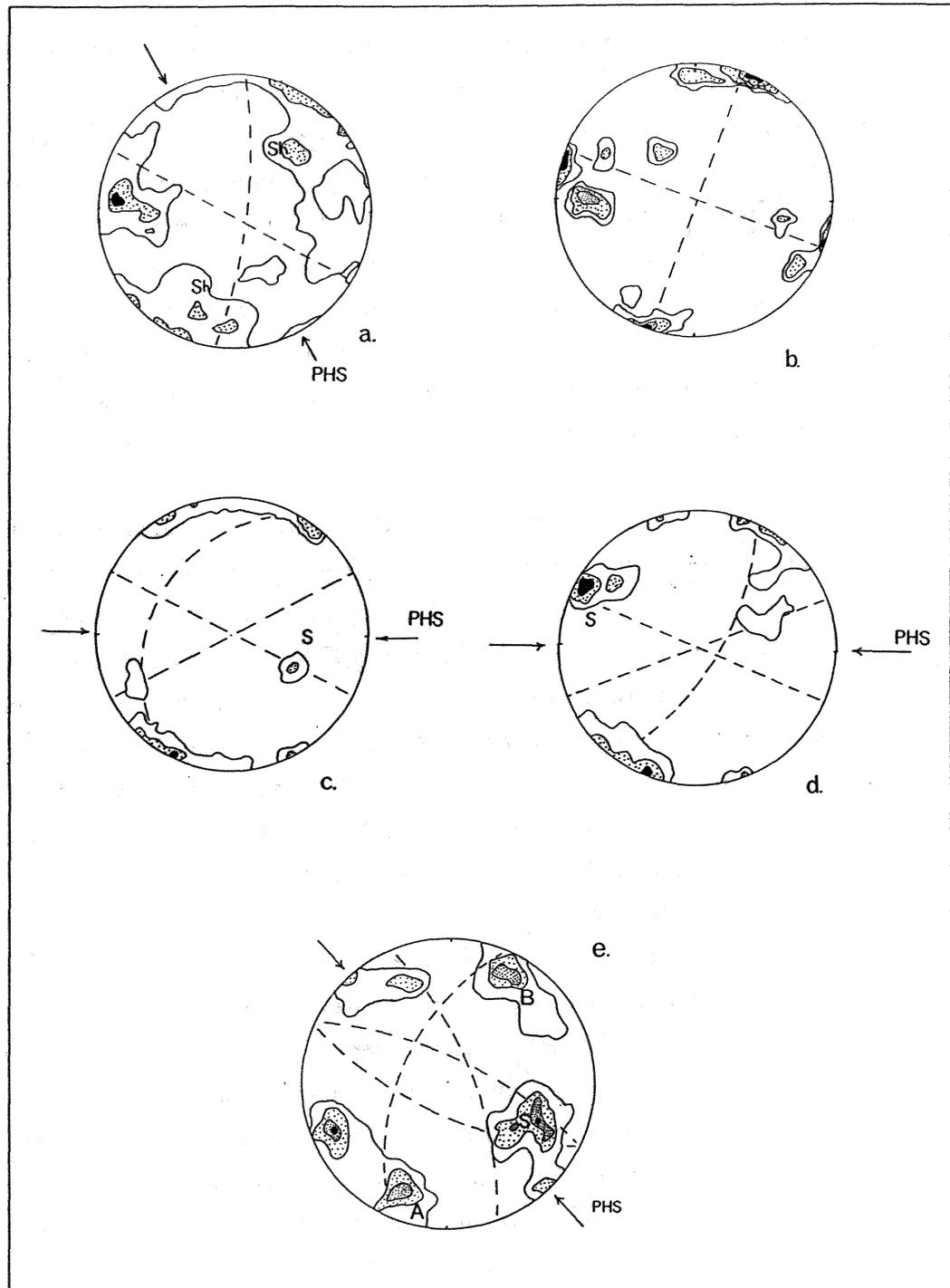


Figure 6.4. Structural geometries (poles to joint planes) in the vicinity of the Main Divide, southern part of Southern Alps, New Zealand. (a) Poles to joints in northern Fiordland. 2, 3, 4% per 1% area. 1345 points. (b) South-central Fiordland. 3, 4, 5, 6% per 1% area. 130 points. (c) Mt Aspiring region. 3, 4, 5% per 1% area. 1140 points. (d) South Westland- Fox to Whymper Glacier area. 4, 6, 8% per 1% area. 450 points. (e) Mt Cook region- Sealy Range to Main Divide. A and B are possible hybrid conjugate shear fracture planes. 3, 4, 5% per 1% area. 352 points. Arrows indicate inferred PHS directions. S: foliation/bedding plane/axial plane trends, Sh: sheeting joints. Lower hemisphere projections

The glacial valley system in northern Fiordland was rectified, and the preferred valley orientations determined (Fig. 6.5a). Five distinct preferred orientations are evident, and they may relate to more than one stress regime over time. Consequently, the unequivocal elucidation of the paleo-PHS direction from the valley trends is not possible. However, the valley trends display a similar pattern to that developed in south-central Fiordland, the implications of which will be discussed shortly. Further, overprinting of the structures by the radial flow of the outlet glaciers from the ice-centres (section 3.2) was probably an important factor in their development.

An additional problem is the possible misinterpretation of fracture origin, and incorrect assignation of the PHS direction, as the fracture surfaces may not be of conjugate shear type, but extensional features (Engelder, 1982b; Nur, 1982; Hancock, 1985). In this case, application of the model of Engelder and Geiser (1980), developed to explain regional joint sets in the Appalachian Plateau, may be valid. The basic premise of their paper was that vertical joints propagate normal to the least principal stress and thus follow the trajectories of the stress field present at the time of propagation. The inland Fiordland Block is a strike-slip regime (Scholz *et al.*, 1973; Davey and Smith, 1983) so maximum ( $\sigma_1$ ) and minor ( $\sigma_3$ ) principle stresses are horizontal. The lack of slickensides or other evidence for shear displacement on the Fiordland joint sets suggests that the shear stress was maintained at a low level. The presence of extension fracturing without shearing indicates that net tensile stresses were present during jointing, and the two near vertical joint sets may have been generated by two independent tensile stress-fields, oriented WNW-ESE and N-S (Fig. 6.4 a).

The state of stress favouring the propagation of extension fractures is one in which the least principal stress ( $\sigma_3$ ) is reduced enough to overcome the tensile strength of the host rocks (Engelder and Geiser, 1980). There are several tectonic sources of tensile strain that may be acting across the Fiordland Block: (1) near surface tensile fracturing may result from shallow tensile regime developed by the stress drop during earthquakes, where, assuming pure shear stress, the tensile component may be 1 to 100 bars (Nur, 1982); (2) Haxby and Turcotte (1976) argued that erosion, uplift and cooling may cause net horizontal tension in the crust so that when previously buried basement is exposed, it may be subject to large tensile stresses which

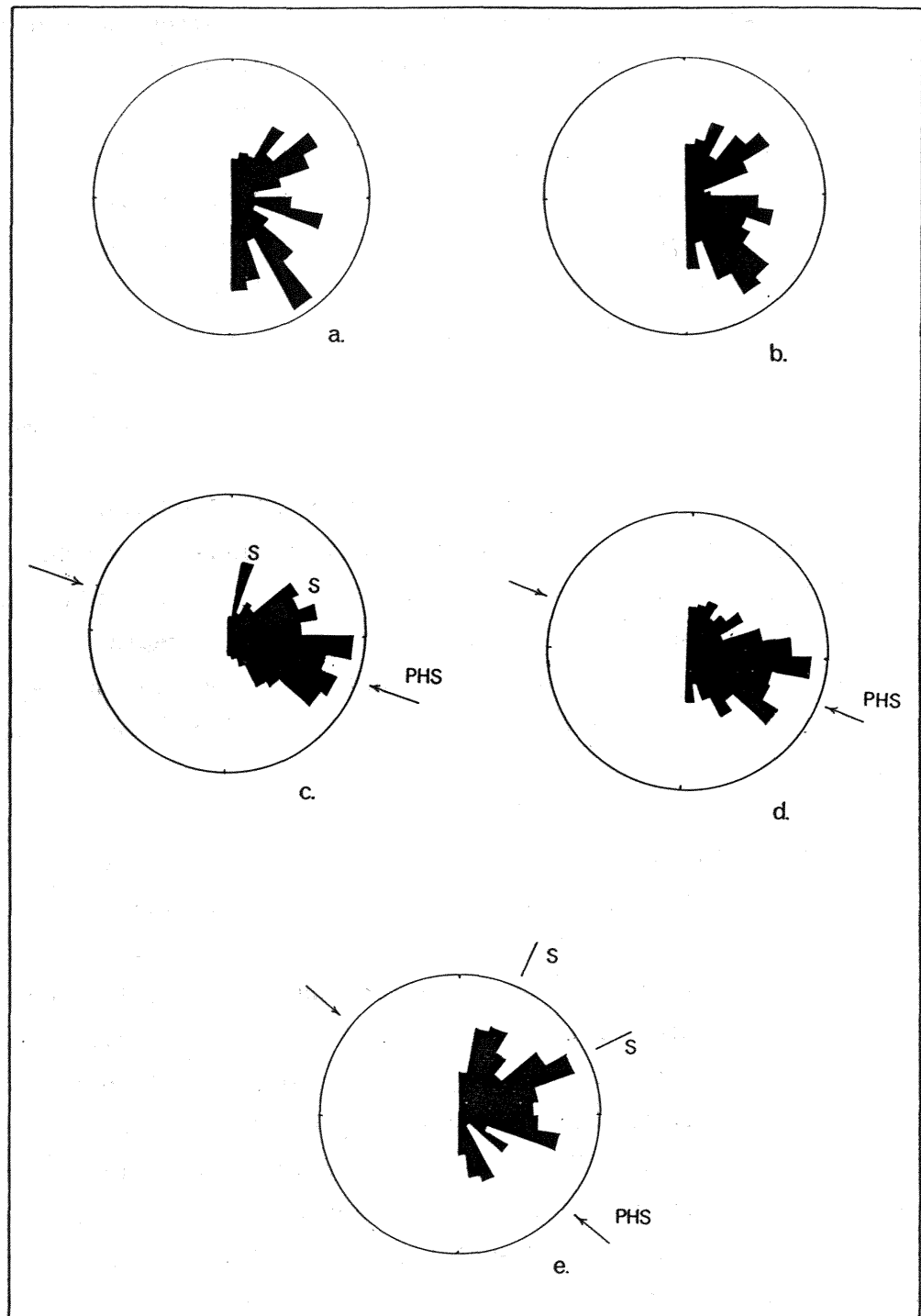


Figure 6.5. Rose diagrams of preferred glacial valley trends and inferred principal stress directions (arrows), southern part of the southern Alps, New Zealand. S: valleys with orientation controlled by foliation/bedding plane/axial surfaces. a. Northern Fiordland. 289 valley segments. b. South-central Fiordland. 189 valley segments. c. Mt Aspiring region. 267 valley segments. d. south Westland. 321 valley segments. e. Mt Cook region. 203 valley segments. Arrows indicate preferred PHS directions.



might produce tensile jointing; (3) local stresses from gravitational forces; and (4) crustal bending extending over a few hundred kilometres in scale may lead to large tensile strains (Nur, 1982). Nur showed that for geologic uplifts of 1.5 km, a crustal half-thickness of 10km and a half-width of 50 km in a bending plate subject to uniform load, extension fractures can develop to a depth of 10km, which is comparable to the brittle part of the crust in which most earthquakes occur. The Fiordland block has similar size constraints, and broadly domed epeirogenic uplift (Ward, 1988a). Further, most Fiordland crustal earthquakes occur at a depth of < 12km (Fig. 6.6). The actual depth of tensile fracturing depends on the ratio of pore pressure to overburden pressure (Price, 1975). However, an approximate depth estimate is provided by the Fiordland topographic relief where deep glacially excavated canyons up to 2 km deep exist, so that tensile fracture may persist to at least this depth. All four modes of tensile strain development may act in Fiordland so that deciphering the boundary conditions controlling joint development is problematical at best.

To explain the development of the Fiordland landscape it is necessary to postulate pre-glacial valleys cut into the planation surface defined by the summit accordance (Fig. 3.2). The valleys would then channel ice as soon as the ice-caps and radiating outlet glaciers developed (Linton, 1957). A plan view of the fiords supports this hypothesis, for whilst straight elements tend to dominate the outlet troughs, they form a roughly dendritic pattern when viewed as a whole. This would be expected if they followed pre-existing valleys. This is further supported by the radial nature of the glacial drainage from the peaks of the upland surface (Fig. 3.4), with radial outflow of the glaciers probably over-printing and exploiting the existing tectonic elements. Thus, the valley trends cannot be used to interpret the regional paleo-stress field in northern Fiordland, although it is apparent that there is a degree of structural control on drainage.

#### 6.3.2. South-Central Fiordland Region

Only a limited appraisal of the regional fracture system was possible, but when all the data sets are combined, they are sufficient to define 3 distinct joint maxima (Fig. 6.4b). The two near vertical maxima are assumed to be conjugate shear surfaces in the prevailing strike-slip biaxial stress regime, while the third low angle fracture is interpreted as a structural marker in the foliated metamorphic

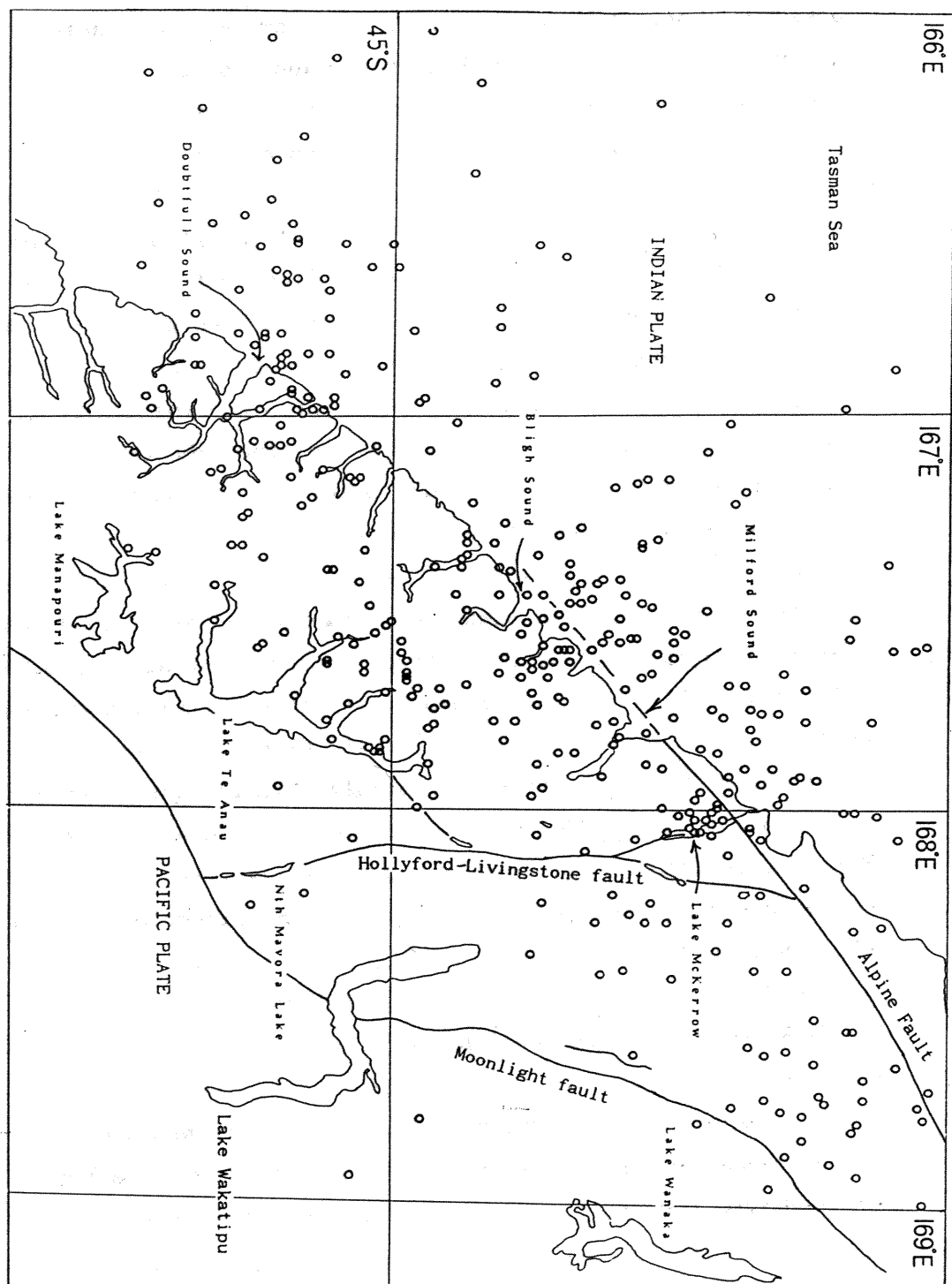


Figure 6.6. Distribution of shallow crustal earthquakes with Richter magnitude  $\geq 4$ . Note localization of epicentres within zone bounded by Alpine and Moonlight-Hollyford fault zones. Data plotted from DSIR earthquake computer file.

rocks. However, the bisectrix of the preferred fracture trends is nearly  $90^\circ$  so that the PHS direction cannot be determined. As suggested for the northern part of the Fiordland Block, a tensile origin for the joint sets may be more appropriate.

The rectification and statistical evaluation of the regional glacial valley trends (Fig. 6.5b), indicated five strong orientation maxima, displaying similar trends to those obtained from the valley trends in northern Fiordland. A high degree of structural control on the glacial drainage pattern is apparent, and the similarity to that developed in northern Fiordland suggests that the Fiordland Block has maintained a uniform stress-field prior to and during development of the radial glacial drainage system.

The micro-earthquake study of Scholz *et al.* (1973) resulted in only two poorly constrained diagrams for the central Fiordland region (Fig. 6.1a). Close to the Tasman coast, thrust faulting was recognized in association with the Alpine Fault, with the stress-field changing to strike-slip in the interior. Scholz *et al.* (1973) defined an E-W oriented PHS, nearly perpendicular to the coast and Alpine Fault. However, in the Te Anau Basin, on the eastern side of the block, geodetic strain data indicate a N-S PHS direction (Walcott, 1978) (Fig. 6.1c).

### 6.3.3. Mt. Aspiring Region

A study of the fracture and valley patterns was undertaken in the Mt. Aspiring region close to the Main Divide. The PHS directions derived from the fracture and valley patterns in the schist terrain (Figs. 6.4c & 6.5c) indicate a consistent PHS direction to that obtained from the first-motion studies. Examination of the fracture pattern (Fig. 6.4c) indicates an E-W compression direction, assuming that the two dominant fracture orientations represent conjugate shear surfaces. The fracture trends correspond closely to the preferred valley trends, and a third major fracture set is associated with the foliation in the schists.

PHS directions obtained from crustal micro-earthquake first-motion studies (Scholz *et al.*, 1973; Reyners *et al.*, 1983) from the Aspiring/Central Otago region, indicate a constant regional stress-field (Fig. 6.1a). In close proximity to the Alpine Fault, a thrusting/reverse fault stress regime is developed, changing to

strike-slip inland. The derived E-W oriented PHS directions are highly oblique to the Alpine Fault. This direction is confirmed by PHS directions derived from the geometry of late Cenozoic movement on the Moonlight and Hollyford fault systems (Norris *et al.*, 1978), suggesting that the present day activity is similar to that of the last few million years.

The geometry of fracture and preferred valley trends indicate that the glacial valley system was developed under a stress regime with PHS direction similar to that acting currently. That is, fluvial and glacial erosional development of the troughs was concurrent with compression and uplift associated with movement on the Alpine Fault. A further strongly developed valley trend oriented NE-SW reflects strong structural control on the development of the glacial drainage pattern. The dominant valley trends developed parallel to the main neotectonic elements are a reflection of the Pleistocene tectonic and erosional history of the region.

#### 6.3.4. South Westland Region

The glacierized landscape of South Westland on the eastern side of the Alpine Fault is a zone subjected to highly oblique compression (Walcott, 1979). The combined fracture orientation data from the region on the western side of the Main Divide indicate that three distinct orientation maxima are developed (Fig. 6.4d). The two near vertical joint sets are interpreted as conjugate shear surfaces, while a third steeply dipping set is associated with the foliation in the schist. The angle between the two vertical sets is  $\sim 45^\circ$ , suggesting a PHS direction oriented  $\sim$ WNW-ESE (Fig. 6.4d). Similarly, the angle between the dominant rectified glacial valley trends is  $\sim 45^\circ$  (Fig. 6.5d), roughly corresponding to the orientation of the fractures. This supports the interpretation of the dominant valley trends as conjugate shear surfaces in the biaxial stress field developed immediately east of the Alpine Fault. The valley geometry suggest a PHS direction at the time of valley formation of  $\sim 110^\circ$ . Further strongly developed N-NE valley trends are related to structural (foliation) control on the drainage and are ignored for the purpose of this analysis.

Earthquake first motion studies by Scholz *et al.* (1973), geodetic strain studies (Walcott, 1978) and studies of recent fracture patterns on recently deglaciated surfaces (Norris and Cooper, 1986), confirm the current oblique convergence within the Southern Alps, and allows

the present WNW-ESE PHS direction to be calculated. In the Waiho Valley, Holm *et al.* (1987) recognized a sequence of mesoscopic structures suggesting a progressive rotation of the subhorizontal PHS direction in an anticlockwise sense. The most recent structures gave PHS directions consistent with the geodetic and micro-earthquake data.

It appears that the valley trends follow lines of brittle failure in shallow crustal rock, recently exposed by movement and erosion along the Alpine Fault (Koons, 1987). Fluvial and glacial incision has been rapid to maintain a balance with the rapid uplift of the schist on the eastern side of the Alpine Fault (J. Adams, 1980; Whitehouse, 1987). The length of the westward flowing rivers reflects a balance between eastward erosion of the valley head and westward crustal shortening, since shortening against the Alpine Fault means that the rivers must erode headward at 15 km/Myr just to maintain a constant length (J. Adams, 1985). The glacial and fluvial drainage radiates from the trend of the Main Divide following the regional slope. Structural weaknesses suitably oriented with respect to the flow patterns were preferentially exploited by fluvial and glacial erosion. Such a scenario has been noted in the Albertan Rocky Mountains (Scheidegger, 1983). Thus, glacial and fluvial erosional development of the troughs occurred under a stress regime associated with uplift along the Alpine Fault similar to that developed today, and the landscape is active and young.

#### 6.3.5. Mt. Cook Region

The Torlesse greywacke and argillite in the Mt Cook region have been subjected to a high level of compression and uplift (J. Adams, 1979). The greywackes are intensely fractured, faulted and folded (Findlay and Spörli, 1984). The regional fracture patterns were determined for the Mt Cook region (Fig. 6.4e) and the absence of rib and hackle marks on greywacke joint surfaces may indicate that the fractures propagated at high speed (Price, 1966). The fracture sets display considerable variation in orientation with respect to topography. However, when all data sets are combined, strong orientation maxima were identified and may be associated with three distinct fracture sets, one of which is associated with the bedding/foliation (Fig. 6.4e). The joint sets display a similar geometry to those measured by Findlay and Spörli (1984). The fresh, clean fractures may be interpreted as conjugate shear surfaces in a

biaxial stress field, and the bisectrix of the acute angle suggests a NW-SE oriented PHS direction. The rectified glacial drainage pattern for the area generates four distinct orientation maxima (Fig. 6.5e), two of which are interpreted as developed along bedding/axial plane weaknesses. However, the bisectrix of the smaller angle does correspond to the known PHS direction, with a trend of  $\sim 310^\circ$ .

Examination of Fig. 6.4e indicates that an alternative interpretation of the fracture data may be just as valid. Joint sets A and B define two surfaces with the same strike but opposite dip. The  $2\theta$  angle is small and, according to the scheme of Hancock (1985) (Fig. 6.2), could be interpreted as conjugate hybrid shear fractures. For this to be the case,  $\sigma_1$  must be vertical, and  $\sigma_2$  and  $\sigma_3$  develop in the horizontal plane (Fig. 6.2). This is contrary to the stress-strain ellipsoid developed from geodetic strain and earthquake first-motion studies (Fig. 6.3a) where  $\sigma_1$  and  $\sigma_3$  at depth are in the horizontal plane. However, perturbations in the stress-field can be created by the extreme relief in the Mt Cook area, so that interpretation of mesoscale kinematic features on or near ridges does not necessarily represent the state of stress at depth (Kohlbeck *et al.*, 1979).

Field (1975) analysed slickenside lineations on shear joint surfaces in the Liebig Range and found that most of the axes of intermediate strain were nearly vertical, confirming that many of the slickensides were formed during strike-slip movement when the axes of extension and compression lay in a horizontal plane. The maximum compression direction was oriented  $\sim 320^\circ$ – $340^\circ$  and is consistent with earthquake first-motion data from the Pukaki network (Haines *et al.* 1979) and geodetic strain (Walcott, 1978) (Fig. 6.1a). Based on this information, it is clear that the fracture data obtained in this study are insufficient to elucidate the microtectonic history of the host rock without knowledge of the joint architecture and angular relationships between sets visible in the field (Hobbs *et al.*, 1976; Hancock, 1985).

Nevertheless, it is apparent that there is a high degree of structural control on the direction of glacial erosion, and thus, development of the glacial valley trends. The major valleys parallel the regional fold axes and bedding strike. The presumed conjugate shear surfaces and associated minor tributary valleys are only a minor element of the landscape, unlike the strong tectonic control on

drainage apparent on the western side of the Main Divide. This is probably a result of the greater age of the erosional landforms east of the divide relative to the rapidly uplifted and denuded landscape developed on schist to the west (Whitehouse, 1987).

#### 6.3.6. Implications of Valley Trends For Landscape Development

Wellman and Willett (1942) developed a summit-level surface for the central Southern Alps and recognized the development of drainage perpendicular to the regional slope on the western side of the Main Divide, with southward flowing, structurally controlled drainage to the east. They felt that the drainage on the western side of the divide was the older landscape element. It is now recognized that uplift and erosion are extremely rapid on the western side of the divide east of the Alpine Fault (Whitehouse, 1987) with up to 25 km of erosion since the initiation of uplift ~5.4 Myr BP (Kamp *et al.*, submitted). Preferential exploitation and erosion of the dominant structural weaknesses occurred on the tectonically active, rapidly uplifted terrain on the western side of the Main Divide. This rapid erosion generated the present youthful tectonically and erosionally adjusted landscape.

Conversely, on the eastern side of the Main Divide, uplift and erosion rates are an order of magnitude lower and the glacial landscape is significantly older (J. Adams, 1985; Whitehouse, 1987), allowing the development of overwidened glacial troughs parallel to structure. The pre-glacial fluvial drainage undoubtedly followed the structural weaknesses and were subsequently exploited and modified by the glaciers. A strong structural control on drainage is also apparent in the Mt. Aspiring area, although the influence of the neotectonic stress-field and associated structural elements on the development of the glacial drainage system is more clearly seen.

The glacial drainage pattern in the Fiordland region differs significantly from that developed in the schist and greywacke terrains. The rectified valley trends for Fiordland indicate some tectonic control on the glacial drainage pattern. However, sinuosity, and the dendritic nature of the drainage networks, when viewed as a whole, suggests that the glacial landscape reflects the pre-glacial drainage system with minimal glacial modification of the overall trends. Glacial deepening and widening has proceeded to develop the overdeepened glacierized morphology, but the massive, erosion

resistant nature of the Fiordland crystalline rocks permitted only slow erosional enlargement of the troughs. This resistance enabled near complete maintenance of the form of the pre-glacial drainage system.

#### 6.4. *In situ* Rock Stress Determinations

##### 6.4.1. Introduction.

The state of stress in the crust has been shown to be an important control on the development of large scale erosional geomorphic features in tectonically active areas (Scheidegger and Ai, 1986). A similar degree of control is evident on the geometry and form of the glacial valleys developed in the vicinity of the Main Divide of the Southern Alps. Whilst the orientation of the principal stresses control aspects of the geometry of erosional features, it has been shown in engineering studies of rock slopes that the magnitude and orientation of the principal stresses influence rock slope failure, location of erosional forms and thus the final form of the slopes (Yu and Coates, 1970; Stacey, 1973). This theme is the subject of the next chapter, but before potential stress control on landforms can be examined, some information on the regional *in situ* stress field would be useful. Unfortunately, unlike in North America (Zoback and Zoback, 1980) and Western Europe (Scheidegger, 1978; Illies and Hoffers, 1981), measurements of crustal stress in New Zealand are few. Nevertheless, what few data exist has implications for the near surface stress fields and erosional landform generation.

##### 6.4.2. Central Otago

Successful *in situ* stress measurements have been made in the investigation drive near to the outfall end of the Mt. Difficulty Tunnel, Kawarau Damsite (Mills and Gray, 1985), using hydrofracture, overcoring, and rock deformation techniques. The overcoring results are consistent with a model of overburden induced stresses beneath the centre of the mountain. At the level of the proposed tunnel and test site, the stress distribution can be expected to be influenced by the tectonic stresses acting in the basement rock and being distributed into the mountain range (Brown *et al.*, 1980). The predominance of reverse faulting in the area would suggest that the horizontal tectonic stresses are compressive and higher stresses can be expected



closer to the mountain. Tunnel sections indicate that a crush zone aligned parallel to the valley wall is likely to have caused destressing of the excavation area (Halliday and Beetham, 1985).

At the Clyde Damsite, *in situ* stress measurements using the hydrofracture technique were carried out (Enever and Woollorton, 1984). High magnitude principal stresses were measured, and the possibility of topography affecting the result was discounted. However, Halliday and Beetham (1985) considered that the measured stresses could represent localized stress concentration effects rather than the regional stress field. The results of Enever and Woollorton (1984) suggest a high level of horizontal stress ( $\sigma_h$ ) at least six times the vertical stress ( $\sigma_v$ ). Thus, the conflicting stress patterns obtained from nearby sites do not enable the unequivocal elucidation of the crustal stress field.

The finite element model of Brown *et al.* (1980) at Nevis Bluff indicated the importance of the spacing and orientation of the shear/crush zones in the schist on the local stress-field and stress-magnitudes. Engineering experience of stress redistribution in valleys at damsites (Broch and Nilsen, 1979; Broch and Sorheim, 1984; Zhi *et al.*, 1985), along with the extreme topography and the presence of shear zones, suggests that the stress-field and its geometry will have an important influence on the development of the erosional landforms.

#### 6.4.3. Fiordland

Probably the most conspicuous structural feature of the northern Fiordland plutonic rock is the pervasive sheet jointing (exfoliation) that has developed parallel or subparallel to the topographic surfaces. Sheets 3-20 cm thick at the surface, typically increasing to more than 3 m at depths of 7-15 m, are contemporaneous with similar curved rebound fracturing encountered during the construction of the Homer Tunnel (Fyffe, 1954; MacFarlane, 1983). According to the Brunner and Scheidegger (1973) model of exfoliation development in surface rock, tensional stresses are induced in uniaxial compression. If the induced tensional stresses exceed the tensional strength of the rock at the most dangerous point, a progressive tensile fracture develops which is aided by notch effects. This model explains the parallelism

between exfoliation joints and the surface, and the fact that the separation of the sheeting joints increases with depth into the rockmass.

*In situ* stress measurements in tunnels in Norway near to fiord walls (Myrnang and Grimstad, 1984), and steep river valleys (Zhi *et al.*, 1985) show that the regional stress field is invariably affected by the steep valley topography, with the major stress ( $\sigma_1$ ) aligned sub-parallel to the valley slope, the minor stress axis ( $\sigma_3$ ) normal to the slope, and the intermediate stress ( $\sigma_2$ ) parallel to the valley itself. Locally, these stresses were found to be affected by the lithological changes (changes in rock strength) and wide discontinuities (faults), where stresses are shed to more competent rock thus leading to localized stress concentrations. In these areas of high relief, there is a concentration of stress beneath the valley floor, with the horizontal stresses greatly exceeding the vertical stresses (Brown *et al.*, 1980; Zhi *et al.*, 1985).

In a study of rock stresses in granite and gneiss near Mt Waldo, Maine, Lee *et al.* (1979) found that the magnitudes of the deepest stress-relief measurements were approximately three times as great at the mountain location in massive rock as in the valleys underlain by more closely sheeted/jointed rock. The rate of stress increase with depth was much greater than could be accounted for by the rock load. Release of residual strain energy explained the *in situ* stresses that were reduced and re-orientated in the energy-consuming sheeting process (Lee *et al.*, 1979).

The Fiordland region shows many similarities to Norway, with similar geology, extreme glacierized nature of the relief, and in the pervasiveness of sheet jointing. However, little is known of the regional stress regime in Fiordland, especially that which influenced the development of surfacial features. Nevertheless, aspects of the stress field can be inferred indirectly from the few large rock excavations attempted in the Fiordland region.

During the construction of the Homer Tunnel, considerable rock spalling problems were encountered. Within the tunnel the dominant jointing was found to be a closely spaced platy jointing striking obliquely at angles of less than 45° degrees to the tunnel walls (Fyffe, 1954). The same platy jointing was exposed on most of the ice-

scoured surfaces near to the tunnel. The fact that the platy jointing in the tunnel tends to arch in conformity with the roof and walls, suggests that it bears some relationship to the rock surface. Where the tunnel intersects faulted country, or where the regional joint pattern is closely spaced, the stresses have been relieved and platy jointing is not developed. Extensive rockfalls due to popping of the surface rock from the roof and walls were experienced immediately after widening operations, and these falls continued at increasing intervals over the next four years (MacFarlane, 1983).

Geomechanical tests were made during the construction of the West Arm Manapouri Power House. The machine hall arch is under more than 210 metres of cover, and is excavated out of hard, massive gneiss, pegmatite and granite (Betchel, 1967). Before the main excavation began, the *in situ* stress regime, and response of the rock mass to excavation, were determined by means of flatjacks and borehole extensometers installed in adjacent excavations and investigation drives (Perrin, 1984). Modified versions of similar instruments were installed during the excavation of the main cavern to monitor the immediate post-excavation response of the rock mass and long term stability. The results from the rock movement indicators have shown a steady decrease in the rate of rock relaxation after construction. The high measured vertical and horizontal stresses were much greater than would be expected from the input of overburden stresses alone, suggesting the release of residual strain energy and/or a horizontal geotectonic stress component (R. Thomson, pers comm.).

Further evidence for a high magnitude crustal stress-field comes from the recorded shallow crustal seismicity across the Fiordland-Mt Aspiring regions (Fig. 6.6). Plotting all earthquake epicentres with a strength greater than 4.0 indicates a distinctive concentration of seismic activity along and east of the Fiordland extension of the Alpine Fault (Fig. 6.6). Few epicentres are located east of the boundary defined by the the Moonlight-Fiordland Boundary Fault system. The offshore activity dies away to the east where the thicker continental crust on the Australian Plate is reached. Within the Fiordland micro-plate, a distinct pattern of shallow crustal seismicity emerges.

Concentrations of seismic activity are evident along the Hollyford Fault. The earthquake activity is regarded as being representative of the current level of stress-strain adjustments taking place in the

crustal rocks in the area of concern (Reyners *et al.*, 1983). The high uniaxial compressive strength, high dynamic elastic moduli and massive nature of the northern Fiordland rock suggests that high levels of stress can be sustained by the rock without failure. When failure does occur, it is brittle, allowing the rapid release of large amounts of stored strain. That transcurrent motion on the Alpine fault is spread over a region of shear through Fiordland, is supported by the existence of earthquake activity as far east as Te Anau (Fig. 6.6).

#### 6.5. Summary and Conclusions

The fracture and valley patterns developed close to the Main Divide of the Southern Alps reflect the tectonic regime developed by movement and compression along the Alpine Fault. Although the valleys often develop along conjugate shear surfaces, this direction is not consistent, and other factors such as radial glacier flow patterns away from the Main Divide, have imprinted their own patterns on the mountain landscape (section 3.2). Furthermore, the valley trends frequently reflect a paleo-stress regime similar to the present tectonic stress pattern, suggesting that the tectonic regime is similar to that pertaining at inception of uplift. Measurements of the *in situ* stress field confirm that the horizontal tectonic stresses are of considerably greater magnitude than the vertical gravitational stresses. A high magnitude crustal stress-field is developed in the Fiordland block, the mode of release of which may be an important control on the development of the erosional landforms.

## **Chapter Seven**

# **Stress Modelling and the Development of Glacial Troughs**

### 7.1. Introduction

Whether or not rock failure will occur and erosional removal of debris be allowed to proceed, is largely dependent on the magnitude and geometry of the stress-field acting on the rock slope (Stacey, 1973). If the applied stresses exceed the rock strength, failure may occur. The rock quality parameters -elastic moduli, Poisson's Ratio, joint density and continuity- are usually taken as the controls on the distribution and magnitude of the stresses within the slope rock (Goodman, 1977). In tectonically affected rock masses, a balanced state of stress develops as a result of the gravitational forces, as well as other physical and chemical processes (Scheidegger and Ai, 1986). During fluvial/glacial erosion, part of the rock mass is removed, and stresses are redistributed with subsequent deformation in the vicinity of the free surface created (Nichols, 1980).

Stress concentrations have been modelled in numerous photo-elastic and finite element (FE) studies of elastic materials (Stacey, 1973). They have also been inferred from rock bursts near the base of steep fiord slopes in Norway (Bjerrum and Jorstad, 1968; Broch and Sorheim, 1984; Myrnang and Grimstad, 1984). Fjords generally lie at the foot of mountain ridges which are frequently in excess of 1500 m high. In addition, most steep fiord slopes have extremely sparse jointing limited almost entirely to stress-relief, sheeting joints.

In hard, slightly fractured, tectonically-stressed rock, brittle fractures develop rupture with sudden relief of the rock stresses. Thus, on the valley slopes, either new joints are created or the rock mass failure proceeds by exploiting pre-existing, suitably oriented joints. These fractures control the progressive deformation and failure of the slope rock. Jointed rock is regarded as a 'no tension' material (Zienkiewicz *et al.*, 1968) i.e., it cannot transmit or hold tensile stresses, so that failure of the jointed rock mass is likely if joint orientations permit. Stress-relief fracturing increases the permeability and deformability of the rock mass, and reduces the rock mass strength (RMS). This fracturing expedites rock weathering, alteration and solution, and influences groundwater flow (Gerber and

Scheidegger, 1969, 1973). This further reduces the RMS and slope stability, and increases the probability of failure.

The vast majority of the work on gravitationally deformed slopes has been carried out in glaciated terrain (Jahn, 1964; Beck, 1968; Mahr, 1977; Mollard, 1977; Radbruch-Hall *et al.*, 1976; Bovis, 1982; Savage and Varnes, 1987). Many authors have suggested that the removal of lateral support of glaciers from valley sides has been the primary cause of gravitational deformation, the magnitude of which is controlled by local factors such as structure, lithology and seismicity (Bovis, 1982; Pearce and O'Loughlin, 1985).

Due to the mathematical complexity, few exact solutions exist for stresses in even simple symmetrical ridge and valley systems (Savage *et al.* 1985). An indirect approach to the problem is estimation of the *in situ* stress field via the finite element technique (FE). The method was developed in 1956 to analyse the stresses in aviation structures (Turner *et al.*, 1956) and has since seen application to a wide variety of engineering problems (Yu and Coates, 1978). In this study, regional *in situ* stresses are modelled and their potential impact on the development of the glacial landscapes examined.

#### 7.1.1. Review of Modelling Of Valley-Ridge Systems

Few applications of the FE method have been made to the study of the development of erosional geomorphic features. Matheson and Thomson (1973) used the technique to study rebound in fluvial valleys. Radbruch-Hall *et al.*, (1976) employed it to study the development of sackung-type ridges in mesas of layered igneous and sedimentary rock. The model allowed them to predict the development of uphill-facing scarps in closely fractured rocks near ridge crests as the sides of the ridge bulge outward under gravity. Sturgul *et al.* (1976) developed a FE model of the Hochkönig Massif in Austria. Similarly, Kohlbeck *et al.* (1979) modelled the stresses acting in an alpine valley in Austria, and argued that gravitationally induced-stresses due to local topographic conditions, explained the measured *in situ* stresses.

Savage and Varnes (1987) enlarged on the approximate analysis of Radbruch-Hall *et al.* (1976), establishing a mechanical basis for the large scale gravitational spreading and fracture development in steep-

sided ridges. This was achieved by combining relevant results of previous elastic (Savage *et al.*, 1985) and plastic (Savage and Smith, 1987) solutions for gravity-induced deformation. Savage and Varnes (1987) argued that sackungen have developed in response to valley-wall oversteepening by Pleistocene alpine valley glaciation. As the valley glaciers retreated during interglacial stages, the ridges were subjected to increased gravity-induced stresses. In parts of a ridge, with rock of low cohesive strength and closely spaced joints, these stress differences were sufficient to initiate plastic flow and, high on the ridge sides, uphill-facing scarps developed. Augustinus (1987) applied the FE method to help study the development of glacial troughs in the New Zealand Southern Alps.

Studies by Yu and Coates (1970, 1978) and Stacey (1973) of the stresses induced by open pit mines with a range of physical properties, depths, shapes and volumes, indicate the value of the FE technique when used as a simulator of a large range of slope conditions. Yu and Coates (1970) conducted a series of studies for which a total of 45 slope conditions were examined, taking into account the slope angles, slope shapes and various loading conditions. Stacey (1973) undertook a similarly exhaustive FE modelling study of a range of slope angles, different floor widths and loading conditions. Stacey also evaluated the influence of rock jointing on the *in situ* stresses in the rock slope. In Fig. 7.1c,d the effect of varying the coefficient of lateral earth pressure alone is shown to be great. The dominant stresses are nearly vertical and parallel to the hillslope when  $K_0 = 1/3$  ( $K_0 = \sigma_h/\sigma_v$  = coefficient of lateral earth pressure at rest), but with an increase in lateral pressure ( $K_0 = 3$ ) the orientation of the principal stress changes and a large tensile zone develops at the toe of the slope (Fig. 7.1d).

McTigue and Mei (1981), Savage *et al.* (1985) and Amadei *et al.* (1987) showed that large horizontal stresses develop under valleys, and decrease and become compressive at low values of the Poisson's ratio, although this simple pattern is changed by rock anisotropy and jointing (Amadei and Savage, 1985). It is unlikely that bedrock can withstand large tensile stresses, so that heave and fracture are probable leading to increases in the effectiveness of erosion processes. Amadei *et al.* (1987) showed that the magnitude and orientation of the *in situ* stress field induced in a rock mass under gravity is strongly related to the rock mass structure.



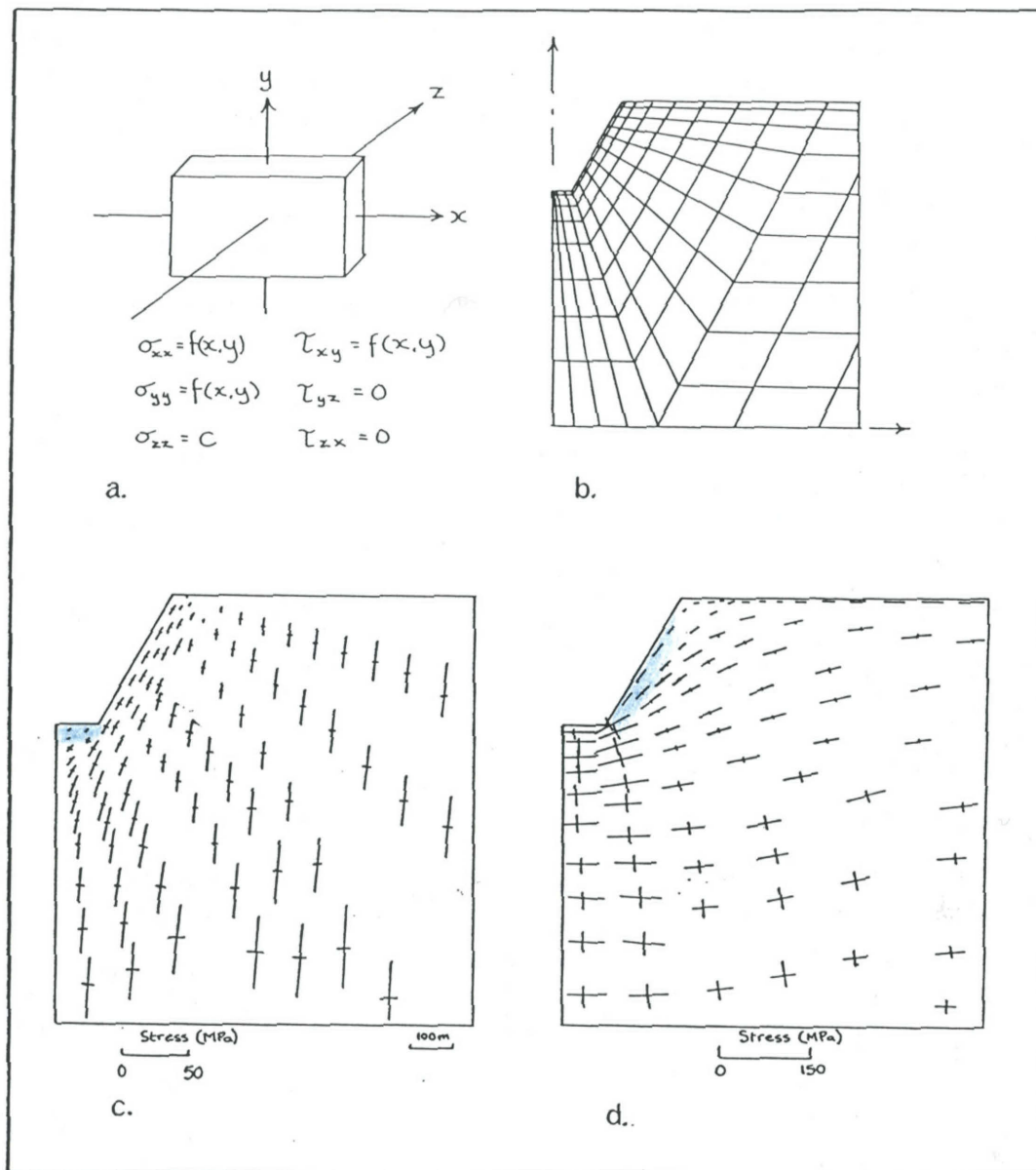


Figure 7.1. (a) Boundary stress conditions for finite element models. (b) FE mesh for a simple 60° slope. (c) Trajectories of principal stresses for a 60° slope model with  $K_0 = 0.33$ . (d) Principal stress trajectories for  $K_0 = 3$ . Note the development of zones of tensile stress near the toe of the slope under a compressive horizontal stress-field (coloured region). Bar length indicates stress magnitude. After Yu and Coates (1970).

## 7.2. Finite Element Method

### 7.2.1. Introduction

Excellent works on the FE technique are those of Desai and Abel (1973) and Zienkiewicz (1977). Essentially, the method assumes that the response of a body to various loading conditions can be approximated by considering a cross-section of the body to be made up of deformable elements. These are either triangular or quadrilateral in shape and each is connected at the corner or nodes (Fig. 7.1b). The amount of deformation will depend on the amount of load, and how close the element is to the applied load. The elements are chosen small enough that the straight lines that make up the sides of the elements remain straight after deformation (Yu and Coates, 1978).

The mathematical formulation of the FE method is based on the principle that when loads are applied to a body, the total potential energy of the system remains at a minimum (Zienkiewicz, 1977). It can be shown that for the total potential energy of the system ( $U$ ) to be minimized, the following conditions hold:

$$(\delta) = [K]^{-1} (Q) \quad (1)$$

where  $[K]$  is the total stiffness matrix of the system (sum of the total stiffness matrices of each element);  $(\delta)$  = the nodal displacement, and  $(Q)$  is the total loading of the system. Once the displacement at each node has been determined, it is a simple matter to calculate the strains from the relation:

$$(\epsilon) = [D] (\delta) \quad (2)$$

where  $[D]$  is the displacement strain matrix. The stresses are then found to be:

$$(\sigma) = [E] (\epsilon) \quad (3)$$

where  $[E]$  is the elastic matrix, i.e., the relationship between the stresses and strains.

### 7.2.2. Mesh Development

For each valley slope profile, a mesh was constructed to simulate the structure. The mesh elements were closely spaced at the slope surface and as breaks of slope are approached (Fig. 7.2.a-e). The stress changes are mainly induced at the free-surfaces, so that deep into the structure only large elements are required.

The nodal points were numbered to reduce the bandwidth of the matrix and to reduce the computational cost. The selection of the boundary conditions for the model analyses is critical for a realistic simulation of the stress field. It is essential to have at least one fixed point otherwise the structure is not in static equilibrium (Zienkiewicz, 1977).

With gravity as the only load on the system, the nodes at the two lower corners (i.e., the one at the bottom right and the bottom left of the structure) were fixed. The nodes along either side were constrained to move only vertically and those along the bottom could move only horizontally. Conversely with the imposition of horizontal loading ( $\sigma_h$ ) only, a node along the bottom centre of the mesh was fixed. The nodes along either side were constrained to move only horizontally and those along the bottom only vertically. All other nodes were free to move in any direction.

### 7.2.3. Data Input To The Model

The stresses applied to the slope system are additive, and may not by themselves be important controls on rock failure. In a tectonically active, glacierized mountain belt, the input of tectonic and thermal stresses may be an important additional input. Further, in compressional terrain the resultant extreme relief would be expected to induce large gravitational stresses. These would combine with the tectonic and any thermal stress component to generate rock failure and so control the location and direction of the modifying geomorphic processes.

The formal assumptions of the FE model are : (1) the body is a continuum in (2) static equilibrium; (3) the body behaves in a linearly elastic fashion and is homogeneous and isotropic; (4) elastic

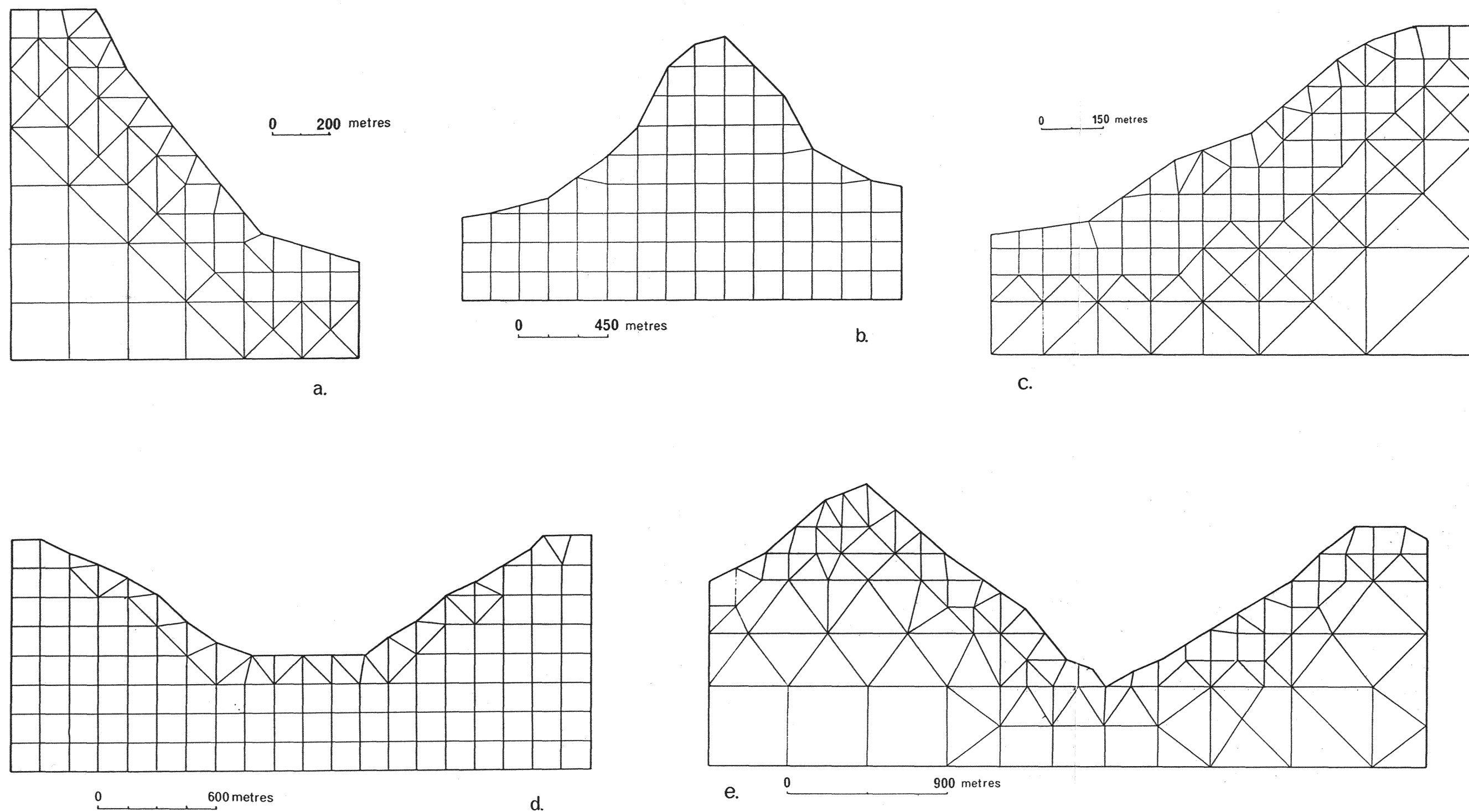


Figure 7.2. Finite element grids representing: (a) one-half of a symmetrical ridge, Darran Mountains, northern Fiordland; (b) profile across Barrier ridge, Darran Mountains; (c) one-half of a symmetrical ridge, West Arm, Lake Manapouri; (d) profile across the Tasman Valley at Ball Shelter, Mt Cook National Park; and e. profile across the Whymper Glacier, South Westland.

distortions of the body occur under a condition of plane strain. From the stress concentrations at each point:

$$\begin{vmatrix} \sigma_x & \tau_{xy} \\ \tau_{yx} & \sigma_y \end{vmatrix} \quad (4)$$

the principal stresses and their orientations are calculated.

The rock quality parameters required as input for the model are: unit weight of the material, Elastic Moduli (E) and Poisson's ratio ( $\nu$ ). E and  $\nu$  are simple inputs where isotropic media are concerned, but for materials showing strong strength anisotropy such as schists, the complete stress/strain ellipsoid must be determined (Read *et al.*, 1987).

In the FE analyses, the loads imposed on the structures are a self-weight induced vertical stress ( $\sigma_v$ ), and a horizontal ( $\sigma_h$ ) stress to simulate load induced tectonically. A thermal stress component ( $\sigma_{th}$ ) was used to simulate stress induced in the rock mass by an advancing/retreating glacier. In practice, the effects of these stresses would be reduced by the displacements of the valley walls and the presence and density of the bedrock joints (Stacey, 1973). In the self-weight analysis,  $K_0 = 0$  ( $K_0$  is the coefficient of earth pressure at rest,  $K_0 = \sigma_h/\sigma_v$ ) where the vertical stress  $\sigma_v$  is given by:

$$\sigma_v = \rho gh \quad (5)$$

where  $\rho$  is the dry density of the rock, and  $h$  is the overburden thickness.

An arbitrary value of  $K_0 = 1$  was used in the analyses, with the input of a horizontal stress such that the magnitude of the applied load will depend on the elastic properties of the bedrock. Jamison and Cook (1979) (Fig. 7.3) showed that  $K_0$  values of  $>2$  and  $<7$  are common in regions of thrust faulting, whilst zones of normal faulting are associated with crustal extension and  $K_0$  is usually  $<1$ , if all horizontal stresses are relieved. Where strike-slip faulting is present, the stress field may be weakly compressional but  $K_0$  approaches unity. Thus,  $K_0 = 1$  is used as input to the models for the strike-slip terrains adjacent to the Main Divide of the Southern Alps.

For best approximations it must be assumed that the 2-dimensional plane of the FE model coincides with an *in situ* principal stress plane

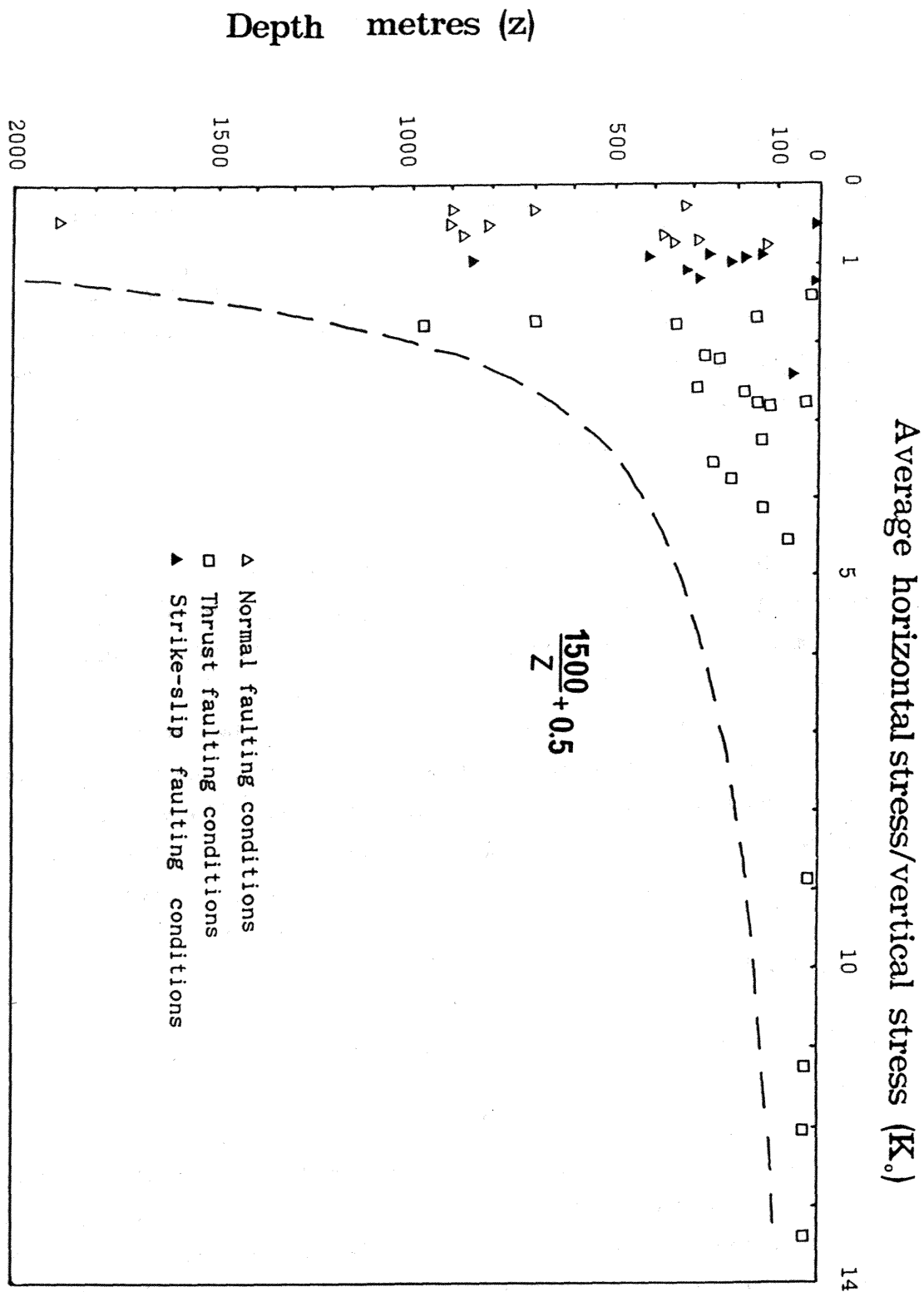


Figure 7.3. Effect of tectonic processes on the coefficient of earth pressure at rest ( $K_0$ ). The diagram relates the ratio of the vertical to horizontal stress, to the value of the vertical component of stress as a function of depth below surface. The data are divided into three groups corresponding to stress conditions associated with normal, thrust and strike-slip faulting. After Jamison and Cook (1979).

(a reasonable assumption for a planar analysis oriented perpendicular to the face of a rock cut or slope). By applying a lateral hydrostatic stress to a finite element, the shear stresses at the lateral boundaries remain zero. The stress conditions for a finite element under these assumptions are shown in Fig. 7.1a. The horizontal boundary force component was assumed to be constant with depth.

#### 7.2.4. Model Output

The results were obtained as numerical values for the displacements at each node and the values of their stresses at the centre of each element (horizontal stress component:  $\sigma_x$ , vertical component:  $\sigma_y$ , and the shear stress:  $\tau_{xy}$ ). The stress and displacement vector data were contoured automatically in the programme and the results displayed for each load case and model.

### 7.3. Finite Element Models

#### 7.3.1. Northern Fiordland

Two different meshes were developed to simulate the typical Darran Mountain valley profiles. Firstly, a simple mesh representing half a symmetrical valley was constructed based on a profile drawn of the north wall of the Gertrude Valley below Mt. Talbot (Fig. 7.2a). A second mesh was constructed from a profile drawn through the Barrier Range from Lake Adelaide to the Gertrude Valley (Fig. 7.2b). The geotechnical properties of the assumed isotropic, linearly elastic diorite/gabbro are given in Table 7.1.

In the iteration with material self-weight as the only load on both meshes, low magnitude tensile stresses are generated at the slope toe and trough base, changing to compressive at the trough wall and crest (Fig. 7.4a & 7.5a). Zones of high shear stress would be developed on the slopes, but are probably insufficient to cause failure of the intact material. Similarly, the induced tensional stresses are unlikely to be of sufficient magnitude to cause material failure. The stress magnitude increases with trough slope inclination and height.

In northern Fiordland, high  $\sigma_h$  tectonic stresses are probably present, developed by northward oblique-slip movement along the Alpine

Table 7.1. Rock strength properties assumed for finite element calculations.

Study area	Rock type	Dynamic elastic moduli (GPa)	Dynamic Poisson's ratio	Unit weight (kg/m <sup>3</sup> )	Cohesion (MPa)	Brazil tensile strength (MPa)
N. Fiordland	Gabbro	52.6	0.2	2880	50	8.5
S. Fiordland	Granite	45.0	0.25	2850	33	7.3
S. Westland	Biotite schist	63.5 *	0.13 *	3176 *	13.5	5.0
Mt Cook	Greywacke	8.0	0.35	2354	140	22.5
McMurdo Dry	Dolerite	88.7	0.24	2910	60	13.9
Valleys	Orthoquartzite	26.1	0.37	2340	22.1	3.3
	Arena Sandstone	11.0	0.45	2350	10.1	1.9

All strength values from vacuum saturated state. \* values from Brown *et al.* (1980), all others from this study (Appendix 3).



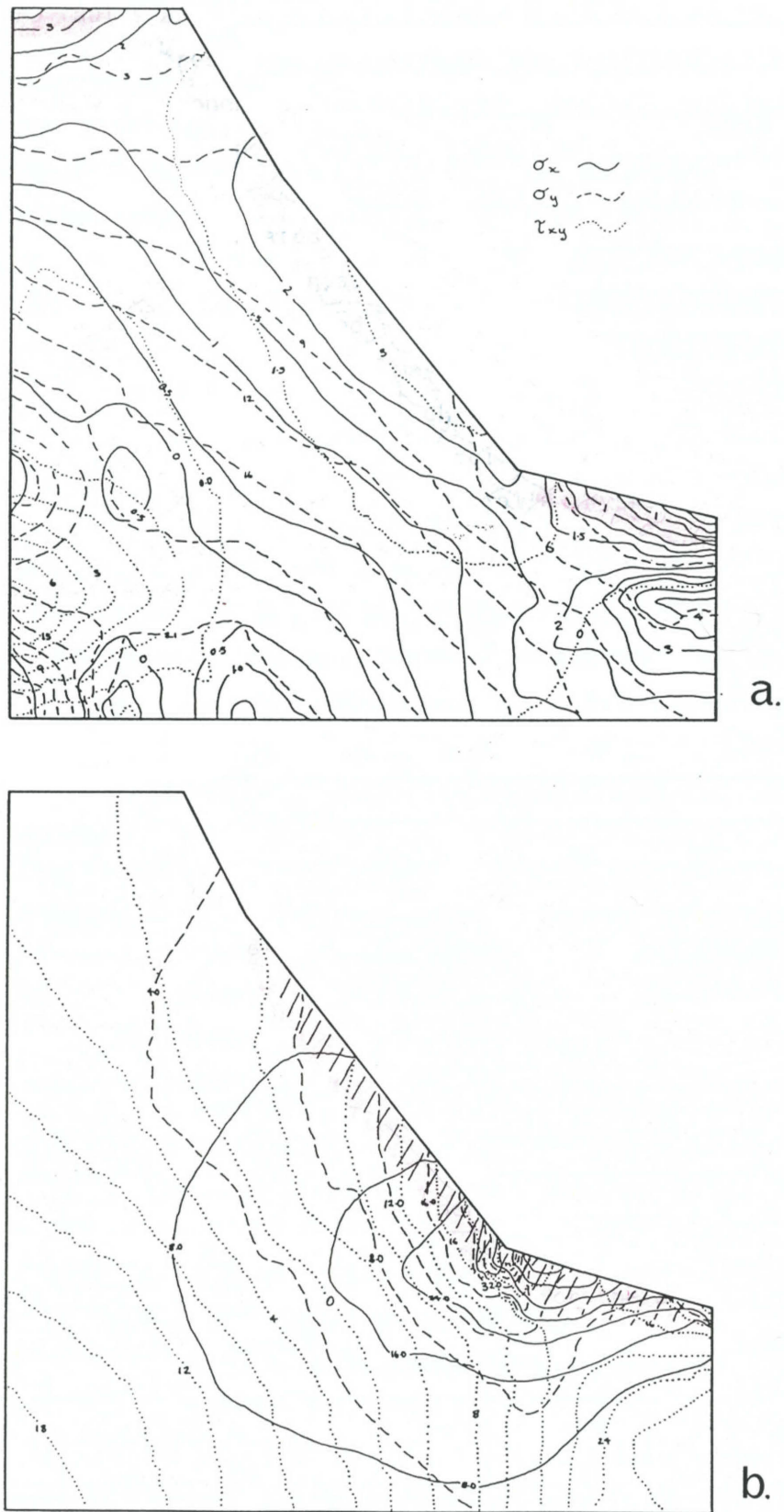
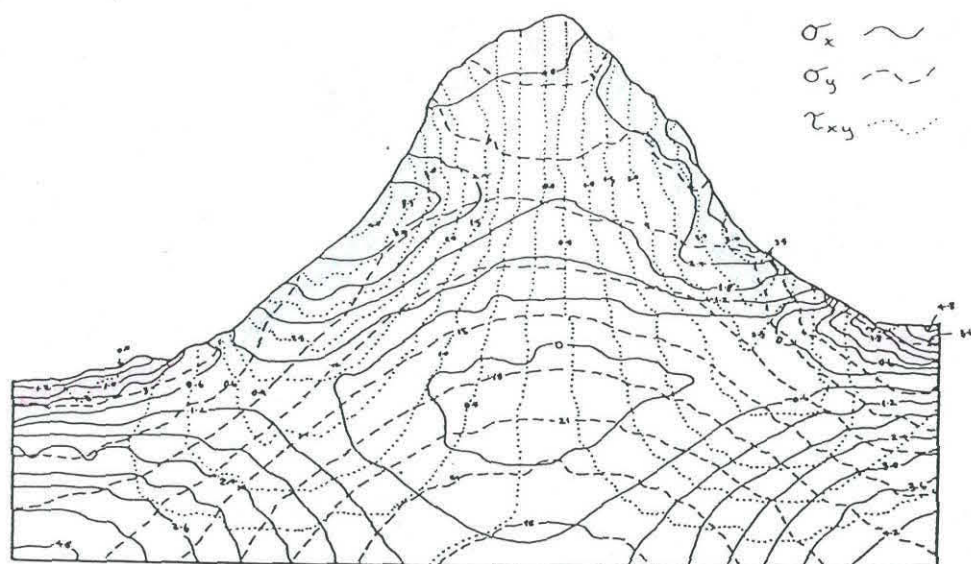
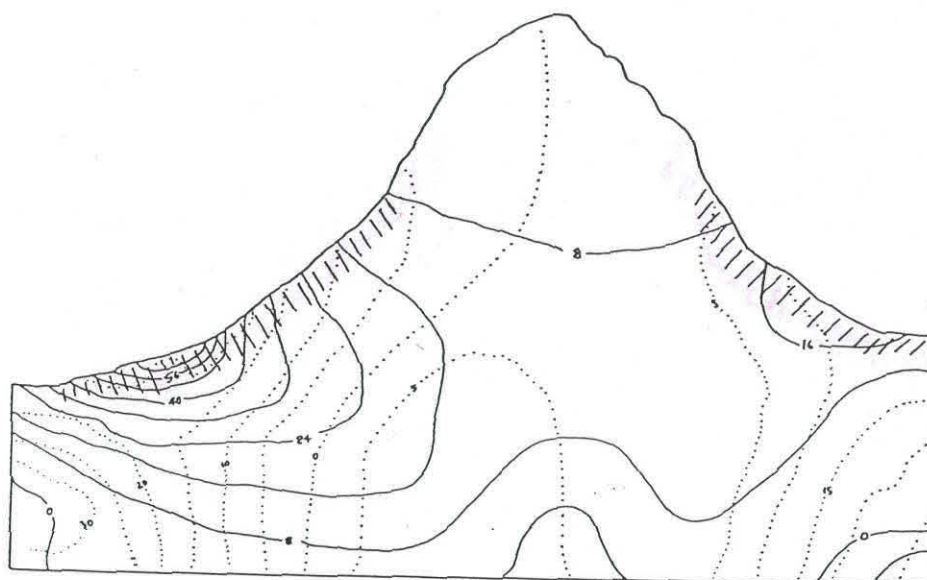


Figure 7.4. Modelled stress contours within half of a symmetrical valley, northern Fiordland, with: (a)  $K_0 = 0$ ; b.  $K_0 = 1.0$ . Slope region shaded pink indicates a tensional zone, blue: compressional. Hatched zone indicates areas of induced tensile failure along the trough cross-profile.



a.



b.

Figure 7.5. Modelled stresses within a profile across Barrier Ridge northern Fiordland, with: (a)  $K_0 = 0$ ; b.  $K_0 = 1.0$ . Shading as for Fig. 7.4.

and Hollyford faults and associated uplift. To simulate the input of horizontal tectonic stresses, each model was loaded with a horizontal compressive stress component so that  $K_0 = 1$ , and the resultant stress fields plotted for each model (Fig. 7.4b, 7.5b). Examination of Figs. 7.4b & 7.5b, indicates that a contrasting stress pattern and magnitude is developed to that generated by only self weight-induced loading (Fig. 7.4a & 7.5a). With horizontal loading (Figs. 7.4b & 7.5b), high stress concentrations are developed towards the slope toe and valley bottom. The stresses are tensile and may be of sufficient magnitude to cause tensile failure of the intact rock material (Table 7.1). Curved sheeting joints of probable stress-relief origin are commonly developed towards the base of the trough walls (Fyffe, 1954) and the existence of these stress-relief joints is consistent with a model of the development of high magnitude tensile stresses in the slope.

An increase in the horizontal loading ( $K_0 = 3$ ) simply increases the magnitude of the stresses concentrated at the base of the valley with little change in their geometry. The additional input of thermal stresses developed under a fluctuating glacial regimen is a potentially important component of the stress system. Assuming a laterally confined elastic half-space, the thermal stress generated by a temperature change  $\Delta T$  is given by:

$$\sigma_{th} = \frac{\alpha \cdot E \cdot \Delta T}{1 - \nu} \quad (6)$$

where  $\alpha$  is the linear coefficient of thermal expansion,  $E$  is Young's modulus and  $\nu$  is Poisson's ratio. Assuming a  $\alpha$  of  $7 \times 10^{-6}$  and elastic moduli of 52.6 GPa and Poisson's ratio of 0.2 for the plutonic rocks, with an advancing glacier, a temperature change of only  $6^\circ\text{C}$  is sufficient to generate a horizontal tensile stress of 2.8 MPa; a  $10^\circ\text{C}$  reduction in temperature will generate a tensile stress of 4.6 MPa. These stresses have a magnitude nearly 50% of the tensile strength of the granite/gabbro, and suggest that zones of fluctuating thermal stress in the bedrock could aid the processes of rock weakening when added to the cycles of repeated loading of the rock mass.

Scheidegger (1963) proposed the existence of a stress reversal at the valley shoulder, and argued that these steep, stress weakened slopes may be where most rock falls are initiated. Such a distinct low angle valley shoulder persists across northern Fiordland (Fig. 2.2c),

below which are steep but stable compressively stressed slopes. The presence of high tensile stresses at the valley shoulder is suggested by the presence of tensile fissures, joint blocks and shatter zones.

The input of horizontal compression to the models induces tensile stresses at the slope toe and valley bottom, with the stresses reducing in magnitude with increasing valley width. As long as the tensile strength of the slope rock is exceeded and pre-existing weakness planes exist allowing the break up of the massive joint bound blocks, erosion by an advancing valley glacier will result in preferential deepening of the trough and eventual development of the overdeepened and steepened glacial valleys apparent across northern Fiordland (Fig. 2.2a). The high *in situ* rock mass strength of the trough slopes (Fig. 4.2) prevents non-glacial processes from reducing their slope angle despite the development of tensile fissures in the slope rock. Consequently, the overdeepened trough form will be maintained so that erosion during glacier re-advances will probably enhance the tectonically and glacially adjusted trough slope and valley cross-profile forms.

#### 7.3.2. West Arm Manapouri

A FE mesh was developed to simulate the valley profile at the site of the West Arm power station, Lake Manapouri (Fig. 7.2c). The model is of half a symmetrical valley. The rock quality inputs to the model are given in Table 7.1. Gravitational and tectonically-induced stress-fields were modelled using  $K_0 = 0$  and 1.0 and the stress fields are shown in Fig. 7.6a,b. Flat jacks were inserted and stress measurements were made during the construction of the West Arm power station. Shortly after the excavation of the chamber,  $\sigma_v$  values of up to 120 MPa and  $\sigma_h$  values of up to 54 MPa were measured, and these reduced rapidly to a constant low value of  $\sigma_v \sim 6$  MPa and  $\sigma_h \sim 3$  MPa (Perrin, 1984).

With the input of only overburden induced loads to the model, a low magnitude compressive stress field is generated in the vicinity of the relatively low-angle slopes and valley floor (Fig. 7.6a). At the base of the slope, only low magnitude compressive stresses are developed at the surface and the shear stresses are probably insufficient to cause the rupture of even jointed rock slope material. However, using the same FE mesh, and the input of horizontal loading ( $K_0 = 1$ ), a region of high stress concentration is generated at the

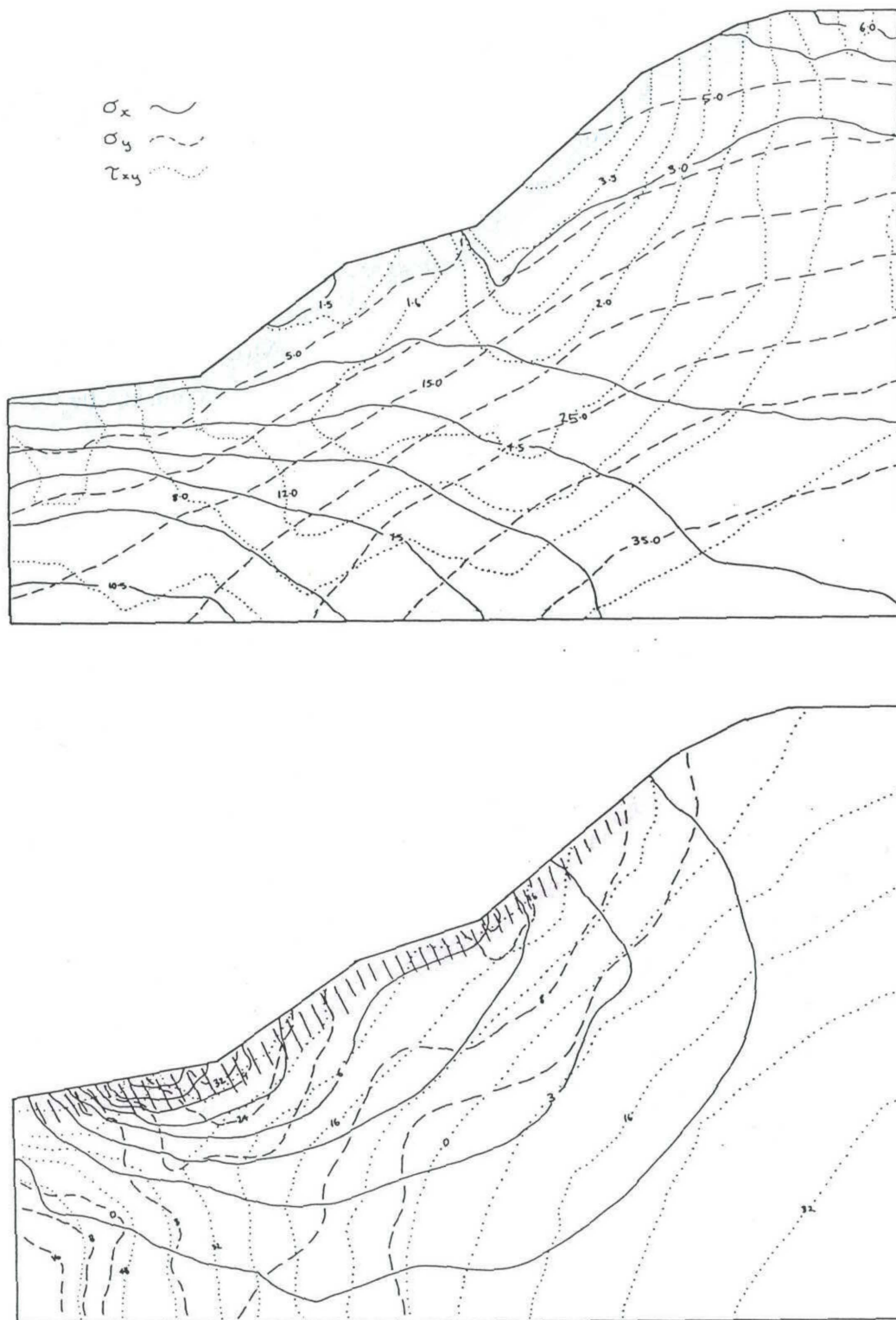


Figure 7.6. Modelled stress contours within half of a symmetrical ridge profile at West Arm, Lake Manapouri, with: (a)  $K_0 = 0$ ; (b)  $K_0 = 1.0$ . Shading as for Fig. 7.4.

slope toe. The stresses generated in the slope rock are tensional and persist upslope towards the ridge crest (Fig. 7.6b).

From the preceeding analysis, it may be expected that glacially oversteepened slopes and broken rock/sheeting joints would develop with the presence of a horizontal tectonic stress component. However, in the south-central Fiordland region, the slopes are relatively low-angle, troughs relatively shallow and the slopes stable and heavily vegetated, displaying little evidence of stress-relief, sheet jointing. Thus, the glacierized morphology supports a model of the input of only gravitational stress to the valley system. This model is compatible with the stress measurements made during the construction of the West Arm power station. The high *in situ* stresses measured by the flatjacks are probably due to the release of residual stresses locked-in the rock. These may be the result of an earlier tectonic stress regime, and/or depth of burial, and released in a time-dependent fashion shortly after excavation. According to Perrin (1984) the West Arm underground power house appears to have reached a state of equilibrium with the rockmass.

High magnitude tectonic stresses are believed to have been generated across northern Fiordland by movements on the Alpine and Hollyford Faults (Davey and Smith, 1983), with a large component of locked-in stress being generated by deep burial and erosion (MacFarlane, 1983). J. Adams (1981) argued that earthquakes are an important mechanism of crustal stress relief, and while the frequency of large ( $M > 6$ ) earthquakes is low, they release large amounts of stored strain energy.

### 7.3.3. Greywacke Model-Mt Cook

A single model of a typical glacial valley cross-profile was developed for the greywacke terrain, Mt Cook region. A mesh was constructed to simulate a profile across the Tasman Valley at De la Beche Ridge consisting of 123 nodes and 102 elements (Fig. 7.2d). The geotechnical properties of the greywacke used in the analysis are given in Table 7.1.

The low  $E$  and high  $\nu$  values associated with the intercalated greywacke and argillite bands (Table 7.1) developed an *in situ* stress regime different from that developed in the plutonic basement of Fiordland. The FE model was loaded with self-weight ( $K_0 = 0$ ), and a

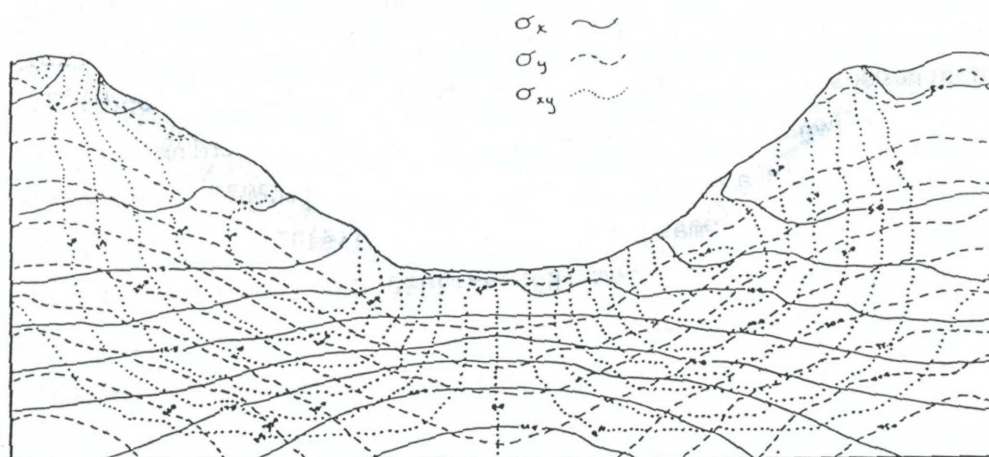


horizontal component ( $K_0 = 1$ ) to simulate load induced tectonically. Loading of the model with material self-weight generates a strongly compressive stress regime (Fig. 7.7a), with the *in situ* rock stresses probably being insufficient to cause failure of the intact rock. However, the density and continuity of the jointing would considerably reduce the stresses required for failure to occur. In the slope rock,  $\sigma_1 \gg \sigma_2$ , so that tensile failure may be induced with arching parallel to the slope (Brunner and Scheidegger, 1973), although the closely jointed nature of the rock mass makes this unrealistic. Loading of the mesh with a horizontal component ( $K_0 = 1$ ), develops a high stress concentration in the trough walls and valley base (Fig. 7.7b). The induced stresses are tensile and may enhance the failure of the rock slope.

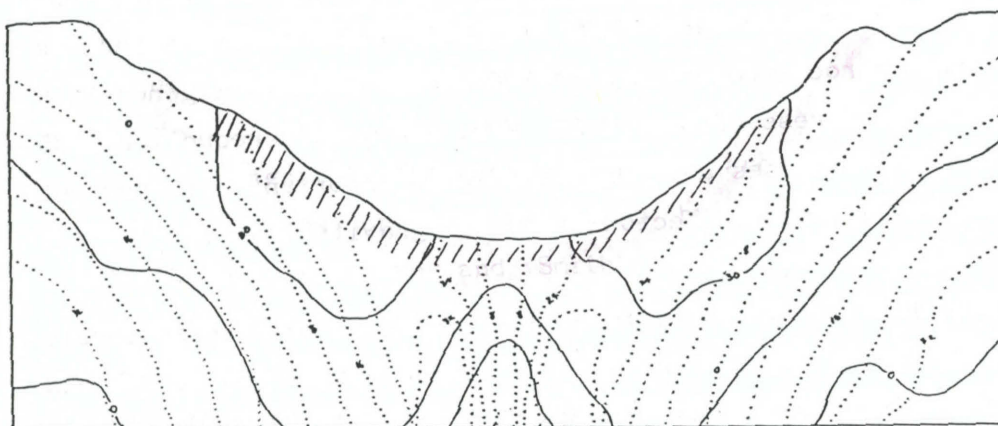
The input of a thermally-induced stress developed under a fluctuating glacial regimen was considered. Assuming a coefficient of thermal expansion of  $11 \times 10^{-6}$  for greywacke, and Elastic moduli and Poisson's ratio of 8 GPa and 0.35 respectively, for an advancing glacier, a drop in rock temperature of  $6^\circ\text{C}$  is sufficient to generate a horizontal tensile stress of only 0.81 MPa, and a  $10^\circ\text{C}$  reduction 1.35 MPa. Thus, thermal stresses are unlikely to be important with respect to the rock stresses induced tectonically and gravitationally.

In closely jointed rock, failure can occur at low stress levels and a yielding of the total rock mass is commonly observed (Broch and Sorheim, 1984). Weaker rocks can be expected to produce a deep zone of stress weakened rock with stress-relief along pre-existing discontinuities without slabbing (Fergusson and Hamel, 1981). The geometry and magnitude of the shear stresses across the profile suggests that the distribution of valley bottom defects is such that they do not experience shearing displacements parallel to the valley axis. This results in the *in situ* shear strengths of the valley bottom rock often exceeding the residual level and approaching the peak shear strength for intact rock. Thus, glacial erosion of the greywacke/argillite basement should result in the preferential widening of the trough.

During the retreat of the glacier, the unbuttressed rock slope will equilibrate to the changed stress conditions. Depending on the RMS characteristics of the slope rock, this adjustment can take



a.



b.

Figure 7.7. Modelled stress contours within a profile across the Tasman Valley, Mt Cook National Park, with: (a)  $K_0 = 0$ ; (b)  $K_0 = 1.0$ . Shading as for Fig. 7.4.



several forms. Features such as antisllope scarps are frequently developed in the Mt Cook area, but almost exclusively in a direction perpendicular to the PHS direction, and parallel to the ridge crests. Beck (1968) and Cave (1980) noted similar slump rents developed in the Torlesse rocks in the Kelly Range, Arthur's Pass National Park. These authors attributed the ridge rents to gravitational slumping of the greywacke along the bedding plane weaknesses and ridge core foundering following glacial deepening and widening of the valleys. However, Beck's (1968) interpretation is open to question and the features are more likely to be the result of rock mass bulging with downslope movement creating the scarp (Prebble, 1987).

The FE modelling suggests that the steepening of the valley-sides increases the shear stress in the valley wall rock, and is probably the most important cause of the tensional displacements and downslope flexuring of the heavily jointed rock where the bedrock structure is favourable. Depending on the geometry of the jointing and resultant blocks, a temporary steepening of the rock face by a few degrees may reactivate the slope failure, i.e., sliding/toppling on many joint planes presently not critical for stability. The FE model is compatible with a model of the development of the anti-slope scarps by tension and flexural slip.

#### 7.3.4. Schist Model-South Westland

A NW-SE oriented profile was drawn across the Whymper Glacier, South Westland. The mesh was constructed to simulate the valley and surrounding ridges, and comprises 123 nodes and 112 elements (Fig. 7.2e). The geotechnical properties of the schist are displayed in Table 7.1. Although the schist displays a strong strength anisotropy (Read *et al.*, 1987), lack of time and resources made its evaluation difficult and the schist was idealized as an isotropic, homogeneous material as suggested by Brown *et al.* (1980).

Loading of the mesh with material self-weight develops a complex compressional stress field (Fig. 7.8a). Tensional stresses are induced at the base of the trough, but are of low magnitude and probably insufficient to cause failure of the intact material (Table 7.1). The closely spaced foliation and fracture spacing of the schist would significantly reduce the stresses required for rock failure. The input of a horizontal loading component ( $K_0 = 1$ ) generates a contrasting stress pattern and magnitude (Fig. 7.8b). The pattern is complex and

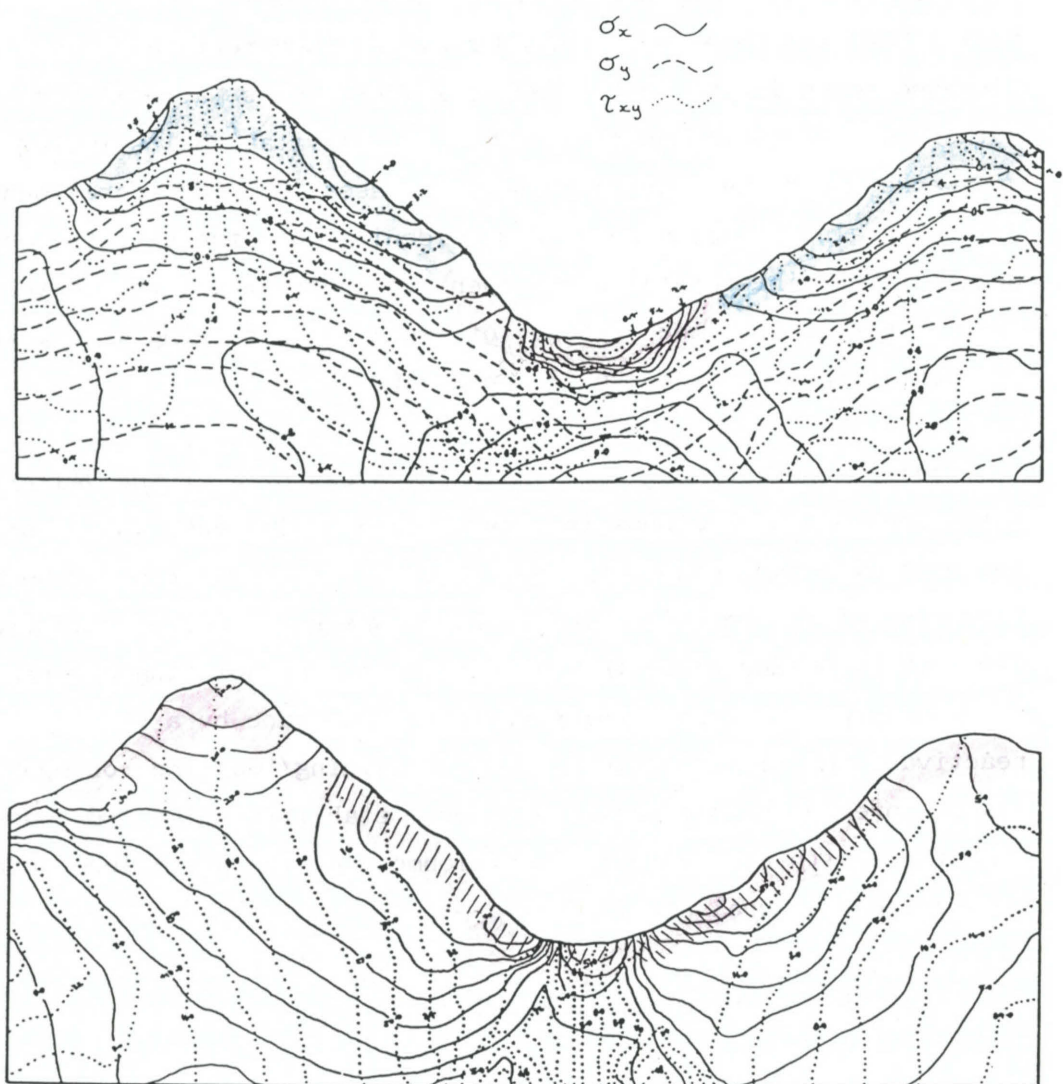


Figure 7.8. Modelled stress contours within a profile across the Whymper Glacier, South Westland, with: (a)  $K_0 = 0$ ; (b)  $K_0 = 1.0$ . Shading as for Fig. 7.4.

displays stress concentrations and induced tensile regions along the complete rock slope profile (Fig. 7.8b). The tensional stresses are of sufficient magnitude to cause failure of the slope and valley bottom rock, so that slope failure and erosion of the surface rock are probably rapid, enhancing the rapid denudation of the schist terrain in the central Alps.

The high regional PHS field and foliation defined anisotropy in the schist results in foliation-plane controlled glacial deepening and widening of the trough. This structural control causes the development of trough asymmetry when the trough parallels the foliation, but the schist behaves almost like an isotropic medium when the foliation is highly oblique or perpendicular to the trend of the valley axis. The Franz Josef glacial valley is excavated perpendicular to the foliation and has developed a steep, canyon-like lower valley segment. The cross-valley profile is symmetrical, and stress-relief slabbing cuts across the foliation at high-angles, bearing no apparent relationship to the structures in the schist (Fig. 2.12c). Stress-induced failure of the valley bottom rock combined with the foliation and tectonic joint sets, provides weakened, easily erodible rock. The high RMS of the rock slopes allows the maintenance of apparently oversteepened slopes until cross-joints gradually open; weathering, release of residual stresses and high joint water pressures cause gradual weakening of the rock mass.

#### 7.4. Stress Evaluation: Implications For Slope Stability and Erosion Processes

In the previous two chapters, the regional and *in situ* stress fields have been argued to have a major influence on the development of the glacial valley morphology in the New Zealand Southern Alps. The regional state of stress controls the type of fracturing that occurs, creating zones of preferential weakness in the rockmass to be exploited by the fluvial and glacial processes. This supports the premise of Gerber (1980) that many features of glaciated mountains owe much of their form to the stress patterns in the rocks, rather than to the erosional processes which are most effective as removers of pre-fractured rock. However, it must be emphasized that the models developed here are highly idealized, ignoring the input of lithological and structural variations in the bedrock. Thus, the models may not correspond to the real situation. However, they do

indicate the potential importance of the stresses in the rock mass on erosional landform generation, and provide some ideas for further research.

Following development of the valley system, the *in situ* stress field has controlled the destabilization, modification and development of the glacial valley cross-profiles by working in conjunction with the rock mass strength of the slope rock. The following results are readily apparent from the FE modelling:

- 1) The stress field along the mountain slopes is controlled by a combination of the tectonic stress field and that induced locally by the topography.
- 2) The rock slopes with high  $\nu$  and low  $E$  (e.g. Fiordland rock slopes) display a weak compressional stress field at the trough base. This changes to a stress concentration with strong tensional elements at the trough slope and base with the input of a horizontal load simulating the stresses induced tectonically. The stresses may induce tensile and shear failure of the slope rock along the whole profile.
- 3) The rock slopes with low  $\nu$  and high  $E$  (e.g. Mt. Cook region rock slopes) display a tensile stress field at the trough base oriented perpendicular to the slope. The input of a horizontal load simulating horizontal tectonic stress develops a stress concentration towards the base of the slope. The stresses perpendicular to the slope are tensile and may induce tensile failure of the rockmass at the slope toe and valley floor.
- 4) Thermal stresses induced in the rock mass by a fluctuating glacier are an important potential input to the system, with the magnitude of the induced tensile stresses sometimes approaching the tensile strength of the intact rock.
- 5) The pattern of stress-induced failure of the rock mass may selectively control the direction and extent of glacial exploitation of the trough rock and subsequent slope modification. The deep, narrow troughs developed in northern Fiordland reflect preferential glacial deepening, whilst the relatively over-widened glacial troughs developed in the Mt Cook region reflect erosional widening in tandem with rapid destabilization of the low RMS trough slopes. The extent

and geometry of this erosion is strongly influenced by the elastic and intact strength properties of the bedrock, although the RMS properties of the eroded basement control the final trough form.

## 7.5. Influence of the In Situ Stress Regime on the Development of Some Antarctic Dry Valley Landforms

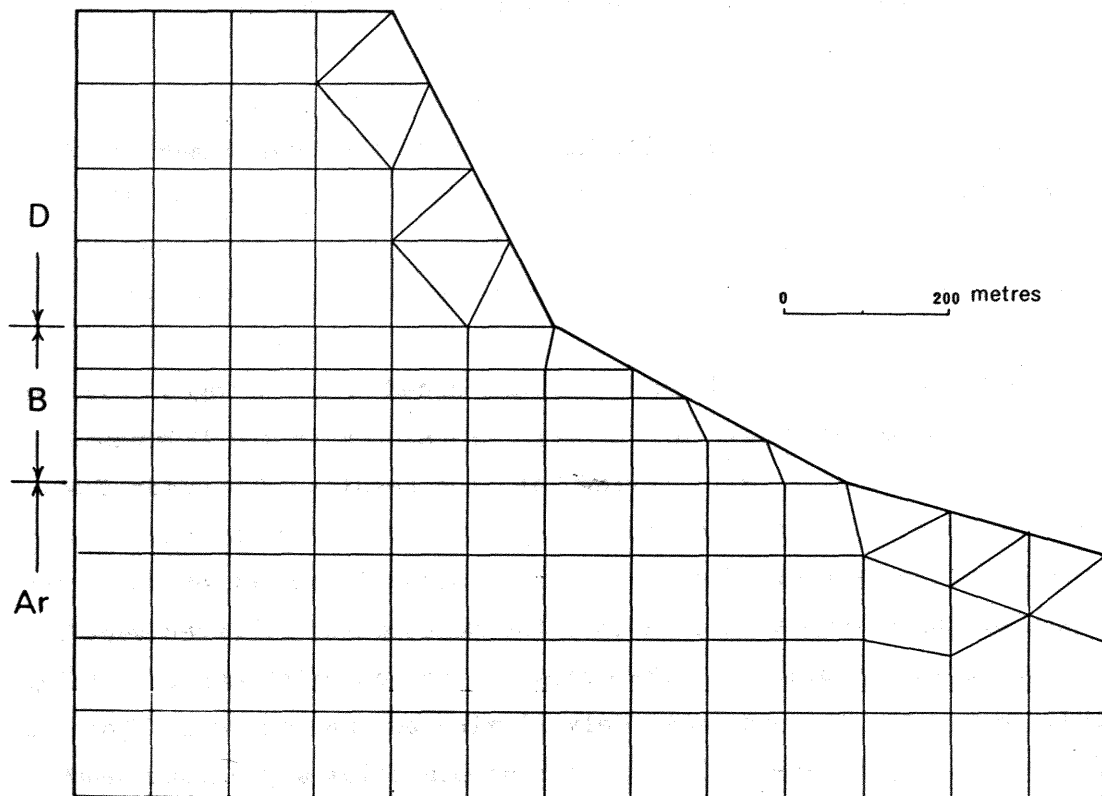
### 7.5.1. Introduction

Gravitational deformation of steep-sided rock ridges will be examined with reference to a variety of slopes in the McMurdo Dry-Valleys, Antarctica. A brief review of the results of section 4.5 is given here, as it is considered to be important for the analysis of the FE modelling study. The relatively high intact strength of the capping Beacon Orthoquartzite allows the development of often vertical RMS equilibrium slopes on the capping Beacon Orthoquartzite (Fig. 4.12). However, the more finely laminated and densely jointed underlying low RMS Arena Sandstone, displays low-angle rock benches usually falling outside the equilibrium envelope.

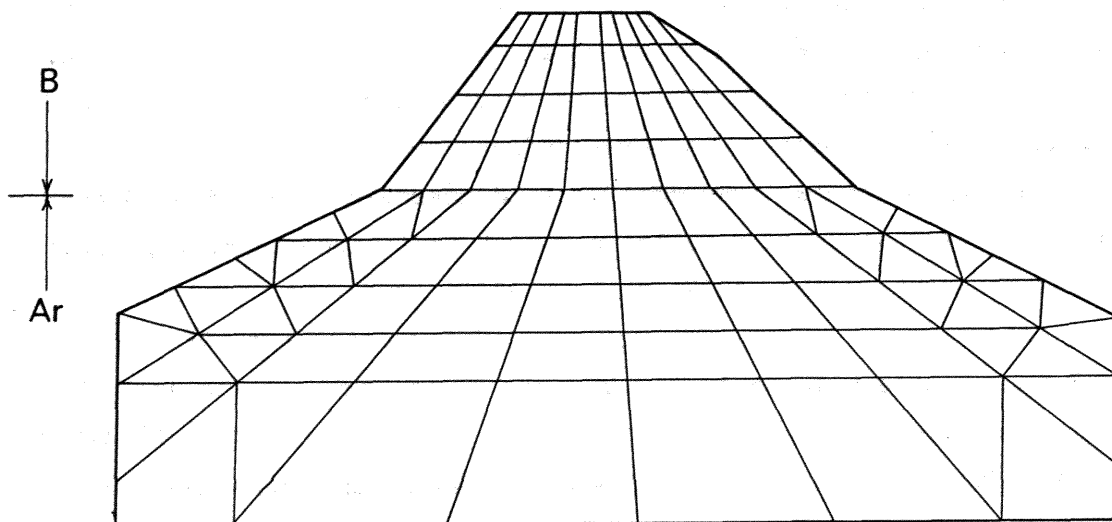
Consequently, it appears that the controlling factors on the slope form and landform genesis are the fracture frequency and orientation, with the closely jointed Aztec Sandstone being more susceptible to: (a) glacial erosion, and (b) rapid weathering (both physical and chemical), due to increased joint surface area. A further factor is the relative hardness (cementation/case-hardening) of the Beacon Orthoquartzite that would give the cap rock resistance to both glacial and wind abrasion (Selby, 1977; Malin, 1984).

### 7.5.2. Finite Element Analysis

The models applied in this study are 2-dimensional and represent a section through a two and three-layered ridge. In the three-layered Mt Thor model, strong elastic material representing a dolerite cap, rests on a base of weak material representing bedded sandstone. The stresses and displacements on half of the symmetrical mass, as it deformed under its own weight, were generated (Fig. 7.9a). In the two layered Mt Cerce model, a cap of Beacon Orthoquartzite overlies closely bedded Aztec Formation Sandstone (Fig. 7.9b).



a.



b.

Figure 7.9. Finite element meshes representing: (a) one-half of a symmetrical, self gravitating, three-layered ridge, Mt. Thor, Asgard Range; (b) profile across a self-gravitating two-layered ridge, Mt Cerce, Olympus Range. D = Ferrar Dolerite, B = Beacon Heights Orthoquartzite, Ar = Arena Sandstone.

The profile sections were digitized by hand and a FE mesh chosen that consisted of 105 and 112 elements for the Mt. Cerce and Thor profiles respectively (Fig. 7.9a,b). Isotropic, elastic materials were assumed, and the geological input to the models were unit weight of the rock, dynamic Elastic Moduli and the Poisson's ratio. The relevant strength values are given in Table 7.1. The problem was taken to be one of plane-strain. The load imposed on each structure was self-weight induced. Boundary conditions employed are those given in Fig. 7.1a.

#### 7.5.3.1. FE Model- Mt. Thor

Figure 7.10a shows the expected stress trajectories and magnitudes for  $\sigma_x$  and  $\sigma_y$ . For  $\sigma_x$ , note the large tensile stresses generated in the dolerite just above the contact with the sandstone. Similarly in Fig. 7.10a, it can be seen that large shear stresses are developed along the contact. Both of these features may be attributed to the extension of the dolerite mass in response to lateral ductile flow in the relatively weak Arena Sandstone. Large stresses exist near the base of sandstone slopes in response to the weight of the overlying rock. Fig. 7.10b shows the distorted shape of the mass in response to the gravitational loading. The weaker sandstone bulges slightly in response to the lateral flow, a feature seen in the sandstone underlying the dolerite cap.

#### 7.5.3.2. FE Model- Mt. Cerce

The FE model of Mt. Cerce (Fig. 7.11a,b), a layered model with Beacon Orthoquartzite overlying the Aztec Sandstone, indicates a lack of high tensile or shearing stresses at the contact. High tensile stresses are expected from the observed tensile jointing in the near vertical slopes developed in the orthoquartzite. This may be due to the similar unit weights,  $E$  and  $\nu$  of the two materials. Nevertheless, field examination of the 'mesas' indicates the breakup of the capping orthoquartzite into blocks of 200-300m size (Fig. 7.12), although the modelled *in situ* stress field is not conducive to the development of stress-relief free faces.

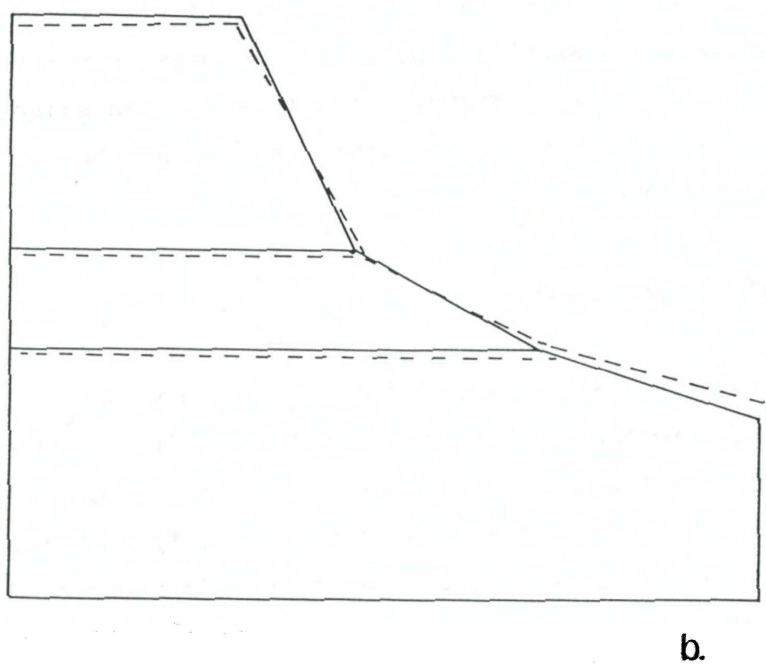
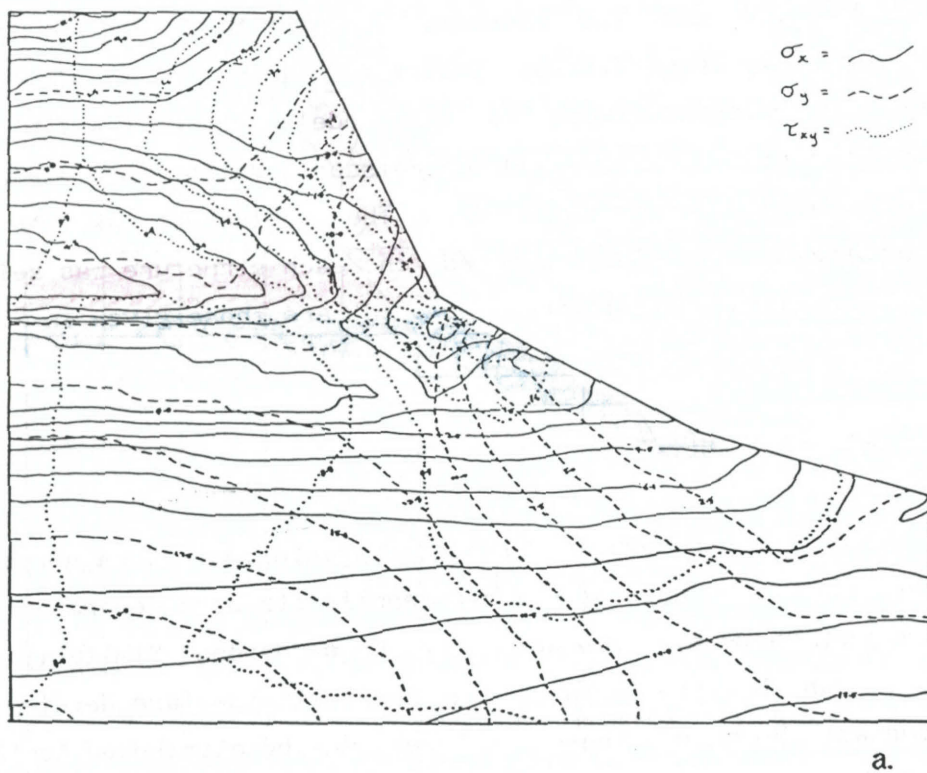
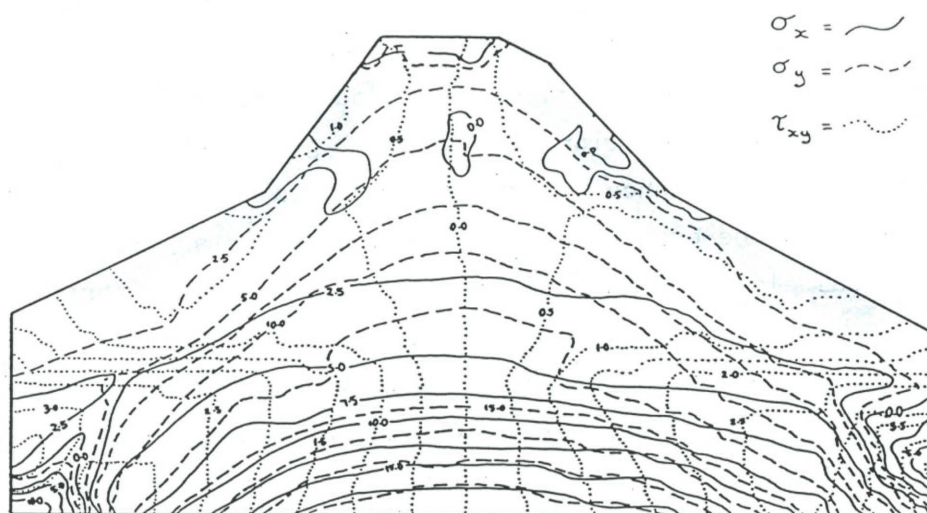
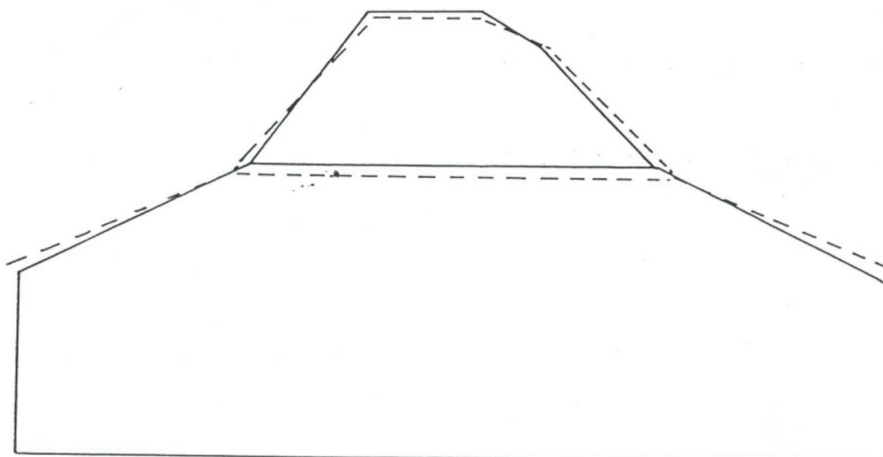


Figure 7.10. (a) Modelled stress contours within a three-layered model of Mt Thor with  $K_0 = 0$ . (b) Comparison of the original (solid line) and final (dashed line) outlines of the layered Mt Thor model. Shading as for Fig. 7.4.





a.



b.

Figure 7.11. (a) Modelled stress contours within a two-layered model of Mt Cerce with  $K_0 = 0$ . (b) Comparison of the original (solid line) and final (dashed line) outlines of the layered Mt Cerce model. Shading as for Fig. 7.4.

### 7.5.3. Development of Residual Stresses In Sandstone

A possible explanation for this apparent anomaly lies in the geologic and more recent erosional history of the mesa. During the deposition and induration of the sandstone and subsequent loading imposed by the thick dolerite cap, residual stresses were locked into the Aztec Sandstone by sintering and pressure annealing at the quartz grain contacts. The Beacon Heights Orthoquartzite is remarkably uniform in composition, and composed almost entirely of very mature quartz arenites. On average the bedding units are between 0.1-0.3 m thick. In thin-section the quartz grains show grain/grain point contacts and evidence of sintering and a predominance of cementation by quartz. The examination of clastic sedimentary rocks has shown that residual elastic strains can reside within their fabric (Friedman and Logan, 1970). Experimentally, Riek and Curry (1974) demonstrated that residual elastic strain locked into quartz sandstone could be released by subjecting samples to cycles of uniaxial loading. Hence, it is argued here that elastic locked-in stress was imparted during the cementation and diagenesis of the Beacon Supergroup sandstones. In this period of initial loading a differential compression was imparted to the grains. This state of differential stress was given permanence in the rock fabric by continuing diagenesis, and deposition of cement around and between grains.

A model of the 'locking in' of the residual stress by baking of the sandstones by the dolerite intrusions, as well as by compression and diagenesis, is supported by the frequent development of columnar jointing in the Altar Mountain Sandstone (Fig. 7.13). This feature was first described by Spletstoeser and Jirsa (1985) from Hatherton Sandstone in the Britannia Range, with the jointing developed within ~1 m of the dolerite contact. No preferred growth orientation for the quartz overgrowths was noted, indicating that the crystallization does not appear to have occurred under stress.

In the ensuing period of tectonism and epeirogenic uplift, jointing was accentuated as later uplift and erosional unloading became important processes. In the course of joint development due to uplift and unloading, compression on the grains was substantially relieved in a direction perpendicular to the structure by the formation of sheeting joints aligned close to the regional trend. Consequently, it appears that the development of the sheeting joints in



Figure 7.12. Sheet jointing in Beacon supergroup Sandstone, Mt. Dido, Olympus Range.

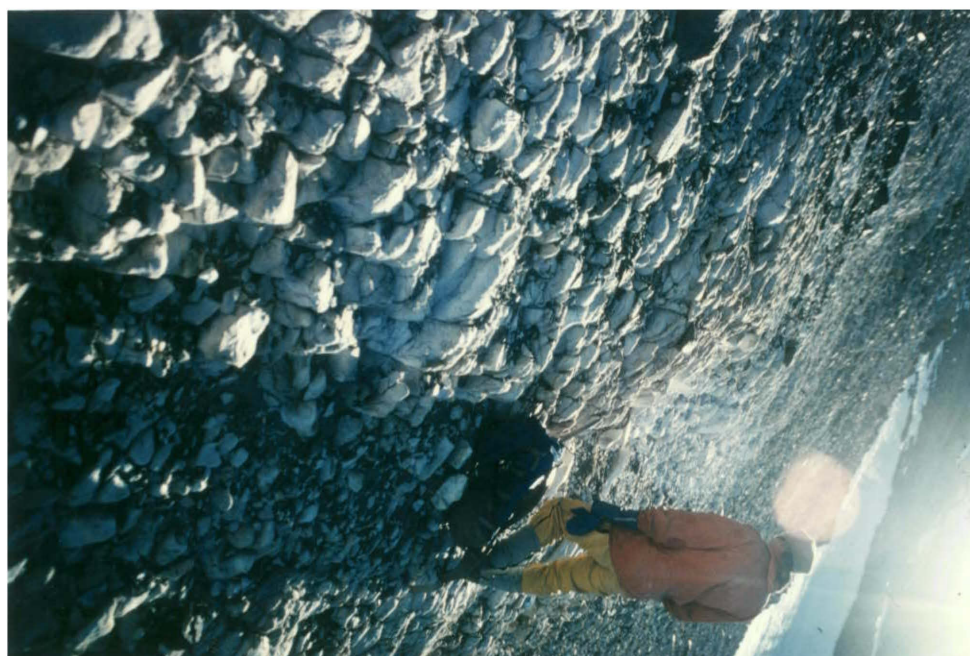


Figure 7.13. Columnar jointing in Altar Mountain Sandstone, Jeremy Sykes Glacier, Asgard Range.

the indurated Beacon Heights Orthoquartzite and Altar Mountain Sandstone is largely a consequence of rock failure consequent upon the release of residual strains in the rock. However, the current gravitational unloading under a thick cap of high density Ferrar Dolerite is a major stress input that must be considered when evaluating the stability of the appropriate sandstone slopes.

#### 7.5.4. Summary and Conclusions

The landscape of the McMurdo Dry valleys preserves remnant features of Miocene and Pliocene glacial erosion, although the details of the present morphology are dominated by subaerial erosion and stress-relief induced erosion effects. Release of residual and overburden-induced stresses is indicated by the pervasiveness of sheeting joints in both the igneous and sedimentary rocks. Further input to the *in situ* rock stress field may result from the input of overburden-induced stresses imparted by a dolerite cap, that may act with the residual locked-in stresses to further weaken the rock and so enhance slope rock failure and erosion. Significant differences in rock strength were found between the Arena Sandstone and overlying Beacon Heights Orthoquartzite but it is the RMS properties of the slope rock that control the slope form. RMS with respect to subaerial processes controls the final form of the trough slopes and future directions of erosion of the remanent erosional features. Thus, these landforms no longer owe their detailed morphology to the glacial processes, even though the main ice-free troughs are clearly of glacial origin.

## Chapter Eight

### Synthesis

### 8.1. Introduction

The morphology and morphogenesis of tectonically active regions adjacent to the Main Divide of the Southern Alps have been examined. The glacierized terrains are characterized by steep, frequently unstable slopes that rapidly equilibrate to the changed stress conditions upon the retreat of the buttressing valley glacier. Subsequent slope modification and the final form of the valley, is largely controlled by the RMS properties of the slope rock. The RMS of slopes in tectonically active areas is further influenced by the stress-induced joint development in the rock mass. This theme has been investigated and enlarged into a model of the development and modification of glacial valley cross-profiles.

### 8.2. Valley Initiation and Development

The initiation of rapid uplift and glaciation of the Southern Alps commenced about 2.5 Myr BP (H. Wellman, 1979, J. Adams, 1979). This is evident from the first appearance of schist in conglomerates west of the Alpine Fault, indicating that the schist of the Southern Alps was exposed and eroded for the first time. The growing ridges were deeply incised by fluvial processes that have since been enhanced and modified by repeated glacial action. Glacial exploitation of structural weaknesses such as faults, foliation planes and rock joints, is suggested by the regularity of the glacial valley drainage pattern. This trend is strengthened by the close correspondence between the orientations of the dominant vertical fracture sets and trends of the main glacial valleys in the vicinity of the Main Divide.

Once the valley pattern became established, the dominant drainage trends were maintained and enlarged by the glaciers, as the latter were constrained by the position of the ridges. The catchments contributed ice to the glaciers in proportion to their size except in the case of ice-caps, where asymmetry could develop depending on insolation and wind-drift effects (Linton, 1957). The strong correlation between fiord trough size and glacier contributing area to each outlet trough, indicates that fiord size had adjusted to the volume of ice discharged through them.

The best fit regression equations developed for the relationship between the size of the fiords and their glacier contributing areas, were applied to the inland lakes cut into schist and greywacke/argillite on the eastern side of the Main Divide. Lakes such as Wanaka, Tekapo and Pukaki are all over-widened with respect to the volume of ice discharged through them. To a first approximation it was argued that the densely jointed and strongly foliated schists and greywackes have suffered glacial erosion by trough widening rather than deepening.

The rock intact strength properties bear little relationship to the form and size of alpine-type outlet glacier troughs. Outlet trough size was largely controlled by the activity of the glaciers, i.e., the volume of ice discharged through them, while the trough cross-section form was largely a result of the RMS properties of the slope rock and mode of post-glacial destabilization. The structural properties of the bedrock are the dominant influence on final trough slope form in highly foliated and tectonically fractured rock.

A modified RMS method was developed, incorporating weightings and those elements considered to be important with respect to glacial erosion. The modified RMS values display a strong inverse correlation with various measures of trough shape, i.e., the more densely jointed and weaker the rock mass with respect to subglacial erosion processes, the broader and flatter the valley developed.

### 8.3. Interaction of RMS and Stress Field on Valley Development

The finite element models developed for typical valley profiles in Fiordland, Mt Cook and South Westland, support and enhance the RMS-form model for the development of the glacial troughs. It is first assumed that the rock mass before glaciation stood at an angle below that of limiting stability, and that only with the advent of glacial undercutting did these rock masses develop a steeper angle. When these assumptions are made, and the nature of the rock slope failure and glacial removal of the slope debris are considered, models of development of the glacial valley cross-profile can be developed (Fig. 8.1).



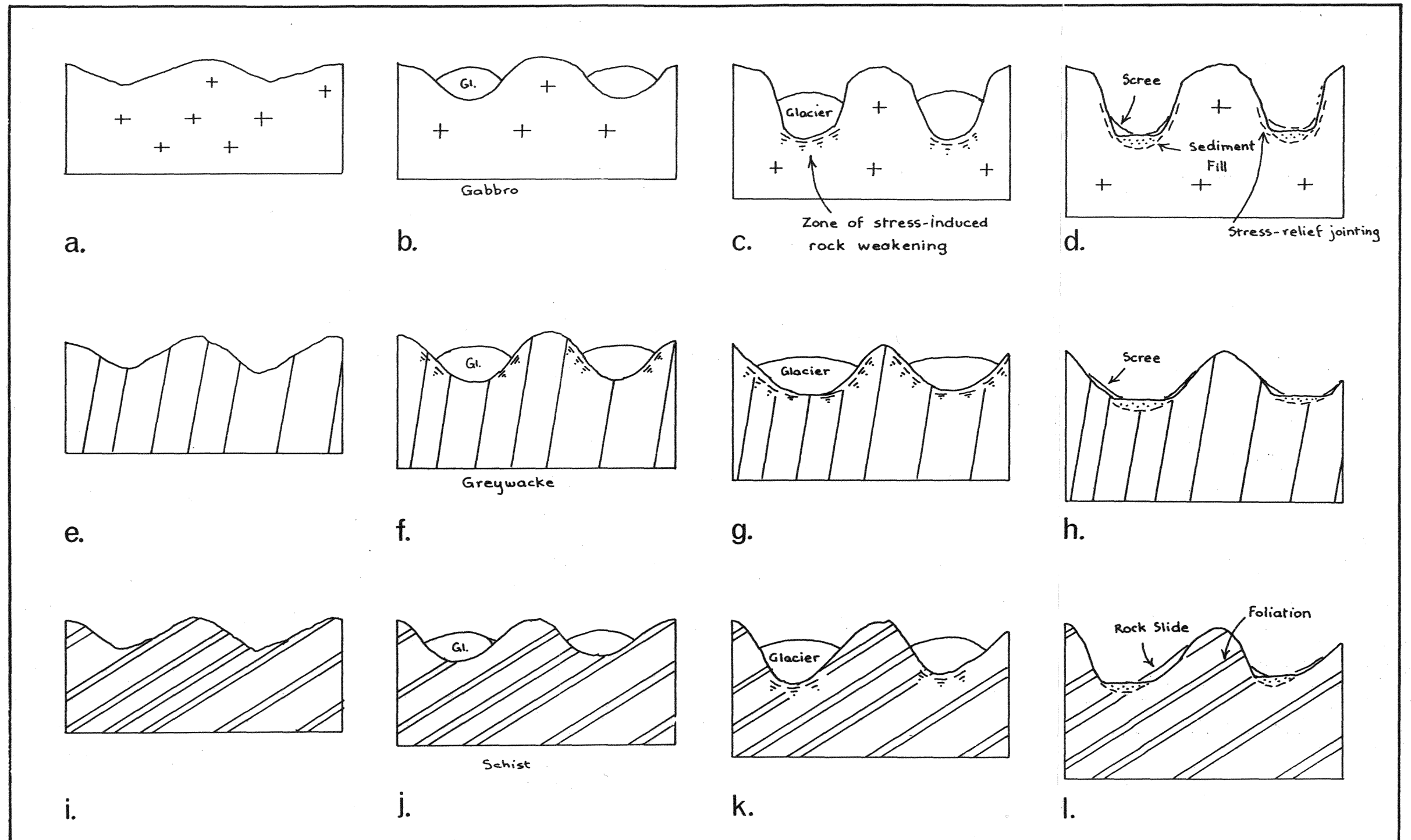


Figure 8.1. Models of the development of glacial valley shape, Southern Alps, New Zealand. a-d. Northern Fiordland plutonic rocks. Note preferential glacier deepening associated with stress-induced failure of valley bottom rock. e-h. Mt. Cook greywacke/argillite. Note progressive widening of the trough associated with stress-induced rock slope rock failure and low RMS to slope processes. i-l. South Westland schist basement. Note foliation control on asymmetric valley development.



Figures 8.1a-d are simple models of the development and modification of a glacial valley in Northern Fiordland. Initial planation of the crystalline basement was followed by uplift and development of an early Pleistocene fluvial drainage system. With continued epeirogenic uplift of the Fiordland block, small cirque and valley glaciers eventually coalesced to produce ice-caps with large radiating outlet glaciers. An equilibrium glacial system was established adjusted to the glacier activity, and the stress and RMS properties of the host rock mass. The stress-field developed in the trough rock would result in the tensile failure of the slope and trough bottom rock by a combination of self-weight, tectonic and thermally-induced stresses. The process of stress-induced weakening of the massive rock will allow excavation and removal of the weakened rock at the trough base, so that the end product of glacial excavation is relatively deep, narrow troughs. The high RMS of the bedrock allows the maintenance of steep slopes, despite tensile sheeting, that will be minimally modified following recession of the buttressing valley glacier. Subsequent glacier readvances will not be provided with weakened slope rock so that deepening, rather than widening will proceed.

Figures 8.1e-h are simplified sketches of the development of the Tasman Valley. Crustal shortening and uplift of the schist and Torlesse rocks of the Mt. Cook region initiated a fluvial drainage system. Following inception and development of cirque and small valley glaciers, the pre-existing fluvial drainage system was enhanced by glacial erosion. Glacial recession caused gravitationally (horizontal spreading of the slope rock due to removal of the lateral support of the glacier) and tectonically-induced destabilization of the trough slopes, enhanced failure and slope recession. These displacements may have commenced when the valley was still occupied by a glacier, given the large disparity between the unit weights of the ice and rock (Lewis, 1954). In unbuttressed densely jointed rock, subsequent to glacier recession, the joint sets favourable for failure opened up. This provided weakened zones along the rock slope profile that were exploited by major glacier readvances. The debris from the slope failure further enhanced erosion through the contribution of excess debris tools for abrasion, as well as controlling the site of erosion through the provision of weakened bedrock.

Figures 8.1i-1 are simplified sketches of a glacial valley developed in highly anisotropic, foliated schist. Pre-existing lines of weakness, i.e., fault/shear zones, allowed the development of rectilinear fluvial drainage patterns in the schist, that were further exploited and enhanced by the imposition of a glacial system on the landscape. Foliation controls the RMS and stability of the trough slopes resulting in the development of valley asymmetry.

An attempt has been made to quantify and explain variations in the RMS and its influence on glacial erosion and subsequent slope modification. The magnitude of the effects of glacial erosion on the landscape is directly controlled by the size and physical properties of the glacier (Roberts and Rood, 1984; Harbor *et al.*, 1988). However, this is an over-simplification and ignores the rock mass strength properties of the eroded bedrock. It is apparent that the form of the glacial troughs developed in the vicinity of the Main Divide of the Southern Alps is a direct consequence of the RMS properties of the slope rock, and *in situ* stress-field (Augustinus, 1987; Selby *et al.*, 1988).

#### 8.4. Implications of Uplift, Erosion and Rock Strength for the Development of the Southern Alps Landscape

##### 8.4.1. Introduction

The landscape changes eastward across the central Southern Alps from intensely dissected, to strongly glaciated, to more subdued landscapes. The average age of the landforms increases eastwards, reflecting changes in erosion rates, lithology and relief (Fig. 8.2). These are controlled by variation in precipitation and uplift rates, which, in turn, reflect the nature of the plate boundary in the central South Island and the interaction with the mountains produced by plate convergence.

Several attempts have been made to relate the landforms to the rate of erosion and uplift (J.Adams, 1985; Whitehouse, 1987). However, quantitative estimates of erosion rates are limited, and the magnitude and frequency of individual erosion processes vary both spatially and temporally. Nevertheless, a broad balance between uplift and erosion appears to be maintained (J.Adams, 1980; Whitehouse, 1987)(Fig. 8.2), suggesting that the landforms are in a state of equilibrium despite

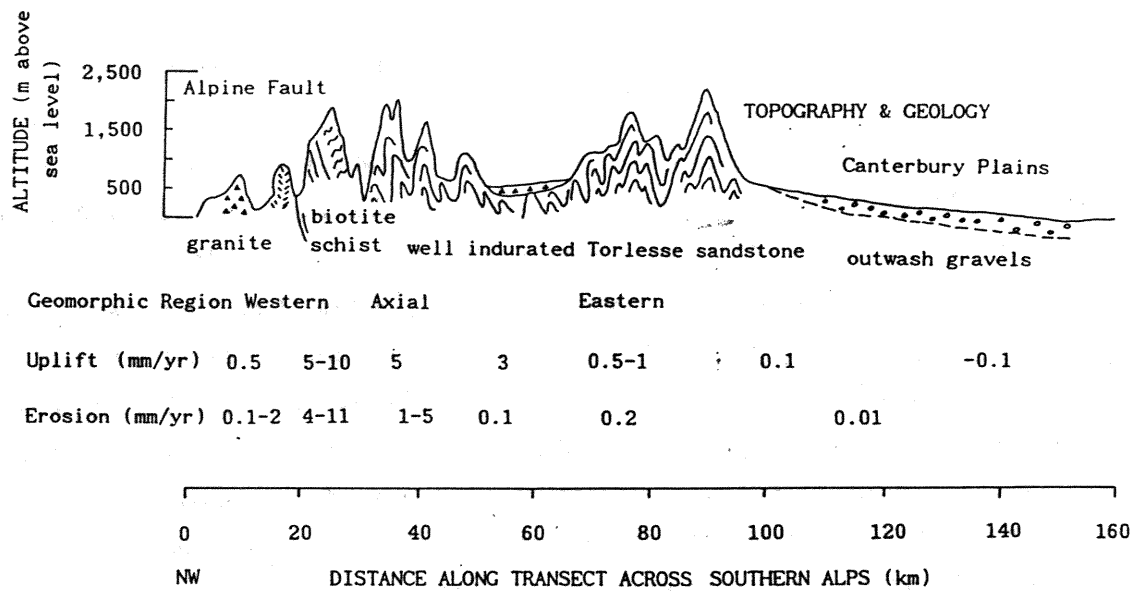


Figure 8.2. Cross-section through the Southern Alps showing uplift and erosion rate variations across the Main Divide. After Whitehouse (1987).

minor perturbations created by glacial/interglacial erosion cycles. Griffiths (1981) argued that present glaciers are eroding at rates little different to that in adjacent non-glaciated catchments, suggesting that fluvial erosion is the predominant erosion process. However, at the peak of the Last Glaciation, the glaciers in the central Southern Alps were considerably larger than the present sluggish, retreating ice-masses. Evidence for fluvial erosion dominating valley development on the western side of the Main Divide comes largely from the observation (i.e., Whitehouse, 1987) that Pleistocene glacial landforms and deposits are poorly preserved.

The relative proportion of debris transported as bedload and suspended load is critical for the denudation analysis. Abrasion transforms the bed load into suspended load and the latter increases with distance of transport. Adams (1980) noted that there was a lack of reliable sediment load measurements for South Island rivers, and formulated models that rely on several critical assumptions to derive his sediment load and erosion rate estimates. Griffith (1981) calculated actual suspended sediment loads from many of the same rivers studied by J.Adams (1980) and obtained significantly different results. Adams' estimates were long term, as against the short term estimates of Griffith (1981), so that any agreement may be purely fortuitous. Despite the problems, the derived denudation rates allow an investigation of the erosional development of the valleys in the vicinity of the Main Divide.

#### 8.4.2. Fiordland Region

In northern Fiordland, the estimated denudation rates of 0.07 mm/yr for the Cleddau river, and 0.2 mm/yr from the rate of sediment infilling of Milford and Nancy Sounds (J.Adams, 1980) are significantly lower than the uplift rates of ~2-2.2 mm/yr (Williams, 1985; Hull and Berryman, 1986). This suggests that uplift of the Fiordland Block exceeds the denudation rate by an order of magnitude. Adams (1980) argued that uplift and erosion were about balanced in Fiordland, but this model was based on inadequate data. Assuming a constant erosion rate of ~0.2 mm/yr since the initiation of subaerial erosion ~2 Myrs BP. (Ward, 1988a), only ~200 m of downcutting would have occurred. However, this is belied by the extreme relief developed in northern Fiordland, where the largest outlet troughs have been eroded ~1900 m below the level of the summit-level envelope (planation surface).

An obvious explanation for this apparent anomaly is that glacial erosion during glacial maxima has been far more effective than fluvial processes, the former exploiting weakened rock at the slope base and thalweg. This scenario is enhanced by the modelled stress-induced failure of the rock towards the base of the trough cross-profile. The current low erosion rates reflect the stability of the valley slopes and minimal infilling of the coastal fiords. Thus, the mountains of northern Fiordland will continue to grow at a faster rate than their relief until the inception of large active glaciers renews rapid trough downcutting. Glacial erosion will increase the relief, until the RMS of the slope rock has been exceeded and failure and slope modification occurs.

#### 8.4.3. Mt Aspiring-South Westland Region

For the Mt Aspiring region immediately north of Fiordland, Griffiths (1981) estimated a denudation rate of 5.3 mm/yr from specific sediment yield for the Haast River. This result is at variance with the long term rate derived by J.Adams (1980) of 0.4 mm/yr from gravel infilling of onshore sediment traps, although the latter is certainly a minimum estimate due to underestimation of the suspended load. Kamp *et al.* (submitted) used fission track ages of partially annealed zircons and apatites in schist to estimate 14-25 km of erosion for the past 5.4 Myrs, giving overall erosion rates of 2.6-4.6 mm/yr since the inception of rapid uplift. However, on the eastern side of the Main Divide, Griffiths (1981) calculated denudation rates of 0.4 and 0.1 for the Shotover and Arrow River catchments respectively. Closer to the Main Divide, J.Adams (1980) calculated higher rates of 0.8-1.2 mm yr for lakes Wanaka and Wakatipu catchments from the thickness of the lake sediment fill. Estimated uplift rates on the western side of the Divide of ~5 mm/yr were derived from the displacement of uplifted marine terraces (Cooper and Bishop, 1979; Bull and Cooper, 1986).

At the gross scale, erosion seems to be broadly balanced by uplift. However, the Haast River erosion estimate of Griffiths (1981) probably does not reflect the long term post-glacial denudation rate of the Mt Aspiring region. The Haast River catchment largely drains the eastern side of the Main Divide, breaching the Divide to flow towards the west coast. The major tributaries source in the central Alps (Fig. 2.10) where uplift and erosion rates are significantly

higher. The lower denudation rates estimated from Lakes Wanaka and Wakatipu by J.Adams (1980) may in a large part reflect differential uplift and lower erosion rates on the eastern side of the Moonlight Fault.

Assuming the denudation rates derived from the over-filled fiords on the west coast and volume of lake sediment east of the Divide (J.Adams, 1980) are realistic minimum estimates of long term postglacial erosion rates, then uplift has outstripped erosion since deglaciation in Mt Aspiring region. A balance can only be maintained by enhanced erosion during glacial maxima. Thus, the morphogenesis of the Mt Aspiring area is largely a product of glacial rather than fluvial erosion. This model is supported by deep-sea sediment cores from SE of the Otago coast of New Zealand (Griggs *et al.*, 1983). Glacial maxima outlet glaciers and pro-glacial rivers transported much greater volumes of sediment to offshore area than was transported during the interglacial episodes. The lower interglacial sedimentation rate was in response to higher sea-levels as glaciers retreated and deposited much of their loads in newly formed glacial lakes and on the plains. Details of the relative importance of erosion during glacial/interglacial cycles will necessitate the coring and appraisal of offshore sediment traps.

#### 8.4.4. Central Southern Alps - Westland to Mt Cook Regions

For the central Southern Alps, from the Waiho to Cropp River, high denudation rates of 4-11 mm/yr have been estimated for the western side of the Main Divide (J.Adams, 1980; Griffiths, 1981; Griffiths and McSaveney, 1983; Whitehouse, 1987)(Fig. 8.2). These rates compare with uplift rates of 10-20 mm/yr (H.Wellman, 1979), 11 mm/yr (Griffiths and McSaveney, 1983), and 7.8 mm/yr (Bull and Cooper, 1986), suggesting that the uplift rates are broadly balanced by denudation.

The rapid erosion of the schist on the western side of the Main Divide is enhanced by glacial undercutting of the slopes, oversteepening and consequent increase in material addition to the valley base. Headward erosion of 15 km/Myr is required just for the rivers to maintain a constant length. Rapid removal of the schist is further enhanced by freeze-thaw and hydration-induced physical weathering. These processes help explain the extremely rapid removal of the schist basement on the western side of the Main Divide. Close stream spacing coupled with rapid glacial and fluvial erosion enables

rapid removal of the schist interfluves, which are continually rejuvenated by uplift. Continual rapid uplift and removal of the breakdown products of the schist, resulted in the development and maintenance of a young mountain landscape.

However, on the eastern side of the Main Divide, the uplift rate is significantly lower and roughly balanced by the denudation rate of ~1-5 mm/yr (Whitehouse, 1987). However, the greywacke mountains are significantly higher than the schist mountains on the eastern side of the Divide. The Torlesse rocks are highly abrasion resistant, yet their relatively low mass strength (a result of closely spaced jointing) suggests that denudation should be rapid. The height of the greywacke mountains is a reflection of the spacing of the major valleys (Ahnert, 1984) and relative erosivity of the denudation processes. Greater valley spacing in the Torlesse greywacke mountains, despite the lower RMS, allows the development of higher mountains than the rapidly denuded interfluves in the schist.

East of the Main Divide, currently active erosion processes largely rework glacial debris and slope debris so that the low measured erosion rates are a reflection of the sluggish, low erosivity of the present valley glaciers. At the peak of the Last Glaciation, large, active glaciers occupied all the major troughs in the vicinity of the Main Divide, so that erosion of trough bottom and trough wall rock was considerably enhanced. The rate of glacial and subaerially-induced slope retreat was broadly balanced by uplift so that the overwidened nature of the greywacke mountains is maintained without the complete removal of the interfluves.

#### 8.4.5. Antarctica

Whilst uplift and erosion of the Southern Alps is rapid, a contrasting mode of landscape development exists in Antarctica. The coastal uplands of East Antarctica and Lambert Glacier region of the Prince Charles Mountains are undergoing slow isostatic rather than tectonic uplift (P.Wellman, 1983, 1988). Using high peaks as an estimate of erosion, P.Wellman (1983) estimated 0.3-0.6 km of erosion for the past 30 Myrs, giving an overall glacial denudation rate of ~10-20 m/Myrs. Similarly, in the Lambert Glacier region, glacial denudation varies from 1.3-2.0 km, to give a denudation rate of ~50 m/Myrs since the initiation of glaciation (P.Wellman, 1988).

The Transantarctic Mountains (TAM) have a contrasting tectonic origin to the East Antarctic highlands. Fitzgerald *et al.*, (1986) proposed that TAM uplift is by a combination of asymmetric extension of the lithosphere followed by crustal underplating. Gleadow and Fitzgerald (1987) employed zircon fission track ages to infer that TAM uplift commenced ~50 Myrs BP to give a total uplift of ~4.8-5.3 km. Compensating for isostatic effects, gives a total tectonic uplift since the Jurassic of 1.4 km, and a denudation rate for the past 50 Myrs of ~68-78 m/Myrs (P.Wellman, 1988).

Clearly the denudation rates of 10-80 m/Myrs estimated for the Antarctic highlands are two to three orders of magnitude lower than the mean denudation rate for the tectonically active Southern Alps (5 km/Myrs, H.Wellman, 1979). The rapid denudation of the Southern Alps is by a combination of fluvial and glacial processes, with gravitationally and tectonically-induced destabilization and failure of the trough wall rock a major element in the overall denudation process. The size of the valleys draining the Main Divide appears to be adjusted to the volume of ice discharged through them during glacial maxima. This pattern is repeated for the major outlet glaciers and ice streams draining the East Antarctic Ice Sheet, indicating the importance of glacial erosion in development of the present landscape. However, the similarities end there, for the Antarctic outlet troughs have probably been almost exclusively ice-filled since the development of the East Antarctic Ice Sheet in late Oligocene (25-30 Myrs ago)(Barrett *et al.*, 1987; Barron *et al.*, 1988), so that subaerial and fluvial processes have had minimal, if any, impact on the outlet trough slope and cross-profile development.

Since the uplift of the Antarctic highlands is largely isostatic in origin, with a tectonic component of uplift only in the TAM, trough slope oversteepening and tectonically-induced rock slope weakening has not occurred, so that the low denudation rates are purely a reflection of slow glacial erosion by the occupying ice streams. This is despite the fact that subaerial and glacial denudation has proceeded in the TAM since the early Cainozoic rifting of the Ross Sea. This difference emphasizes the importance of tectonic and gravitationally-induced processes on denudation rates in alpine areas. P.Wellman (1988) similarly concluded that the difference between plate margin and interior denudation rates is similar to the contrast between other geological processes such as horizontal crustal strain and the frequency of earthquakes.



## 8.5. Conclusions

The erosional morphology, in the vicinity of the Main Divide of the Southern Alps and Fiordland, appears to be a product of the interaction between Alpine Fault-induced tectonic processes, rock mass strength of the uplifted and eroded bedrock, and the processes acting to denude the developing mountain landscape. The magnitude of the effects of glacial erosion on the landscape is directly controlled by the size and physical properties of the glacier, whilst the form of the trough is a direct consequence of the RMS properties of the slope rock and the *in situ* stress-field. The site of rock failure, and hence the existence of weakened erodible rock, may selectively control the site of maximum subglacial erosion. Consequently, the shape of an enlarged glacial trough depends not only on the properties of the glacier and idealized rock intact strength, but on the RMS properties of the host rock mass and stress-induced controls on the site of rock mass failure. This study has implications for the development and modification of alpine glacial troughs in similar tectonic settings elsewhere, and is a further example of the control of the mass strength properties of the bedrock on the development of hard rockslopes and erosional landforms.

## References Cited

- Abdullatif, D.M. and Cruden, B.M.; 1983, The relationship between rock mass quality and ease of excavation.  
Bulletin International Association Engineering Geology, 28, p.183-187.
- Abrahams, A.D. and Parsons, A.J.; 1987, Identification of strength equilibrium rock slopes: further statistical considerations.  
Earth Surface Processes and Landforms, 12, p.631-635.
- Adams, C.J.; Age and origin of the Southern Alps.  
In: Origin of the Southern Alps, Walcott, R.I and Cresswell, M.M. (Eds.), Royal Society of New Zealand Bulletin 18, p. 73-78.
- Adams, C.J.; 1981, Uplift rates and thermal structure in the Alpine Fault zone and Alpine Schists, Southern Alps, New Zealand.  
Geological Society of London Special Publication, 9, p.211-222.
- Adams, J.; 1979, Vertical drag on the Alpine Fault.  
In: Origin of the Southern Alps, Walcott, R.I and Cresswell, M. (Eds.), Royal Society of New Zealand Bulletin 18, p.47-54.
- Adams, J.; 1980, Contemporary uplift and erosion of the Southern Alps, New Zealand.  
Bulletin Geological Society of America, 91, Part 2, p.1-114.
- Adams, J.; 1981, Earth-quake dammed lakes in New Zealand.  
Geology, 9, p.215-219.
- Adams, J.; 1985, Large scale geomorphology of the Southern Alps, N.Z.  
In: Tectonic Geomorphology, Morisawa, M. and Hack, J.T., (Eds.), Allen and Unwin, London, p.105-128.
- Addison, K.; 1981, The contribution of discontinuous rock mass failure to glacial erosion.  
Annals of Glaciology, 2, p.3-10.
- Ahnert, F.; 1984, Local relief and the height of mountain ranges.  
American Journal of Science, 284, p.1035-1055.
- Ai, N.S; and Scheidegger, A.E.; 1981, Valley trends in Tibet.  
Zeitschrift für Geomorphologie, 25 (2), p.203-212.
- Allen, A.D. and Gibson, G.W.; 1962, Geological investigations in South Victoria land, Antarctica. Part VI: Outline of the geology of the Victoria Valley Region.  
New Zealand Journal of Geology & Geophysics, 5, p.234-242.
- Allis, R.G.; 1981, Continental underthrusting beneath the Southern Alps.  
Geology, 9, p.303-7.
- Allis, R.G.; 1986, Mode of crustal shortening adjacent to the Alpine Fault, New Zealand.  
Tectonics, 5(1), p.15-32.
- Amadei, B. and Savage, W.Z.; 1985, Gravitational stresses in regularly jointed rock masses - A keynote lecture.  
In: Fundamentals of rock joints, Stephansson, O. (Ed.), Centek, Sweden, p.463-474.
- Amadei, B., Savage, W.Z. and Swolfs, H.S.; 1987, Gravitational stresses in anisotropic rock masses.  
Int. J. Rock Mech. Min. Sci. & Geomech. Abstr., 24, p.5-14.

- Andrews, J.T.; 1972, Glacier power, mass balances, velocities and erosion potential.  
Zeitschrift für Geomorphologie Supplementband, 13, p.1-17.
- Andrews, J.T.; 1975, Glacial Systems.  
Duxbury Press, North Scituate, Mass.
- Andrews, J.T. and Le Masurier, W.E.; 1973, Rates of Quaternary glacial erosion and corrie formation, Marie Byrd Land, Antarctica.  
Geology, 3, p.75-80.
- Aniya, M. and Welch, R.; 1981a, Morphological analyses of glacial valleys, and estimation of sediment thicknesses on valley floors, Victoria Valley system, Antarctica.  
Japanese Antarctic Bulletin, 71, p.77-95.
- Aniya, M. and Welch, R.; 1981b, Morphometric analyses of some Antarctic cirques.  
Geografiska Annaler, 63 A (1-2), p.41-53.
- Augustinus, P.C.; 1987, Tectonics, stresses and glacial erosion: an appraisal.  
In: Programme with Abstracts, 12th INQUA Congress, Ottawa, p.123.
- Bakker, J.P. and Le Heux, J.W.N.; 1952, A remarkable new geomorphological law.  
Koninklijke Nederlandsche Akademie van Wetenschappen, B55, p.339-410.
- Bandis, S., Lumsden, A.C., and Barton, N.; 1981, Experimental studies of scale effects on the shear behaviour of rock joints.  
Int. J. Rock Mech. Mining Sci. & Geomech. Abstr., 18, p. 1-21.
- Barrett, P.J., Elston, D.P., Harwood, D.M., McKelvey, B.C. and Webb, P.N.; 1987, Mid-Cenozoic record of glaciation and sea-level change on the margin of the Victoria Land basin, Antarctica.  
Geology, 15, p.634-637.
- Barron, J. *et al.* (Leg 119 Shipboard Scientific Party);  
1988, Early Glaciation of Antarctica.  
Nature, 333, p.303-304.
- Barton, C.; 1982, Variables in fracture energy and toughness testing of rock.  
In: Proceedings 23rd U.S. Rock Mechanics Symposium, Berkeley, p.449-462.
- Barton, N.; 1971, Progressive failure of excavated rock slopes.  
In: 13th U.S. Rock Mechanics Symposium, University of Illinois, p.130-137.
- Barton, N. and Choubey, V.; 1977, The shear strength of rock joints in theory and practice.  
Rock Mechanics, 10, p.1-54.
- Batley, M.H.; 1960, Geological factors in the development of Veslgjuv-botn and Vesl-Skautbotn.  
In: Investigations of Norwegian cirque glaciers, Lewis, W.V. (Ed.), Royal Geographical Society Research Series 4, p. 5-10.
- Beck, A.C.; 1968, Gravity faulting as a method of topographic adjustment.  
New Zealand Journal of Geology and Geophysics, 11, p. 111-119.

- Beckedahl, H.R.; 1987, Rock mass strength determinations as an aid to landscape interpretation.  
In: International Geomorphology 1986, Part 1. Gardiner.V (Ed.), Wiley, London, p. 393-405.
- Bell, D.H.; 1976, Slope evolution and slope stability, Kawarau Valley, Central Otago, New Zealand.  
Bulletin International Association of Engineering Geology, 14, p.5-16.
- Bell, D.H.; 1982, Geomorphic evolution of a valley system: the Kawarau Valley, Central Otago.  
In: Landforms of New Zealand, Soons, J.M. and Selby, M.J. (Eds.), Longman Paul, Auckland, p.317-342.
- Benson, W.N., Bartrum, J.A. and King, L.C.; 1934, The geology of the region about Preservation and Chalky Inlets, southern Fiordland, New Zealand, Part 2.  
Transactions Royal Society of New Zealand, 64, p.51-87.
- Bentley, C.R.; 1983, Crustal structure of Antarctica from geophysical evidence-a review.  
In: Antarctic Earth Science, Oliver, R.L., James, P.R. and Jago, J.B. (Eds.), Australian Academy of Science, Canberra.
- Bentley, C.R.; 1987, Antarctic ice streams: a review.  
Journal of Geophysical Research, 92 (B9), p.8843-8858.
- Betchel, 1967, Report on construction geology of the West Arm Powerhouse and associated works.  
Ministry of Works and Development Report No.14-R-4545 (Unpubl.)
- Bevan, T.G. and Hancock, P.L.; 1986, A late Cenozoic regional mesofracture system in southern England and northern France.  
Journal of the Geological Society, London, 143, p.355-362.
- Bieniawski, Z.T.; 1974, Geomechanics classification of rock masses for the design of tunnel support.  
Proceedings 3rd ISRM Congress, Vol.2, Balkema, Rotterdam, p.27-32.
- Bieniawski, Z.T.; 1975, Point load test in engineering practice.  
Engineering Geology, 9 (1), p.1-11.
- Bieniawski, Z.T.; 1979, The geomechanics classification in rock engineering applications.  
In: Proceedings 4th I.S.R.M. Congress, Montreux, Vol. 2, Balkema Rotterdam, p. 41-47.
- Birot, P.; 1968, Les developpements recents des theories de l'erosion glaciaire.  
Annales de Géographie, 419, p. 1-14.
- Bishop, D.G. and Hislop, W.F.; 1983, Things that go bang in the night.  
Landscape, 13, p.2-5.
- Bishop, D.G.; 1985, Inferred uplift rates from raised marine surfaces Southern Fiordland, New Zealand.  
New Zealand Journal of Geology and Geophysics, 28, p. 243-51.
- Bjerrum, L., and Jorstad, F.A.; 1968, The stability of rock slopes in Norway.  
Norwegian Geotechnical Institute Publication 79, 11pp.

- Blair, 1972, Influence of variations in lithology and structure in Torlesse Supergroup upon erosion processes in Blackley Stream catchment, Torlesse Range.  
Unpublished M.Sc Thesis, University of Canterbury, New Zealand.
- Blattner, P.; 1978, Geology of the crystalline basement between Milford Sound and Hollyford Valley, New Zealand.  
New Zealand Journal of Geology and Geophysics, 21, p.33-47.
- Boulton, G.S.; 1974, Processes and patterns of glacial erosion.  
In: Glacial Geomorphology, Coates, D.R. (Ed.), Binghampton, New York, p. 41-87.
- Boulton, G.S.; 1979, Processes of glacial erosion on different substrata.  
Journal of Glaciology, 23 (89), p.15-38.
- Boulton, G.S and Jones, A.S.; 1979, Stability of temperate ice caps and ice sheets resting on beds of deformable sediment.  
Journal of Glaciology, 24 (90), p.29-44.
- Boulton, G.S., Morris, E.M., Armstrong, A.A. and Thomas, A.; 1979, Direct measurement of stress at the base of a glacier.  
Journal of Glaciology, 22 (86), p.3-24.
- Bovis, M.J.; 1982, Uphill-facing scarps in the Coast Mountains, British Columbia.  
Bulletin Geological Society of America, 93, p.804-812.
- Bradshaw, J.Y.; 1985, Geology of the Northern Franklin Mountains.  
Unpublished PhD Thesis, Otago University, New Zealand.
- Broch, E.; 1974, The influence of water on some rock properties.  
In: Proceedings 3rd ISRM Congress, Montreal, Vol.2, Balkema, Rotterdam, p.33-38.
- Broch, E.; Changes in rock strength caused by water.  
In: Proceedings 4th ISRM Congress, Montreux, Vol.2, Balkema, Rotterdam, p.71-75.
- Broch, E. and Franklin, J.A.; 1972, Point load strength test.  
Int. J. Rock Mech. Min. Sci. & Geomech. Abstr., 9, p.669-697.
- Broch, E. and Nilsen, B.; 1979, Comparison of calculated, measured and observed stress at the Ortfjell open pit, Norway.  
Norwegian Soil & Rock Engineering Association, Publication No.1.
- Broch, E., and Sorheim, S.; 1984, Experiences from the planning, construction and supporting of a road tunnel subjected to heavy rock bursting.  
Rock Mechanics and Rock Engineering, 17, p.15-35.
- Brown, E.T. (Ed.); 1981, Rock characterization, testing and monitoring Pergamon, Oxford.
- Brown, I.R., Goodman, R.E. and Hittinger, M.; 1980, Finite element study of Nevis Bluff rock-slope failure.  
Rock Mechanics, 12, p. 231-45.
- Bruce, I. and Cruden, D.; 1977, The dynamics of the Hope Slide.  
Bulletin International Association of Engineering Geology, 16, p.94-98.

- Bruun, A.F., Brodie, J.W., and Fleming, C.A.; 1955, Submarine geology of Milford Sound, New Zealand.  
New Zealand Journal of Science and Technology, 36, p. 397-410.
- Brunner, F.K., and Scheidegger, A.E.; 1973, Exfoliation.  
Rock Mechanics, 5, p.43-62.
- Bull, W.B.; 1975, Allometric change of landforms.  
Bulletin Geological Society of America, 86, p.1489-1498.
- Bull, W.B. and Cooper, A.F.; 1986, Uplifted marine terraces along the Alpine Fault, New Zealand.  
Science, 234, p.1225-1228.
- Bull, W.B. and Cooper, A.F.; 1988, Response to comment by C.M. Ward on "Uplifted marine terraces along the Alpine Fault".  
Science, 240, p.804-805.
- Caine, N.; 1982, Toppling failures from alpine cliffs on Ben Lomond, Tasmania.  
Earth Surface Processes and Landforms, 7, p.133-152.
- Carol, H.; 1947, The formation of roches moutonnées.  
Journal of Glaciology, 1 (1), p.57-59.
- Cave, M.P.; 1982, Stratigraphy and structure of Torlesse rocks, Arthur's Pass National Park.  
Unpublished PhD thesis, Geology Dept. University of Auckland.
- Chinn, T.J. and Whitehouse, I.E.; 1978, Glacier snowline variations in Southern Alps, New Zealand.  
In: World Glacier Inventory, IAHS-AISH Publ. No.126, p. 219-228.
- Church, M. and Mark, D.M.; 1980, On size and scale in geomorphology.  
Progress in Physical Geography, 4, p.342-390.
- Colback, P.S.B. and Wiik, B.L.; 1965, Influence of moisture content on the compressive strength of rocks.  
In: Proceedings 3rd Canadian Rock Mechanics Symposium, Toronto, p.65-83.
- Cooks, J.; 1981, Rock quality measured by seismic wave velocity as a factor in landform development.  
South African Journal of Science, 77, p.517-521.
- Cooks, J.; 1983, Geomorphic response to rock strength and elasticity.  
Zeitschrift für Geomorphologie, 27, p.483-493.
- Cooper, A.F. and Bishop, D.G.; 1979, Uplift rates and high level marine platforms associated with the Alpine Fault at Okuru River, South Westland.  
In: The Origin of the Southern Alps, Walcott, R.I. and Cresswell, M.M. (eds.), Royal Society of New Zealand Bulletin 18, p. 35-43.
- Crabtree, R.D. and Doake, C.S.M.; 1982, Pine Island Glacier and its drainage basin: results from radio-echo sounding.  
Annals of Glaciology, 3, p.65-70.
- Craw, D.; 1984, Lithologic variations in Otago Schist, Mt. Aspiring area, NW Otago, New Zealand.  
New Zealand Journal of Geology & Geophysics, 27, p. 151-166.

- Craw, D.; 1985, Structure of the schist in the Mt Aspiring region, northwestern Otago, New Zealand.  
New Zealand Journal of Geology & Geophysics, 28, p.55-76.
- Craw, D., Rattenbury, M.S. and Johnstone, R.D.; 1987, Structural geology and vein mineralisation in the Callery River headwaters, Southern Alps, New Zealand.  
New Zealand Journal of Geology & Geophysics, 30, p.273-286.
- Cruden, D.M.; 1976, The influence of discontinuities on the stability of rock slopes.  
In: Mass Wasting, Proceedings 4th Guelph Geomorphology Symposium. Yatsu, E., Ward, A.J. and Adams, F. (Eds.), Geo Abstracts, Norwich, p.57-68.
- D'Andrea, D.V., Fisher, R.L. and Fogelson, D.E.; 1964, Prediction of compressive strength from other rock properties.  
Colorado School of Mines Quarterly, 59(4B), p.623-640.
- Davey, F.J., and Smith, E.G.C.; 1983, Tectonic setting of the Fiordland region, south-west New Zealand.  
Geophysics Journal of Royal Astronomical Society, 72, p. 23-38.
- Day, M.J.; 1980, Rock hardness: field assessment and geomorphic importance.  
Professional Geographer, 32, p.72-81.
- Decker, E.R., and Bucher, G.J.; 1982, Geothermal studies in the Ross Island, Dry Valleys region.  
In: Antarctic Geoscience, Craddock, C. (ed.), University of Wisconsin Press, Madison, p.887-894.
- Deere, D.U. and Miller, R.P.; 1966, Engineering classification and index properties for intact rock.  
Technical Report No. AFNL-TR-65-116, Air Force Weapons Laboratory, New Mexico.
- Denton, G.H., Prentice, M.L., Kellogg, D.E. and Kellogg, T.B.; 1984, Late Tertiary history of the Antarctic Ice-Sheet: Evidence from the Dry- Valleys.  
Geology, 12, p. 263-267.
- Desai, C.S. and Abel, J.F.; 1972, Introduction to the finite element method.  
Van Nostrand Reinhold, New York.
- Doornkamp, J.C. and King, C.A.M.; 1971, Numerical Analysis in Geomorphology.  
Arnold, London.
- Drewry, D.H.; 1972, Radio-echo sounding in Antarctica.  
In: Polar Geomorphology, Institute of British Geographers Special Publication No. 4, p. 43-57.
- Drewry, D.H.; 1982, Ice flow, bedrock, and geothermal studies from radio-echo sounding inland of McMurdo Sound, Antarctica.  
In: Antarctic Geoscience, Craddock, C. (ed.). University of Wisconsin Press, Madison, p.977-983.
- Drewry, D.H.; 1983, Antarctic ice sheet: aspects of current configuration and flow.  
In: Mega-Geomorphology, Gardner, R. and Scoging, H. (eds.), Clarendon, Oxford, p.18-38.



- Drewry, D.H. and Robin, G. de Q.; 1983, Form and flow of the Antarctic ice sheet during the last million years.  
In: The climatic record in polar ice sheets, Robin, G. de Q. (ed.), Cambridge University Press, p.28-38.
- Drewry, D.H.; 1986. Glacial Geologic Processes.  
Edward Arnold, London.
- Eiby, G.A.; 1968, A descriptive catalogue of New Zealand earthquakes, Part 1-Shocks felt before the end of 1845.  
New Zealand Journal of Geology & Geophysics, 11, p.16-40.
- Embleton, C. and King, C.A.M.; 1975, Glacial Geomorphology.  
Edward Arnold, London.
- Embleton, C. and Whalley, B.; 1979, Energy, forces, resistances and responses.  
In: Process in Geomorphology, Embleton, C. and Thorne, J. (Eds.), Edward Arnold, London, p.11-38.
- Emerson, J.W.; 1985, A simple topographic method for determining structural trends.  
Journal of Geological Education, 33, p.215-216.
- Enerver, J and Woollorton, B.; 1984, Stress measurements at the Clyde Damsite, New Zealand.  
CSIRO Division of Geomechanics, site investigation report No.15.
- Engelder, T. and Geiser, P.; 1980, On the use of regional joint sets as trajectories of paleostress fields during the development of the Appalachian Plateau.  
Journal of Geophysical Research, 85 (B11), p.6319-6341.
- Engelder, T.; 1982a, Is there a genetic relationship between selected regional joints and contemporary stress within the lithosphere of North America?  
Tectonics, 1, p.161-178.
- Engelder, T.; 1982b, Reply to comment by A.E. Scheidegger on "Is there a genetic relationship between selected region joints and contemporary stress within the lithosphere of North America?".  
Tectonics, 1 (5), p.465-470.
- England, J.; 1986, Glacial erosion of a high Arctic valley.  
Journal of Glaciology, 32 (110), p.60-64.
- Fahey, B.D.; 1983, Frost action and hydration as rock weathering mechanisms on schist: a laboratory study.  
Earth Surface Processes and Landforms, 8, p.535-546.
- Fergusson, H.F. and Hamel, J.V.; 1981, Valley stress in flat lying sedimentary rocks.  
In: Proceedings International Symposium on Weak Rock, Vol. 3, p.1235-1240.
- Ficker, E., Sonntag, G. and Weber, E.; 1980, Ansätze zur mechanischen Deutung der Rissentstehung bei Parabelrissen und Sichelbrüchen auf glazialgeformten felsoberflächen.  
Zeitschrift für Gletscherkunde Und Glazialgeologie, 16, p.25-43.
- Field, B.; 1975, Geology of the Central Liebig Range.  
Unpublished M.Sc Thesis, Auckland University, New Zealand.

- Findlay, R.M.; 1979, Summary of structural geology of Haast Schist terrain, central Southern Alps, New Zealand: implications of structure for uplift and deformation within the Southern Alps. In: Origin of the Southern Alps, Walcott, R.I. and Cresswell, M.M. (eds.), Royal Society of New Zealand Bulletin, 18, p.113-120.
- Findlay, R.M.; 1987, Structure and interpretation of the Alpine schists in Copland and Cook River Valleys, South Island, New Zealand.  
New Zealand Journal of Geology and Geophysics, 29, p. 117-138.
- Findlay, R.M. and Spörli, K.B.; 1984, Structural geology of the Mt. Cook Range and Main Divide, Hooker Valley region, New Zealand.  
New Zealand Journal of Geology and Geophysics, 27, p. 257-276.
- Findlay, R.M., Skinner, D.N.B. and Craw, D.; 1984, Lithostratigraphy and structure of the Koettlitz Group, McMurdo Sound, Antarctica.  
New Zealand Journal of Geology and Geophysics, 27, p. 513-536.
- Fitzgerald, P.G., Sandiford, M., Barrett, P.J. and Gleadow, A.J.W.; 1986, Asymmetric extension associated with uplift and subsidence in the Transantarctic Mountains and Ross Embayment.  
Earth and Planetary Science Letters, 81, p.67-78.
- Fitzharris, B.B.; 1967, Some aspects of the Late Quaternary geomorphology of the Mid-Waiau and Monowai valleys, South Island, New Zealand.  
In: Proceedings 5th New Zealand Geography Conference, Auckland, p.181-187.
- Fitzharris, B.B. and Owens, I.F.; 1980, Avalanche atlas of the Milford Road and an assessment of the hazard to traffic.  
New Zealand Mountain Safety Council. Avalanche Committee Report No.4.
- Fitzharris, B.B., Campbell, P.I., Smith, G.M., Blucher, P.R. and Ho, C.W.; 1984, Avalanche atlas of the Ball Hut Road, & assessment of hazard to traffic.  
N.Z. Mountain Safety Council, Avalanche Rept.6, Dept. of Internal Affairs, Wellington.
- Fitzharris, B.B. and Owens, I.F., 1984, Avalanche tarns.  
Journal of Glaciology, 30 (106), p. 308-312.
- Franklin, J.A.; 1985, Suggested method for determining point load strength.  
Int. J. Rock Mech. Min. Sci. & Geomech. Abstr., 22, p.51-60.
- Friedman, M. and Logan J.M.; 1970, Influence of residual elastic strain on the orientation of experimental fractures in three quartzose sandstones.  
Journal of Geophysical Research, 75 (2), p. 387-405.
- Fujii, Y., 1981, Aerophotographic interpretation of surface features and an estimation of ice discharge at the outlet of the Shiraze drainage basin, Antarctica.  
Japanese Antarctic Record, 78 (33), p.1-15.
- Fyffe, H.E.; 1954, The Homer Tunnel - jointing and stability.  
Unpublished New Zealand Geological Survey Report to Ministry of Works and Development, NZGS file D40/924.
- Gage, M.; 1966, Franz-Josef Glacier,  
Ice, 20, p. 26-27.

- Gardner, J.S.; 1980, Frequency, magnitude and spatial distribution of mountain rockfalls and rockslides in the Highwood Pass area, Alberta, Canada.  
In: Thresholds in Geomorphology, Coates, D.R. and Vitek, J.D. (Eds.), Allen and Unwin, p.267-295.
- Gerber, E.; 1980, Geomorphological problems in the Alps.  
Rock Mechanics Supplement, 9, p.93-107.
- Gerber, E. and Scheidegger, A.E.; 1969, Stress-induced weathering of rock masses.  
Ecologiae Geologicae Helveticae, 62 (2), p. 401-415.
- Gerber, E. and Scheidegger, A.E.; 1973, Erosional and stress-induced features on steep slopes.  
Zeitschrift für Geomorphologie Supplementband., 18, p. 38-49.
- Gerber, E. and Scheidegger, A.E.; 1975, Geomorphological evidence for the geophysical stress-field in mountain massifs.  
Rivista Italiana Di Geofisica, 2 (1), p. 47-52.
- Gibson, G.M.; 1982, Stratigraphy and petrography of some metasediments and associated metamorphic rocks from central Fiordland, New Zealand.  
New Zealand Journal of Geology & Geophysics, 25, p.21-43.
- Gibson, G.M., McDougall, I. and Ireland, T.R.; 1988, Age constraints on metamorphism and the development of a metamorphic core complex in Fiordland, southern New Zealand.  
Geology, 16, p.405-408.
- Girard, W.; 1976, Size, shape and symmetry of the cross-profiles of glacial valleys.  
Unpublished PhD. Thesis, University of Iowa.
- Gleadow, A.J.W., and Fitzgerald, P.G.; 1987, Uplift history and structure of the Trans Antarctic Mountains: new evidence from fission track dating of basement apatites.  
Earth and Planetary Science Letters, 82, p.1-14.
- Goodman, R.E.; 1977, Analysis in jointed rocks.  
In: Finite elements in geomechanics, Gudehus, G. (Ed.), Wiley, London. p.351-375.
- Gordon, J.E.; 1981, Ice scoured topography and its relationship to bedrock structure and ice movement in parts of Northern Scotland and Western Greenland.  
Geografiska Annaler, 63 A (1-2), p. 55-65.
- Gough, D.I. and Gough, W.I.; 1987, Stress near the surface of the earth.  
Annual Reviews Earth & Planetary Science, 15, p. 545-566.
- Graf, W.L.; 1970, Geomorphology of the glacial valley cross-section.  
Arctic and Alpine Research, 2, p. 303-312.
- Graf, W.L.; 1976, Cirques as glacier locations.  
Arctic and Alpine Research, 8, p.79-90.
- Griffiths, G.A.; 1981, Some suspended sediment yields from South Island catchments, New Zealand.  
Water Resources Bulletin, 18(4), p.662-671.

- Griffiths, G.A. and McSaveney, M.J.; 1983, Hydrology of a basin with extreme rainfalls - Cropp River, New Zealand.  
New Zealand Journal of Science, 26, p.293-306.
- Griggs, G.B., Carter, L., Kennett, J.P. and Carter, R.V.; 1983, Late Quaternary marine stratigraphy southeast of New Zealand.  
Bulletin of Geological Society of America, 94, p.791-797.
- Gunn, B.M.; 1960, Structural features of the Alpine schists of Franz Josef-Fox Glacier region.  
New Zealand Journal of Geology and Geophysics, 3, p. 287-308.
- Gunn, B.M. and Warren, G.; 1962, Geology of Victoria Land between the Mawson and Mulock Glaciers, Antarctica.  
New Zealand Geological Survey Bulletin no. 71.
- Gunsallus, K.L. and Kulhawy, F.H.; 1984, A comparative evaluation of rock strength measures.  
Int. J. Rock Mech. Min. Sci. & Geomech. Abstr., 21, p.233-248.
- Hack, J.T.; 1957, Studies of longitudinal stream profiles in Virginia and Maryland.  
U.S. Geological Survey Professional Paper 294B.
- Hagen, J.O., Wold, B., Leistol, O., Ostrem, G. and Sollid, J.L.; 1983, Subglacial processes at Bondhusbreen, Norway: preliminary results  
Annals of Glaciology, 4, p. 91-98.
- Haines, A.J., Calhaem, I.M. and Ware, D.E.; 1979, Crustal seismicity near Lake Pukaki, South Island.  
In: Origin of the Southern Alps, Walcott, R.I. and Cresswell, M.M. (Eds.), Royal Society of New Zealand Bulletin 18, p.87-94.
- Hall, K.; 1986, Rock moisture content in the field and the laboratory and its relationship to mechanical weathering studies.  
Earth Surface Processes and Landforms, 11, p.131-142.
- Hall, K., 1987, The physical properties of quartz-mica schist and their application to freeze-thaw weathering studies in the maritime Antarctic.  
Earth Surface Processes and Landforms, 12, p. 137-149.
- Hallett, B.; 1979, A theoretical model of glacial abrasion.  
Journal of Glaciology, 23 (89), p. 39-50.
- Hallett, B.; 1981, Glacial abrasion and sliding: their dependence on the debris concentration in basal ice.  
Annals of Glaciology, 2, p. 23-28.
- Halliday, G.S. and Beetham, R.D.; 1985, Kawarau River power investigations.  
New Zealand Geological Survey Report EG 386.
- Hancock, P.L.; 1985, Brittle microtectonics: principles and practice.  
Journal of Structural Geology, 7, p.437-457.
- Hancox, G.T., Beanland, S., and Brown, I.R.; 1985, Seismotectonic hazard evaluation for the Kawarau Power development.  
New Zealand Geological Survey Report EG 384.
- Harbor, J.M., Hallett, B. and Raymond, C.F.; 1988, A numerical model of landform development by glacial erosion.  
Nature, 333, p.347-349.

- Harland, W.B., 1957, Exfoliation joints and ice action.  
Journal of Glaciology, 3, p. 8-10.
- Haxby, W.F. and Turcotte, D.L.; 1976, Stresses induced by the addition and removal of overburden and associated thermal effects.  
Geology, 5, p. 181-184.
- Haynes, V.M., 1972, The relationship between the drainage areas and sizes of outlet troughs of Sukkertoppen Ice-cap, West Greenland.  
Geografiska Annaler, 54 A (2), p. 66-75.
- Haynes, V.M.; 1977, The modification of valley patterns by ice-sheet activity.  
Geografiska Annaler, 59 A (3-4), p.195-207.
- Hobbs, B.E., Means, W.D. and Williams, P.F.; An outline of structural geology.  
Wiley, New York.
- Hoek, E.; 1983, Strength of jointed rock masses.  
Géotechnique, 33, p.187-223.
- Holm, D.K., Norris, R.J. and Craw, D.; 1987, Brittle-ductile transition displayed by schists uplifted to the Alpine Fault, Franz Josef, Westland.  
In: Geological Society of New Zealand Dunedin Conference Programme and Abstracts, Geological Society of New Zealand Miscellaneous Publication 37A.
- Holst, T.B.; 1982, Regional jointing in the northern Michigan Basin.  
Geology, 10, p.273-277.
- Hull, A.G. and Berryman, K.R.; 1986, Holocene tectonism in the region of the Alpine Fault at Lake McKerrow, Fiordland, N.Z.  
Royal Society of New Zealand Bulletin, 24, p. 315-331.
- Illies, J.H. and Hoffers, B.; 1981, Stress patterns and strain release in the Alpine Foreland.  
Tectonophysics, 71, p.157-172.
- Jaeger, J.C. and Cook, N.G.W.; 1979, Fundamentals of rock mechanics.  
3rd Edition, Chapman and Hall, London.
- Jahns, R.M.; 1943, Sheet structures in granites: its origins and use as a measure of glacial erosion in New England.  
Journal of Geology, 12, p.71-98.
- Jahn, A.; 1964, Slopes morphological features resulting from gravitation.  
Zeitschrift für Geomorphologie Supplement Band, 5, p.59-72.
- Jamison, D.B. and Cook, N.G.W.; 1979, An analysis of the measured values for the state of stress in the earth's crust.  
Unpublished paper quoted in Jaeger and Cook (1979).
- Kamp, P.J.J. and Fitzgerald, P.G.; 1987, Geologic constraints on the Cenozoic Antarctic-Australia-Pacific relative plate motion.  
Geology, 15, p.694-697.
- Kamp, P.J.J., Green, P.F. and White, S.H.; Southern Alps Orogen, New Zealand: Uplift age and structure of a continental collision zone derived from fission track geochronology.  
Submitted to Tectonics.

- Kanasewich, E.R.; 1963, Gravity measurements on the Athabasca Glacier.  
Journal of Glaciology, 4, p.617-631.
- Kansky, K.J.; 1963, Structure of transport networks: relationships between network geometry and regional characteristics.  
University of Chicago, Dept. of Geography, Research Paper, 84.
- Kazi, A. and Al-Mansour, Z.R.; 1980, Empirical relationship between Los Angeles abrasion and Schmidt hammer strength tests with application to aggregates around Jeddah.  
Quarterly Journal of Engineering Geology London, 13, p.45-52.
- King, M.S.; 1983, Static and dynamic elastic properties of rocks from the Canadian Shield.  
Int. J. Rock Mech. Mining Sci. & Geomech. Abstr., 20 (5), p.237-241.
- Kohlbeck, F. and Scheidegger, A.E.; 1977, On the theory of the evaluation of joint orientation measurements.  
Rock Mechanics, 9, p.9-15.
- Kohlbeck, F., Scheidegger, A.E. and Sturgul, J.R.; 1979, Geomechanical model of an alpine valley.  
Rock Mechanics, 13, p.1-14.
- Koons, P.O.; 1987, Some thermal and mechanical consequences of rapid uplift: an example from the Southern Alps, New Zealand.  
Earth and Planetary Science Letters, 86, 307-319.
- Lee, F.T., Miller, D.R. and Nichols, T. Jr.; 1979, The relation of stresses in granite and gneiss near Mt. Waldo, Maine, to structure, topography and rock bursts.  
In: Proceedings 20th U.S. Rock Mechanics Symposium, Austin, Texas, p.663-674.
- Lewis, W.V.; 1954, Pressure release and glacial erosion.  
Journal of Glaciology, 2 (16), p.417-422.
- Linton, D.L.; 1957, Radiating valleys in glaciated lands.  
Tijdschrift van Heft Koninklijk Nederlansch, LXXIV (3), p.297-312.
- Luckman, B.H.; 1976, Rockfalls and Rockfall Inventory Data, some observations from Surprise Valley, Jasper National Park, Canada.  
Earth Surface Processes, 1, 287-298.
- Luckman, B.H.; 1981, Geomorphology of the Alberta Rocky Mountains: A review and commentary.  
Zeitschrift fur Geomorphologie Supplementband, 37, p.91-119.
- MacFarlane, D.; 1983, Geologic comment on widening and maintenance proposals, Homer Tunnel.  
Unpublished New Zealand Geological Survey EG Immediate Report 83/043.
- McGarr, A., Spottiswoode, S.M. and Gay, N.C.; 1975, Relationship of mine tremors to induced stresses and rock properties in the focal region.  
Bulletin Seismological Society of America, 65 (4), p.981-993.
- McIntyre, N.F., 1985a, The dynamics of ice-sheet outlets.  
Journal of Glaciology, 31 (108), p.99-107.
- McIntyre, N.F., 1985b, A re-assessment of the mass balance of the Lambert Glacier drainage basin, Antarctica.  
Journal of Glaciology, 31 (107), p.34-38.

- McKellar, I.C.; 1973, Geology of the Te Anau-Manapouri District 1:50,000. New Zealand Geological Survey Miscellaneous Series, Map 4. Dept. of Scientific and Industrial Research, Wellington.
- McKellar, I.C.; 1982. Fiordland.  
In: Landforms of New Zealand, Soons, J.M. and Selby, M.J. (Eds.), Longman Paul, Auckland.
- McKelvey, B.C. and Webb, P.N.; 1962, Geological investigations in Southern Victoria Land, Antarctica: Part. 3 - geology of Wright Valley.  
New Zealand Journal of Geology & Geophysics, 5, p.143-162.
- McKelvey, B.C., Webb, P.N. and Kohn, B.P.; 1977, Stratigraphy of the Taylor and Lower Victoria Groups (Beacon Supergroup) between Mackay Glacier and Boomerang Range, Antarctica.  
New Zealand Journal of Geology & Geophysics, 20 (5), p.813-863.
- McTigue, D.F. and Mei, C.C.; 1981, Gravity induced stresses near the topography of a small slope.  
Journal of Geophysical Research, 86 (B10), p.9268-9278.
- Malin, M.C.; 1984, Abrasion rate observations in Victoria Land, Antarctica.  
Antarctic Journal of the U.S., 18 (6), p.14-16.
- Mahr, T.; 1977, Deep-reaching gravitational deformations of high mountain slopes.  
Bulletin International Association of Engineering Geology, 16, p.121-127.
- Matheson, D.S. and Thompson, S.; 1973, Geological implications of valley rebound.  
Canadian Journal of Earth Sciences, 10, p.961-978.
- Mathews, W.H.; 1967, Profiles of late Pleistocene glaciers in New Zealand.  
New Zealand Journal of Geology & Geophysics, 10, p.146-163.
- Matsuoka, N.; 1985, Rock control on the distribution of linear depressions on the Main Divide of the Akaishi Range, Southern Japanese Alps.  
Geographical Review of Japan, Series A (7), p.411-427.
- Mattinson, J.M., Kimbrough, D.L. and Bradshaw, J.K.; 1986, Western Fiordland orthogneiss: Early Cretaceous arc magmatism and granulite facies metamorphism, New Zealand.  
Contributions to Mineralogy and Petrology, 92, p.383-392.
- Meier, S., Portrait of an Antarctic outlet glacier.  
Journal of Hydrological Science, 28 (3), 403-416.
- Metcalf, R.C.; 1979, Energy dissipation during subglacial abrasion at Nisqually Glacier, Washington, USA.  
Journal of Glaciology, 23 (89), p.233-246.
- Michalopoulos, A.P. and Triandafilidis, G.E.; 1976, Influence of water on hardness, strength and compressibility of rock.  
Bulletin Association of Engineering Geologists, 13, p.1-22.
- Mills, K.W. and Gray, W.J.; 1985, Kawarau River power investigations in situ stress measurements and laboratory testing.  
Ministry of Works and Development Central laboratories Report 2-85/3.

- Mollard, J.D.; 1977, Regional landslide types in Canada.  
In: Reviews in Engineering Geology, Vol.3., Geological Society of America Special Publication, p.29-58.
- Moon, B.P. and Selby, M.J.; 1983, Rock mass strength and scarp forms in Southern Africa.  
Geografiska Annaler, 65 A (1-2), p.135-145.
- Moon, B.P.; 1984, Refinement of a technique for determining rock mass strength for geomorphological purposes.  
Earth Surface Processes and Landforms, 9, p.189-193.
- Moon, B.P.; 1986, Controls on the form and development of rock slopes in fold terrane.  
In: Hillslope Processes, Abrahams, A.D. (Ed.), Allen and Unwin, Boston, p.227-243.
- Morgan, V.I., Jacka, T.H., Akerman, G.J. and Clarke, A.L.; 1982, Outlet glacier and mass-balance studies in Enderby, Kemp and Mac. Robertson Lands, Antarctica.  
Annals of Glaciology, 3, p.204-210.
- Morland, L.W. and Boulton, G.S.; 1975, Stress in an elastic hump: the effect of glacier flow over elastic bedrock.  
Proceedings Royal Society London Series A, 344 (1637), p.157-173.
- Morland, L.W. and Morris, E.M.; 1977, Stress in an elastic bedrock hump due to glacier flow.  
Journal of Glaciology, 18 (78), p.67-75.
- Myrnang, A.M. and Grimstad, E.; 1984, Coping with the problem of rock bursts in hard rock tunnelling.  
Tunnels and Tunnelling, 14, p.13-15.
- Nicholas, R.M. and Dixon, J.C.; 1986, Sandstone scarp form and retreat in the Land of Standing Rocks, Canyonlands National Park, Utah.  
Zeitschrift für Geomorphologie, 30 (2), p.167-187.
- Nichols, T.C.; 1980, Rebound, its nature and effect.  
Quarterly Journal of Engineering Geology, 13, p.133-150.
- Nilsen, T.H.; 1973, The relation of joint patterns to the formation of fiords in Western Norway.  
Norsk Geologisk Tidsskrift, 53, p.183-194.
- Norris, R.J.; A geometrical study of finite strain and bending in the South Island.  
In: The Origin of the Southern Alps, Walcott, R.I. and Cresswell, M.M. (eds.), Royal Society of New Zealand Bulletin 18, p.21-28.
- Norris, R.J., Carter, R.M. and Turnbull, I.M.; 1978, Cainozoic sedimentation in basins adjacent to a major continental transform boundary in southern New Zealand.  
Journal of Geological Society of London, 135, p.191-205.
- Norris, R.J. and Carter, R.M.; 1980, Offshore sedimentary basins at the southern end of the Alpine Fault, New Zealand.  
In: Sedimentation at Oblique-slip Mobile Zones, Ballance, P.F. and Cresswell, M. (Eds.), Special Publication International Association of Sedimentologists, 4, p.237-265.



- Norris R.J. and Carter, R.M.; 1982, Fault-bounded blocks and their role in localising sedimentation and deformation adjacent to the Alpine Fault, southern New Zealand.  
Tectonophysics, 87, p.11-23.
- Norris, R.J. and Cooper, A.F.; 1986, Small-scale fractures, glaciated surfaces and recent strain adjacent to the Alpine Fault, New Zealand.  
Geology, 14, p.687-690.
- Nur, A.; 1982, The origin of tensile fracture lineaments.  
Journal of Structural Geology, 4 (1), p.31-40.
- Nye, J.F.; 1965, Flow of a glacier in a channel of rectangular, elliptic, or parabolic cross-section.  
Journal of Glaciology, 5, p.661-690.
- Oerlemans, J.; 1984, Numerical experiments in large scale glacial erosion.  
Zeitschrift für Gletscherkunde Und Glazialgeologie, 20, p.107-126.
- Oliver, G.J.H. and Coggon, J.H.; 1979, Crustal structure of Fiordland New Zealand.  
Tectonophysics, 54, p.253-292.
- Oliver, P.J.; 1983, Seismotectonic, structural, volcanologic, and geomorphic study of New Zealand.  
In: Landsat II over New Zealand: monitoring our resources from space, Ellis P.J., Thomas, I.L. and McDonnell, M.J. (Eds.), New Zealand Department of Scientific and Industrial Research Bulletin 221, p.298-332.
- Olyphant, G.A.; 1981a, Allometry and cirque evolution.  
Geological Society of America, 92, p.679-685.
- Olyphant, G.A.; 1981b, Interaction among controls on cirque development: Sangre De Cristo Mountains, Colorado, U.S.A.  
Journal of Glaciology, 27 (97), p.449-458.
- Olyphant, G.A.; 1983, Analysis of the factors controlling cliff burial by talus within Blanca Massif, southern Colorado, U.S.A.  
Arctic and Alpine Research, 15, p.65-75.
- Penck, A.; 1905, Glacial features in the surface of the Alps.  
Journal of Geology, 13, p.1-17.
- Perrin, N.D.; 1984, Manapouri Power Project rock mechanics instrumentation results 1966-1984.  
Unpublished New Zealand Geological Survey EG. Immediate Report 84/045.
- Pickrill, R.A. and Irwin, J.; 1983, Sedimentation in a deep glacier fed lake, Lake Tekapo, New Zealand.  
Sedimentology, 30, p.63-75.
- Pearce, A.J. and O'Loughlin, C.L.; 1985, Landsliding during an M7.7 earthquake: influence of geology and topography.  
Geology, 13, p.855-858.
- Pearce, A.J. and Watson, A.J.; 1986, Effects of earthquake-induced landslides on sediment budget and transport over a 50-yr period.  
Geology, 14, p.52-55.

- Porter, S.C.; 1975, Equilibrium-line altitudes of late Quaternary glaciers in the Southern Alps, New Zealand.  
Quaternary Research, 5, p.27-47.
- Prebble, W.M.; 1987, Rock slope movements in limestone and shales, NE Marlborough, New Zealand.  
Unpublished PhD thesis, University of Auckland, New Zealand.
- Price, N.J.; 1966, Fault and joint development in brittle and semi-brittle rock.  
Pergamon, Oxford.
- Price, N.J.; 1975, Rheology of crustal rocks.  
In: Geodynamics today: a review of earth's dynamic processes, Royal Society, London, p.150-163.
- Protod'yakonov, M.M.; 1969, Methods of determining the shear strength of rocks.  
In: Mechanical Properties of Rocks (Israel Program for Scientific Translations), p.15-27.
- Rabia, H. and Brook, N.; The Shore hardness of rock.  
Int. J. of Rock Mech. Mining Sci. & Geomech. Abstr., 16, p.335-6.
- Radbruch-Hall, D.H., Varnes, D.J. and Savage, W.; 1976, Gravitational spreading of steep-sided ridges in western U.S.A.  
Bulletin International Association of Engineering Geology, 14, p.23-35.
- Rastas, J. and Seppala, M.; 1981, Rock jointing and abrasion forms on roches moutonnées in SW Finland.  
Annals of Glaciology, 2, p.159-163.
- Read, S.A.L., Perrin, N.D. and Brown, I.R.; 1987, Measurement and analysis of laboratory strength and deformability characteristics of schistose rocks.  
Paper given at 6th I.S.R.M. Conference, Montreal.
- Reynaud, L.; 1973, Flow of a glacier with a solid friction law.  
Journal of Glaciology, 12 (65), p.251-258.
- Reyners, M., Ingham, C.E. and Ferris, B.G.; 1983, Micro-seismicity of the Upper Clutha Valley, South Island, New Zealand.  
New Zealand Journal of Geology & Geophysics, 26, p.1-6.
- Riek, G.A. and Currie, J.B.; 1974, A study of the relationship between rock fabric and joints in sandstone.  
Canadian Journal of Earth Sciences, 11, p.1253-1268.
- Roberts, D.; 1974, A discussion: The relation of joint patterns to the formation of fjords in western Norway.  
Norska Geologiska Tidsskrift, 54, p.213-215.
- Roberts, M.C. and Rood, R.M.; 1984, The role of ice contributing area in the morphology of transverse fiords, British Columbia.  
Geografiska Annaler, 66A (4), p.381-393.
- Robin, G de Q.; 1976, Is the basal ice of a temperate glacier at pressure melting point?  
Journal of Glaciology, 16 (74), p.183-196.
- Robinson, P.H.; 1984, Ice dynamics and thermal regime of Taylor Glacier, South Victoria Land, Antarctica.  
Journal of Glaciology, 30 (105), p.153-160.

- Rose, K.E.; 1979, Characteristics of ice flow in Marie Byrd Land, Antarctica.  
Journal of Glaciology, 24 (90), p.63-75.
- Röthlisberger, H. and Iken, A.; 1981, Plucking as an effect of water pressure variation at the glacier bed.  
Annals of Glaciology, 2, p.51-62.
- Ryder, J.M.; 1981, Geomorphology of the southern part of the Coast Mountains of British Columbia.  
Zeitschrift für Geomorphologie Supplementband., 37, p.120-147.
- Sara, W.A.; 1968, Franz Josef and Fox Glaciers, 1951-1967.  
New Zealand Journal of Geology & Geophysics, 11, p.768-780.
- Savage, W.Z., Swolfs, H.S. and Powers, P.S.; 1985, Gravitational stresses in long symmetric ridges and valleys.  
Int. J. Rock Mech. Min. Sci. & Geomech. Abstr., 22 (5), p.291-30.
- Savage, W.Z. and Smith, W.K.; 1987, A model for the plastic flow of landslides.  
U.S. Geological Survey Professional Paper 1385.
- Savage and Varnes, 1987, Mechanics of gravitational spreading of steep-sided ridges (sackung).  
Bulletin International Association of Engineering Geology, 35, p.31-35.
- Scheidegger, A.E.; 1963, On the tectonic stresses in the vicinity of a valley and a mountain range.  
Proceedings of Royal Society of Victoria, 76, p.141-145.
- Scheidegger, A.E.; 1978, Comparative aspects of the geotectonic stress-field.  
Rock Mechanics Supplement, 6, p.55-64.
- Scheidegger, A.E.; 1979a, Enigma of jointing.  
Rivista Italiana Di Geophysica, 5, p.1-4.
- Scheidegger, A.E.; 1979b, On the tectonics of the Western Himalayas.  
Arch. Meteorol. Geophys. Bioklimatol., A 28, p.89-106.
- Scheidegger, A.E.; 1980, Alpine joints and valleys in the light of the neotectonic stress-field.  
Rock Mechanics Supplement, 9, p.109-124.
- Scheidegger, A.E.; 1982a, Principles of Geodynamics.  
Springer, Berlin, 3rd edition.
- Scheidegger, A.E.; 1982b, Comment on "Is there a genetic relationship between selected regional joints and contemporary stress within the lithosphere of North America?" by T. Engelder.  
Tectonics, 2, p.463.
- Scheidegger, A.E.; 1983, Interpretation of fracture and physiographic patterns in Alberta, Canada.  
Journal of Structural Geology, 5 (1), p.53-59.
- Scheidegger, A.E. and Ai, N.S.; 1986, Tectonic processes and geomorphological design.  
Tectonophysics, 136, p.285-300.

- Scholz, C.H., Rynn, J.M., Weed, R.W. and Frohlich, C.; 1973, Detailed Seismicity of the Alpine Fault zone Fiordland region, New Zealand. Bulletin Geological Society of America, 84, p.3297-3316.
- Schumm, S.A. and Chorley, R.J.; 1966, Talus weathering and scarp recession in the Colorado Plateau. Zeitschrift für Geomorphologie, 10, p.11-35.
- Selby, M.J.; 1971, Slopes and their development in an ice-free, arid area of Antarctica. Geografiska Annaler, 53A, p.235-245.
- Selby, M.J.; 1974, Slope evolution in an Antarctic oasis. New Zealand Geographer, 30, p.18-34.
- Selby, M.J.; 1977, Transverse erosion marks on ventifacts from Antarctica. New Zealand Journal of Geology & Geophysics, 20, p.949-969.
- Selby, M.J.; 1980, A rock mass strength classification for geomorphic purposes. Zeitschrift für Geomorphologie, 24, p.31-51.
- Selby, M.J.; 1982, Controls on the stability and inclinations of hill slopes formed on hard rock. Earth Surface Processes & Landforms, 7, p.449-467.
- Selby, M.J.; 1985, Evidence of Miocene Ice-Sheet overriding of the Trans Antarctic Mountains: an agnostic view. New Zealand Antarctic Record, 6, p.50-51.
- Selby, M.J.; 1987, Rock Slopes. In: Slope Stability, Anderson, M.G. and Richards, K.S. (Eds.), Wiley, London, p.475-504.
- Selby, M.J. and Wilson, A.T.; 1971, Possible Tertiary age for some Antarctic cirques. Nature, 229, p.623-624.
- Selby, M.J., Augustinus, P.C., Moon, V.G. and Stephenson, R.J., 1988, Slopes on strong rock masses: modelling and influences of stress distributions and geochemical properties. In: Modelling Geomorphological Systems, Anderson, M. (Ed.) Wiley, London, p.341-374.
- Seppala, M.; 1975, Influence of rock jointing on the asymmetric form of the Ptarmigan Glacier valley, south-eastern Alaska. Bulletin Geological Society of Finland, 47, p.33-44.
- Shabtaie, S., Whillans, I.M. and Bentley, C.R.; 1987, The morphology of ice streams A, B, and C, West Antarctica, and their environs. Journal of Geophysical Research, 92 (B9), p.8865-8884.
- Simmons, G. and Brace, W.F. 1965, Comparison of static and dynamic measurements of the compressibility of rocks. Journal of Geophysical Research, 70, p.5649-5656.
- Smorodinov, M.I. Motovilov, E.A. and Volkov, V.A.; 1970, Determination of correlation relationships between strength and some physical characteristics of rocks. In: Proceedings 2nd ISRM Congress, Vol.2, p.35-37.

- Sommerville, P., Mark, A.F. and Wilson, J.B.; 1983, Plant succession on moraines of the Upper Dart Valley, southern South Island, N.Z. New Zealand Journal of Botany, 20, p. 227-244.
- Speight, R.; 1935, Notes on the Franz Josef Glacier, February, 1934. Transactions Royal Society of New Zealand, 64, p.315-322.
- Spletstoeser, J.F. and Jursa, M.A.; 1985, Columnar jointed sandstone in the Beacon Supergroup, Britannia Range, Antarctica (Note). New Zealand Journal of Geology & Geophysics, 28, 761-764.
- Spörli, K.B.; 1979, Structure of the South Island Torlesse in relation to the origin of the Southern Alps.  
In: Origin of the Southern Alps, Walcott, R.I. and Cresswell, M.M. (eds.), Royal Society of New Zealand Bulletin, 18, p.99-104.
- Spörli, K.B.; 1987, Airphoto lineaments and fracturing in the axial ranges of the central North Island, New Zealand.  
Journal of the Royal Society of New Zealand, 17, p.139-156.
- Stacey, T.; 1973, The stability of rock slopes in mining and civil engineering situations.  
C.S.I.R. National Mechanical Engineering Research Institute Report ME 1202.
- Stanton, B.R. and Pickard, G.L.; 1981, Physical oceanography of the New Zealand fiords.  
New Zealand Oceanographic Institute Memoir 88.
- Statham, I. and Francis, S.C.; 1986, Influence of scree accumulation and weathering on the development of steep mountain slopes.  
In: Hillslope Processes, Abrahams, A.D. (Ed.), Allen and Unwin, Boston, p.245-268.
- Sturgul, J.R., Scheidegger, A.E. and Grinshpan, Z.; 1976, Finite element model of a mountain massif.  
Geology, 4, p.439-442.
- Sugden, D.E.; 1974, Landscapes of glacial erosion in Greenland and their relationship to ice, topography and bedrock conditions.  
In: Progress in Geomorphology, Brown, E.H. and Watters, K.S. (Eds.), Inst. Brit. Geogr. Spec. Publ. 7, p.177-193.
- Sugden, D.E.; 1978, Glacial erosion by the Laurentide Ice-Sheet.  
Journal of Glaciology, 20 (83), p.367-390.
- Sugden, D.E. and John, B.; 1976, Glacial Systems and Environments. Arnold, London.
- Suggate, R.P.; 1978, The Geology of New Zealand. Government Printer, Wellington. 2 vols.
- Suggate, R.P.; 1982, The geological perspective.  
In: Landforms of New Zealand, Soons, J.M. and Selby, M.J. (Eds.), Longman Paul, Auckland.
- Svensson, H.; 1959, Is the cross-section of a glacial valley a parabola?  
Journal of Glaciology, 3, p.362-363.
- Szlavin, J.; 1974, Relationships between some physical properties of rock determined by laboratory tests.  
Int. J. Rock Mech. Min. Sci. & Geomech. Abstr., 11, p.57-66.

- Terzaghi, K.; 1945, Stress conditions for failure of saturated concrete and rock.  
In: Proceedings American Society For Testing of Materials, 45, p.777-801.
- Turnbull, I.M., Barry, J.M., Carter, R.M. and Norris, R.J.; 1975, The Bobs Cove Beds and their relationship to the Moonlight Fault Zone.  
Journal of Royal Society of New Zealand, 5, p.355-394.
- Turner, M.J., Clough, R.W., Martin, G.C. and Topp, L.J.; 1956, Stiffness and deflection analysis of complex structures.  
Journal of Aeronautical Science, 23, p.805-824.
- Vivian, R. and Bocquet, G.; 1973, Subglacial cavitation phenomena under the glacier d'Argentière.  
Journal of Glaciology, 12 (66), p.439-451.
- Vivian, R.; 1980, The nature of the ice-rock interface: the results of investigation on 20,000 m<sup>2</sup> of the rock bed of temperate glaciers.  
Journal of Glaciology, 25 (92), p.267-277.
- Walcott, R.I.; 1978, Present tectonics and late Cenozoic evolution of New Zealand.  
Geophysics Journal Royal Astronomical Society, 52, p.137-164.
- Walcott, R.I.; 1979, Plate motions and shear strains in the vicinity of the Southern Alps.  
In: Origin of the Southern Alps, Walcott, R.I. and Cresswell, M. (Eds.), Bulletin Royal Society of New Zealand 18, p.5-12.
- Walder, J. and Hallett, B.; 1985, A theoretical model of rock fracture during freezing.  
Bulletin Geological Society of America, 96, p.336-346.
- Ward, C.M.; 1988a, Marine terraces of the Waitutu district and their relation to the late Cenozoic tectonics of the southern Fiordland region, New Zealand.  
Journal of the Royal Society of New Zealand, 18, p.1-28.
- Ward, C.M.; 1988b, New Zealand marine terraces: uplift rates.  
Science, 240, p.803-804.
- Wardle, P.; 1973, Variations of glaciers of Westland National Park and the Hooker Range, New Zealand.  
New Zealand Journal of Botany, 11, p.349-388.
- Warren, G.; 1967, Sheet 17 Hokitika, Geological Map of New Zealand 1:250,000.  
Department of Scientific and Industrial Research, Wellington.
- Waterhouse, J.B.; 1985, Preliminary account of the geology of the Malte Brun Range, New Zealand.  
Australian Geologist, 57, p.7-13.
- Wellman, H.W. and Willett, R.W.; 1942, The geology of the West Coast from Abut Head to Milford Sound: Part I.  
Royal Society of New Zealand Transactions, 71, p.423-457.
- Wellman, H.W.; 1979, An uplift map for the south Island of New Zealand and a model for the uplift of the Southern Alps.  
In: Origin of the Southern Alps, Walcott, R.I. and Cresswell, M.M. (Eds.), Royal Society of New Zealand Bulletin 18, p.13-20.

- Wellman, P.; 1983, Origin and subglacial erosion of part of the coastal highland of East Antarctica.  
Journal of Geology, 91, p.471-480.
- Wellman, P.; 1988, Tectonic and denudational uplift of Australian and Antarctic highlands.  
Zeitschrift für Geomorphologie, 32, p.17-29.
- Whalley, W.B., Douglas, G.R. and Jonsson, A.; 1983, The magnitude and frequency of large rock slides in Iceland during the postglacial.  
Geografiska Annaler, 65 A, 99-109.
- Wheeler, D.A.; 1984, Using parabolas to describe cross-sections of glaciated valleys.  
Earth Surface Processes & Landforms, 9, p.391-394.
- Whitehouse, I.E.; 1983, Distribution of large rock avalanche deposits in the central Southern Alps, New Zealand.  
New Zealand Journal of Geology & Geophysics, 26, p.271-279.
- Whitehouse I.E.; 1987, Geomorphology of a compressional plate boundary, Southern Alps, New Zealand.  
In: International Geomorphology 1986, Part.1, Gardiner, V. (Ed.), Wiley, London, p.897-924.
- Williams, J.G. and Harper, C.T.; 1978, Age and status of the MacKay Intrusives in Eglinton- Upper Hollyford area.  
New Zealand Journal of Geology & Geophysics, 21, 733-742.
- Williams, J.G. and Smith, I.E.M.; 1983, The Hollyford Gabbro-norite-a calcalkaline cumulate.  
New Zealand Journal of Geology & Geophysics, 26, p.345-357.
- Williams, P.W.; 1985, Origin and age of Aurora- Te Ana-Au Cave.  
In: Aurora- Te Ana-Au Cave: a survey and interpretation of scientific resources.  
Williams, P.W. (Ed.), Unpublished Rept. to Fiordland National Park.
- Williams, R.B.G. and Robinson, D.A.; 1983, The effect of surface texture on the determination of the surface hardness of rock using the Schmidt hammer.  
Earth Surface Processes and Landforms, 8, p.289-292.
- Wood, B.L.; 1960, Sheet 27 Fiord. Geological Map of New Zealand 1:250,000. Department of Scientific and Industrial Research, Wellington.
- Wood, B.L.; 1962, Sheet 22 Wakatipu. Geological Map of New Zealand 1:250,000. Department of Scientific and Industrial Research, Wellington.
- Wyrwoll, K.H.; 1977, Causes of rock-slope failure in a cold area: Labrador-Ungava.  
In: Reviews In Engineering Geology, 3, p.59-67, Geological Society of America Special Publication.
- Yatsu, E., 1966, Rock Control in Geomorphology, Sozisha, Tokyo.
- Yeats, R.S.; 1987, Tectonic map of Central Otago based on Landsat imagery.  
New Zealand Journal of Geology and Geophysics, 30, p.261-271.

- Yu, Y.S. and Coates, D.F.; 1970. An analysis of rock slopes using the finite element method.  
Research Report R229, Mines Branch, Department of Energy, Mines & Resources, Ottawa.
- Yu, Y.S. and Coates, D.F.; 1978, Canadian experience in simulating pit slopes by the finite element method.  
In: Landslides and Avalanches, Voight, B. (Ed.), Elsevier, p.709-757.
- Zhi, W., Li, G. and Wang, K.; 1985, Analyses of discing phenomenon and stress-field in the region of an underground powerhouse.  
Rock Mechanics & Rock Engineering, 18, p.1-15.
- Zienkiewicz, O.C.; 1977, The finite element method in engineering science.  
McGraw-Hill, London, 3rd Edition.
- Zienkiewicz, O.C., Valliappan, B.E. and King, I.P.; 1968, Stress analysis of rock as a no tension material.  
Geotechnique, 18, 56-66.
- Zoback, M.L. and Zoback, M.; 1980, State of stress in the conterminous United States.  
Journal of Geophysical Research, 85 (B11), p.6113-6156.
- Zumberge, J.H.; 1955, Glacial erosion in tilted rock layers.  
Journal of Geology, 63 part.2, p.149-158.



## Appendices

## Appendix One

Table A1.1a. Rock mass strength of some rock slopes from the McMurdo Dry Valleys, Antarctica.

Profile no.	1	2	3	4	5	6	7	8	9	10	11	12	13	14	15	16	17	18	19	20
RMS properties																				
Slope inclination	80	24	45	58	27	70	81	86	42	80	40	71	38	68	67	84	72	31	58	66
Intact strength 'R'	12	13	18	16	13	11	19	17	17	17	14	17	15	19	19	18	14	15	18	13
Weathering	7	7	9	7	9	7	9	9	7	10	7	7	7	7	7	9	7	7	9	9
Joint spacing	26	24	23	23	20	22	24	22	24	24	24	22	27	27	27	22	24	20	25	24
Joint orientation	14	14	14	5	14	14	14	14	9	14	14	14	14	9	9	14	20	14	14	14
Joint width	4	5	6	5	5	6	5	5	5	4	5	6	4	6	6	6	6	6	5	4
Joint continuity	6	5	5	5	5	6	5	5	5	5	4	5	6	5	5	5	6	6	5	6
Groundwater outflow	6	6	6	6	6	6	6	6	6	6	6	6	6	6	6	6	6	6	6	6
Total rating	75	74	81	67	72	72	82	78	73	80	74	77	79	79	79	80	83	74	82	76

Table A1.1b. RMS properties of some slopes from McMurdo Dry Valleys

Profile no.	21	22	23	24	25	26	27	28	29	30	31	32	33	34	35	36	37	38	39	40
RMS properties																				
Slope inclination	62	57	43	67	35	33	27	25	26	30	38	22	73	30	35	27	36	85	81	77
Intact strength 'R'	18	19	19	17	19	12	13	12	14	16	17	13	17	17	12	13	17	14	17	16
Weathering	7	7	9	9	9	9	7	7	9	9	7	7	9	7	7	9	9	7	9	9
Joint spacing	25	22	15	19	14	23	24	25	17	18	17	19	30	18	18	18	16	29	30	30
Joint orientation	14	20	14	18	20	18	18	14	14	14	9	14	14	14	14	14	14	14	14	14
Joint width	4	5	6	6	6	4	4	5	6	6	6	6	5	5	6	5	6	5	5	6
Joint continuity	5	6	5	7	5	6	6	6	6	4	6	6	7	6	5	6	6	6	7	7
Groundwater outflow	6	6	6	6	6	6	6	6	6	6	6	6	6	6	6	6	6	6	6	6
Total rating	79	85	74	82	79	78	78	75	72	73	68	71	82	73	68	71	74	81	88	88

'R' = Schmidt hammer rebound

Table A1.1c. RMS properties of some rock slopes from McMurdo Dry Valleys, Antarctica.

Profile no.	41	42	43	44	45	46	47	48	49	50	51	52	53	54
Slope inclination	20	34	57	21	87	39	73	67	81	86	36	17	35	43
Intact strength 'R'	13	17	16	13	14	18	19	18	18	19	18	19	17	18
Weathering	7	9	7	7	9	9	7	7	9	9	9	7	7	7
Joint spacing	19	16	17	19	30	16	20	19	29	18	19	23	20	24
Joint orientation	14	14	9	14	14	20	14	18	9	18	9	14	9	14
Joint width	7	6	5	5	6	5	6	4	7	6	6	4	4	5
Joint continuity	6	5	4	5	7	4	5	4	5	5	5	4	4	5
Groundwater	6	6	6	6	6	6	6	6	6	6	6	6	6	6
Total rating	72	73	64	69	86	79	77	76	83	81	72	72	67	79

Profile numbers refer to site locations in Fig. 2.23.

Table A1.2a. Rock mass strength data for some slopes from northern Fiordland.

Profile no.	1	2	3	4	5	6	7	8	9	10	11	12	13	14	15	16	17	18	19
RMS Properties																			
Slope inclination	68	70	62	31	31	46	55	0	0	59	44	76	46	38	80	36	68	39	74
Intact strength 'R'	18	19	19	18	19	19	19	19	19	18	19	19	19	18	19	19	19	18	19
Weathering	9	10	9	10	10	10	9	10	10	10	9	10	10	10	10	10	9	10	10
Joint spacing	27	23	20	22	24	21	21	21	20	21	21	21	21	20	20	22	20	25	18
Joint -sa	18	20	20	20	18	20	18	-	-	14	20	14	14	18	14	20	14	18	14
orientation -ice	18	14	18	14	18	18	20	14	18	18	18	18	18	20	18	20	20	20	14
Joint width	7	6	7	7	7	7	6	7	7	7	7	6	7	6	7	7	6	5	6
Joint continuity	6	6	6	5	6	5	6	5	6	6	6	5	5	6	7	6	6	6	5
Groundwater	6	6	6	5	5	5	6	6	6	6	6	6	5	5	6	6	5	6	5
Total rating -sa	91	90	87	87	89	87	85	-	-	82	88	81	81	83	83	90	79	88	78
Total rating -ice	72	66	66	64	71	68	69	64	73	67	67	68	68	67	67	71	68	73	62

Table A1.2b

Profile no.	20	21	22	23	24	25	26	27	28	29	30	31	32	33	34	35	36
Slope inclination	51	50	52	48	60	32	51	0	20	28	0	67	35	70	55	77	61
Intact strength 'R'	19	18	19	19	19	19	19	19	19	19	19	19	19	19	19	19	19
Weathering	10	9	10	10	10	9	10	9	9	10	9	10	10	10	10	10	10
Joint spacing	19	28	25	24	29	24	27	28	30	29	28	18	17	19	18	20	24
Joint -sa	20	20	9	18	20	20	20	-	20	20	-	14	14	18	18	18	18
orientation -ice	18	18	20	14	18	18	20	20	18	20	18	18	20	14	14	18	18
Joint width	6	7	6	6	5	6	7	5	4	7	6	6	6	6	7	7	5
Joint continuity	6	6	7	6	6	6	7	7	5	7	5	6	5	6	6	6	6
Groundwater outflow	6	6	6	6	6	6	6	6	5	6	5	6	5	6	6	6	6
Total rating -sa	86	94	78	89	85	90	96	-	92	98	-	79	76	84	84	86	88
Total rating -ice	66	73	74	67	66	70	76	76	76	78	74	65	66	62	61	67	69

sa = subaerial, ice = with respect to ice flow.

Profile numbers refer to site locations in Fig. 2.6.

Table A1.3. Rock mass strength data of some slope from South-central Fiordland.

Profile no. Strength parameters	1	2	3	4	5	6	7	8	9
Slope inclination	-	-	80	35	57	68	35	74	42
Intact strength 'R'	19	19	19	19	20	18	19	19	19
Weathering	9	10	10	9	9	9	9	9	10
Joint spacing	21	20	20	29	25	23	30	23	21
Joint -sa	-	-	20	14	14	14	9	14	18
orientation -ice	18	14	14	18	14	14	18	14	18
Joint width	7	7	6	7	7	7	7	7	7
Joint continuity	6	7	5	7	5	6	6	5	6
Groundwater	6	6	5	6	6	5	6	5	6
Total rating -sa	-	-	85	91	86	82	86	82	87
Total rating -ice	67	63	63	75	68	64	76	65	68

sa = subaerial, ice = with respect to ice flow.

Profile numbers refer to site locations in Fig. 2.7.

Table A1.4a. Rock mass strength data for some rock slopes in Mt Aspiring region.

Profile no. RMS properties	1	2	3	4	5	6	7	8	9	10	11	12	13	14	15	16	17	18	19	20
Slope inclination	80	82	45	0	64	80	48	47	41	44	46	53	40	80	30	48	90	32	79	57
Intact strength 'R'	14	13	17	17	20	19	11	14	14	18	13	12	17	19	16	19	19	18	19	17
Weathering	9	9	8	7	10	10	7	9	9	9	9	7	9	10	9	10	10	9	9	9
Joint spacing	21	19	26	15	22	23	19	20	22	26	20	19	26	30	17	30	30	25	29	22
Joint -sa	20	20	18	-	18	14	18	20	20	14	5	5	20	14	5	18	14	5	14	20
orientation -ice	9	14	9	14	14	5	14	14	9	14	9	9	9	-	5	14	5	5	-	14
Joint width	7	6	6	5	7	6	5	6	5	6	5	4	5	7	5	5	5	5	7	6
Joint continuity	6	6	4	5	6	5	4	5	5	6	4	4	5	7	5	6	6	4	6	5
Groundwater outflow	4	5	6	5	5	4	6	6	5	5	6	5	5	5	5	5	5	5	5	5
Total rating -sa	81	78	85	-	88	81	70	80	80	84	62	56	87	92	62	93	89	71	89	84
Total rating -ice	53	55	60	53	66	57	51	57	54	67	51	47	61	-	47	73	64	57	-	62

Profile numbers refer to site locations in Fig. 2.8.

Table A1.4b. Rock mass strength data for some rock slopes from Mt. Aspiring

Profile no.	21	22	23	24	25	26	27	28	29	30	31	32	33	34	35	36	37	38	39	40
Slope inclination	75	46	39	90	52	72	78	80	42	76	75	90	85	47	71	57	79	69	38	39
Intact strength 'R'	14	10	13	14	16	18	19	13	16	12	11	16	17	16	13	17	18	17	18	17
Weathering	7	7	7	7	7	7	9	9	9	9	7	7	8	9	7	7	7	7	7	7
Joint spacing	21	25	19	25	26	30	29	22	29	20	21	23	21	27	26	25	25	25	21	20
Joint -sa	18	14	14	20	18	14	14	14	5	20	18	18	20	5	18	18	18	14	9	9
orientation -ice	-	18	14	9	9	9	-	18	-	14	9	-	-	14	14	9	9	9	14	-
Joint width	6	4	5	5	5	7	7	6	6	5	4	6	7	6	6	6	5	4	4	5
Joint continuity	6	4	6	5	5	6	6	6	6	6	5	6	6	5	5	5	4	5	5	5
Groundwater outflow	5	4	6	5	6	5	5	6	6	5	6	6	6	5	6	5	5	6	5	6
Total rating -sa	77	68	70	81	83	87	89	76	77	76	72	82	85	73	81	83	82	78	69	69
Total rating -ice	-	60	53	55	58	64	-	62	-	54	48	-	-	66	60	58	59	58	60	-

sa = subaerial, ice = with respect to ice flow

Table A1.4c. RMS properties of some Mt Aspiring schist slopes (continued)

Profile no.	41	42	43	44	45	46	47	48	49
RMS Properties									
Slope inclination	29	43	54	34	34	82	46	49	0
Intact strength 'R'	17	15	17	16	17	15	11	17	18
Weathering	7	7	7	7	7	7	7	7	7
Joint spacing	19	19	17	30	24	29	29	25	29
Joint -sa	20	9	18	9	14	-	-	14	-
orientation -ice	9	14	-	-	-	9	14	14	18
Joint width	5	4	6	7	7	5	6	7	4
Joint continuity	5	5	5	5	6	5	4	6	6
Groundwater outflow	5	6	6	6	6	6	6	6	6
Total rating -sa	78	65	76	80	81	-	-	82	-
Total rating -ice	52	55	-	-	-	60	61	63	72

Profile numbers refer to site locations in Fig. 2.8.

Table A1.5. RMS data from some schist slopes from South Westland

Profile no.	1	2	3	4	5	6	7	8	9	10	11	12	13	14	15	16	17	18	19	20
RMS Properties																				
Slope inclination	36	47	41	0	40	67	69	70	51	0	0	80	0	53	74	0	57	79	39	65
Intact strength 'R'	17	19	16	16	16	18	15	17	17	19	17	18	17	17	18	17	17	18	13	18
Weathering	9	10	9	9	9	10	10	10	10	10	10	10	10	10	10	10	10	10	9	9
Joint spacing	29	29	25	29	19	20	23	25	29	29	20	22	24	20	21	23	24	20	24	18
Joint -sa	20	14	18	-	9	20	14	9	14	-	-	14	-	14	18	-	20	18	5	20
orientation -ice	18	18	18	20	14	14	18	9	14	18	18	14	20	18	9	14	14	18	9	14
Joint width	6	6	7	7	6	5	5	6	6	7	6	7	7	6	7	7	6	7	5	6
Joint continuity	7	7	7	6	6	5	6	7	7	7	6	7	7	6	7	7	7	6	5	6
Groundwater outflow	6	6	6	6	6	5	6	6	5	5	6	6	5	6	6	6	6	5	5	6
Total rating -sa	94	91	88	-	71	83	79	80	88	-	-	84	-	79	87	-	90	84	66	83
Total rating -ice	73	76	68	74	58	62	66	61	70	76	65	64	71	65	58	64	65	66	55	59

sa = subaerial, ice = joint orientation relative to ice flow.

Profile number refers to site locations in Fig. 2.11.

APPENDIX 2.1. Alpha-indices used in defining ice-divides  
over Fiordland-Mt Aspiring regions.

Grid Coordinates	V	E	G	$\alpha$
1. S157 300750	39	37	4	4.2
2. S157 200630	32	30	4	3.4
3. S157 250760	58	62	6	9.0
4. S157 370740	97	109	3	7.9
5. S166 150490	59	59	3	2.7
6. S166 230500	31	30	2	1.8
7. S166 150550	47	45	4	2.3
8. S166 050420	27	25	2	2.0
9. S165 850600	58	61	5	7.2
10. S157 200900	46	54	5	14.9
11. S157 000850	53	53	5	5.0
12. S148 150050	26	24	3	2.1
13. S148 250000	61	66	3	6.8
14. S148 050940	76	83	3	6.1
15. S149 420000	158	196	3	10.9
16. S148 360130	94	104	3	7.1
17. S148 150130	81	88	4	7.0
18. S139 300255	68	73	4	6.9
19. S139 100210	40	41	2	0.4
20. S139 080380	34	34	2	0.3
21. S139 030240	33	31	4	0.3
22. S139 260420	27	23	4	0.2
23. S139 180420	51	51	4	0.4
24. S139 340370	63	63	7	5.8
25. S140 460310	72	82	3	9.4
26. S140 530400	44	51	1	9.6
27. S140 670340	69	67	8	6.0
28. S140 410220	47	51	2	6.7
29. S149 540180	80	86	3	5.8
30. S140 615230	80	73	10	2.0
31. S140 445445	24	22	3	10.5
32. S139 350450	69	75	4	7.5
33. S129 300520	26	27	1	4.3
34. S139 155495	20	13	7	2.9
35. S129 220525	28	21	8	2.0
36. S130 500520	45	44	7	7.1
37. S140 650450	49	52	3	6.5
38. S130 480620	38	38	4	5.6
39. S130 560590	47	51	3	7.9
40. S130 550710	40	39	4	4.0
41. S130 675690	52	55	4	7.1
42. S130 720570	38	37	3	2.8
43. S129 330600	74	77	4	4.9
44. S129 340680	22	16	6	2.6
45. S130 410700	41	31	9	2.6
46. S121 500890	48	50	5	6.6
47. S121 600920	49	43	9	3.2
48. S121 700920	47	46	3	2.3
49. S121 580800	69	70	6	5.3
50. S121 680820	30	30	2	3.6
51. S130 790730	68	73	5	7.6
52. S121 790890	50	52	4	6.3
53. S122 900030	37	39	1	4.3
54. S122 860940	52	53	4	3.0
55. S121 730090	54	55	5	3.9
56. S112 800120	40	41	2	4.0
57. S121 650050	32	31	2	1.7
58. S121 020030	22	24	1	7.7



59. S121 980880	46	52	3	10.3
60. S131 950700	56	55	3	1.9
61. S113 990170	57	65	3	10.1
62. S113 870240	47	47	4	4.5
63. S113 970310	53	56	4	6.9
64. S113 880370	44	36	9	2.4
65. S113 060340	36	34	5	4.5
66. S105 080440	34	31	5	3.2
67. S156 860850	88	101	5	10.5
68. S157 960680	39	40	3	5.5
69. S166 280600	34	26	7	1.6
70. S166 990590	58	59	5	3.6
71. S165 780500	32	34	3	2.9
72. S165 920530	35	28	8	1.5
73. S166 370500	66	65	6	3.8
74. S166 350420	36	32	5	1.5
75. S167 480570	36	34	2	1.49
76. S158 570610	55	44	11	0
77. S158 530730	73	79	2	5.7
78. S158 580880	84	96	4	9.8
79. S149 550960	49	51	5	7.5
80. S149 400000	78	88	3	8.6
81. S148 350915	78	90	3	9.9

#### Mt Aspiring area

Grid Coordinates	V	E	G	$\alpha$
1. S131 120670	77	76	8	4.7
2. S131 030740	34	26	9	1.5
3. S131 240670	32	34	2	6.8
4. S131 130760	31	22	10	1.8
5. S131 020580	30	27	5	3.6
6. S131 950700	66	65	7	4.7
7. S122 150990	52	59	3	10.1
8. S122 230930	44	39	7	2.4
9. S122 080810	40	41	4	6.7
10. S122 170840	56	59	3	5.6
11. S131 260720	39	38	5	5.5
12. S114 450230	46	52	1	6.7
13. S114 590210	66	65	4	2.8
14. S114 440150	40	38	8	8.0
15. S123 400960	28	26	3	2.0
16. S123 500880	41	34	8	1.3
17. S123 490890	48	41	8	1.1
18. S123 390840	30	19	11	0
19. S132 450780	55	51	7	2.9
20. S132 510730	26	24	3	2.1
21. S132 420710	23	21	3	2.4
22. S142 530490	37	36	3	2.9
23. S132 510550	37	29	6	2.9
24. S142 430390	67	75	2	7.8
25. S142 390330	36	28	6	-3.0
26. S141 270330	57	53	6	1.8
27. S142 320420	31	33	4	10.5
28. S132 390520	93	89	9	2.8
29. S141 200470	54	53	4	2.9
30. S141 090430	41	36	6	1.3
31. S113 130150	38	39	2	4.2
32. S113 290150	24	20	3	2.3
33. S113 300240	20	18	3	2.9
34. S113 160130	48	53	1	6.6

35.	S113	515220	58	61	5	7.2
36.	S132	300565	38	37	2	2.8
37.	S105	180510	18	16	3	3.0
38.	S105	240590	24	18	5	2.0
39.	S105	110630	32	30	3	1.7
40.	S105	250430	63	65	3	4.1
41.	S106	330540	44	40	6	2.4
42.	S106	400680	49	47	3	1.1
43.	S97	440900	55	51	3	1.0
44.	S97	620830	26	23	4	2.1
45.	S97	310790	44	45	2	3.6
46.	S106	460400	40	40	4	5.3
47.	S106	620480	54	53	4	2.9
48.	S106	690640	54	58	3	6.8
49.	S98	000830	72	81	3	8.6
50.	S98	890700	30	31	2	5.4
51.	S107	870590	19	19	2	6.1
52.	S107	810440	40	39	4	0.4
53.	S115	800320	43	38	5	3.7
54.	S98	820920	18	14	4	3.2
55.	S98	950980	16	14	3	3.7
56.	S98	050970	30	29	3	3.6
57.	S107	030600	24	26	1	7.0
58.	S97	740890	28	27	2	2.0
59.	S107	060520	55	59	4	7.6
60.	S107	090630	38	38	3	4.2
61.	S98	140740	28	26	3	2.0
62.	S99	220880	33	31	3	1.6
63.	S87	040110	34	29	7	3.2
64.	S87	140090	18	14	5	3.2
65.	S114	590210	22	21	1	0
66.	S114	660320	24	19	5	0
67.	S114	470220	32	35	1	6.8

V = total number of vertices (nodes). In the present study these are defined as the beginning, end or intersection of any valley; E = total number of edges (links). These are the valley sectors between the vertices; G = the number of separate sub-graphs.  $\alpha$ -index as given in section 3.3.

All grid coordinates from NZMS 1, 1:63360 topographic maps

# APPENDIX 2.2. Glacial valley morphometry.

Grid Coordinates	Perimeter length (km)	Cross-section Area (km <sup>2</sup> )	Shape Factor (f)	Width (km)	Depth (km)	Form Ratio (FR)
------------------	--------------------------	--	------------------------	---------------	---------------	--------------------

## Northern Fiordland

1. S122 929063	3.49	1.64	0.44	2.35	1.08	1.09
2. S122 924034	2.99	1.25	0.42	1.73	0.99	0.87
3. S122 932018	3.65	1.65	0.38	2.20	1.18	0.93
4. S122 952984	1.74	0.38	0.39	1.15	0.56	1.03
5. S122 887048	3.07	1.22	0.41	2.10	0.96	1.10
6. S122 901068	2.58	0.88	0.39	1.64	0.87	0.94
7. S122 912000	2.97	1.17	0.38	1.76	1.05	0.84
8. S122 902947	2.35	0.67	0.42	1.55	0.68	1.14
9. S112 812152	4.24	2.30	0.42	2.75	1.28	1.07
10. S121 810901	3.56	1.53	0.40	2.41	1.08	1.12
11. S121 809954	3.11	1.28	0.42	2.01	0.97	1.04
12. S121 787027	4.05	2.10	0.44	2.85	1.19	1.20
13. S113 013160	2.68	1.00	0.50	1.86	0.74	1.26
14. S113 945195	3.59	1.84	0.49	2.29	1.05	1.09
15. S113 909192	3.11	1.34	0.48	2.14	0.90	1.19
16. S122 038041	1.88	0.49	0.46	1.25	0.56	1.12
17. S122 024995	2.32	0.67	0.47	1.70	0.62	1.37
18. S122 982012	2.08	0.60	0.47	1.38	0.62	1.11

mean f = 0.43 ± 0.04

mean FR = 1.08 ± 0.13

## South-central Fiordland

1. S148 253968	2.97	1.19	0.47	2.29	0.86	1.33
2. S148 287962	2.01	0.50	0.40	1.52	0.62	1.23
3. S148 313926	2.12	0.55	0.48	1.76	0.54	1.63
4. S148 362955	1.56	0.30	0.39	1.11	0.49	1.13
5. S148 377980	1.19	0.52	0.49	1.55	0.53	1.46
6. S148 268028	1.95	0.52	0.43	1.36	0.62	1.10
7. S148 291058	3.14	1.26	0.41	2.37	0.99	1.20
8. S148 374046	2.62	0.93	0.53	2.17	0.65	1.67
9. S148 215921	1.77	0.43	0.41	1.27	0.59	1.08
10. S148 053030	2.42	0.82	0.46	1.83	0.73	1.25
11. S148 077086	2.01	0.54	0.50	1.64	0.54	1.52
12. S148 128932	3.11	1.34	0.44	2.32	0.99	1.17
13. S157 294750	3.07	1.02	0.43	1.95	0.77	1.27
14. S157 273788	3.22	1.26	0.48	2.72	0.81	1.68
15. S157 304672	2.87	0.98	0.46	2.41	0.74	1.63
16. S157 361875	2.99	1.26	0.52	2.45	0.81	1.51
17. S157 357828	2.95	1.27	0.46	2.38	0.80	1.49
18. S157 231852	3.47	1.46	0.45	2.79	0.93	1.50
19. S157 143863	3.25	1.12	0.44	2.72	0.79	1.72

mean f = 0.46 ± 0.04

mean FR = 1.39 ± 0.22

## Mt. Aspiring

1. S106 437668	3.34	1.38	0.47	2.79	0.87	1.60
2. S106 650489	3.31	1.22	0.42	2.72	0.87	1.56
3. S106 542452	3.46	1.52	0.50	2.88	0.87	1.66
4. S106 571435	2.31	0.74	0.54	1.83	0.59	1.55
5. S114 398268	3.73	1.31	0.48	3.50	0.73	2.40
6. S114 388344	2.64	0.76	0.46	2.26	0.62	1.82
7. S114 410365	2.08	0.48	0.46	1.73	0.50	1.73

8. S114 472363	3.97	1.93	0.54	3.44	0.90	1.91
9. S114 315140	3.10	1.07	0.49	2.63	0.71	1.85
10. S114 587378	3.48	1.53	0.47	2.79	0.93	1.50
11. S113 275270	4.68	2.63	0.55	4.12	1.02	2.02
12. S114 492288	2.06	0.51	0.47	1.76	0.53	1.66
13. S106 630610	3.99	1.57	0.49	3.62	0.80	2.26
14. S98 838766	3.18	1.27	0.44	2.60	0.90	1.44
15. S98 960733	3.54	1.54	0.50	2.94	0.87	1.69
16. S98 861857	3.71	1.57	0.44	3.03	0.96	1.58
17. S98 012920	3.68	1.51	0.49	3.19	0.84	1.90
18. S99 223733	3.69	1.38	0.45	3.16	0.84	1.88
19. S88 611200	4.09	1.88	0.51	3.50	0.90	1.94

mean f = 0.48 ± 0.04

mean FR = 1.79 ± 0.25

#### South Westland

1. S71 020700	3.58	1.49	0.45	3.0	0.93	1.61
2. S71 005670	3.66	1.68	0.48	3.03	0.96	1.58
3. S71 063665	3.60	1.66	0.51	2.94	0.90	1.63
4. S71 028640	2.33	0.68	0.43	1.86	0.68	1.37
5. S71 954642	3.70	1.67	0.52	3.19	0.87	1.83
6. S71 940720	2.04	0.49	0.52	1.73	0.46	1.88
7. S71 941690	3.24	1.25	0.48	2.75	0.80	1.72
8. S71 957660	1.98	0.50	0.56	1.70	0.45	1.89
9. S71 919650	2.70	0.92	0.49	2.20	0.70	1.57
10. S71 833648	3.36	1.33	0.45	2.69	0.87	1.55
11. S71 967727	3.77	1.59	0.40	2.91	1.05	1.39
12. S71 800621	1.78	0.41	0.46	1.36	0.50	1.36
13. S72 204726	2.28	0.69	0.47	1.80	0.65	1.38
14. S72 261798	2.37	0.74	0.46	1.89	0.68	1.39
15. S88 324221	2.00	0.60	0.51	1.39	0.59	1.18
16. S88 382268	2.21	0.65	0.50	1.67	0.59	1.42
17. S79 733410	2.76	0.88	0.49	2.32	0.65	1.78

mean f = 0.48 ± 0.04

mean FR = 1.56 ± 0.21

#### Mt. Cook

1. S79 903425	4.89	3.02	0.56	4.21	1.10	1.91
2. S79 531013	3.22	1.27	0.53	2.79	0.74	1.89
3. S79 030569	3.02	1.17	0.48	2.45	0.80	1.53
4. S79 914545	3.25	1.32	0.48	2.63	0.84	1.57
5. S79 881515	4.93	2.50	0.50	4.49	1.02	2.20
6. S79 797366	4.19	2.36	0.55	3.50	1.02	1.72
7. S79 780392	4.04	1.99	0.51	3.40	0.96	1.77
8. S79 424783	3.29	1.46	0.53	2.66	0.84	1.58
9. S79 311715	2.67	0.88	0.51	2.23	0.65	1.72
10. S79 887557	2.55	0.78	0.54	2.18	0.57	1.91
11. S79 948557	1.51	0.30	0.40	1.61	0.50	1.61
12. S79 060481	1.32	0.24	0.53	1.05	0.34	1.54
13. S79 948379	1.56	0.33	0.54	1.30	0.39	1.67
14. S79 078614	3.15	1.23	0.51	2.94	0.77	1.91
15. S79 022402	3.36	1.29	0.52	2.94	0.74	1.99
16. S72 474846	3.96	1.77	0.50	3.56	0.90	1.98
17. S72 277730	2.92	1.08	0.50	2.38	0.74	1.61

mean f = 0.52 ± 0.02

mean FR = 1.77 ± 0.19

All grid coordinates from NZMS 1 1:63360 topographic maps.

## APPENDIX 2.3. Fitting second order polynomials equations to glacial valley cross-profiles

$$y = a + bx + cx^2$$

### Northern Fiordland

#### Grid Coords.

#### Quadratic Equation

1. S122 929063	$y = 4363 - 1.912x + 2.41 \times 10^{-4}x^2$	$r = 0.99$	$n = 14$
2. S122 924034	$y = 5878 - 2.584x + 3.63 \times 10^{-4}x^2$	$r = 0.96$	$n = 11$
3. S122 887048	$y = 5838 - 1.948x + 2.59 \times 10^{-4}x^2$	$r = 0.97$	$n = 12$
4. S122 901068	$y = 5644 - 2.416x + 3.88 \times 10^{-4}x^2$	$r = 0.99$	$n = 13$
5. S122 912000	$y = 7930 - 3.266x + 4.29 \times 10^{-4}x^2$	$r = 0.98$	$n = 13$
6. S112 812152	$y = 5146 - 1.848x + 2.03 \times 10^{-4}x^2$	$r = 0.98$	$n = 13$
7. S121 809954	$y = 5374 - 1.981x + 2.86 \times 10^{-4}x^2$	$r = 0.98$	$n = 16$
8. S121 787027	$y = 4147 - 1.676x + 1.85 \times 10^{-4}x^2$	$r = 0.98$	$n = 17$
9. S113 013160	$y = 5657 - 2.057x + 2.80 \times 10^{-4}x^2$	$r = 0.98$	$n = 12$
10. S113 945195	$y = 4479 - 1.945x + 2.52 \times 10^{-4}x^2$	$r = 0.97$	$n = 17$
11. S113 909192	$y = 4802 - 1.568x + 2.25 \times 10^{-4}x^2$	$r = 0.97$	$n = 14$
12. S122 038041	$y = 6133 - 2.365x + 4.07 \times 10^{-4}x^2$	$r = 0.98$	$n = 11$
13. S122 024995	$y = 6487 - 2.022x + 2.60 \times 10^{-4}x^2$	$r = 0.97$	$n = 11$
14. S122 948045	$y = 8047 - 3.009x + 4.22 \times 10^{-4}x^2$	$r = 0.98$	$n = 10$
15. S122 932018	$y = 5286 - 1.958x + 2.85 \times 10^{-4}x^2$	$r = 0.98$	$n = 13$
16. S122 901068	$y = 5644 - 2.416x + 3.88 \times 10^{-4}x^2$	$r = 0.99$	$n = 14$
17. S122 902947	$y = 4638 - 1.743x + 3.48 \times 10^{-4}x^2$	$r = 0.98$	$n = 10$
18. S121 810901	$y = 5157 - 1.823x + 2.19 \times 10^{-4}x^2$	$r = 0.96$	$n = 14$

$$y = 5592 - 2.141x + 3.02 \times 10^{-4}x^2$$

$$\begin{matrix} +1140 & +0.442 & +0.78 \times 10^{-4} \end{matrix}$$

### Southern Fiordland

1. S148 253968	$y = 6595 - 1.979x + 1.90 \times 10^{-4}x^2$	$r = 0.99$	$n = 10$
2. S148 313926	$y = 4711 - 1.105x + 1.85 \times 10^{-4}x^2$	$r = 0.94$	$n = 9$
3. S148 377980	$y = 6187 - 1.866x + 2.65 \times 10^{-4}x^2$	$r = 0.99$	$n = 10$
4. S148 291058	$y = 6618 - 2.033x + 1.97 \times 10^{-4}x^2$	$r = 0.96$	$n = 11$
5. S148 374046	$y = 2882 - 1.273x + 1.70 \times 10^{-4}x^2$	$r = 0.98$	$n = 13$
6. S148 053030	$y = 3373 - 1.720x + 2.46 \times 10^{-4}x^2$	$r = 0.99$	$n = 11$
7. S148 077086	$y = 3393 - 1.552x + 2.41 \times 10^{-4}x^2$	$r = 0.98$	$n = 11$
8. S148 128932	$y = 3924 - 1.796x + 2.12 \times 10^{-4}x^2$	$r = 0.99$	$n = 10$
9. S157 294750	$y = 3792 - 1.110x + 1.30 \times 10^{-4}x^2$	$r = 0.98$	$n = 13$
10. S157 273788	$y = 4255 - 1.130x + 1.25 \times 10^{-4}x^2$	$r = 0.97$	$n = 10$
11. S157 304672	$y = 3669 - 1.133x + 1.25 \times 10^{-4}x^2$	$r = 0.98$	$n = 11$
12. S157 361875	$y = 4247 - 1.298x + 1.57 \times 10^{-4}x^2$	$r = 0.98$	$n = 12$
13. S157 357828	$y = 5009 - 1.394x + 1.57 \times 10^{-4}x^2$	$r = 0.98$	$n = 10$
14. S157 238879	$y = 4082 - 1.193x + 0.89 \times 10^{-4}x^2$	$r = 0.98$	$n = 12$
15. S157 143863	$y = 3647 - 1.097x + 1.74 \times 10^{-4}x^2$	$r = 0.94$	$n = 12$
16. S148 287962	$y = 3563 - 1.529x + 2.09 \times 10^{-4}x^2$	$r = 0.96$	$n = 12$

$$y = 4372 - 1.451x + 1.795 \times 10^{-4}x^2$$

$$\begin{matrix} +1126 & +0.325 & +0.47 \times 10^{-4} \end{matrix}$$

### South Westland

1. S71 800621	$y = 6471 - 1.756x + 3.02 \times 10^{-4}x^2$	$r = 0.99$	$n = 11$
2. S71 833648	$y = 7223 - 1.580x + 1.35 \times 10^{-4}x^2$	$r = 0.95$	$n = 12$
3. S71 919650	$y = 6972 - 1.624x + 1.66 \times 10^{-4}x^2$	$r = 0.99$	$n = 12$
4. S71 957660	$y = 6533 - 1.286x + 2.03 \times 10^{-4}x^2$	$r = 0.99$	$n = 10$
5. S71 941690	$y = 6149 - 1.001x + 1.10 \times 10^{-4}x^2$	$r = 0.98$	$n = 15$
6. S71 940720	$y = 7019 - 1.315x + 1.81 \times 10^{-4}x^2$	$r = 0.99$	$n = 10$
7. S71 994642	$y = 5508 - 0.846x + 0.90 \times 10^{-4}x^2$	$r = 0.94$	$n = 12$
8. S71 028640	$y = 6081 - 1.266x + 2.11 \times 10^{-4}x^2$	$r = 0.95$	$n = 13$

9. S71 063665  $y = 6147 - 1.190x + 1.24 \times 10^{-4}x^2$ ,  $r = 0.96$ ,  $n = 14$
10. S71 005670  $y = 6403 - 1.320x + 1.20 \times 10^{-4}x^2$ ,  $r = 0.98$ ,  $n = 14$
11. S72 261798  $y = 6756 - 1.536x + 2.20 \times 10^{-4}x^2$ ,  $r = 0.98$ ,  $n = 10$
12. S79 733410  $y = 5705 - 1.044x + 1.35 \times 10^{-4}x^2$ ,  $r = 0.98$ ,  $n = 14$
13. S88 382268  $y = 5163 - 1.620x + 2.59 \times 10^{-4}x^2$ ,  $r = 0.97$ ,  $n = 10$
14. S88 324221  $y = 5035 - 1.631x + 3.40 \times 10^{-4}x^2$ ,  $r = 0.99$ ,  $n = 12$
15. S72 204726  $y = 6304 - 1.592x + 2.35 \times 10^{-4}x^2$ ,  $r = 0.99$ ,  $n = 13$

---


$$y = 6231 - 1.374x + 1.89 \times 10^{-4}x^2$$

$$\quad \quad \quad \pm 634 \quad \quad \pm 0.263 \quad \quad \pm 0.71 \times 10^{-4}$$

#### Mt. Aspiring

1. S106 437668  $y = 5812 - 1.449x + 1.24 \times 10^{-4}x^2$ ,  $r = 0.96$ ,  $n = 14$
2. S106 650489  $y = 6658 - 1.401x + 1.25 \times 10^{-4}x^2$ ,  $r = 0.94$ ,  $n = 11$
3. S106 542452  $y = 6467 - 1.297x + 1.21 \times 10^{-4}x^2$ ,  $r = 0.98$ ,  $n = 11$
4. S114 398268  $y = 4890 - 0.691x + 0.69 \times 10^{-4}x^2$ ,  $r = 0.95$ ,  $n = 14$
5. S114 388344  $y = 6002 - 1.086x + 1.34 \times 10^{-4}x^2$ ,  $r = 0.95$ ,  $n = 10$
6. S114 472363  $y = 6721 - 1.015x + 0.88 \times 10^{-4}x^2$ ,  $r = 0.98$ ,  $n = 15$
7. S114 315140  $y = 6190 - 1.075x + 1.10 \times 10^{-4}x^2$ ,  $r = 0.96$ ,  $n = 11$
8. S114 587378  $y = 8498 - 1.783x + 1.38 \times 10^{-4}x^2$ ,  $r = 0.98$ ,  $n = 14$
9. S113 275270  $y = 6723 - 1.226x + 0.70 \times 10^{-4}x^2$ ,  $r = 0.99$ ,  $n = 12$
10. S114 492288  $y = 7057 - 1.278x + 1.84 \times 10^{-4}x^2$ ,  $r = 0.95$ ,  $n = 13$
11. S106 630610  $y = 4654 - 0.806x + 0.69 \times 10^{-4}x^2$ ,  $r = 0.98$ ,  $n = 18$
12. S99 223933  $y = 6313 - 1.165x + 0.86 \times 10^{-4}x^2$ ,  $r = 0.96$ ,  $n = 14$
13. S98 838766  $y = 5782 - 1.402x + 1.43 \times 10^{-4}x^2$ ,  $r = 0.99$ ,  $n = 12$
14. S98 960733  $y = 6408 - 1.517x + 1.17 \times 10^{-4}x^2$ ,  $r = 0.98$ ,  $n = 12$
15. S98 012920  $y = 5833 - 1.236x + 0.92 \times 10^{-4}x^2$ ,  $r = 0.97$ ,  $n = 13$

---


$$y = 6267 - 1.228x + 1.11 \times 10^{-4}x^2$$

$$\quad \quad \quad \pm 873 \quad \quad \pm 0.267 \quad \quad \pm 0.31 \times 10^{-4}$$

#### Mt. Cook

1. S79 903425  $y = 7281 - 1.170x + 0.74 \times 10^{-4}x^2$ ,  $r = 0.99$ ,  $n = 11$
2. S79 531013  $y = 5918 - 0.828x + 0.94 \times 10^{-4}x^2$ ,  $r = 0.99$ ,  $n = 11$
3. S79 030569  $y = 7593 - 1.185x + 1.32 \times 10^{-4}x^2$ ,  $r = 1.0$ ,  $n = 10$
4. S79 914545  $y = 7040 - 1.081x + 1.12 \times 10^{-4}x^2$ ,  $r = 0.98$ ,  $n = 10$
5. S79 881515  $y = 7775 - 0.900x + 0.53 \times 10^{-4}x^2$ ,  $r = 0.97$ ,  $n = 12$
6. S79 797366  $y = 6627 - 1.247x + 1.02 \times 10^{-4}x^2$ ,  $r = 1.0$ ,  $n = 14$
7. S79 780392  $y = 7734 - 1.290x + 0.94 \times 10^{-4}x^2$ ,  $r = 0.98$ ,  $n = 13$
8. S79 424783  $y = 7526 - 1.431x + 1.42 \times 10^{-4}x^2$ ,  $r = 0.99$ ,  $n = 11$
9. S79 311715  $y = 7163 - 1.266x + 1.55 \times 10^{-4}x^2$ ,  $r = 0.98$ ,  $n = 10$
10. S79 887557  $y = 7360 - 1.087x + 1.41 \times 10^{-4}x^2$ ,  $r = 0.98$ ,  $n = 11$
11. S79 948557  $y = 7095 - 1.409x + 1.88 \times 10^{-4}x^2$ ,  $r = 0.98$ ,  $n = 10$
12. S72 277730  $y = 6140 - 1.326x + 1.58 \times 10^{-4}x^2$ ,  $r = 0.97$ ,  $n = 12$
13. S79 022402  $y = 7026 - 1.135x + 1.01 \times 10^{-4}x^2$ ,  $r = 0.98$ ,  $n = 13$
14. S88 611200  $y = 6073 - 0.970x + 0.89 \times 10^{-4}x^2$ ,  $r = 0.97$ ,  $n = 13$
15. S72 474846  $y = 6880 - 1.008x + 0.84 \times 10^{-4}x^2$ ,  $r = 0.98$ ,  $n = 14$

---


$$y = 7015 - 1.156x + 1.146 \times 10^{-4}x^2$$

$$\quad \quad \quad \pm 574 \quad \quad \pm 0.173 \quad \quad \pm 0.355 \times 10^{-4}$$

'r' = correlation coefficient, n = number of data points.

#### APPENDIX 2.4. Glacial valley drainage density.

<u>Mt Cook region</u>	Valley Length (km)	Drainage Basin Area (km <sup>2</sup> )	Drainage Density (km/km <sup>2</sup> )
Hopkins River	104	255	0.41
Dobson River	106	331	0.32
Cass River	84	180	0.47
Jollie River	64	141	0.45
Macaulay River	88	175	0.5
Mueller Glacier	43	120	0.36
Tasman Glacier	125	388	0.32
Godley Glacier	156	381	0.41
Havelock River	121	276	0.44
Clyde River	71	164	0.43
Rakaia River	86.5	251	0.34
Mathais River	110	261	0.42
Lawrence River	43	116	0.37

Mean density = 0.40 ± 0.06

#### Mt Aspiring region

Matukituki River	106	502	0.21
Dart River	160	447	0.36
Rees River	97	244	0.40
Arawata River	268	754	0.36
Waiatoto River	135	452	0.30
Makarora River	284	831	0.34
Young River	39	102	0.38
Blue River	26	58	0.45
Wilkin River	65	270	0.24
Albert Burn	48	139	0.35
Burke River	52	119	0.44
Haast River	664	1969	0.34
Okuru River	80	220	0.36
Turnbull River	63	149	0.42
Forgotten River	40	101	0.40

Mean density = 0.36 ± 0.07

#### South Westland region

Waitaha River	83	123	0.67
Wanganui River	231	342	0.68
Paringa River	118	220	0.54
Matatahi River	83	153	0.54
Jacobs River	70	122	0.57
Copeland River	87	155	0.56
Karangarua River	82	181	0.45
Cook River	78	131	0.60
Waiho River	37	67	0.55
Callery Stream	60	97	0.62
Fox River	55	95	0.58
Perth River	94	224	0.42
Clarke River	87	166	0.52
Landsborough R.	213	358	0.59

Mean density = 0.56 ± 0.08

Fiordland Region

Lake Te Anau:

NW Arm	77	123	0.63
Worsely Arm	81	156	0.52
Glade Arm	109	218	0.50
SW Arm	179	196	0.91
North Fiord	179	273	0.66
George Sound			
Alice Arm	57	73	0.78
SW Arm	11	15	0.73
Milford Sound	275	519	0.53
First Arm	21	27	0.78
Precipace Cove	55	69	0.80
Gaer Arm	137	167	0.82
Nancy Sound	71	90	0.79
Caswell Sound	186	272	0.68
Emelius Arm	110	143	0.77
Vancouver Arm	58	100	0.58
Broughton Arm	60	70	0.86

Mean density =  $0.71 \pm 0.13$



#### **A3.1. Rock Density and Porosity**

The density or unit weight of rock can be correlated with the UCS of the material (Deere and Miller, 1966). Consequently, for each rock-type tested, the density in both an oven-dried and saturated state was determined (Tables A3.1-5). The ISRM standard methods for density determination using short-cores, were followed exactly (Brown, 1981).

Apparent porosity was determined from the same short-cores used for the density calculations, and followed the water content method detailed in Brown (1981).

#### **A3.2. Point Load Strength**

The point load strength index was used both as a surrogate measure of uniaxial compressive strength (UCS), and tensile strength, both to complement other laboratory tests and where sufficient material was not available for coring. The tests were mainly carried out on irregular lumps of rock, although diametral and axial tests on short-cores were used where sufficient material was available. The ISRM suggested methods given in Franklin (1985) were followed. All the tests enumerated had valid failure modes (Franklin, 1985). The resulting data are given in Tables A3.1-5. For isotropic rock, at least 20 samples were tested at each site, while for anisotropic material (schist), at least 20 tests were undertaken both parallel and perpendicular to the foliation, except where otherwise indicated in Tables A3.1-5.

#### **A3.3. Brazil Tensile Strength**

This is an indirect measure of tensile strength involving compressive diametral loading to induce tensile stress in a thin disc of rock. The determination of indirect tensile strength followed the ISRM suggested methods (Brown, 1981). The tests were carried out on short-cores of rock in both a saturated and oven-dried state when sufficient material was available. The tensile strength results and number of tests are given in Tables A3.1-5. For anisotropic rock, the tests were carried out both parallel and perpendicular to the foliation/bedding.

#### A3.4. Intact Shear Strength

This test was described originally by Protod'yakonov (1969) and enables the determination of internal cohesion ( $\tau_0$ ) and internal friction angle ( $\phi$ ) of intact rock. Vacuum-saturated short cores were used, 54 mm diameter with a length/diameter ratio of 1:1.

In order to construct a Mohr envelope, it is necessary to carry out the tests at no less than three angles. The best results for the hard rock were achieved with angles of 45°, 40°, 35° and 30° to the direction of applied stress. Variations in strength between samples usually required 2-3 tests per angle.

The cores were placed in dies, loaded to failure and the peak value recorded. Normal and shearing stresses were then calculated and a linear regression analysis was carried out to enable determination of the internal cohesion and friction angle. The results and number of tests are given in Tables A3.1-5. Insufficient rock material precluded a comparison of shear strength in oven-dried and saturated samples.

#### A3.5. Dynamic Elastic Moduli & Poisson's Ratio

Dynamic elastic moduli were calculated for selected rock types using vacuum-saturated short cores. Three tests per rock type were undertaken where sufficient material was available. The method involved measuring the arrival times of p- and s- waves through short cores under a uniaxial stress-field and entering the data into elasticity equations given by King (1983). Calculations were limited to an upper stress-level of 50% of ultimate strength. The results of the dynamic elastic moduli and Poisson's ratio calculations are given in Tables A3.1-3.

The relationships between static and dynamic elastic moduli have been studied by several workers (e.g. Simmons and Brace, 1965; King, 1983). These workers showed that at low confining stresses the static elastic modulus was significantly less than the dynamic moduli for dry rock, which was explained by the presence of micro-cracks. However, when the rock is water saturated, the static modulus decreases and the dynamic modulus increases, with the increase in the latter due to the higher seismic-wave velocities in saturated rock. King (1983) found that there is a good correlation between static and dynamic elastic

moduli, with the two values converging as the moduli increase. Thus, the dynamic elastic moduli derived in this study are regarded as valid. The elastic moduli and Poisson's ratio values were used as input to the finite element models discussed in Ch. 7.

### A3.6. Los Angeles Abrasion Resistance

This is a measure of the abrasion resistance of the rock, and involves grinding a given mass of certain size fractions of a sample in a ball-mill. This was attempted to enable the quantification of the variations in abrasion resistance of rock to subglacial erosion processes.

The machinery used was as per ISRM designation (Brown *et al.*, 1981), but recommended sample sizes and gradings were not followed due to the lack of sufficient sample. However, preliminary tests on greywacke showed that there were few differences between the results of the standard and modified methods used in this study. Instead of the recommended 5 kg of sample, 2.5 kg was used, involving the size fractions 37.5-19.0 and 19.0-1.7 mm respectively, with only half the recommended charge. The sample was revolved in the ball-mill 100 times and the fraction coarser than 1.7 mm was weighed. All material was then returned to the mill for a further 400 revolutions, and the fraction coarser than 1.7 mm was weighed and the percentage wear calculated. The results are given in Tables A3.1-5. The abrasion index was calculated for dry tests only.

### A3.7. Shore Scleroscope Hardness

The Shore Scleroscope provides an index of the intact strength by means of a standard measure of rock hardness. It may also be used as an estimate of the abrasion resistance of the rock (Deere and Miller, 1966). The equipment and methods used in this study are as set out in ISRM suggested methods (Brown, 1981). Short-cores were mainly used, involving tests with the rock in both an oven-dried and vacuum-saturated state. Rabia and Brook (1979) found a marked decrease in strength when the rock was tested in a saturated state, although the effect was most noticeable on porous rather than compact rock. For isotropic rock, at least 25 tests were conducted on each material, while for anisotropic rock, the variability induced by foliation required a minimum of 50 impact tests for each sample. The results are detailed in Tables A3.1-5.

### A3.8. Schmidt Hammer Rebound

Field estimations of the compressive strength of *in situ* rock were obtained by means of a Schmidt hammer. Although the instrument actually measures hammer rebound due to rock elasticity, this value has been directly correlated with compressive strength (Day, 1980). However, the use of the Schmidt hammer can be limited by the nature of the rock surface, especially for schists which often have uneven surface textures and this can have an effect on the readings (Williams and Robinson, 1983). In addition, the use of the hammer parallel to the schistosity was frequently inhibited by the destructive collapse of the mica laminae under hammer impact (Hall, 1987). The method given in Selby (1980) was followed in this study and the Schmidt hammer rebound data presented in Tables A3.1-5.

Table A3.1. Selected physical and intact strength properties of some McMurdo Dry Valley rocks

	Ferrar Dolerite	Larsen Granodiorite	Irizar Granite	Vida granite	Olympus Granite- gneiss
Specific gravity (kg/m <sup>3</sup> ) (wet)	2.928 $\pm$ 0.014(8) 2.932 $\pm$ 0.014(8)	2.755 $\pm$ 0.042(12) 2.765 $\pm$ 0.037(12)	2.568 $\pm$ 0.013(8) 2.586 $\pm$ 0.014(8)	2.532 $\pm$ 0.012(6) 2.555 $\pm$ 0.010(6)	2.719 $\pm$ 0.010(10) 2.728 $\pm$ 0.012(10)
Porosity (%)	0.40 $\pm$ 0.12(8)	1.01 $\pm$ 0.50(12)	1.58 $\pm$ 0.23(8)	2.15 $\pm$ 0.24(6)	0.85 $\pm$ 0.16(10)
Point load (dry) strength (MPa)(sat)	12.0 $\pm$ 1.56(13) 12.37 $\pm$ 3.45(12)	5.29 $\pm$ 1.55(10) 4.31 $\pm$ 0.9(12)	4.79 $\pm$ 1.24(14) 5.80 $\pm$ 0.96(16)	2.32 $\pm$ 0.52(15) 2.30 $\pm$ 0.52(14)	5.13 $\pm$ 1.22(20) 4.44 $\pm$ 1.6 (16)
Brazil tensile (dry) strength (MPa) (sat)	18.12 $\pm$ 2.04(8) 13.89 $\pm$ 1.43(10)	6.19 $\pm$ 0.66(3) 5.21 $\pm$ 0.48(7)	5.13 $\pm$ 0.27(5) 4.1 $\pm$ 0.32 (4)	5.96 $\pm$ 0.41(6) 4.58 $\pm$ 0.51(11)	7.73 $\pm$ 0.77(5)
Sonic velocity (dry) (m/s) (sat)	5.600 $\pm$ 0.313(5) 5.908 $\pm$ 0.220(9)	3.051 4.284 $\pm$ 0.41(14)	3.180 $\pm$ 0.15(3) 4.077 $\pm$ 0.14(9)	2.534 $\pm$ 0.533(11) 2.015 $\pm$ 0.462(7)	4.493 $\pm$ 0.323(8) 4.669 $\pm$ 0.314(13)
Internal cohesion (MPa) (sat)	60.4	15.2	64.1	57.8	31.8
Internal friction angle	40°	47.7°	37.6°	40.4°	41.7°
Dynamic elastic moduli (GPa) (sat)	88.7 $\pm$ 3.6(3)	53.6	47.3 $\pm$ 8.5(3)	34.4 $\pm$ 8.3(3)	47.0 $\pm$ 1.3(2)
Dynamic Poisson's ratio (sat)	0.23 $\pm$ 0.03(3)	0.27	0.31 $\pm$ 0.01(3)	0.32 $\pm$ 0.06(3)	0.3 $\pm$ 0.04(2)
Shore hardness (dry) (sat)	77.85 $\pm$ 2.2 74.08 $\pm$ 4.4	79.6 $\pm$ 4.1 73.1 $\pm$ 4.3	88.6 $\pm$ 4.1 78.3 $\pm$ 4.4	74.6 $\pm$ 3.1 70.8 $\pm$ 4.7	86.3 $\pm$ 2.6 82.9 $\pm$ 4.1
Los Angeles (dry) abrasion(%)	16.4 $\pm$ 4.6(2)	41.3 $\pm$ 4.4(2)	31.1 $\pm$ 1.3(3)	45.7 $\pm$ 4.6(2)	26.1 $\pm$ 6.7(2)
Schmidt hammer rebound	62.0 $\pm$ 4.0	46.0 $\pm$ 5.2	50.2 $\pm$ 5.2	48.4 $\pm$ 3.7	54.7 $\pm$ 2.8

Numbers in ( ) refer to no. of tests, except where standardized as indicated in text.

Dry = tests in oven-dried state, sat = vacuum saturated.

Table A3.2. Selected physical and intact strength properties of some Beacon Supergroup Sandstones

	Beacon Heights Orthoquartzite	Arena Sandstone	Altar Mtn Sandstone	New Mtn Sandstone
Specific gravity (dry) (kg/m <sup>3</sup> )	2.337+0.016(6)	2.266+0.013(6)	2.339+0.024(8)	2.47
(sat)	2.388+0.014(6)	2.361+0.015(6)	2.408+0.022(8)	2.52
Porosity (%)	5.15+0.57(6)	9.57+0.30(6)	6.6+0.48(8)	5.5
Point load (dry) strength (MPa) (sat)	3.9+0.59(20) ---	1.86+0.43(13) ---	3.15+0.64(14) 2.85+0.82(12)	0.41+0.12(10) ---
Brazil tensile (dry) strength (MPa) (sat)	4.45+0.10(3) 3.26+0.2 (5)	2.69+0.29(4) 1.86+0.78(4)	5.59+0.77(4) 3.58+0.6 (6)	1.26+0.1 (4)
Sonic velocity (dry) (km/s) (sat)	0.830+0.100(3) 2.320+0.414(9)	--- 2.947+0.112(9)	2.954 3.375+0.292(6)	3.3 3.77
Internal cohesion (MPa) (sat)	22.1	10.7	22.6	4.2
Internal friction angle (sat)	38.4°	39.7°	33.2°	43.9°
Dynamic elastic moduli (GPa) (sat)	23.7+8.8(3)	10.87	22.7+5.5(3)	---
Poisson's ratio (sat)	0.34+0.1(3)	0.45	0.39+0.03(3)	---
Shore hardness (dry) (sat)	53.9+4.5 44.0+4.0	48.3+6.0 41.6+3.2	65.5+4.9 44.2+8.3	--- ---
Los Angeles abrasion (%) (dry)	94.1	97.4	79.7	99.6
Schmidt hammer rebound	53.8+3.6	49.3+2.6	56.8+4.3	43.5+3.5

Number in ( ) = no. of tests, except where standardized as indicated in text.

Dry = tests in oven-dried state, sat = vacuum saturated.

Table A3.3 Selected physical and intact strength properties of some Darran Mtns plutonic rocks

	Gabbro	Leucogabbro	Diorite	Gabbro	Gabbro
Specific Gravity (kg/m <sup>3</sup> ) (dry)	2.888±0.004(3)	2.871±0.064(6)	2.813±0.024(5)	2.901±0.010(7)	2.904±0.049(5)
Specific Gravity (kg/m <sup>3</sup> ) (sat)	2.895±0.004(3)	2.880±0.065(6)	2.825±0.024(5)	2.907±0.009(7)	2.932±0.010(5)
Porosity (%)	0.66±0.06(3)	0.83±0.13(6)	1.15±0.095(5)	0.61±0.08(7)	0.53±0.05(5)
Point load (MPa) (dry)	5.06±1.26(15)	5.82±1.53(13)	3.81±0.99(14)	5.03±1.01(16)	7.79±1.49(15)
Point load (MPa) (sat)	---	---	---	---	7.80±1.98(16)
Brazil tensile strength (MPa) (dry)	7.74	7.95±1.12(5)	5.58±0.65(4)	10.78±1.45(12)	10.41±1.05(8)
Brazil tensile strength (MPa) (sat)	6.36±0.30(4)	4.27±0.23(4)	7.27±0.82(7)	7.13±0.13(4)	---
Sonic velocity (km/s) (dry)	5.473±0.060(3)	3.929±0.192(5)	3.389±0.262(3)	3.691±0.430(5)	3.248±0.100(3)
Sonic velocity (km/s) (sat)	5.563±0.100(3)	4.170±0.298(10)	3.908±0.292(8)	5.045±0.370(12)	4.751±0.343(9)
Internal cohesion (MPa) (sat)	105	60	33.1	58.3	68.3
Internal friction angle	43°	42.2°	41.8°	42°	37.5°
Dynamic elastic moduli (GPa) (sat)	---	50.88	10.55	47.0±10.6(3)	47.4±7.7(3)
Poisson's ratio (sat)	---	0.29	0.31	0.29±0.03(3)	0.19±0.02(3)
Shore hardness (dry)	75.5±2.8	77.3±3.6	70.2±4.1	78.6±3.5	81.3±3.5
Shore hardness (sat)	71.5±3.2	56.0±3.0	69.7±3.7	67.7±3.9	
Los Angeles abrasion (%) (dry)	29.9±2.2(2)	28.8±1.2(2)	38.9±0.4(2)	27.8±0.4(3)	20.5±1.0(2)
Schmidt hammer hardness	52.4±1.1	55.6±1.3	59.5±1.1	57.7±1.2	58.3±1.2

Number in ( ) refers to no. of tests, except where no. is standardized in text.  
 Dry = tested in oven-dried state, sat = vacuum saturated.

Table A3.4. Selected physical and intact strength properties of some schists from the Mt Aspiring region, and Torlesse rocks from Mt Cook.

	Pyritic Greenschist	Speckled Green Schist	Pelitic Grey Schist	Greywacke	Argillite
Specific gravity (dry) (kg/m <sup>3</sup> ) (sat)	3.058+0.012(6) 3.070+0.009(6)	2.860+0.008(3) 2.868+0.005(3)	2.750+0.001(5) 2.757+0.002(5)	2.707+0.015(10) 2.708+0.015(1)	2.796+0.007(5) 2.798+0.006(5)
Porosity (%)	1.27+0.19(6)	0.81+0.30(3)	0.74+0.19(5)	0.19+0.05(10)	0.13+0.03(5)
Point load (dry) strength (MPa) (sat)	10.11+2.18(20) ---	5.28+0.98(14) + 1.11+0.88(8) // ---	4.63+1.34(19) + 1.59+0.78(9) // ---	11.35+3.5(15) 12.08+1.89(14)	11.06+3.92(15)+ 4.41+2.61 (10)// 12.68+0.87(16)+ 4.87+0.92(9) //
Brazil tensile (dry) strength (MPa) (sat)	8.27+1.87(7) 5.99+0.64(4)	5.45+0.74(3)+ 6.64+0.76 (5)// 3.94+0.38(4)+ 3.78+0.05 (4)//	15.23+1.53(4)+ --- 6.36+1.62 (4)+ ---	18.80+2.63(17) 24.45+3.87(8)	21.47+2.17(5) + --- 26.73+1.57(5) +
Sonic velocity (dry) (km/s) (sat)	2.755+0.155(3) 3.720+0.25(3)	2.713+0.400(3)+ 4.932+0.040(3)// 3.800+0.060(3)+ 5.278+0.050(3)//	3.043+0.120(3)+ --- 3.815+0.245(3)+ ---	5.579+0.100(5) 5.602+0.121(5)	5.547+ --- 5.490+ ---
Internal cohesion (MPa) (sat)	19.2	---	18.2	140	27.9 //
Internal friction angle (sat)	29°	---	35.4°	35.9°	48.2°
Shore hardness (dry) (sat)	40.4+3.5 37.2+4.4	47.0+3.0 42.1+5.8	61.6+11.8 + 46.2+17.4 +	91.72+1.36 90.06+2.32	75.54+2.44 + 73.81+2.48 +
Los Angeles abrasion (%) (dry)	34.0+3.8	47.2	33.2+1.8	11.1+2.4	15.3+1.66
Schmidt hammer rebound	47.8+3.6	49.0+0.82	59.0+3.9	66.2+1.7	62.8+2.4

'+' = rock tested perpendicular to foliation, '//' = rock tested parallel to foliation.  
Numbers in ( ) refer to no. of tests except where no. is standardized in text.



Table A3.5. Selected physical and strength properties of some schists from South Westland

	Q-F-G-B Schist	Q-F-B Schist	Q-B Schist	Q-F-B Schist	Q-B Schist	Q-F-B Schist
Specific gravity (dry) (kg/m <sup>3</sup> ) (sat)	2.698+0.006(3) 2.711+0.005(3)	2.658+0.012(3) 2.672+0.014(3)	2.736+0.004(4) 2.745+0.005(4)	2.736+0.004(3) 2.738+0.019(3)	2.728+0.02(3) 2.653+0.04(3)	2.642+0.032(3) 2.714+0.007(3)
Porosity (%)	1.26+0.14(3)	1.31+0.17(3)	0.91+0.07(4)	1.05+0.06(3)	1.12+0.18(3)	1.46+0.20(3)
Point load (dry) + strength (MPa) //	9.2+1.46(19) 2.82+0.94(16)	10.01+0.97(8) 2.86+0.62(10)	7.4+1.05(10) 2.53+0.84(10)	8.92+2.31(15) 3.45+1.90(14)	6.76+1.7(15) 2.61+1.52(10)	6.83+0.82(8) 2.87+1.0(15)
Brazil tensile (dry) + strength (MPa) //	12.16+1.61(6) ---	12.54+0.3(3) 4.92+1.04(3)	14.91+0.87(3) 5.04+0.40(2)	10.31+0.28(4) 5.27+1.20(3)	8.22+2.21(4) ---	8.03+0.12(3) 1.94+0.24(2)
Sonic velocity (km/s) + (sat) //	2.729+0.331(3) ---	--- 4.869+0.16(3)	--- 5.224+0.08(4)	--- 5.313+0.26(3)	--- ---	2.149+0.34(3) 5.045+0.06(3)
Internal cohesion (MPa) (sat)	29.6	10.0	16.7	13.5	---	23.8
Internal friction angle (sat)	38.2°	45.5°	42.3°	40.6°	---	38.6°
Shore hardness (dry) // (sat) //	52.5+12.9 57.0+7.2	72.3+14.6 50.0+7.3	67.0+10.3 52.7+14.1	63.1+15.9 56.4+16.5	56.3+15.0 ---	59.0+15.0 54.6+9.1
Los Angeles abrasion (%) (dry)	27.7+0.8(2)	26.0+0.1(3)	27.5+1.1(2)	25.4	23.3+2.4(2)	34.2+1.9(2)
Schmidt hammer rebound	52.1+1.7	52.6+2.7	52.6+2.4	54.7+2.7	54.5+2.3	52.2+3.4

Q = quartz, F = feldspathic, B = biotite, C = chlorite

Number s in ( ) refer to no. of tests, except where standardized as in text.

Dry = tested in oven-dried state, sat = vacuum saturated.